THE UNIVERSITY OF QUEENSLAND

AUSTRALIA

Bioeroding sponges in a time of change: insights into the physiology and cell biology of a photosymbiotic coral-eroding sponge

Michelle Achlatis

Master of Science; Bachelor of Science

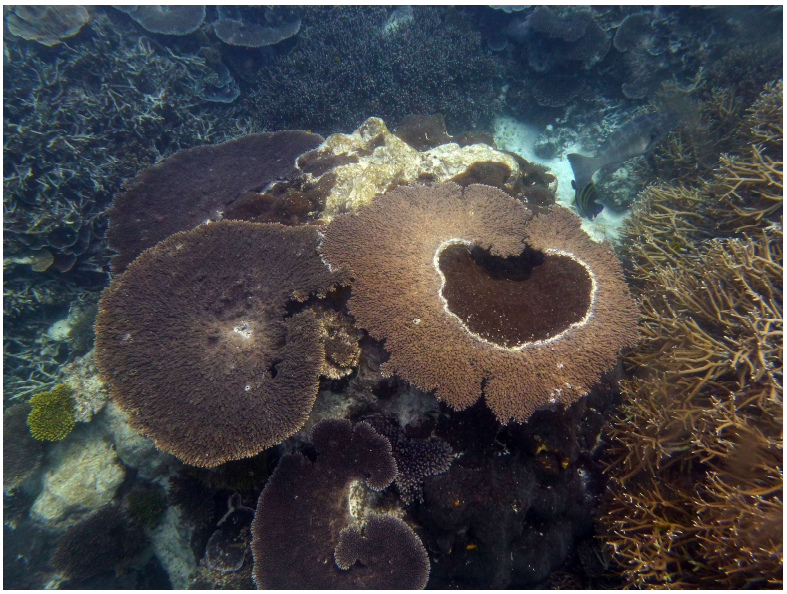

A thesis submitted for the degree of Doctor of Philosophy at

The University of Queensland in 2018

School of Biological Sciences

Abstract

Anthropogenic climate change is altering the ecological balance of the world around us, and coral reefs are among the first ecosystems to reveal these fundamental changes. Consequently, there is an urgent need to understand how key services provided by reefs will change in the future. The ability of reefs to maintain positive carbonate balances despite their exposure to the erosive power of waves is fundamental to many services they provide. An important, but relatively unexplored facet of the carbonate balance of reefs, is their biological erosion by excavating sponges. Gaining greater insight into the physical drivers of this biological erosion, in addition to the potential responses of excavating sponges to future conditions is therefore the goal of this thesis.

While healthy reefs maintain a positive budget, or at least equilibrium between construction and destruction of calcium carbonate ($CaCO_3$), warming and ocean acidification have the potential to tip the scales towards net erosion. Excavating sponges, which are one of the major groups of $CaCO_3$ bioeroders, belong to the perceived "winners" under future scenarios with their bioerosion rates expected to increase disproportionately. Despite the critical relevance of the effect of climate change on the excavating activity of bioeroding sponges, the physiological and metabolic processes that underpin the ecological success of such sponges on coral reefs are poorly understood.

Some of the most competitive and destructive (to the $CaCO_3$ framework) bioeroding sponges form a symbiosis with photosynthetic dinoflagellates of the genus *Symbiodinium.* The Great Barrier Reef sponge *Cliona orientalis*, used as a model in the current study, is an aggressive competitor that often overgrows and kills the calcareous corals that it erodes. A key question is: Is the vigour and competitive superiority of such sponges associated with the symbiosis they form with photosynthetic dinoflagellates? The role of dinoflagellates in host metabolism and host bioerosion capacity remains relatively unexplored. The first study in the present thesis attempts to shed light on the interaction between *C. orientalis* and its photosymbionts, while assessing the contribution of photosynthetic energy to the bioerosion activity (Chapter 2). The bioerosion rates of bleached (relatively free of symbionts), photosynthetically inactivated (treated with diuron) and control sponges were quantified in the light (day) and in the dark (night). These experiments show a clear relation between the holobiont photosynthetic activity and the day-time bioerosion capacity of the sponge. Night-time bioerosion was only partially explained by respiration rates and day-time photosynthetic activity that might lead to storage of photosynthetic outputs for night-time use.

The presence of a small prokaryotic community in the sponge, however, complicates the definitive attribution of all photosynthetic activity to *Symbiodinium*. There are multiple potential candidates for uptake of inorganic carbon (i.e. photosynthesis) or inorganic nitrogen within a clionaid holobiont, the latter potentially even carried out by the sponge itself. In a second study, isotopically enriched ^{13}C-bicarbonate and ^{15}N-ammonium were used to track the entry and distribution of inorganic carbon and nitrogen in the sponge holobiont (Chapter 3). Capitalizing on recent integration of isotopic labelling, transmission electron microscopy and nanoscale secondary ion mass spectrometry, isotopic enrichment of individual cell types and tissue structures of interest were visualized and quantified inside the outer photosynthetic layer of the sponge. This experiment unequivocally pinpointed *Symbiodinium* as the primary source of inorganic assimilation into organic material, illustrating that assimilated material is subsequently translocated to proximate sponge cells, in the absence of symbiont digestion.

Finally, to assess the resilience of the symbiosis as well as the host's dependence on *Symbiodinium*, the sponge holobiont was subjected to prolonged warming and acidification, under increased heterotrophic potential (Chapter 4). In a fully-crossed design that respects diurnal and seasonal fluctuations in seawater conditions, the sponges were exposed to independent and concomitant warming and acidification (projected as appropriate for a typical end of century, non-El Niño summer under "business-as-usual" carbon dioxide emissions), as well as diet supplementation with nitrogen-rich particulates. While acidification did not strongly affect erosion rates, diet supplementation accelerated them. Warming decelerated bioerosion rates and caused extensive bleaching and prevailing mortality of sponges, overriding the other factors and confirming a strong metabolic dependence of the sponge on its resident symbionts. This experiment indicates that the growth, bioerosion capacity and likelihood of survival of *C. orientalis* and similar photosymbiotic excavating sponges could be substantially reduced rather than increased on end-of-the-century reefs under "business-as-usual" emission profiles. In other words, although photosymbiotic excavating sponges benefit in many ways from their resident *Symbiodinium*, they are nonetheless vulnerable to prolonged heat stress, implying that they may not share the title of "winners" alongside their non-*Symbiodinium*-hosting counterparts on future coral reefs.

Declaration by author

This thesis is composed of my original work, and contains no material previously published or written by another person except where due reference has been made in the text. I have clearly stated the contribution by others to jointly-authored works that I have included in my thesis.

I have clearly stated the contribution of others to my thesis as a whole, including statistical assistance, survey design, data analysis, significant technical procedures, professional editorial advice, financial support and any other original research work used or reported in my thesis. The content of my thesis is the result of work I have carried out since the commencement of my higher degree by research candidature and does not include a substantial part of work that has been submitted to qualify for the award of any other degree or diploma in any university or other tertiary institution. I have clearly stated which parts of my thesis, if any, have been submitted to qualify for another award.

I acknowledge that an electronic copy of my thesis must be lodged with the University Library and, subject to the policy and procedures of The University of Queensland, the thesis be made available for research and study in accordance with the Copyright Act 1968 unless a period of embargo has been approved by the Dean of the Graduate School.

I acknowledge that copyright of all material contained in my thesis resides with the copyright holder(s) of that material. Where appropriate I have obtained copyright permission from the copyright holder to reproduce material in this thesis and have sought permission from co-authors for any jointly authored works included in the thesis.

Publications during candidature

Peer-reviewed publications related to this thesis:

Achlatis M, van der Zande RM, Schönberg CHL, Fang JKH, Hoegh-Guldberg O, Dove S. (2017). Sponge bioerosion on changing reefs: ocean warming poses physiological constraints to the success of a photosymbiotic excavating sponge. *Sci Rep* **7**: 10705.

Achlatis M, Pernice M, Green K, Guagliardo P, Kilburn MR, Hoegh-Guldberg O, Dove S. (2018). Single-cell measurement of ammonium and bicarbonate uptake within a photosymbiotic bioeroding sponge. *ISME J* **12**: 1308–1318.

Peer-reviewed publications not related to this thesis:

Alexander BE, **Achlatis M**, Osinga R, van der Geest HG, Cleutjens JPM, Schutte B, de Goeij JM. (2015). Cell kinetics during regeneration in the sponge *Halisarca caerulea*: how local is the response to tissue damage? *PeerJ* **3**: e820.

Ramsby BD, Hill MS, Thornhill DJ, Steenhuizen SF, **Achlatis M**, Lewis AM, LaJeunesse TC. (2017). Sibling species of mutualistic *Symbiodinium* clade G from bioeroding sponges in the western Pacific and western Atlantic oceans. *J Phycol* **53**: 951–960.

Fang JKH, Schönberg CHL, Mello-Athayde MA, **Achlatis M**, Hoegh-Guldberg O, Dove S. (2018). Bleaching and mortality of a photosymbiotic bioeroding sponge under future carbon dioxide emission scenarios. *Oecologia* **187**: 25-35.

Brown KT, Bender-Champ D, Kubicek A, van der Zande R, **Achlatis M,** Hoegh-Guldberg O, Dove SG (2018). The dynamics of coral-algal interactions in space and time on the southern Great Barrier Reef. *Front Mar Sci* **5**: 181.

Hoegh-Guldberg O, Jacob D, Taylor M, Bindi M, Brown S, Camilloni I, Diedhiou A, Djalante R, et al. (2018). Chapter 3: Impacts of 1.5ºC global warming on natural and human systems. In: Global Warming of 1.5 °C, an IPCC special report on the impacts of global warming of 1.5 °C above pre-industrial levels. Intergovernmental Panel on Climate Change. (**contributing author**).

Conference abstracts related to this thesis and presented by the candidate:
"Future bioerosion on the Great Barrier Reef by the excavating sponge *Cliona orientalis",* 89th Australian Coral Reef Society Conference, 2015, Daydream Island, Australia.

"Putting the success of bioeroding sponges on future reefs into perspective: Enhanced bioerosion versus physiological constraints of *Cliona orientalis*", 13th International Coral Reef Symposium, 2016, Hawaii, USA.

"Single-cell measurement of metabolic interactions between a bioeroding sponge and its endosymbiotic dinoflagellates", 10th World Sponge Conference, 2017, Galway, Ireland and
2nd Queensland Mass Spectrometry Symposium, 2017, Brisbane, Australia.

"Metabolic interactions between an aggressive bioeroding sponge and its endosymbiotic dinoflagellates revealed through novel technologies", 91st Australian Coral Reef Society Conference, 2018, Exmouth, Australia.

Publications included in this thesis

Achlatis M, van der Zande RM, Schönberg CHL, Fang JKH, Hoegh-Guldberg O, Dove S. (2017). Sponge bioerosion on changing reefs: ocean warming poses physiological constraints to the success of a photosymbiotic excavating sponge. *Sci Rep* **7**: 10705. (Incorporated as Chapter 4).

Contributor	Statement of contribution
Achlatis M (Candidate)	Conception and design (40%) Analysis and interpretation (45%) Drafting and production (50%)
van der Zande RM	Conception and design (0%) Analysis and interpretation (20%) Drafting and production (0%)
Schönberg CHL	Conception and design (0%) Analysis and interpretation (15%) Drafting and production (20%)
Fang JKH	Conception and design (0%) Analysis and interpretation (5%) Drafting and production (0%)

Hoegh-Guldberg O	Conception and design (20%) Analysis and interpretation (0%) Drafting and production (10%)
Dove S	Conception and design (40%) Analysis and interpretation (15%) Drafting and production (20%)

Achlatis M, Pernice M, Green K, Guagliardo P, Kilburn MR, Hoegh-Guldberg O, Dove S. (2018). Single-cell measurement of ammonium and bicarbonate uptake within a photosymbiotic bioeroding sponge. *ISME J* **12**: 1308–1318. (Incorporated as Chapter 3).

Contributor	Statement of contribution
Achlatis M (Candidate)	Conception and design (40%) Analysis and interpretation (35%) Drafting and production (50%)
Pernice M	Conception and design (30%) Analysis and interpretation (15%) Drafting and production (25%)
Green K	Conception and design (0%) Analysis and interpretation (10%) Drafting and production (0%)
Guagliardo P	Conception and design (0%) Analysis and interpretation (10%) Drafting and production (0%)
Kilburn MR	Conception and design (0%) Analysis and interpretation (5%) Drafting and production (0%)
Hoegh-Guldberg O	Conception and design (10%) Analysis and interpretation (10%) Drafting and production (5%)
Dove S	Conception and design (20%) Analysis and interpretation (15%) Drafting and production (20%)

Manuscripts included in this thesis

No other submitted manuscripts included.

Contributions by others to the thesis

Sophie Dove and Ove Hoegh-Guldberg at The University of Queensland (UQ) were the principal advisors of this thesis, and Lars Nielsen at UQ was the secondary advisor. Christine Schönberg at the Australian Institute of Marine Science provided external supervision on most parts of the research, and contributed significantly to writing Chapter 2 and Chapter 4. Mathieu Pernice at the University of Technology Sydney provided essential guidance for the NanoSIMS study (Chapter 3). Sophie Dove and David Kline (currently at the University of California San Diego) designed the temperature and acidification system at Heron Island utilised in Chapter 4. Aaron Chai and Giovanni Bernal Carrillo at UQ were the maintenance technicians of this system. Dorothea Bender-Champ, Andreas Kubicek, Rene van der Zande and Kristen Brown at UQ assisted in the experimental setup during fieldwork on Heron Island. Todd C. LaJeunesse at the Pennsylvania State University is thanked for the preliminary *Symbiodinium* genetic analysis (Chapter 2). Selina Ward and Ian Tibbetts at UQ are gratefully acknowledged for being the expert readers of this thesis. Sophie Dove and Ove Hoegh-Guldberg funded the project through the funding bodies listed in the "Financial support" section below. All research was conducted under sample permit nr. G14/37212.1 issued by the Great Barrier Reef Marine Park Authority.

Statement of parts of the thesis submitted to qualify for the award of another degree

None

Research involving human or animal subjects

Ethics approval was not required for this research.

Acknowledgements

I have heard many say that the PhD is a marathon, not a sprint. At times though it resembles a relay race, and in this section I would like to thank all the people who have helped me reach the finish line.

First of all I am grateful to my main advisors, Sophie and Ove, for giving me the opportunity to start my PhD and for supporting and encouraging me along the journey. You have both been a source of inspiration. Sophie, thank you for teaching me to never stop questioning. Special thanks to my external advisor Christine for her endless enthusiasm about sponges, and for keeping the great work up. I am indebted to you Christine of all the tireless work you have put into revising my manuscripts. Although not officially an advisor of my project, Mathieu has generously shared his knowledge on all things NanoSIMS with me, and without his help my NanoSIMS studies would not have been possible. It has been a pleasure working with you Mathieu, and it was fun to finally meet you in person.

I would also like to acknowledge the staff of the Centre for Microscopy and Microanalysis, the Advanced Water Management Centre, and the Elemental Microanalysis facility at UQ, as well as the NanoSIMS facility at the University of Western Australia. In particular I would like to thank Kathryn for teaching me Electron Microscopy despite my unconventional rock-hard sponges, and Paul for patiently bombarding hundreds of sponge cells at the NanoSIMS. The School of Biological Sciences at UQ also deserves praising, amongst others for the Friday rooftop social mixers.

I have spent more than a year over 12 trips on the small island cay named Heron Island. For all the fun times there, and for all the things I learned, I would firstly like to thank the leading post-docs of the Laureate team, Doro and Andreas. You have both been extremely helpful over the years, and thanks again for your patience with all our questions. Rene, Kristen and later “adopted” Mat, thank you for all the hard teamwork and the good laughs. I promise I will bake a banana bread without bananas of all of us soon, it’s too bad Andreas and Doro will miss out this time. I would also like to thank Aaron and Gio for their contributions in building experiments as well as building fun memories (including Aaron’s famous pancake breakfasts) on the island. Yannick, Ramona, Lauren, Bobby and my dear friend Zoi, thank you all for volunteering your time to help. I hope the surprise manta visits were a good payoff. Special thanks to Maureen and all the staff of the Heron Island Research Station for their support over the years. To the numerous researchers and fellow students that I have shared sunset beers and island fever with over the years, thank you for making the hard work enjoyable.

Back on the mainland, I would like to express my gratitude to all the past and present members of the Coral Reef Ecosystems lab, In particular: Annamieke, Hayley and Mark for tirelessly accommodating my requests over the years and for keeping us all under check; my officemate and friend Veronica, for the daily fun and for sharing her motivation and chocolate during our long office hours. All the best writing up Veronica; in addition to those mentioned above, the remaining members of our PhD cohort, Catherine and Dom, for the good times and the baked goods - we are almost there now! Dr. Anjani, congratulations again on your title and hope to catch up soon in the Caribbean. Francisco, Norbert, Robert, Siham and our inspirational postdocs Manuel, Beto, Emma, Julie, Carolina and most of all Pim, thank you for all your support. I would like to stop and acknowledge James; although we unfortunately never overlapped in Australia, I must admit that your PhD offered me great inspiration, and a great toolbox for my work. To the overseas sponge researchers Vassia, Brittany and Jasper, thank you for helping me and for getting me excited about sponges in the first place.

I would like to extend my appreciation to my friends and family in Europe and beyond, especially my grandmother who gave me a roof to sleep under while I was a masters student, my γιαγιά and παππού and his 'άνθρωπος αγράμματος, τούβλο απελέκητο' saying, my friend Marialena who always encourages me, my UOC, tzelavi and UVA friends, the Erasmus b…. group, and many more. Here in Australia, thanks to the crazy Greek Panagopoulos family for the fun times, and a huge thanks to Ebony and Giorgo (and Alexi πού και πού) for putting up with living with two nerdy wannabe academics for all these years. Brisbane city council pools, author G.R.R. Martin and Shady Palms are acknowledged for providing regular escape routes.

Finally but most importantly, I have no words to thank my parents Marjan and Panagiotis and my sister Ebony for always believing in me, Ierapetra for making me love the sea, and Rene for making me love coral reefs.

Financial support

The Australian Research Council Laureate grant FL120100066 (Ove Hoegh-Guldberg), the ARC Centre of Excellence for Coral Reef Studies grant CE0561435 (Ove Hoegh-Guldberg and Sophie Dove) and the ARC Linkage – NOAA grant LP11020087 (Ove Hoegh-Guldberg and Sophie Dove) funded this study. The Holsworth Wildlife Research Endowment (Michelle Achlatis) by the Ecological Society of Australia significantly contributed and is gratefully acknowledged. The PhD candidature was supported by an Australian Government Research Training Program Scholarship.

Keywords

bioerosion, calcium carbonate, climate change, *Cliona*, DCMU, Great Barrier Reef, NanoSIMS, *Symbiodinium*, symbiosis, sponge

Australian and New Zealand Standard Research Classifications (ANZSRC)

ANZSRC code: 050101, Ecological Impacts of Climate Change, 30%

ANZSRC code: 060603, Animal Physiology − Systems, 60%

ANZSRC code: 060705, Plant Physiology, 10%

Fields of Research (FoR) Classification

FoR code: 0606, Physiology, 50%

FoR code: 0602, Ecology, 40%

FoR code: 0607, Plant Biology, 10%

To Marjan and Panagiotis

"The question at once arises, how is it that even the stoutest corals, resting with broad base upon the ground, and doubly secure from their spreading proportions, become so easily a prey to the action of the same sea which they met shortly before with such effectual resistance? The solution of this enigma is to be found in the mode of growth of the corals themselves. Living in communities, death begins first at the base or centre of the group, while the surface or tips still continue to grow, so that it resembles a dying centennial tree, rotten at the heart, but still apparently green and flourishing without, till the first heavy gale of wind snaps the hollow trunk, and betrays its decay. Again, innumerable boring animals establish themselves in the lifeless stem, piercing holes in all directions into its interior, like so many augers, dissolving its solid connexion with the ground, and even penetrating far into the living portion of these compact communities. The number of these boring animals is quite incredible, and they belong to different families of the animal kingdom […]. But however efficient these boring animals may be in preparing the coral stems for decay, there is yet another agent, perhaps still more destructive. We allude to the minute boring-sponges, which penetrate them in all directions, until they appear at last completely rotten throughout."

Prof. Louis Agassiz, 1851
Annual report of the Superintendent
of the US Coast Survey, Florida Keys

Table of Contents

List of Figures and Tables

List of Abbreviations

ANOVA	analysis of variance
AOI	area of interest
ATP	adenosine triphosphate
$CaCO_3$	calcium carbonate
Ctrl	control
DCMU	N'-(3,4-dichlorophenyl)-N,N-dimethylurea
DHW	degree heating weeks
DOC	dissolved organic carbon
GBR	Great Barrier Reef of Australia
GHD	glutamate dehydrogenase
GS/GOGAT	glutamine synthetase/ glutamate synthase
HMA	high microbial abundance
IPCC	intergovernmental panel on climate change
LMA	low microbial abundance
MMM	maximum monthly mean temperature
NanoSIMS	nanoscale secondary ion mass spectrometry
NOAA	national oceanic and atmospheric administration
PAM	pulse amplitude modulation
PAR	photosynthetically active radiation
pCO_2	partial pressure of carbon dioxide
PD	present day
PERMANOVA	permutational (multivariate) analysis of variance
POC	particulate organic carbon
PSII	photosystem II
RCP8.5	representative concentration pathway 8.5
TEM	transmission electron microscopy
TOC	total organic carbon

Chapter 1

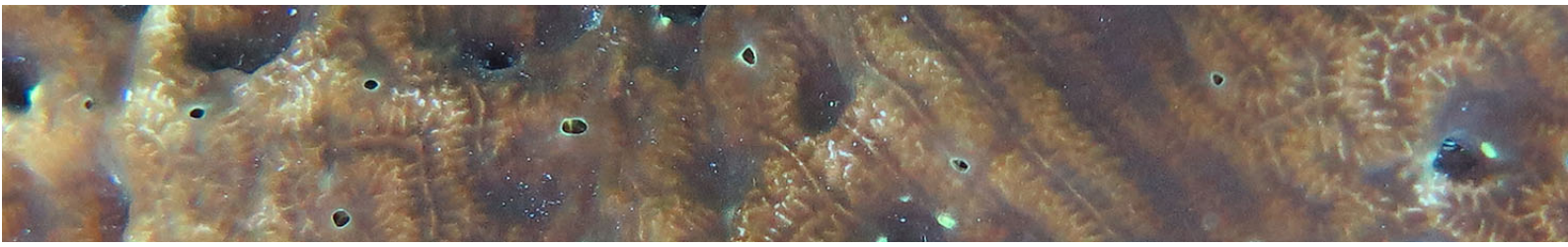

Thesis Introduction

1.1. Sponge bioerosion on coral reefs

Possibly one of the most astonishing interactions between biotic and abiotic components of nature is the interplay between living organisms and calcium carbonate structures. Biologically-mediated carbonate precipitation is ubiquitous in marine ecosystems, from the spherical skeletons of coccolithophores to the intricate shells of molluscs and the massive reefs built by scleractinian corals. Just as ubiquitous, however, is another suite of organisms that specialize in the erosion of calcium carbonate structures, scraping away on the surface as they feed, or excavating micro- or macroscopic galleries as they grow and acquire shelter within these limestone-like structures.

Carbonate coral reefs are distinguished by their ability to produce a three-dimensional calcium carbonate framework within which at least a million species live (Reaka-Kudla, 1997; Knowlton *et al.*, 2010; Fisher *et al.*, 2015). Such reefs are the result of a balance between constructive and destructive forces that are driven by calcifying and decalcifying mechanisms respectively. The reef framework is maintained by simultaneous accretion of calcium carbonate ($CaCO_3$) due to calcifying organisms and weathering of $CaCO_3$ by physical, chemical or biological erosion (Glynn, 1997). Coral biomineralization, marine cementation and binding by coralline algae lead to skeleton growth and reef formation, which are counteracted by loss of substrate resulting in rubble, sand and silt, some of which are subsequently carried out to the open ocean (Manzello *et al.*, 2008; Kennedy *et al.*, 2013).

A substantial proportion of the biodiversity that reefs host is responsible for eroding and weakening the calcareous skeletons of reef-building species (Schönberg *et al.*, 2017a). The contribution of eroding organisms to carbonate budgets and reef maturation has been well established over the past century, with their activity traced back to Precambrian and Cambrian times (Vogel, 1993). Biological erosion (or bioerosion) refers to the breakdown of consolidated substrate by the direct action of organisms and is mediated by a number of taxa (Neumann, 1966). Microbioerosion is performed by microorganisms such as bacteria, cyanobacteria, protozoans and algae that can dissolve limestones due to the acidic by-products of their metabolism (Macintyre, 1984; Le Campion-Alsumard *et al.*, 1995). Macrobioerosion ranges from coelobites sculpting inside cavities and crevices to internal eroders such as bivalves and external eroders such as grazing fish and sea urchins (Glynn, 1997). Many bioeroders mechanically and/or chemically bore into the $CaCO_3$, thereby providing themselves with shelter and protection from predators (Neumann, 1966; Schönberg *et al.*, 2012). Their endolithic lifestyle may weaken the substrates they inhabit, rendering

infested substrates more susceptible to physical or chemical erosion (Glynn, 1997; Hutchings, 1986). Inversely, physical erosion caused by wave action, storms or cyclones can create dead substrate which will then be colonized by bioeroding organisms.

Bioeroding sponges are a highly significant group on tropical and sub-tropical coral reefs. Up to 90% of macro-bioerosion and 40% of sediment production on reefs has been ascribed to these often abundant sponges (Futterer, 1974; Rützler, 1975; MacGeachy, 1977; Mallela and Perry, 2007). At localities that are heavily invaded by bioeroding sponges, coral calcification rates can be met or even overpassed by sponge bioerosion, as is the case in some Caribbean and East Pacific reefs (Acker and Risk, 1985; Nava and Carballo, 2008). Were these localities to encompass the entirety of a given reef, then it would be questionable to classify such a reef as a carbonate coral reef.

Bioeroding sponges belong to a number of different families (Schönberg *et al.*, 2017b), but the most prominent excavating sponges are found in the family Clionaidae D'Orbigny, 1851 of the order Hadromerida. Clionaid sponges are readily recognizable as yellow, brown or orange spots coating the interior of corroded coral skeletons, but some growth forms spread laterally encrusting the limestone surface ("alpha" versus "beta" form respectively, Schönberg *et al.*, 2017a). This is particularly true for a number of rigorous excavators of the "*Cliona viridis* species complex" which form symbioses with photosynthetic dinoflagellates of the genus *Symbiodinium.* Of the 76 *Cliona* species currently recognized by the World Porifera Database (van Soest *et al.*, 2018), roughly a quarter host *Symbiodinium*, and half of this quarter display particularly rapid lateral expansion and high bioerosion rates (Mote *et al*., in review; CHL Schönberg, pers.comm.). In this relationship, the *Symbiodinium*, and potentially the host sponge, benefit from lateral expansion that increases the light-harvesting surface of the sponge and *Symbiodinium* contained within (e.g. Rützler, 1975; Vicente, 1978; Schönberg *et al.*, 2001; López-Victoria *et al.*, 2006). While excavating beneath the surface, bioeroding sponges cause polyp death by removing the structural support of coral calyces (López-Victoria *et al.*, 2006; Chaves-Fonnegra and Zea, 2007). Without skeletal support, the coral tissue retreats and, in the absence of defensive nematocysts and mucus, the sponge is able to spread rapidly. Once the coral is heavily infested, the sponge can even overgrow and kill surface tissues (Glynn, 1997; Schönberg, 2000).

Sponge erosion is thought to be accomplished by a combination of chemical and mechanical boring, yet the details of this process remain ambiguous and controversial (Schönberg, 2008). In order to penetrate the substrate, the sponge employs etching cells (amoebocytes) that

chemically carve a groove in the $CaCO_3$ (Fig.1.1a). The extended pseudopodial sheets of these cells mechanically expand the groove and release minute $CaCO_3$ chips when they coalesce centrally (Rützler and Rieger, 1973; Pomponi, 1979a; 1979b; 1980) (Fig.1.1b). The chips are then expelled through the sponge's aquiferous system into the water column (Zundelevich *et al.*, 2007). The resulting cavities are filled with sponge biomass as the etching front proceeds deeper into the substrate.

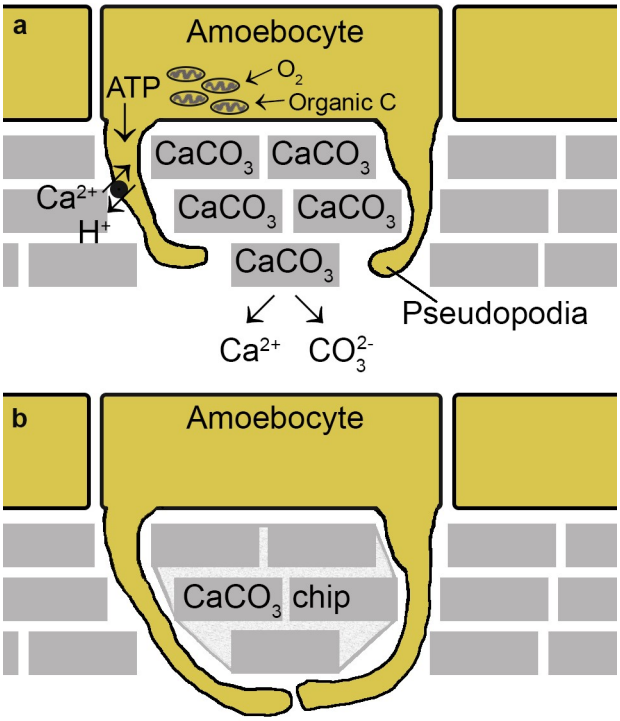

Figure 1.1: Conceptual schematic of the etching process in bioeroding sponges. (a) At the etching front, amoebocytes manipulate the local acid balance to protrude parts of their cell surface (pseudopodia) into the porous $CaCO_3$. The exact chemical agents that dissolve the $CaCO_3$ remain unknown, but calcium and protons pumps could be involved as hypothesized here. Potentially these pumps are driven by ATP produced by mitochondria (shown here as elliptical organelles) that feed on O_2 and organic carbon (C), both of which are particularly abundant in photosymbiotic bioeroding sponges. **(b)** When the pseudopodia coalesce centrally, a minute chip of $CaCO_3$ is mechanically freed and ejected through the sponge's aquiferous canals.

The exact enzymes or acids involved in the bioerosion process remain unidentified and highly controversial despite early attempts to ascertain their nature (reviewed by Schönberg, 2008). Pomponi (1979c) used electron microscopic cytochemistry with acid phosphatase as a marker to demonstrate that a lysosomal system is involved in the etching process, and Hatch (1980) demonstrated that carbonic anhydrase has an active role in erosion by *Cliona celata*. Recently, interest in the etching process has been revived, with a new study confirming previous suggestions that extracellular pH is reduced (i.e. is more acidic) at the etching sites

as compared to ambient seawater and sponge tissue (Schönberg, 2008; Webb *et al.*, unpubl. data). It is plausible that oxygen and organic carbon fuel large numbers of mitochondria in etching cells, which in turn produce sufficient ATP to drive Ca^{2+}/H^{+} antiporters that pump protons into the site of decalcification (as hypothesized in Fig.1.1a). This unconfirmed hypothesis is the reverse of the calcification process established in corals (Allemand *et al.*, 2004), and could be boosted in photosymbiotic sponges where photosynthetically-produced oxygen and organic carbon molecules are plentiful.

Rates of substratum colonization by bioeroding sponges can depend on a number of biotic and abiotic variables such as nutrient availability, temperature, substrate type and physiological condition of the organism (Risk *et al.*, 1995; Hill, 1996; Hutchings, 1986). Regardless of the erosion rate, the bioerosion process appears to be an energetically-costly process, and as such it presumably confers competitive advantages to the sponges' fitness. Early studies hypothesized that the sponges obtain nutrition from the removed material and/or tissues (Ward and Risk, 1977), but this has yet to be demonstrated. Instead, the literature supports that the bioerosion habit of sponges is a product of the sheltering, shading and shielding function of the surrounding limestone. Out of reach of most predators, clionaid sponges, which most likely lack other means of chemical or mechanical defence (but see Chavez-Fonnegra *et al.*, 2008 for compounds potentially used to attack corals), have the competitive advantage of establishing their habitat in a substrate that other organisms cannot invade or compete for (Schönberg and Wisshak, 2012). In that way, their soft tissue is adequately protected without the need to defend it, replace material lost to predation, or invest largely into spicule formation. The porous limestone may also protect the sponge (and its microbial community) from excess light or desiccation in the intertidal zone (Schönberg 2000, 2001; Schönberg & Suwa 2007), as well as parasites or disease vectors (Schönberg and Wisshak, 2012).

Clionaid sponges play an important ecological role on reefs by hosting a number of organisms inside their water channels (e.g. polychaetes, sipunculans, ophiuroids, and bivalves), changing the space availability, shaping the reef framework and influencing seawater chemistry (Zundelevich *et al.*, 2007). Bioeroding sponges also most likely actively contribute to the "sponge loop" which recycles nutrients on coral reefs (De Goeij *et al.*, 2008, 2013; Rix *et al.*, 2016a, 2016b, 2017) given that the nutrition of at least two Caribbean excavating species relies on dissolved organic carbon (Mueller *et al.*, 2014). Their excavating activity significantly increases the porosity of the coral frameworks, resulting in

honeycombed $CaCO_3$ structures that are more susceptible to physical stressors such as storms and cyclones or other biological agents of erosion such as parrotfish grazing (Hutchings, 1986).

1.2. Bioerosion in the context of global change

Approximately 30% of the anthropogenic carbon dioxide (CO_2) emissions to date have been absorbed by the oceans (IPCC, 2013), disturbing their natural buffering system. As a result, the pH values of seawater are decreasing (Raven *et al.*, 2005). Ocean acidification poses significant risks to coral reefs and the calcifying organisms that they host (De'ath *et al.*, 2009; Pörtner *et al.*, 2014; Hoegh-Guldberg *et al.*, 2007; 2014). Acidification, however, is just one of the many threats coral reefs face. The enhancement of the greenhouse effect caused by human emissions has further triggered a series of rapid changes to our oceans. Since the 1980s, anthropogenic global warming has caused numerous bleaching events (i.e. disruption of the symbiosis between the coral host and its symbiotic dinoflagellates) on coral reefs worldwide, leading to unprecedented coral mortality and deleterious downstream effects for the ecosystems and the human populations they support (Hoegh-Guldberg, 1999; Hoegh-Guldberg *et al.*, 2007b, De'ath *et al.*, 2009; Hoegh-Guldberg, 2012; Hughes *et al.*, 2017a). Over the past years, the phenomenon of coral bleaching has intensified and during 2015-2016, the third and most severe so far pantropical bleaching event occurred (Hughes *et al.*, 2017b).

As opposed to other reef stressors such as overfishing, disease, pollution by land-runoff and eutrophication that act at a local level, tackling the global stressors of acidification and warming requires action on an international level. Despite a 3-year period of relatively slow growth in CO_2 emissions from fossil fuels and industry (+0.4% yr^{-1} during 2014-2016 as opposed to an average of +1.8% yr^{-1} from 2007-2016), growth returned to +2.0% in 2017 (Peters *et al.*, 2017; Le Quéré *et al.*, 2017; Jackson *et al.*, 2017). So far, humanities actions have fallen short of the changes needed to detour from the business-as-usual trajectory and to contain global warming to the United Nations Paris Agreement target of "well below 2ºC", let alone below 1.5ºC which is considered the maximum warming under which >10% of coral reefs worldwide could still be conserved (Frieler *et al.*, 2013; Schleussner *et al.*, 2016; Hughes *et al.*, 2017a).

CO_2-driven impacts on coral calcification have received significant attention in recent years (Orr *et al.*, 2005; Kleypas and Langdon, 2006; Wernberg *et al.*, 2012; Kroeker *et al.*, 2013).

Numerous studies have projected that there will be less $CaCO_3$ accretion on reefs worldwide due to increased mortality or decreased calcification potential (see references in Hoegh-Guldberg *et al.*, 2007) and such changes have already been described from various locations including the Great Barrier Reef of Australia (GBR) (e.g. Cooper *et al.*, 2008; De'ath *et al.*, 2009; Hughes *et al.*, 2017b; Frieler *et al.*, 2013). However, despite a recent increase in interest, decalcification and in particular bioerosion responses to ocean acidification, warming and eutrophication remain poorly understood, even though their role is of equal significance to the carbonate budgets of reefs (Tribollet and Golubic, 2011; Andersson and Gledhill, 2013; Fang and Schönberg, 2015; Schönberg *et al.*, 2017a, 2017b). Decalcifying mechanisms are understudied in comparison to calcifying mechanisms, especially in the context of global change. Only recently have bioerosion and its associated processes started to be included in ecological modelling (González-Rivero *et al.*, 2011b; Kennedy *et al.*, 2013; Perry *et al.*, 2014; Bozec *et al.*, 2015).

Although bioeroding sponges are better studied than other endolithic bioeroders (Schönberg *et al.*, 2017b), they remain poorly understood compared to other reef taxa, partly due to technical difficulties in their laboratory and field handling. Their endolithic growth form causes complex taxonomy and hampers *in situ* observations. Even when they encrust surfaces, it is difficult to accurately estimate the extent of growth in the underlying substrate. In addition, the fine intertwinement of their soft tissue with the substrate allows only destructive biomass quantification (Fang *et al.*, 2013b; Schönberg *et al.*, 2017b).

A growing body of studies has nevertheless suggested that concurrent global warming and acidification will enhance the abundance and bioerosion efficiency of excavating sponges on reefs, tipping the balance to the disadvantage of calcifying organisms (see references in Schönberg *et al.*, 2017a, 2017b; Chaves-Fonnegra *et al.*, 2017). One of the proposed hypotheses is that the energetic cost of bioerosion will be reduced in more acidified oceans as the dissolution threshold will be more readily met, since $CaCO_3$ dissolution by sponges is thought to entail excretion of acids (Wisshak *et al.*, 2012; Schönberg *et al.*, 2017a). This hypothesis presumes access of seawater to the decalcifying space, which may be achieved to a certain extent through the porous $CaCO_3$ skeleton, especially if it is in some part unprotected by host tissue (Fig. 1.1). Since pH buffering potential is dictated by the ratio of total alkalinity to dissolved inorganic carbon, reductions in the energetic cost of bioerosion might be further stimulated by decreased aragonite saturation states on future reefs (Feely *et al.*, 2004). Manzello *et al.* (2008) found high bioerosion rates on reefs in the Eastern Pacific

that have naturally high levels of partial pressure of CO_2 (pCO_2) and therefore low pH waters. By having siliceous and not calcareous skeletons, bioeroding sponges are not affected much by changes to the water chemistry that disfavour calcification and therefore decrease erosion activity of other bioeroders such as bivalves or urchins (Fabry *et al.*, 2008), as long as the pH changes are not severe enough to cause direct acidosis of the sponge cells.

In comparison to other reef organisms, bioeroding sponges may only be slightly affected by warming (Márquez *et al.*, 2006; Schönberg *et al.*, 2008; Duckworth and Peterson, 2013; Wisshak *et al.*, 2013; Enochs *et al.*, 2015), and on a number of occasions they have in fact appeared to benefit from warming events that caused widespread coral mortality (Rützler, 2002; Carballo *et al.*, 2013; Chaves-Fonnegra *et al.*, 2017). Temperature effects on sponge bioerosion remain unclear, especially in the absence of long term studies testing the effects of extreme temperatures associated with business-as-usual summer conditions. With regards to chemical bioerosion, warming may act in two contradicting ways: $CaCO_3$ dissolves less readily in warmer waters (Mehrbach *et al.*, 1973; Andersson *et al.*, 2008), but the speed of bioerosion as a biochemical reaction should be positively correlated to temperature, within physiological limits (Atkins and De Paula, 2009).

Bioeroding sponges may preferentially settle on clean, recently dead corals (Marulanda-Gómez *et al.*, 2017), and they erode more rapidly in dead rather than living corals (Le Campion-Alsumard *et al.*, 1995; Schönberg and Wilkinson, 2001). Therefore, increased coral mortality on future reefs may further promote greater rates of bioerosion (Chaves-Fonnegra *et al.*, 2017). Schönberg and Ortiz (2008) have demonstrated an increase in the number of excavating sponges following a large coral mortality event on the central GBR, which had increased the available colonization area. Certain excavating sponges, however, are superior competitors capable of overgrowing living coral as well (Aerts, 1999; Schönberg, 2000), especially as a result of the reduced coral resistance arising from frequent disturbance events. Such events can lead to greater numbers of bioeroders and greater colonization rates given the relatively diminished effect of these same events so far on sheltered endolithic bioeroders (Schönberg and Suwa, 2007).

Being filter feeders, bioeroding sponges may benefit from eutrophication (e.g. Rose and Risk, 1985; Ward-Paige *et al.*, 2005; Fabricius *et al.*, 2005). Organic pollution, which is rich in bacterioplankton, stimulates sponge growth [until the toxicity threshold is met, (Rützler, 2002)]. As early as 1985, Rose and Risk had linked the presence of bioeroding sponges with sewage discharge in the Caribbean, where both their abundance and land-based runoff have

since increased considerably (Chaves-Fonnegra *et al.*, 2007; Mueller *et al.*, 2014). Although there is need for direct experimental evidence of the relation between nutrient loads and sponge bioerosion, field studies have indicated that populations of boring sponges increase on inshore eutrophic reefs. For example, macrobioerosion rates are significantly higher on the GBR inshore region, which receives substantial terrestrial runoff, as compared to offshore oligotrophic reefs (Sammarco *et al.,* 1990; Risk *et al*, 1995; Tribollet and Golubic, 2005).

In conclusion, the limited evidence on the survival and growth of bioeroding sponges under a changing climate suggests that they are likely to be more resilient and hence less affected than corals. Given their advantageous position, it is plausible that sponge bioerosion will increase if current disturbance trends continue. Although competition with macroalgae may control the growth of bioeroding sponges to a certain extent (González-Rivero *et al.*, 2011b, 2016; Chaves-Fonnegra *et al.*, 2011; 2017; Chaves-Fonnegra and Zea, 2011), current evidence suggests that in the extreme case the increase in bioeroding sponges may tip the balance towards net reef dissolution (reviewed by Schönberg *et al.*, 2017b). Evidence has already emerged of increasing abundances of bioeroding sponges on individual perturbed reefs (e.g. Rützler, 2002; López-Victoria and Zea, 2005; Ward-Paige *et al.*, 2005; Schönberg and Ortiz, 2008; Carballo *et al.*, 2013; Kelmo *et al.*, 2013; Wisshak *et al.*, 2014; Ramsby *et al.*, 2017a) and of their potential role in phase shifts towards alternate steady or temporarily reversible states (Norström *et al.*, 2009; González-Rivero *et al.*, 2011a; Bozec *et al.*, 2015; Chaves-Fonnegra *et al.*, 2017). The prediction of increased abundance of bioeroding sponges is in accordance with a more general hypothesis of shifts towards sponge (and algae) dominated reef systems in the Caribbean and elsewhere, with important implications for nutrient cycling on coral reefs (Diaz and Rützler, 2001; Norström *et al.*, 2009; McMurray *et al.*, 2010; Colvard and Edmunds, 2011; Bell *et al.*, 2013; Ruzicka *et al.*, 2013; Villamizar *et al.*, 2014; De Bakker *et al.*, 2017; De Goeij *et al.*, 2017). Recent studies have elucidated that both bottom-up (e.g. supply of dissolved and particulate food sources) and top-down processes (e.g. predation) on coral reefs control such growing sponge abundance, but the relative contribution of these processes remains debatable to date (Lesser, 2006; Trussell *et al.*, 2006; Lesser and Slattery, 2013; Pawlik *et al.*, 2013, 2015a, 2015b; Slattery and Lesser, 2015; De Goeij *et al.*, 2017).

Although a number of bioeroding sponge species are likely to be “winners” on future reefs, this might not be the case for all types of bioeroding sponges. Bioeroding sponges often associate with symbiotic microbial communities (prokaryotic as well as eukaryotic) that can

confer advantages as well as disadvantages to the host sponge, depending on the symbiont type and the environmental conditions in question. A particular example can be found in some of the most aggressive bioeroding sponges that form symbioses with photosynthetic eukaryotic microbes which purportedly contribute to the sponge's metabolism. While such symbioses may benefit from increased CO_2 concentrations, a potentially limiting substrate for photosynthesis (Kübler *et al*., 1999), they might also render the sponges vulnerable to heat stress and increased turbidity/nutrient loads on future reefs. To date, bleaching of *Cliona* spp. has rarely been observed during coral bleaching events, and in some cases sponge abundance actually increased following coral mortality (Zea and Weil, 2003; Márquez *et al.*, 2006; Schönberg and Ortiz, 2008; Chaves-Fonnegra *et al.*, 2017). The first report of a natural bleaching event in *Cliona* sponges comes from the lower Florida Keys in 2015, and even though the sponges were only partially bleached and they recovered (Hill *et al.*, 2016; M. Hill, pers. comm.), more severe bleaching may become more common in the near future if warming persists. Although there is some experimental evidence that the association between *Cliona* sponges and their symbionts is relatively heat-tolerant compared to corals (Schönberg *et al.*, 2008; Schönberg and Suwa, 2007; Schönberg and Wisshak, 2012), generally little is known about heat-stress in sponges and, thus, it remains unclear whether photosymbiotic sponges will share the success of other bioeroding sponges under future warming. Similarly, it remains unclear if the premise that nutrient loads stimulate bioerosion holds for photosymbiotic excavating sponges which depend on high water quality and light conditions suitable for symbiont photosynthesis. Understanding how the stability of sponge-symbiont associations is regulated can be key to predicting the future trajectory of individual bioeroding sponge species.

1.3. Photosymbiotic bioeroding sponges

On coral reefs and other nutrient-poor marine systems, symbiotic interactions between invertebrates and microbes fuel high nutrient cycling and species richness. The partnership of sponges and microbes stems from the Precambrian, and has contributed significantly to the evolutionary success of sponges in aquatic habitats (Wilkinson, 1984; Jackson *et al.,* 2010; Uriz *et al.*, 2012). Marine sponges host diverse and abundant communities of metabolically distinct microbes (Thomas *et al.*, 2016; Webster and Thomas, 2016), and based on the magnitude of these communities, individual species are generally divided into low or high microbial abundance sponges (LMA and HMA respectively). Although commonly used, this dichotomy is controversial and may be better described as a continuum with most species

found on the extreme edges (Gloeckner *et al.*, 2014), while its functional meaning for the sponge holobiont is still under examination (Hill and Sacristán-Soriano, 2017). Whilst LMA sponges contain no more microbes than the surrounding seawater, HMA sponges host communities of 2-4 orders of magnitude more concentrated than the surrounding seawater (Hentschel *et al.*, 2006). LMA sponges have generally increased heterotrophic feeding in comparison to HMA sponges where the symbionts purportedly boost the host metabolism, be it through heterotrophic and/or chemo- or photo-autotrophic contributions of the microbes (Poppell *et al.*, 2013; Pita *et al.*, 2018). The interactions between host and photoautotrophic symbionts, in particular, differ vastly in terms of function across different sponge species (Thacker and Freeman, 2012), even though, in principle, the autotrophic activity of the symbionts would often suffice to cover the metabolism of the entire holobiont (the sum of the microbial communities and the host) (Venn *et al.*, 2008; Usher, 2008). If energy sharing occurs from photosymbiont to host, then the partnership with photosynthetic symbionts provides the host with an additional feeding source, namely the inorganic nitrogen and carbon sources that are relatively inaccessible to animal cells (Freeman and Thacker, 2011; Freeman *et al.*, 2013, 2014). It is through such energy sharing that bioeroding sponges that host dinoflagellates of the genus *Symbiodinium* are hypothesized to attain their competitiveness and fast growth rates on nutrient-poor reefs (e.g. Hill, 1996; Weisz *et al.*, 2010; Schönberg *et al.*, 2017b). These photosymbiotic sponges are commonly regarded as being especially competitive and threatening against live corals compared to their non-photosymbiotic counterparts (Schönberg *et al.*, 2017b).

Although *Symbiodinium* forms symbioses with a variety of hosts such as corals and clams, in the phylum Porifera it appears to preferentially partner with sponges of the Clionaidae family (Schönberg and Loh, 2005; Schönberg and Suwa, 2007; Hill *et al.*, 2011; Hill, 2014). Increases in the magnesium to calcium ratio in seawaters of the past 100 million years may have resulted in calcium becoming a limiting factor, thereby driving *Symbiodinium* (that requires calcium for its photochemistry) to invade hosts capable of regulating calcium availability, and hence clionaid sponges (magnesium inhibition hypothesis, Hill and Hill, 2012). Potentially clionaids are a preferred habitat for *Symbiodinium* because they increase the local availability of calcium ions (Ca^{2+}) either in the immediate seawater microenvironment or, even stronger so, inside the sponge body due to Ca^{2+} uptake through cellular transporters (as hypothesized in Fig.1.1a). Ca^{2+} concentration was elevated deep inside the body for a clionaid sponge in comparison to a non-clionaid sponge (Schönberg, 2008). It has been suggested that after invasion, *Symbiodinium* persisted evolutionary in the

host by maintaining a steady excretion of photosynthates, thereby mimicking phagosomal digestion and avoiding detection by the host (Hill and Hill, 2012).

A handful of studies have shown that bioeroding sponges that host *Symbiodinium* erode faster when exposed to sunlight (Rosell and Uriz, 1992; Hill, 1996; Schönberg, 2006) and that decreases in light availability affect the holobiont negatively (Pineda *et al.*, 2016, 2017a, 2017b), but the mechanism behind such observations remains elusive. In such bioeroding sponges, one may ponder on the intriguing possibility that photosynthetic products may stimulate bioerosion. First of all, this possibility conceptually contrasts with the fact that on coral reefs photosynthates and oxygen supply mitochondria to generate ATP that then drives the opposite process, namely calcification by corals that host *Symbiodinium* (Gattuso *et al.*, 1999; Muscatine, 1990; Colombo-Pallotta *et al.*, 2010). The paradigm of *Symbiodinium*-stimulated calcification is both well-established and compatible with biogeochemical principles: although several membranes away from the site of calcification, oxygenic photosynthesis effectively consumes protons, setting up the appropriate proton gradient that allows protons pumped into the calicoblastic layer to flow to the coelom. This gradient changes the thermodynamic balance of calcium carbonate dissolution-precipitation in the calcifying fluid towards mineral precipitation and not dissolution (see Allemand *et al.*, 2004, 2011 for reviews of the process). Concurrent photosynthesis and calcification may even be physiologically beneficial to photosynthetic organisms (McConnaughey and Whelan, 1997). In contrast, decalcification would be disfavoured when photosynthesis is active, unless the two processes do not occur simultaneously, are not co-localized or are linked in a non-chemical way (Garcia-Pichel, 2006). The existence and the nature of a link between sponge bioerosion and photosynthesis of resident symbionts is not well documented and deserves further attention, especially when considered in the context of ocean warming and its impact on the fundamental principles of photosymbioses.

1.4. Introduction to study species: *Cliona orientalis*

The "*Cliona viridis* species complex" consists of bioeroding sponges that are symbiotic with dinoflagellates of the genus *Symbiodinium*. These sponges provide a useful experimental platform to study not only the mechanistic details of bioerosion, but also the dynamics of the interaction between photosynthesis and bioerosion under present as well as future conditions. In the Indo-Pacific region, *Cliona orientalis* Thiele, 1900 consists a particularly abundant representative of the "*Cliona viridis* species complex". *C. orientalis* has been reported from parts of the Coral Triangle, Indian Ocean, West and East coast of Australia, East Asia, as well

as the Red Sea and South African coast (Fang, 2013 and references therein). It is the most common bioeroding sponge of the inshore Great Barrier Reef (Schönberg and Ortiz, 2008), while its occurrence is currently also notable on the offshore GBR, eroding at a rate of approx. 2.5 kg $CaCO_3$ m^{-2} yr^{-1} (Fang *et al.*, 2013a). *C. orientalis* is potentially a solar-powered bioeroding sponge, meaning that it must rely on high water clarity. Therefore, it is not expected to be more abundant inshore than offshore, unless it occupies shallower water inshore than offshore, or it shifts towards a more heterotrophic diet. Interestingly, the abundance of *Cliona orientalis* increased by more than twofold from 1998 to 2004 at one inshore location in the central GBR (Schönberg and Ortiz, 2008). However, more recent surveys of a broader inshore region from 2005-2014 show that increases in the abundance of the sponge are site-specific and depend on local environmental conditions such as fine sediments (negative relationship), competition for space with macroalgae (negative relationship), and dissolved nutrients (chlorophyll a, positive relationship, but only as long as macroalgal growth remains nutrient-limited) (Ramsby *et al.*, 2017a).

Like other bioeroding sponges, *Cliona orientalis* may preferentially settle on clean, recently dead corals (Marulanda-Gómez *et al.*, 2017), yet it is capable of intensively eroding a range of calcium carbonate substrates of varying porosity and density (Schönberg, 2002; Schönberg and Shields, 2008) (Fig.1.2). Colonies of *C. orientalis* are often found eroding massive *Porites* corals on the GBR (Fig. 1.3a), but it can also infest the $CaCO_3$ deposited by corals of diverse genera such as *Acropora*, *Astreopora*, *Cyphastrea*, *Favia*, *Favites*, *Goniastrea*, *Goniopora*, *Lobophyllia* and *Montastrea* (Schönberg and Wilkinson, 2001; Schönberg, 2002; 2003; Holmes *et al.*, 2009). The sponge erodes both live and dead corals, although it most readily infests dead corals (Fang *et al.*, 2016a). The bioerosion rates of the sponge increase in dense solidified material where proportionately more $CaCO_3$ needs to be actively removed in order to create pores and openings that the sponge can then grow into (Schönberg, 2002). Colonies of *C. orientalis* reach several square metres in surface area at over 1 cm of substrate penetration (Schönberg, 2000).

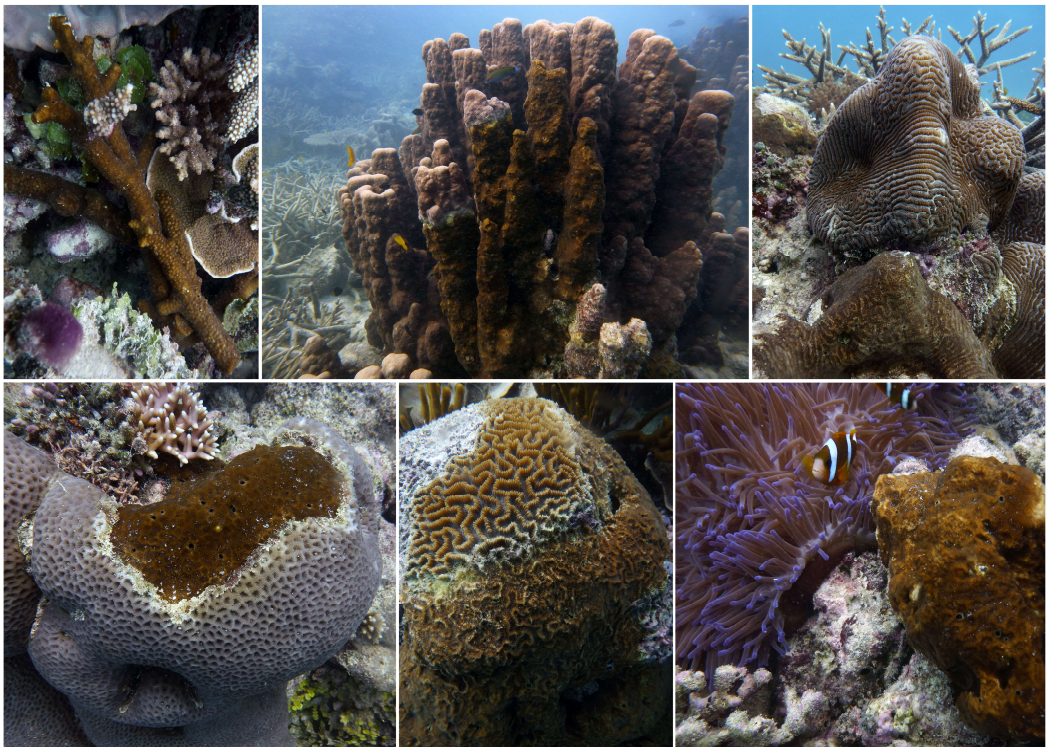

Figure 1.2: The photosymbiotic bioeroding sponge *Cliona orientalis* from the Great Barrier Reef, Australia, eroding various different branching, tubular and massive coral forms (photos taken on a single dive in 2016 on Wistari Reef, Capricorn-Bunker reefs).

The abundance and high erosion rates of *C. orientalis* on the GBR, its symbiosis with *Symbiodinium,* as well as the apparent disparity between its suitability for offshore habitats and its frequent inshore occurrence, make this sponge an interesting study species for the current thesis. A series of tools and experimental methods developed by previous studies demonstrated the species suitability for experimental work (e.g. Schönberg, 2006; Wisshak *et al.*, 2012; Fang *et al.*, 2013a; 2013b, 2014) and enabled further exploration of key mechanisms in the sponge. Over the past 3 years, this sponge has also been used in a number of other studies (discussed throughout the thesis) that have increased our understanding of the physiology of bioeroding sponges (e.g. Fang *et al.*, 2016b, 2017; Strehlow *et al.*, 2016; Pineda *et al.*, 2017a; 2017b). Yet in comparison to other coral reef invertebrates, *C. orientalis* remains a relatively understudied species, especially at the microscopic level. A number of studies have described ultrastructural aspects of the excavation or reproduction of various *Cliona* sponges (Rützler and Rieger, 1973; Pomponi, 1979a, 1979b, 1979c, 1980; Hatch, 1980; Rosell, 1993; Mariani *et al.*, 2000). Similar descriptions of *Cliona orientalis* have focused so far on skeletal structures such as spicule morphology for taxonomic reasons (Schönberg, 2000). Prior to considering physiological experiments, a brief description of the

ultrastructure of our study species was necessary, and it further enabled the use of a wider range of tools when addressing key questions.

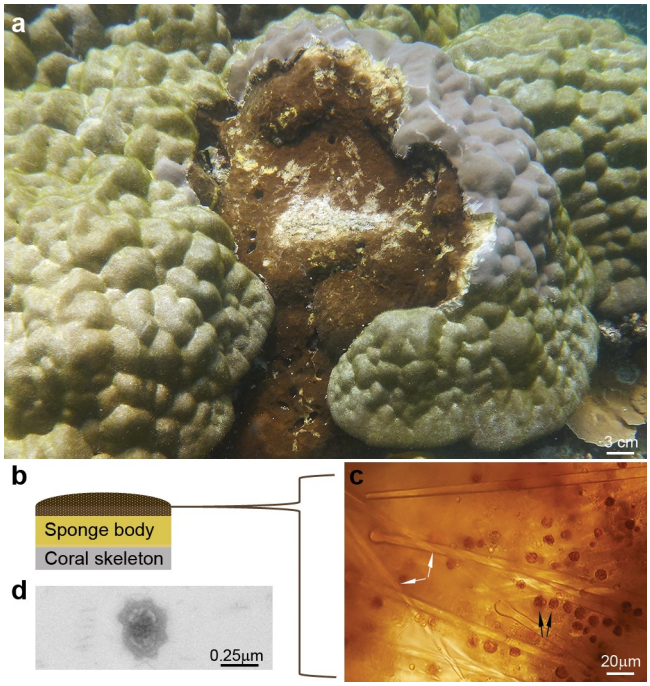

Figure 1.3: The photosymbiotic bioeroding sponge *Cliona orientalis* from the Great Barrier Reef, Australia and its functional tissue layers. **(a)** *C. orientalis* (brown patch) eroding a massive *Porites lobata* colony on Heron Reef. **(b)** Diagram depicting a cross section of the sponge, revealing the different functional layers. The outer sponge layer (brown) hosts dinoflagellates of the genus *Symbiodinium*, while the underlying layer where light does not reach consists of sponge material with very few dinoflagellates (ochre yellow). The lowest layer (grey) consists of coral skeleton that is not yet infested by the sponge. **(c)** The dinoflagellate-rich sponge layer (pinaco-derm, black arrows point at individual dinoflagellates) as seen under the light microscope (×400 magnification). The sponge also secretes its own inorganic skeleton made of siliceous spicules (tylostyles, white arrows). **(d)** TEM image of an unidentified bacterium sparsely found in the mesohyl of the outer layer of *C. orientalis*.

The body mass of *Cliona orientalis* is typically divided into two relatively distinct layers (Fig. 1.3b). The outer brown layer hosts the majority of the symbiotic dinoflagellates, and the underlying ochre-yellow layer which is not exposed to light is relatively void of dinoflagellates. In other words, similar to scleractinian corals, most *Symbiodinium* are found in the body wall that faces the ocean, not the body wall that faces the skeleton. Both layers are solid and hard as the sponge biomass is finely intertwined inside the $CaCO_3$ substrate. A closer look using light and transmission electron microscopy (applying methodology described in Chapter 3) confirmed that these two functional layers are distinct in their cellular composition (Fig. 1.4). Although both layers appear low in bacterial abundance, the outer

layer harbours dense accumulations of *Symbiodinium* cells which are hosted (often in duplicate) inside archaeocyte-like sponge cells (Fig. 1.3c and 1.4a,b). When dinoflagellates were first found in *Cliona* spp. they were reported to be "embedded in an extracellular manner in the sponge parenchyma and more densely near the surface of the sponge" (Sara and Liaci, 1964), but their intracellular positioning is in agreement with a number of more recent observations (Rützler, 1974; Vacelet, 1981; Vicente, 1990; Rosell, 1993; Mariani *et al.*, 2000). The underlying sponge layer is home to an elaborate network of aquiferous canals that circulate water through the body for respiration and heterotrophy (Fig. 1.4c,d). Specialized filter-feeding cells (or choanocytes) equipped with beating flagella line these canals and form choanocyte chambers that are the main uptake point of particulate and probably also dissolved organic material (Hill and Sacristán-Soriano, 2017). Throughout both layers, the abundance of microbial symbionts other than *Symbiodinium* appears to be low [like *C. varians*, (Poppell *et al.*, 2013)] (Fig. 1.3d). Recent analysis has demonstrated that this sparse prokaryotic community consists mainly of alpha, delta and gamma-proteobacteria, with a minor representation of cyanobacteria (Pineda *et al.*, 2016; Ramsby *et al.*, 2018). While this prokaryotic community is metabolically highly diverse and purportedly includes nitrogen fixers as well as microbes that can use a variety of carbon sources (Bryant and Frigaard, 2006), their function inside the present holobiont has yet to be explored. A single *Rhodothalassium*-like alphaproteobacterium dominates the prokaryotic microbiome of *C. orientalis* and has the potential to photosynthesize, oxidize sulphur and fix nitrogen (Ramsby *et al.*, 2018).

The band of *Symbiodinium* cells inside the sponge body is diurnally dynamic rather than stable: chlorophyll fluorescence measurements suggest that by day most of the *Symbiodinium* population is found in the uppermost sunlit layer of the sponge, whereas by night the symbionts are translocated to deeper tissues purportedly by means of host cell migration (Schönberg and Suwa, 2007). Sponges are known to have highly plastic tissues where cell migration is frequent (Gaino *et al*., 1995). In the present case, cell migration serves to maximize photosynthetic output during the day and to prevent loss of symbionts to predation by other reef organisms during the night, while it can also serve as a protective response to light or heat stress (Schönberg and Suwa, 2007). *Symbiodinium* found in *C. orientalis* belong

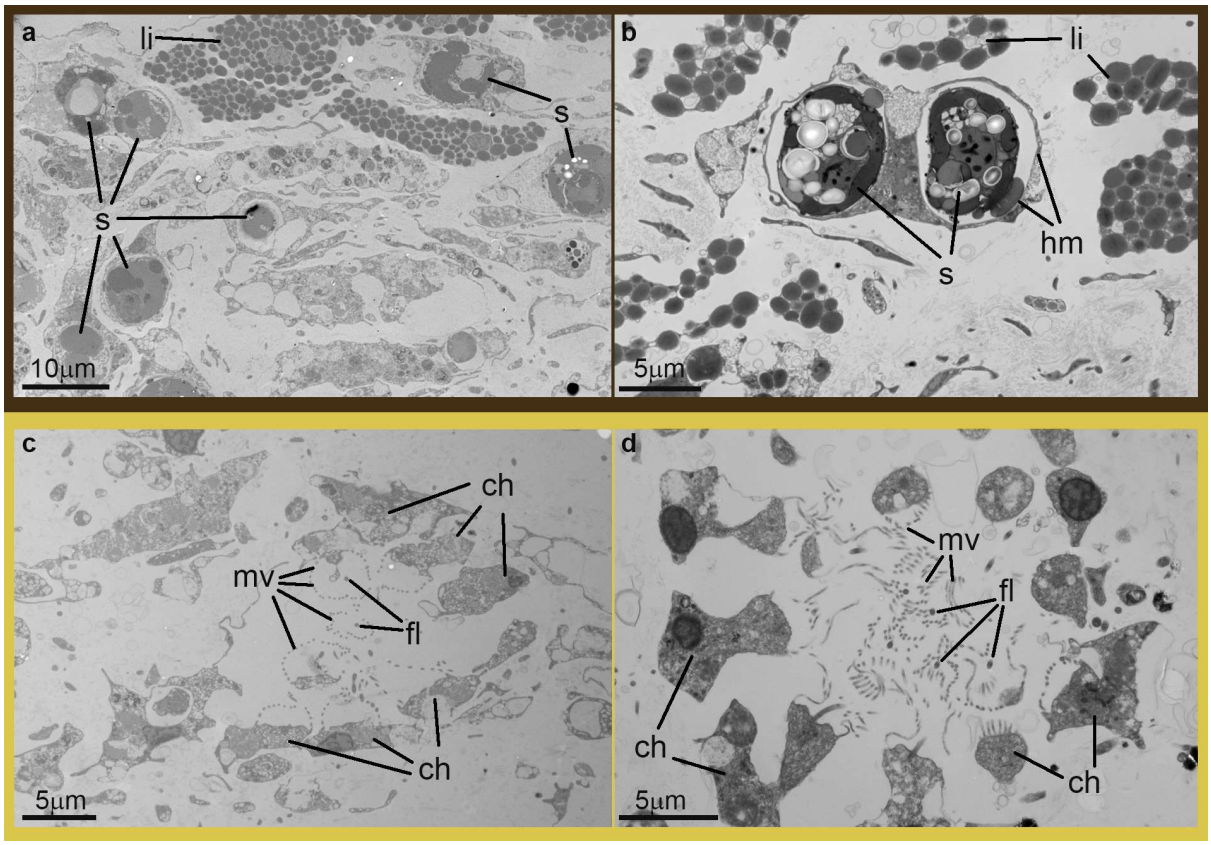

Figure 1.4: Transmission electron micrographs of the outer and inner sponge layers of the photosymbiotic bioeroding sponge *Cliona orientalis.* **(a)** and **(b)** Overview and further magnification respectively of the outer sponge layer illustrating a number of intracellular *Symbiodinium* cells (s) surrounded by the membrane of the archaeocyte-like sponge cells that host them (hm). Note the dense lipid accumulations (li). **(c)** and **(d)** Overview and further magnification of the inner sponge layer illustrating individual filter-feeding cells or choanocytes (ch) forming choanocyte chambers. The flagella (fl) and the collars of microvilli (mv) through which water is filtered to retain nutrients are visible in cross-section. The colours of the image borders correspond to the functional layers depicted in Fig. 1.3b.

to clade G (Schönberg and Loh, 2005; Hill *et al.*, 2011), and within that clade the species *Symbiodinium endoclionum* sp. nov. obtained from *C. orientalis* from the northern GBR and the Japanese island of Okinawa has been recently described (Ramsby *et al.*, 2017b). Interestingly, the same study identified divergent *Symbiodinium* sequences in sponge specimens from the southern GBR (Heron Island in particular, based on sequencing of nuclear large-subunit ribosomal DNA, chloroplast large-subunit rDNA, mitochondrial cytochrome *b* gene, and the photosystem II protein D1), which suggests the presence of a different species that remains to be characterized (Ramsby *et al.*, 2017b).

Cliona orientalis and its bioeroding efficiency under changed climatic conditions have been addressed in a few studies on the Great Barrier Reef: Short-term experiments have demonstrated that ocean acidification accelerates bioerosion by *C. orientalis*; erosion rates in

dead coral were increased by 61% under 1410 µatm pCO_2 over a 10-day experimental period (Wisshak *et al.*, 2012), but the effects of temperature stress remain inconclusive (Wisshak *et al.*, 2013). Short experimental periods however require acute acclimation, which often impairs the physiology of the organism and does not allow distinction of studied-parameter effects from stress effects. In a longer-term experiment, Fang *et al.* (2013a) showed that bioerosion rates and biomass of *C. orientalis* increased under a combined elevation of pCO_2 and temperature that simulated future spring conditions, even though the sponge expelled its symbiotic dinoflagellates. However, the negative energy budget of the sponge (based on a carbon balance model and obtained for a single day at the end of the experiment) implies that this might be a transitional effect and that over the height of future summers the sponge will not be able to sustain its metabolism. Future bioerosion is likely to depend on the sponge's ability to survive (whether bleached or unbleached), which has yet to be tested.

1.5. Rationale, aims and structure of the thesis

The recent pantropical warming event during the 2015-2016 El Niño led to extreme bleaching and subsequent mortality of corals on the Great Barrier Reef, especially in the northern 1000-km-long section (Hughes *et al.*, 2017b). In 2016, the northern GBR experienced heat stress of more than 8 degree heating weeks (peaking at 16 DHW) over approximately 3 months (DHW, °C-weeks; significant coral bleaching is likely when DHW>4°C-weeks, and widespread bleaching and mortality occur at DHW>8°C-weeks; NOAA Coral Reef Watch, 5 km satellite data). Re-occurring coral bleaching in the coming decades is extremely likely according to climate projections, since a) the frequency and intensity of El Niño events is expected to increase (Cai *et al.*, 2014) and b) as global warming progresses, summer temperature thresholds for bleaching are increasingly exceeded throughout non-El Niño phases (Hughes *et al.*, 2018). As coral are declining, there is clearly a need for a more precise understanding of the response of bioeroding sponges to anthropogenic influences, and especially for the response of photosymbiotic bioeroding sponges to warming. This understanding first requires an improved comprehension of sponge and symbiont physiology as well as the capacity for erosion under changed conditions. However, currently the fundamental knowledge that will allow such projections into the future is lacking.

This thesis aims to explore the influence of photosynthesis on the metabolic and bioerosion dynamics of photosymbiotic excavating sponges, and to evaluate the resilience of

photosymbiotic excavating sponges to future environmental conditions, using *Cliona orientalis* from the reefs of Heron Island on the southern Great Barrier Reef. Heron Island is an outer-shelf coral cay in the Tropic of Capricorn at the Southern end of the GBR and is situated on the Western end of a platform reef approximately 70 km off the mainland. It has been the site of the Heron Island Research Station since the 1950s, enabling the development of key facilities that have supported a range of invaluable research projects over the years. In recent years a vast amount of knowledge on the response of individual organisms as well as marine communities to well-defined scenarios of climate change has been gained from research on the island. The island allows for a combination of reef flat as well as open ocean research that enables comparison of contrasting regimes and application of research outputs to a broader range of habitats characteristic of the wider GBR. In addition, the island's offshore waters offer an ideal environment to undertake experimental studies, since they are relatively untouched by terrigenous inputs by comparison to inshore reefs (Rasheed *et al.*, 2004; Page and Willis, 2006), enabling manipulation of stress parameters and comparison against pristine control conditions.

In particular, this thesis explores the following main questions:

- **Chapter 2:** How does the symbiosis between the sponge and its photosynthetic symbionts (*Symbiodinium*) influence its bioerosion capacity?

Bioerosion by photosymbiotic excavating sponges has previously been demonstrated to increase under the influence of light. Photosynthesis is thought to be the driving mechanism of this response, as suggested by experiments that manipulated the light levels that the sponges are grown under. Such approaches however do not rule out the possibility that other physiological changes that are related to light levels or diurnal cycles may be driving the response. In the first experimental chapter, bioerosion activity is explored in response to photosynthesis as a manipulative factor. The bioerosion rates of bleached (relatively free of symbionts), photosynthetically inactivated (treated with diuron) and control sponges are compared at light (day-time) and at dark (night-time).

- **Chapter 3:** Which members of the holobiont (symbionts or host) play a key role in the uptake of inorganic nutrients during photosynthesis in the outer sponge body?

Building on the results and conclusions of the previous chapter, Chapter 3 takes a closer look at the photosynthetic (outer) sponge body in the light. While inorganic carbon uptake in *C. orientalis* is usually attributed to the resident dinoflagellates, there may be other autotrophic symbionts that play a part; likewise for inorganic nitrogen uptake, which could potentially

also be carried out by host cells. In this chapter, the recent integration of isotopic labelling, transmission electron microscopy and nanoscale secondary ion mass spectrometry is exercised to explore inorganic nutrient uptake (bicarbonate and ammonium) at the cellular level in the outer body of the intact *C. orientalis* holobiont.

- **Chapter 4:** How tolerant is the sponge to bleaching under ocean warming, with and without the influence of ocean acidification and eutrophication?

Once an insight into the symbiosis between the components of the *C. orientalis* holobiont is obtained, the final experimental chapter exposes the symbiosis to future Austral summer reef conditions. The tolerance of the sponge to end-of-century ocean temperature and acidity levels is examined by simulating summer conditions as predicted by the business-as-usual emissions scenario of the Intergovernmental Panel on Climate Change (IPCC, 2013, 2014). Both the independent and concurrent effects of warming and acidification are explored. Using a unique mesocosm system, the effects of climate change are built on a diurnally and seasonally variable non-El Niño baseline rather than as flat-lined offsets (Dove *et al*., 2013). Diet supplementation with particulate organics (simulating an outcome of eutrophication) is also included in the experimental design to examine whether a boost in heterotrophic feeding can ameliorate effects of the climate stressors. Addressing warming and acidification effects both in isolation as well as concurrently allows realistic simulation of joint impacts (as will be the case in future waters) while still unravelling the physiological impact of each factor (Crain *et al.*, 2008; Wernberg *et al.*, 2012).

- **Chapter 5:** In the final chapter of the thesis, the results from the three experimental chapters are synthesized into a broader discussion and directions for future research are suggested.

All in all, the current thesis explores bioerosion by *C. orientalis* moving stepwise from the micro-level of ultrastructural observations and holobiont metabolics to the macro-level of ecological functioning under climate change. The symbiosis of sponge and dinoflagellate is addressed as a whole but also broken down into the individual physiologies of the two partners. Structurally, a number of basic questions will first be addressed (Chapter 2), whereupon a set of more in-depth questions is built (Chapter 3), focusing always on the interplay of symbiont photosynthesis and sponge metabolism. These answers then feed into the second set of questions where the gained understanding is tested under future reef conditions (Chapter 4). Although each experimental chapter deals with a distinct set of

questions, one could visualize a common conceptual thread running through the thesis as follows:

Chapter 1 (Thesis Introduction)	Despite a growing body of knowledge on bioeroding sponges, a number of crucial questions remain unanswered before the success of photosymbiotic bioeroding sponges on future reefs can be evaluated.
Chapter 2	In particular, does photosynthesis affect bioerosion and, if so, through what mechanism? Is the link energetically driven?
Chapter 3	If yes, then which holobiont components are responsible for harvesting that photosynthetic energy?
Chapter 4	Finally, how does long-term loss of photosynthesis (bleaching due to thermal stress) influence the holobiont's physiology? Do increased acidity and heterotrophy ameliorate the negative effects of thermal stress?
Chapter 5 (General Discussion)	All in all, maintaining the symbiosis between sponge and *Symbiodinium* intact is fundamental to the well-being and survival of photosymbiotic bioeroding sponges on future reefs.

Chapter 2

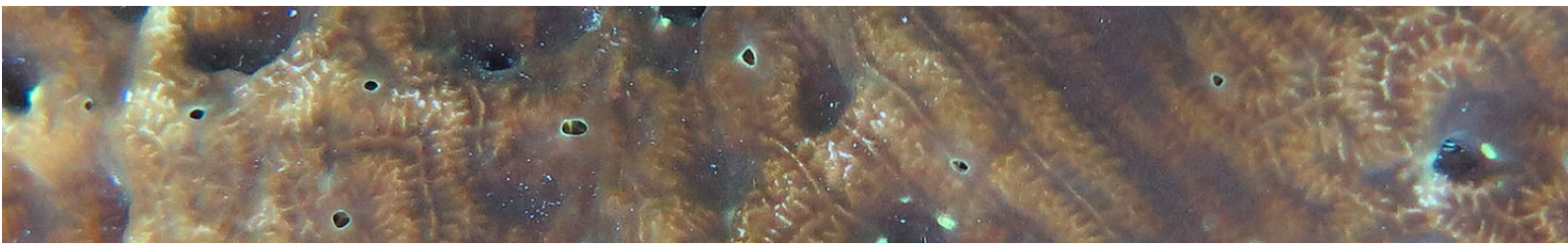

Linking photosynthesis by symbiotic sponges
to enhanced bioerosion

Abstract

Photosynthesis is an important driver of calcium carbonate deposition on tropical coral reefs due to the symbiosis of numerous invertebrates with photosynthetic dinoflagellates of the genus *Symbiodinium.* In bioeroding sponges, however, the same symbiosis appears to support the decalcification of carbonate substrates. The interplay of photosynthesis and decalcification is far less well-studied than that with calcification. Here, the daytime and night-time chemical bioerosion rates of the Indo-Pacific sponge *Cliona orientalis* were examined under varying levels of photosynthetic activity and/or varying abundances of intracellular *Symbiodinium.* Photosynthesis was manipulated either by treating the sponges with the photosynthetic inhibitor diuron (DCMU), or by exposing them to short-term heat stress to achieve bleaching. DCMU resulted in reduced numbers of *Symbiodinium* which lost most of their ability to evolve oxygen. Heat stress, on the other hand, resulted in sponges with far fewer *Symbiodinium* yet with less inhibition of photosynthesis. In both cases, decreases in photosynthetic activity of the symbionts led to proportionately lowered daytime chemical bioerosion rates, stressing the significance of functional symbionts for effective erosion by the sponge. Importantly, increased rates of night-time bioerosion were linked to greater daytime rates of photosynthesis, rather than to the night-time respiration of the sponge holobiont. This study provides strong evidence in support of the model in which photosynthetic products (photosynthates) and/or by-products (oxygen) stimulate bioerosion by the sponge and, thus, this symbiosis appears to be a successful adaptation for thriving in nutrient-poor ecosystems.

2.1. Introduction

Tropical coral reefs thrive in shallow clear waters where sunlight powers productive and diverse food chains. Symbioses between a variety of photosynthetic microorganisms and invertebrates enable high rates of productivity on reefs despite low environmental concentrations of inorganic nutrients (Seckbach, 2004). The evolutionary success that results from hosting phototrophic microbes such as dinoflagellates, diatoms, chlorophytes, rhodophytes, or cyanobacteria is seen in a wide range of invertebrates belonging to taxa as diverse as Cnidaria, Mollusca, Foraminifera, Platyhelminthes, and Porifera (Stat *et al.*, 2006; Lipps and Stanley, 2016).

Presently almost 200 sponge species (Porifera) are known to host microbial photosynthetic symbionts (Schönberg, unpubl. data), which may contribute to the nutrition and health of the

sponge (Wilkinson, 1987; Erwin and Thacker, 2008; Hill *et al.*, 2011; Thacker and Freeman, 2012). Sponge species that receive substantial contributions in this way are often termed "photosymbiotic", or "mixotrophic" given that they also depend on filter-feeding by specialized food-trapping sponge cells. The nutrition of sponges is often further supplemented by inputs from intimate microbial associations formed with heterotrophic bacterial populations of varying density and diversity (high and low microbial abundance sponges) (Hentschel *et al.*, 2003; Taylor *et al.*, 2007).

By far most sponge-inhabiting photosymbionts have been identified as cyanobacteria (Erwin and Thacker, 2007; Diaz *et al.*, 2007; Simister *et al.*, 2012), but many bioeroding sponges of the family Clionaidae stand out by their symbiosis with photosynthetic dinoflagellates of the genus *Symbiodinium*. Invertebrates that host *Symbiodinium* are generally associated with deposition of calcium carbonate ($CaCO_3$) and reef growth, and are exemplified by reef-building corals (Trench et al., 1981; Allemand *et al.*, 2011; Al-Horani, 2016). In contrast, bioeroding sponges inhabit and excavate $CaCO_3$ substrates by manipulating acidity to chemically dissolve calcareous frameworks and to cut out small $CaCO_3$ chips that are then removed mechanically (Pomponi, 1980; Zundelevich *et al.*, 2007). Not all bioeroding sponges host *Symbiodinium*, yet the *Symbiodinium*-hosting "*Cliona viridis* species complex" is one of the groups producing the highest macrobioerosion rates globally, accounting for large fractions of bioerosion of the calcareous frameworks of coral reefs often reaching over 10 kg per metre sponge area and year (Schönberg *et al.*, 2017b). Their remarkable excavating capacity and competitive vigour is commonly attributed to energetic inputs provided by a dense intracellular *Symbiodinium* population (Vacelet, 1981; Rützler, 1990; Weisz *et al.*, 2010; Schönberg *et al.*, 2017b).

Bioeroding sponges predominantly settle on and invade barren calcareous materials, with some species actively competing with coral tissue by laterally displacing or endolithically undermining and occasionally killing polyps (López-Victoria *et al.*, 2006; Chaves-Fonnegra and Zea, 2007). Once established, the photosymbiotic bioeroding sponges expand over the surface of the coral skeleton to harvest light (Glynn, 1997; Schönberg, 2000). Shading experiments have shown that light enhances growth and bioerosion rates of such sponges (Rosell and Uriz, 1992; Hill, 1996; Schönberg, 2006; Pineda *et al.*, 2016), but studies directly addressing the relation between photosynthesis and erosion on a diurnal basis that respects endogenous circadian rythms are lacking. Paradoxically, light-driven oxygenic photosynthesis by their symbionts could potentially increase the local pH due to CO_2 uptake,

making dissolution of $CaCO_3$ less favourable (Garcia-Pichel, 2006). Both temporal and spatial separation of photosynthesis and other competing processes (e.g. N_2 fixation, $CaCO_3$ dissolution) is exhibited in some organisms such as cyanobacteria (Stal and Krumbein, 1987; Berman-Frank *et al*., 2001; Garcia-Pichel, 2006). Interestingly, in bioeroding sponges, photosynthesis and enhanced dissolution take place simultaneously (Fang *et al.*, 2016), suggesting that a model based on temporal separation of the two processes is unlikely. Instead, in bioeroding sponges, the coexistence of photosynthesis and significant $CaCO_3$ dissolution may be made possible, to a certain extent, by the spatial rather than temporal separation of the two processes: the tight insertion of the thin cellular extensions into the etching fissures creates a chemically controllable microenvironment which is void of *Symbiodinium* cells (Rützler and Rieger, 1973; Pomponi, 1980; Schönberg *et al.*, 2017b). Furthermore, in such sponges, most of the *Symbiodinium* population migrates to the surface layer of the sponge by day, and only very few cells remain near the deeper endolithic cell front where bioerosion takes place (Schönberg and Suwa, 2007; M. Achlatis, pers. obs.). There is mounting evidence that keeping the symbiosis between sponge and photosymbionts intact is crucial to the overall health and excavation capacity of photosymbiotic sponges (Fang *et al.*, 2014). However, it remains unclear which exact process powers higher chemical sponge bioerosion in photosymbiotic sponges: a) photosynthesis of the symbiont, supplying carbon-rich photosynthetic compounds and/or an oxygenated environment to drive sponge mitochondria, and/or b) respiration of the symbiont, providing a more acidified environment through net CO_2 production alongside host respiration.

The present study explores bioerosion by the sponge *Cliona orientalis* Thiele, 1900 in response to manipulating the population density of *Symbiodinium* cells and their photosynthetic activity. *C. orientalis* is a strong bioeroder and an effective competitor for space, with a key role in material cycling within coral reef environments (Schönberg and Wilkinson, 2001; Schönberg, 2002). It belongs to the "*Cliona viridis* species complex" and is abundant in the Indo-Pacific and especially on the Great Barrier Reef (Schönberg, 2001; Schönberg and Ortiz, 2008; Ramsby *et al.*, 2017a). To date only G Clade *Symbiodinium* (and no subclades) have been found in *C. orientalis*, suggesting a tight and obligate relationship (Schönberg and Loh, 2005; Schönberg *et al.*, 2005; Hill *et al.*, 2011; Pochon *et al.*, 2014; Ramsby *et al.*, 2017b). The species *S. endoclionum* was recently described in *C. orientalis* from Japan and the central but not southern Great Barrier Reef where possibly a different sibling species of Clade G exists (Ramsby *et al.*, 2017b). After a pilot study determined the treatment conditions used to control photosynthetic activity of the symbionts (described in the

Supplementary Material in the Appendix[1]), the rate of chemical bioerosion by sponges with varying levels of photosynthetic activity and/or *Symbiodinium* abundance were compared in the light (by day) and in the dark (by night). Photosynthetic inhibition and/or reduction of symbiont populations of the sponges was achieved in two ways: a) exposure to the herbicide/algaecide diuron [N'-(3,4-dichlorophenyl)-N,N-dimethylurea or DCMU, the use of which has not been previously reported in sponge-*Symbiodinium* associations] that reversibly binds to the D1 protein of photosystem II (PSII) blocking the electron transport between Q_A^- and the PQ pool (Krause and Weis, 1991), but without directly affecting the host (e.g. Negri *et al.*, 2005; Watanabe *et al.*, 2006; Cantin *et al.*, 2007), and b) exposure to elevated seawater temperature that triggered symbiont loss (as shown in Chapter 4).

We hypothesized that if the symbiont fuels photosynthetic (by)products into bioerosion, then bioerosion rates should be boosted during the day in control sponges. Alternatively, the sponges may store the translocated photosynthetic (by)products and utilize them to erode at night, when pH conditions are more favourable for $CaCO_3$ dissolution due to CO_2 produced by host respiration, and by respiration of the symbionts that now reside slightly deeper in the tissue. We also hypothesized that the reduction in O_2 evolved (CO_2 fixed) by the symbionts in the treated sponges would translate to a loss of bioerosion potential. In particular, we expected that the DCMU treatment would have a relatively greater negative impact on bioerosion by day than by night (relative to control), despite potential adverse effects of DCMU on night-time CO_2 production (chlororespiration) by the symbionts. On the other hand, we expected that the loss of symbionts due to elevated temperature would drive a reduction in the rate of erosion via reduced photosynthetic contributions from the few remaining symbionts by day and potentially via reduced respiratory CO_2 contributions by night.

2.2. Materials and Methods

Sponge collection

Laboratory experiments were done using the bioeroding sponge *Cliona orientalis* Thiele, 1900 collected from the reefs associated with Heron Island on the southern Great Barrier Reef. Encrusting "beta" morphology sponges (Schönberg *et al.*, 2017a) inhabiting dead coral substrates (massive corals) were sampled by SCUBA diving at 5-8 m depth at "Harry's

[1] All Supplementary text, figures (Fig. S…) and tables (Table S…) can be found in the Appendix at the end of the thesis

Bommie" (151.9357°E, 23.4675°S) in January 2015. Standardized cylinders of 15 mm height were produced, containing sponge-penetrated substrate plus an underlying ca. 3 mm thin disc of non-infested $CaCO_3$. The cylinders were cored out of three different sponges using a pneumatic drill with a hole-saw of 35 mm diameter. The species identity was later confirmed by examination of the spicules of the collected sponges (Schönberg, 2000). The bulk density of the sponge-free $CaCO_3$ substrate inhabited by the three sponges was 1.52±0.05 g cm^{-3}, and the porosity was 30.85±2.08% (mean±SEM of 4 substrate cores per sponge). The experimental cores were kept in outdoor aquaria (40L) receiving flow-through seawater and being shaded initially with neutral density shade cloths (~70% light reduction). The shade cloth was later replaced by Marine Blue 131 light filters that mimic the typical light quality and quantity of the collection depth (~40% light reduction, Lee Filters, Andover, UK; Sampayo *et al.*, 2016). Two weeks of healing and acclimation were allowed before the onset of the treatment phase.

Treatment phase

In the treatment phase, 24 sponge cores (8 from each sponge genotype) were labelled and randomly assigned to one of three conditions (per treatment n=2 tanks x 4 cores, Fig. 2.1a):

(a) Exposure to a saturating concentration of DCMU in a closed water system (100µg/L; Falkowski and Raven, 2007; Parrin *et al.*, 2017).
(b) Exposure to elevated temperature in a flow-through regime [peak of +3.1°C above the local maximum monthly mean (MMM; 50-km pixel satellite data, available at http://coralreefwatch.noaa.gov)].
(c) Control conditions in an ambient temperature flow-through regime without DCMU.

All treatments ran over 9 days from the 12th to 21st of February 2015 (Fig. 2.1b, see Table 2.1a for a summary of seawater conditions). All seawater used was filtered through a 10 µm sand filter, thus still containing the main fraction of sponge's common diets (Lynch and Phlips, 2000; Maldonado *et al.*, 2012; Mueller *et al.*, 2014). Duplicate chambers/aquaria were used for every treatment (to lessen the amount of DCMU contamination managed at the offshore site), containing 4 sponge cores each, resulting in n=8 sponges per treatment (as explained in the 'Statistical analysis' section below; Tolosa *et al.*, 2011; Tremblay *et al.*, 2016).

The concentration of DCMU to be used was established in a pilot study done in August 2014 (described in the Supplementary Material in the Appendix). DCMU-treated sponges were

kept in independent 3L chambers that were equipped with a small wave maker and were partially submerged in 40L aquaria for temperature regulation to simulate ambient conditions. To ensure nutrient replenishment, the water of these chambers was changed every morning without exposing the sponges to air, and DCMU dissolved in ethanol was added daily (stock solution of 4.2 mg DCMU in 2.5 ml ethanol, final DCMU concentration 100µg/L) (Negri *et al.*, 2005; Underwood *et al.*, 2006; Suggett *et al.*, 2011). The small quantity of ethanol added did not influence the sponges (Supplementary Material in the Appendix). Despite water replenishment, the pH in the DCMU chambers was lower than in the two flow-through treatments due to build-up of respiratory CO_2 (Table 2.1a).

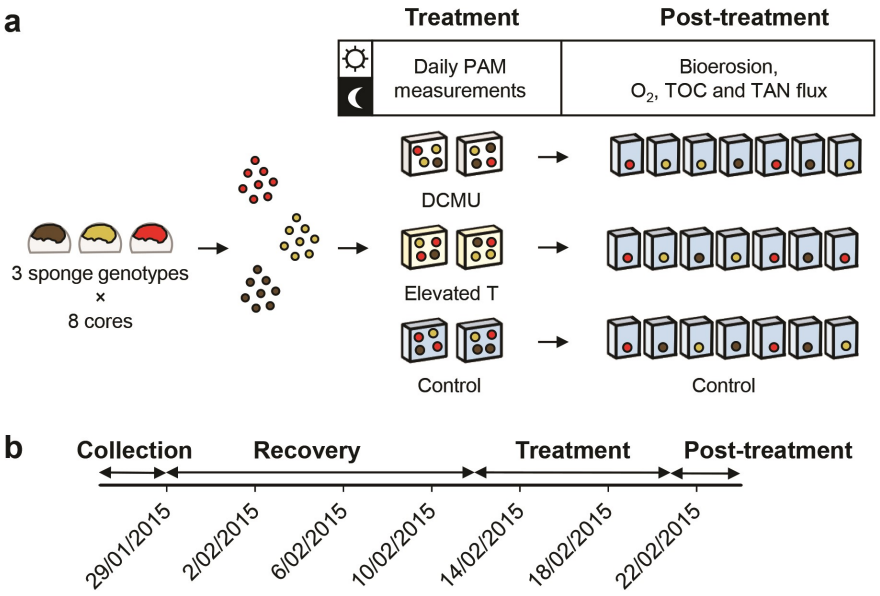

Figure 2.1: Schematic illustration of (a) experimental design and (b) timeline. Three different sponges inhabiting dead massive corals were sampled, and cores were randomly distributed over three experimental treatments: addition of the algaecide DCMU in a closed water system, elevated temperature in a flow-through regime, and control untreated conditions. During the treatment phase, the photosynthetic efficiency of the symbiotic community of the sponge was monitored daily (day and night-time PAM measurements). Post treatment, seven out of eight sponges per treatment were returned to ambient conditions and individual incubations were performed to measure bioerosion rates as well as oxygen, total organic carbon (TOC) and total ammonia nitrogen (TAN) fluxes. One core per treatment was preserved for other purposes. Schematics are not to scale.

Sponges exposed to elevated temperature and control sponges were kept in 40L aquaria that received seawater via the ocean warming and acidification simulation system (baseline simulation and elevated temperature only treatment), as presented in detail by Dove *et al.* (2013) (see also Chapter 4). For the temperature treated sponges, this computer-controlled

system was set to warm the flow-through water by 3.5°C compared to a diurnally-variable baseline measured *in situ* on the reef, while the *in situ* baseline determined the conditions under which the control sponges were kept.

During the treatment phase, daily observations of the tissue colour of the sponges were made in combination with assessment of chlorophyll fluorescence by pulse-amplitude modulated (PAM) fluorometry (Genty *et al.*, 1989). Chlorophyll fluorescence parameters were measured at 21:00 h in the dark (F_v/F_m) and at 14:00 h in the light ($\Delta F/F_m'$) using a Diving-PAM with red LED measuring light with a set distance of 10 mm from the fiberoptics to the sample surface (Walz, Effeltrich, Germany). Light levels were simultaneously monitored, as light affects the response of photosymbioses to DCMU or elevated temperature (Kunert and Dodge, 1989; Jones, 2004; Suggett *et al.*, 2011).

In a photosynthetic measurement system that has been dark-adapted for at least 30 min, dissipation of energy in the form of non-photochemical quenching is minimized, and both the minimum fluorescence (F_o) and the maximum fluorescence (F_m) of PSII chlorophyll can be measured in comparison (provided that alternative mechanisms of chlorophyll fluorescence quenching are not prevalent, as explained below). F_o is the baseline photosynthetic yield and measured in response to a pulse of far red light that is insufficient to excite any reaction centre acceptors i.e. reaction centres remain fully oxidized or "open" to light absorption (Schreiber *et al.*, 1996; Jones *et al.*, 2003). F_m follows "closure" i.e. reduction of all reaction centres when they are fully excited by a saturating pulse of photosynthetically active light (PAR; in this case to >2000 µmol photons m^{-2} s^{-1} for 0.8s). The ratio of variable chlorophyll fluoresence (F_v, which is the difference between F_m and F_o) to F_m is generally – but not always – correlated to the maximum potential quantum yield of PSII (F_v/F_m, Butler, 1978; Krause and Weis, 1991; Consalvey *et al.*, 2005). In illuminated samples, the ratio of variable ($\Delta F = F_m' - F$) to maximum (F_m') chlorophyll fluoresence is used as a measure of the effective quantum yield of PSII ($\Delta F/F_m'$).

DCMU reversibly binds to the exchangeable quinone site (Q_B) of the D1 protein of photosystem II (PSII), preventing further movement of electrons through the plastoquinone pool and cytochrome complex to photosystem I (Renger, 1976; Oettmeier *et al.*, 1980; Astier *et al.*, 1984; Yaakoubd *et al.*, 2002; Suggett *et al.*, 2003; 2011). Instead, the electrons remain trapped in the first stable electron acceptor Q_A on the D2 protein of PSII (Kleczkowski, 1994; Durnford *et al.,* 1998). DCMU therefore saturates with electrons or "closes" at least a subset of reaction centres (which do not necessarily return to their low-energy ground state even

after a few minutes of dark), limiting photochemical quenching of light energy captured by PSII (Krause and Weis, 1991). This leads to a slight increase in F_o. Furthermore, recent studies have shown that an oxidized plastoquinone pool is in itself an effective quencher of chlorophyll fluorescence. Such a pool commonly results from the application of DCMU depending on light and O_2 presence, which means that true F_m is also not achieved under DCMU (Papageorgiou *et al.*, 1972; Krause and Weis, 1991; Hohmann-Marriott *et al.*, 2010). Both these changes to F_o and F_m thus imply that F_v/F_m was expected to decline in the DCMU treatment relative to the control treatment. Such a decline is indicative of the photosynthetic inhibition of the symbionts, which could potentially lead to a reduction of the symbiont population of DCMU-treated sponges.

Increased temperature disrupts the symbiosis between *Symbiodinium* and invertebrate hosts (reviewed by Weis, 2008). In corals, this disruption is related to reactive oxygen species produced by the damaged photosynthetic machinery of the symbiont and subsequent damage to the host tissue. In particular, singlet oxygen ($^1O_2$) produced in the chloroplasts leads to light-induced loss of PSII activity (Krieger-Liszkay, 2004). These changes were again expected to translate as decreases in F_v/F_m, photosynthetic activity and symbiont population of the heat-treated sponges.

PAM fluorometry was used on a day-to-day basis to indicate how effective the treatments were in decreasing the photosynthetic output of the sponges, and to determine the point at which there was a large enough photosynthetic difference between control and treated sponges to commence the post-treatment measurements. This point was reached after 9 days.

Post-treatment measurements

After 9 days of experimental treatment, we assessed daylight and night-time chemical bioerosion rates and other physiological parameters of the sponges that had been subjected to DCMU, elevated temperature or control conditions (see below). Measurements were made in incubation chambers that received the same DCMU-free ambient seawater i.e. all assessments were done under the same untreated conditions (Table 2.1b). In this way, physiological effects of the preceding treatments could be isolated without the need for a negative control for the direct effects of DCMU or temperature elevation on seawater chemistry during the post-treatment incubations. One hour prior to daytime measurements, DCMU-treated sponges were moved from the treatment conditions to ambient running seawater. Since the effects of DCMU on symbiont photosystems are at least partially reversible (Jones *et al.*, 2003), sponges were returned to treatments conditions after

completion of the first round of incubations in preparation for the final incubations of the next day. Sponges of the elevated temperature treatment were moved to ambient running seawater on the evening prior to the first day of incubations to allow them to adjust to the lower temperature.

Actual photosynthetic CO_2 fixation was estimated through photosynthetic/respiratory oxygen flux measurements made post-treatment in the day (14:00, realized CO_2 fixation) and at night (21:00 h) using an OXY-10 oxygen meter as described previously (PreSens, Regensburg, Germany; Fang *et al.*, 2014). Incubations were conducted on seven randomly chosen sponge cores per treatment to match the maximum capacity of the respirometry setup (the eighth core of each treatment was preserved for other purposes). In brief, without exposing them to air, sponges were placed inside sealable chambers containing 0.45 µm-filtered and continuously mixed seawater, the chambers being surrounded by a water bath set at 25°C for temperature stabilization. During the day, and starting at an oxygen saturation of 60%, the sponges were subjected to 30 min of light with an intensity of 450 µmol quanta m^{-2} s^{-1} (Aqua Medic Ocean lights, Bissendorf, Germany), with oxygen levels logged every 15 s. Consecutively, the light was turned off and oxygen levels were logged for an additional 15 min. Maximum net photosynthesis (P_{net}) of the photosymbiotic community of the sponges at saturating light intensity and light-enhanced dark respiration (LEDR) were quantified based on the respective oxygen evolution or depletion (µmol O_2 cm^{-2} h^{-1}) during the light phase or the dark phase immediately thereafter (following Fang *et al.*, 2016b). At night, incubations started at an oxygen saturation of 80% (an average value for forereefs at night; Adey and Steneck, 1985), and oxygen depletion due to dark respiration (DR) was logged every 15 s over 20 min.

Chemical bioerosion rates, as well as the use of total organic carbon and ammonium by the sponges, were determined at the end of the entire study by conducting 4 h incubations by day and by night (11:00 h to 15:00 h and 20:00 h to 24:00 h respectively, using the same seven sponge replicates per treatment). Total organic carbon served as a measure of heterotrophic feeding rates in relation to bioerosion rates. Incubation chambers contained one sponge replicate each, 3 L of seawater, and a small wave maker (Koralia, Hydor, Bassano del Grappa, Italy). Chambers were partially submerged in temperature-stabilizing water baths and covered with lids. Water chemistry was monitored over the 4 h to control appropriate oxygen saturation, temperature and pH. Seawater samples were collected from each chamber at t=0 h and at t=4 h. Chemical sponge bioerosion was quantified as sponge-mediated $CaCO_3$ dissolution by measuring changes in total alkalinity (A_T) of the incubation seawater

(Zundelevich *et al.*, 2007). A_T was measured with Gran titration after Kline *et al.* (2012)

Table 2.1: Physical and chemical conditions in the control and treatment tanks (a) Temperature and pH (NBS scale) during day and night of the treatment phase. Measurements were averaged across replicate tanks and over 9 days of exposure to the algaecide DCMU, elevated temperature or control conditions (Ctrl) (no tank effect, mean ± SEM). **(b)** Post-treatment monitored parameters included temperature (T, in °C), pH (NBS scale), total alkalinity (A_T, in µmol $kgSW^{-1}$), aragonite saturation state (Ω_{Arag}) and photosynthetically active radiation (PAR, µmol quanta m^{-2} s^{-1}). Ω_{Arag} was estimated using the software CO2calc 1.2.0 (Robbins *et al*., 2010) and lacks error values. Note that post-treatment sponge groups were all incubated under the same ambient-temperature seawater in the absence of DCMU.

a Treatment phase

		Time	T	pH
DCMU	Day	10:00 h	26.4 ± 0.5	7.96 ± 0.04
		14:00 h	27.0 ± 0.5	8.17 ± 0.03
	Night	21:00 h	26.8 ± 0.2	7.88 ± 0.02
		02:00 h	26.0 ± 0.3	8.12 ± 0.02
Elevated T	Day	10:00 h	28.6 ± 0.4	8.26 ± 0.03
		14:00 h	29.9 ± 0.3	8.32 ± 0.04
	Night	21:00 h	28.3 ± 0.2	8.27 ± 0.03
		02:00 h	28.2 ± 0.2	8.20 ± 0.01
Ctrl	Day	10:00 h	26.8 ± 0.2	8.29 ± 0.03
		14:00 h	27.4 ± 0.4	8.35 ± 0.03
	Night	21:00 h	26.4 ± 0.2	8.21 ± 0.01
		02:00 h	25.7 ± 0.3	8.20 ± 0.02

b Post-treatment measurements

		Time	T	pH
All	Day	14:00	26.5 ± 0.1	8.11 ± 0.02
groups	Night	21:00	26.1 ± 0.2	8.08 ± 0.03
		A_T	Ω_{arag}	PAR
	Day	2292.1 ± 2.5	3.13	588 ± 10
	Night	2242.3 ± 1.3	2.86	0 ± 0

using an automated titrator (T50, Mettler Toledo, Langacher, Switzerland) calibrated daily with pH NBS scale buffers (Radiometer Analytical, Lyon, France) and Dickson's Standards (University of California, San Diego, USA). The measured total ammonia nitrogen values

served to correct the alkalinity signal for potential ammonia protonation (see below). The change in alkalinity due to $CaCO_3$ precipitation or dissolution ($\Delta A_{T(CaCO_3)}$) was calculated by subtracting the contribution to alkalinity by TAN ($\Delta A_{T(TAN)}$) from the total alkalinity change of the incubation ($\Delta A_{T(inc)}$) [Eqn (1); Schneider *et al.*, 2011]. Chemical sponge bioerosion was subsequently calculated based on Eqn (2):

$$\Delta A_{T(CaCO_3)} = \Delta A_{T(inc)} - \Delta A_{T(TAN)} \quad (1)$$

$$W_{CaCO_3} = (\Delta A_{T(CaCO_3)} /2) \times MW_{CaCO_3} \times V_{sw} \times d_{sw} \quad (2)$$

where W_{CaCO_3} is the weight of the dissolved $CaCO_3$, $\Delta A_{T(CaCO_3)}$ is divided by 2 to match the molar value of dissolved $CaCO_3$, MW_{CaCO_3} is the molecular weight of $CaCO_3$ (100g mol^{-1}), V_{sw} is the incubation volume, and d_{sw} is the seawater density (modified from Zundelevich, *et al.,* 2007). Chemical bioerosion was then expressed as substrate weight loss per area sponge tissue and hour.

Samples for total organic carbon analysis (dissolved and particulate organic carbon) were frozen in sealed pre-combusted and acid-rinsed glass vials until further analysis. Defrosted water samples were analysed at the Advanced Water Management Centre at the University of Queensland using a Total Organic Carbon Analyzer (TOC-L CSH with TNM-L TN unit, Shimadzu). The samples were acidified using HCl and aerated to remove inorganics before determination of non-purgeable organic carbon (Findlay *et al.*, 2010). Total ammonia nitrogen (TAN = $NH_3 + NH_4^+$) was photometrically quantified from seawater samples of the same incubations (Parsons *et al.*, 1984).

Once all incubations were completed, the sponge cores were snap-frozen in liquid nitrogen and stored at -80°C, as the experiment was completed on Heron Island. Once they were transferred to the laboratory at the St. Lucia Campus of The University of Queensland, the samples were thawed and upper surface areas of the cores were quantified using a standard aluminium foil technique (Marsh, 1970). To isolate the sponge tissue from the $CaCO_3$ substrate, an acid decalcification method was used (as described in detail by Fang *et al.*, 2013b). The wet sponge material from seven cores per treatment was homogenized and filtered through a 200 µm sieve followed by a 40 µm sieve to exclude most of the spicules. The homogenate was then centrifuged at 4000g for 5 min at 4°C, washed and centrifuged again (repeated 3 times). The resulting pellet was resuspended in filtered seawater, and *Symbiodinium* concentration was determined using a haemocytometer (Laboroptik, Lancing, UK) under 400x magnification (BX43 microscope, Olympus, Tokyo, Japan) (Fang *et al.*,

2013a). The cell concentrations were then normalized to the surface areas of the sponge cores (cells cm^{-2}). Apart from *Symbiodinium*, *C. orientalis* hosts a low abundance of other microorganisms such as alpha-, delta- and gammaproteobacteria and a limited cyanobacterial population (Poppell *et al.*, 2013; Pineda *et al.*, 2016; Ramsby *et al.*, 2018). Unlike proteobacteria, cyanobacteria are sensitive to DCMU (Sinning, 1992; Angly *et al.*, 2016). Although treatment responses were overall addressed at the holobiont level, analyses focused on *Symbiodinium* since it forms the vastly dominant microbial community in *C. orientalis* and is the primary uptake site of inorganic carbon and nitrogen in this holobiont (Chapter 3 of the current thesis).

Statistical analysis

Statistical analyses were done after testing the assumptions of normality with a Shapiro-Wilk test and homogeneity of variances with a Levene's test. Preliminary analysis showed no significant effect of aquaria (nested within treatment) for any of the variables, therefore data from duplicate aquaria were pooled according to standard methods (Underwood, 1997; Tremblay *et al.*, 2016). We did not incorporate aquaria as a factor within the final design, since unequal numbers of sponges were sampled from each of the duplicate aquaria per treatment (n=3+4). All oxygen flux datasets and the *Symbiodinium* density dataset were analysed by means of one-way ANOVAs. "Treatment" was the between-subjects factor with 3 levels, namely DCMU, elevated temperature, and control. ANOVAs were followed by Tukey's post-hoc tests (Table 2.2). Chemical bioerosion rates, ammonium uptake and carbon uptake were measured both by day and by night. Therefore, these parameters were analysed by means of 2-way mixed model ANOVAs followed by post-hoc comparisons (as listed in Table 2.2). "Treatment" was the between-subjects factor of the mixed model with levels as above, and "Time" was the within-subjects or repeated-measures factor (2 levels: day and night). The chlorophyll fluorescence measurements were analysed separately by day and by night. "Treatment" again was the between-subjects factor of the mixed model, while the within-subjects factor was "Date" and had 9 levels (day 0 to day 9, one data point missing). Datasets analysed with mixed models were additionally tested for equality of covariances using a Box's test and sphericity using a Mauchly's test, where applicable. Simple linear regression models were used between chemical bioerosion and physiological parameters of interest, after assessing normality and homoscedascity of residuals. Statistical tests were evaluated at a 0.05 level of significance and were performed using Statistica 13 (StatSoft, Tulsa, USA). Means and standard errors of means are reported throughout the results (mean±SEM).

2.3. Results

Treatment phase

Chlorophyll fluorescence measurements served as a tool to assess whether the treatments were having the expected effects on the photosynthetic efficiency of the symbiotic community of *Cliona orientalis*, and to determine the minimum duration of the treatment phase for a detectable effect. Over time the effective quantum yield of photosystem II measured in the sponge holobiont was differentially affected by the treatments ($\Delta F/F_m$'; 2-way mixed ANOVA, Treatment x Date, $F_{(16, 168)}=7.15$, $p<0.0001$, Fig. 2.2a, Table 2.2). $\Delta F/F_m$' initially decreased due to DCMU, but not due to elevated temperature. At day 2, $\Delta F/F_m$' in DCMU-treated sponges was only 24% of that in the control, but under elevated temperature $\Delta F/F_m$' increased to 131% of control values (Tukey's post-hoc, $p<0.0001$ for each comparison). At day 3, $\Delta F/F_m$' of the DCMU treatment remained lower than the control ($p=0.022$), before stabilizing for a few days. At day 6 it started to increase again, heading toward the initial levels by the end of the experiment ($p=0.94$). Temperature stress led to a response pattern that was overall more similar to the control, but at day 10 $\Delta F/F_m$' suddenly collapsed and was no longer detectable as F_m' tended to zero.

The maximum potential quantum yield of photosystem II also followed drastically different patterns over time in DCMU- and heat-treated sponges (F_v/F_m, 2-way mixed ANOVA, Treatment x Date, $F_{(16, 168)}=8.90$, $p<0.0001$, Fig. 2.2b, Table 2.2). Although temperature stress did not have an effect at day 1, DCMU exposure resulted in a halving of F_v/F_m levels compared to the control ($p<0.0001$). F_v/F_m rates did not appear to recover over time ($p<0.0001$ at day 9 compared to control). Again, daily values for temperature-stressed sponges did not deviate from the controls, apart from day 10 when F_v/F_m fell to undetectable levels as F_m tended to zero.

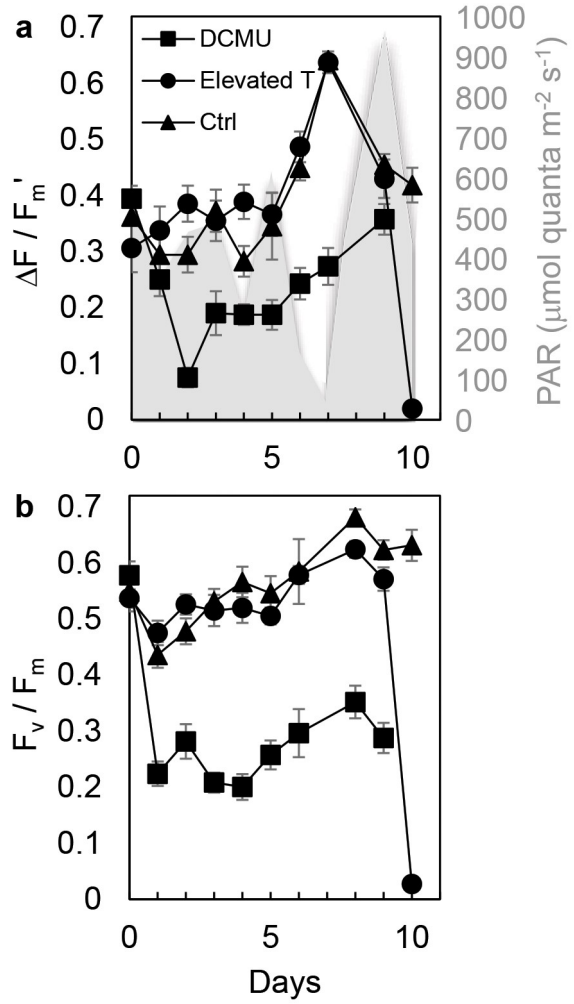

Figure 2.2: (a) Effective quantum yield of photosystem II measured in the day and (b) maximum potential quantum yield of photosystem II measured during the night in photosymbionts of the *Cliona orientalis* holobiont over 9 days of exposure to the algaecide DCMU (added at day 1, 13/02/2015), symbiont loss due to elevated temperature (T) and control treatment (n=8 sponges per treatment after pooling the tanks). The grey area in (**a**) shows simultaneous levels of photosynthetically active radiation (PAR) measured in the aquaria during daytime measurements. At day 10, both effective and maximum potential quantum yield were undetectable in the sponges exposed to elevated temperature. DCMU-treated sponges were removed from the treatments on day 10. No data for F_v/F_m on day 7 as well as $\Delta F/F_m$' and PAR on day 8 were collected due to a cyclone warning (Cyclone Marcia). All days were sunny, apart from day 6 and 7 when PAR fell to 171±0.32 and 42.2±0.37 respectively (mean±SEM).

Post-treatment measurements

By day 10, after 9 days of treatment, autotrophic feeding rates differed between the treatments. Control sponges were daytime net producers of photosynthetically-derived oxygen, whereas heat-treated sponges respired as much as they produced, and DCMU-treated sponges were net consumers of oxygen (4.06±0.13, 0.01±0.20 and -1.02±0.05 µmol O_2 cm^{-2} h^{-1} respectively, ANOVA, $F_{(2,18)}$=355.08, $p<0.0001$ and Tukey's post hoc, $p<0.001$ for both comparisons, Fig. 2.3, Table 2.2). Accordingly, light-enhanced dark respiration measured in

the day was strongest in the control sponges (LEDR, ANOVA, $F_{(2,18)}$=9.66, p=0.001 and Tukey's post hoc, p<0.02 for both comparisons). Although overall weaker than LEDR, night-time consumption of oxygen by the holobiont was also strongest in the control sponges (-2.19±0.14 in controls as opposed to -1.54±012 and -1.20±0.04 µmol O_2 cm^{-2} h^{-1} in the DCMU- and heat-treated sponges respectively; ANOVA, $F_{(2,18)}$=20.09, p<0.0001 and Tukey's post hoc, both p<0.002, Fig. 2.3, Table 2.2). Dark respiration did not differ between the other two treatments (p=0.112).

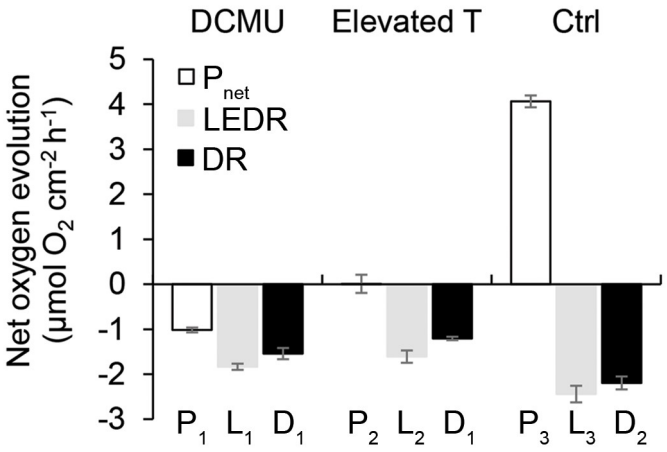

Figure 2.3: Oxygen flux of the bioeroding sponge holobiont *Cliona orientalis* in the day (net photosynthesis, P_{net} and light-enhanced dark respiration, LEDR) and in the night (dark respiration, DR) under three different treatments: exposure to the algaecide DCMU, symbiont loss due to elevated temperature (T), and control treatment (Ctrl). Bars display means ± SEM. Significant differences within P_{net} (P), LEDR (L) and DR (D) across the treatments are indicated by the different number subscripts.

When it comes to heterotrophic feeding, total organic carbon use by the sponges was highly variable and did not differ between the treatments. Total organic carbon uptake was greater by day than by night, with sponges tending to acquire organic carbon by day, but to reduce that uptake or to release carbon into the environment by night (uptake of on average 4.8±0.7 µg C cm^{-2} h^{-1} by day and release of 1.4±1.7 µg C cm^{-2} h^{-1} by night, 2-way mixed ANOVA, diurnal effect, $F_{(1,18)}$=9.59, p=0.006, Table 2.2).

Sponge-generated chemical bioerosion was driven by independent diurnal and treatment effects (2-way mixed ANOVA, $F_{(1,18)}$=12.16, p=0.003 and $F_{(2,18)}$=22.52, p<0.0001 respectively, Fig. 2.4, Table 2.2). Chemical erosion rates were overall higher by night than by day (Tukey's post-hoc, p=0.003), although this diurnal effect tended to be minimal in the control treatment (Fig. 2.4). Net erosion rates gradually decreased from control to heat-treated to DCMU-treated sponges (Tukey's post-hoc, all three comparisons p<0.022).

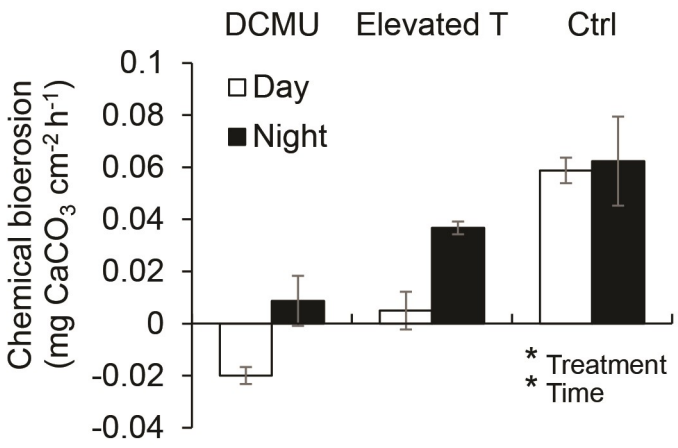

Figure 2.4: Chemical bioerosion rates of the excavating sponge *Cliona orientalis* in the day and in the night under three different treatments: (1) exposure to the algaecide DCMU, (2) symbiont loss due to elevated temperature (T), and (3) control treatment (Ctrl). Asterisks (*) indicate significant main effects. Bars display means ± SEM.

Ammonium use by the sponge holobionts did not follow a diel pattern, but a treatment effect was detected (2-way mixed ANOVA, $F_{(2,18)}$=7.25, p=0.005, Table 2.2). Ammonium was taken up by the sponge holobionts in the control treatment (0.024±0.015 µmol NH_4^+ cm^{-2} h^{-1}) in contrast to the DCMU-treated sponges that released rather than took up ammonium (-0.037±0.014 µmol NH_4^+ cm^{-2} h^{-1}, Tukey's post hoc, p=0.004). Use of ammonium in heat-treated sponges did not differ from the other two treatments (-0.009±0.007 µmol NH_4^+ cm^{-2} h^{-1}).

Overall, exposure of the sponge cores to the chemical and thermal treatments led to visible and statistically significant changes in the symbiotic community of the sponges (ANOVA, $F_{(2,15)}$= 49.91, p<0.0001, Fig. 2.5, Table 2.2). Exposure to the algaecide DCMU over 9 days resulted in moderate paling of the surface tissue of the sponges (viewed by day), and the *Symbiodinium* population decreased by approximately 50% compared to control sponges (Tukey's post-hoc, p<0.001). Exposure to elevated temperature caused a stronger yet still incomplete loss of symbionts (85% loss, Tukey's post-hoc, p<0.001). Per symbiont cell, the net photosynthetic oxygen flux amounted to -2.5±0.2 pmol O_2 h^{-1} in the sponges pre-exposed to DCMU, and -0.5±2.1 pmol O_2 h^{-1} in those exposed to elevated temperature, as opposed to 5.1±0.3 pmol O_2 h^{-1} in the control cells (ANOVA, $F_{(2,15)}$=9.956, p=0.002 and Tukey's post hoc, p<0.05 for control versus the other two treatments). No partial or complete mortality was observed in any of the sponges during the short experimental period, and sponges in all treatments displayed open and pumping oscula.

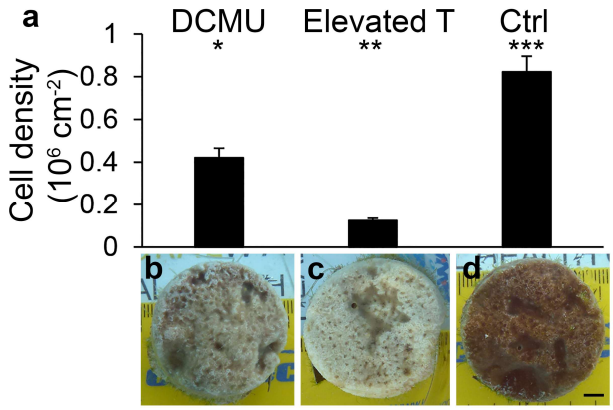

Figure 2.5: Density of *Symbiodinium* cells (a) (mean±SEM) and tissue colour (b-d) of the *Cliona orientalis* sponge holobiont under three treatments with photographs taken by day: **(b)** 9-day exposure to the algaecide DCMU, **(c)** symbiont loss due to elevated temperature, and **(d)** control treatment. Asterisks indicate significant differences between treatments. The scale bar in **(d)** equals 0.5 cm.

Simple regression analysis showed a significant (positive) correlation between net daytime photosynthesis and daytime as well as night-time chemical bioerosion activity in *C. orientalis* ($F_{(1,19)}$=80.21, p<0.001, Fig. 2.6a, and $F_{(1,19)}$=9.28, p=0.007, Fig. 2.6b, respectively). The proportion of variance of daytime chemical bioerosion rates that could be accounted for by net photosynthesis equalled 81%. The equivalent proportion for night-time bioerosion rates was 33% (Fig. 2.6). Night-time respiration explained an additional 8% of the variance in night-time bioerosion rates, but by itself, this correlation was not significant (not shown in Fig. 2.6).

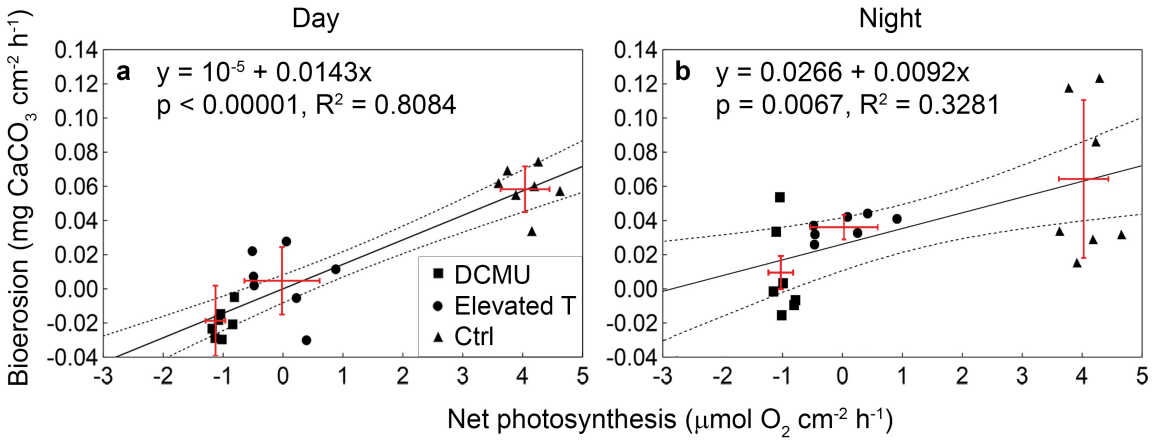

Figure 2.6: Regression analysis between net daytime photosynthesis and chemical bioerosion rates of the bioeroding sponge holobiont *Cliona orientalis* by day **(a)** and by night **(b)**. Net daytime photosynthesis is significantly related to daytime chemical bioerosion rates mostly, but also to night-time chemical bioerosion rates. For each treatment, the mean and standard deviations for each axis are shown in red.

Table 2.2: Results of analysis of variance and follow-up tests where applicable for the key parameters of the experiment presented in Figures 2.2-2.5. The between-subjects factor for all one-way analyses was "Treatment", with 3 levels: exposure to DCMU, elevated temperature (abbreviated as "T"), and control treatment ("Ctrl"). In two-way mixed analyses the within-subjects factor "Time" was added, with levels "Day" and "Night". The chlorophyll fluorescence parameters were analyzed separately by day and by night. Since measured over several days, the within-subjects factor for chlorophyll fluorescence was "Date", and post-hoc comparisons are reported for days/nights of interest as specified. Note that post-hoc comparisons may refer to negative values (i.e. not absolute values). Significant results (evaluated at a 0.05 level) are highlighted in boldface. *Heteroscedastic dataset where a) the significance level was reduced to 0.01 to minimize the risk of a Type I error (Underwood, 1997) and b) multivariate tests were conducted in addition to univariate tests (with overlapping results) due to a violation of sphericity (Girden, 1992). ** Dataset transformed based on log(x+1).

		Analysis of Variance						Post-hoc comparisons		
	ANOVA	Source of variation	DF	SS	MS	F	P	Level	Conclusions	P
Chlorophyll fluorescence (ratio)										
$\Delta F/F_m'$	2-way mixed	Treatment	2	1.243	0.622	23.34	<0.0001	Day 2	**DCMU < T**	**<0.0001**
		Error	21	0.559	0.027				**DCMU < Ctrl**	**<0.001**
		Date	**8**	**1.327**	**0.166**	**25.73**	**<0.0001**		T - Ctrl	0.975
		Treatment × Date	**16**	**0.738**	**0.046**	**7.15**	**<0.0001**	Day 9	DCMU - T	0.999
		Error	168	1.083	0.006				DCMU - Ctrl	0.944
									T - Ctrl	0.999
F_v/F_m*	2-way mixed	Treatment	**2**	**3.033**	**1.516**	**89.47**	**<0.0001**	Night 1	**DCMU < T**	**<0.0001**
		Error	21	0.356	0.017				**DCMU < Ctrl**	**<0.0001**
		Date	**8**	**0.737**	**0.092**	**21.25**	**<0.0001**		T - Ctrl	0.999
		Treatment × Date	**16**	**0.617**	**0.038**	**8.90**	**<0.0001**	Night 9	**DCMU < T**	**<0.0001**

		Error	168	0.728	0.004	89.47			**DCMU < Ctrl**	**<0.0001**
									T - Ctrl	0.999
Oxygen flux (µmol O_2 cm^{-2} h^{-1})										
Net Photosynthesis	1-way	Treatment	**2**	**101.13**	**50.567**	**355.08**	**<0.0001**	-	**DCMU < T**	**<0.001**
		Error	18	2.563	0.142				**DCMU < Ctrl**	**<0.001**
									T < Ctrl	**<0.001**
Dark respiration (DR)	1-way	Treatment	**2**	**3.545**	**1.772**	**20.09**	**<0.0001**	-	DCMU - T	0.112
		Error	18	1.588	0.088				**DCMU > Ctrl**	**<0.002**
									T > Ctrl	**<0.001**
Light-enhanced DR	1-way	Treatment	**2**	**2.594**	**1.296**	**9.66**	**0.001**		DCMU - T	0.495
		Error	18	2.416	0.134				**DCMU > Ctrl**	**0.016**
									T > Ctrl	**0.001**
Organic carbon uptake (mg C cm^{-2} h^{-1})										
	2-way mixed	Treatment	2	0.0001	0.00006	1.51	0.247			
		Error	18	0.0007	0.00004					
		Time	**1**	**0.0004**	**0.0004**	**9.59**	**0.006**	**-**	**Day > Night**	
		Treatment × Time	2	<0.0001	0.00001	0.356	0.705			
		Error	18	0.0008	0.00004					

Bioerosion rates (mg $CaCO_3$ cm^{-2} h^{-1})										
Chemical**	2-way mixed	Treatment	**2**	**0.005**	**0.003**	**22.52**	**<0.0001**	-	**DCMU < T**	**0.021**
		Error	18	0.002	0.0001				**DCMU < Ctrl**	**<0.001**
		Time	**1**	**0.001**	**0.001**	**12.16**	**0.003**		**T < Ctrl**	**0.004**
		Treatment × Time	2	0.0001	0.0002	2.46	0.114			
		Error	18					-	**Day < Night**	**0.003**
Ammonium uptake (µmol cm^{-2} h^{-1})										
	2-way mixed	Treatment	**2**	**0.026**	**0.013**	**7.25**	**0.005**	-	DCMU - T	0.227
		Error	18	0.033	0.002				**DCMU < Ctrl**	**0.004**
		Time	1	0.002	0.002	0.77	0.390		T - Ctrl	0.120
		Treatment × Time	2	0.003	0.001	0.45	0.639			
		Error	18	0.053	0.003					
***Symbiodinium* density (10^6 cells cm^{-2})**										
	1-way	Treatment	**2**	**1.477**	**0.738**	**49.92**	**<0.0001**	-	**DCMU > T**	**0.002**
		Error	15	0.222	0.015				**DCMU < Ctrl**	**<0.001**
									T < Ctrl	**<0.001**

2.4. Discussion

Exposure of the photosymbiotic bioeroding sponge *Cliona orientalis* to the algaecide DCMU or to elevated temperatures resulted in a decrease in the photosynthetic activity and density of *Symbiodinium* dinoflagellates hosted by the sponge. Chemical bioerosion by the sponge decreased steeply as photosynthetic activity declined, demonstrating the presence of a strong and direct link between photosynthetic (by)products and bioerosion. Surprisingly, night-time respiration of the host alone proved insufficient to support high levels of bioerosion despite the favourable water chemistry, revealing that day-time photosynthesis also supports night-time erosion activity. These findings confirm that photosymbioses on coral reefs not only form the energetic basis for how some organisms can build reef frameworks (Muscatine, 1990; Gattuso *et al.*, 1999), but also how some bioeroding organisms such as *C. orientalis* can destroy them.

Photosynthesis and bioerosion rates

Decreases in chemical bioerosion rates went hand in hand with decreases in photosynthetic rates driven by treatment effects, with DCMU-treated sponges eroding the least. In other words, photosynthetic rates explained 81% of the variability found in chemical bioerosion during the day, and 33% by night (see below). While correlations do not imply causation necessarily, and the existence of other non-photosynthetic treatment effects on bioerosion were not observed but cannot be excluded, this link between photosynthesis and bioerosion is consistent with previous studies, and may result from photosynthate transfer to and/or boosted oxygen supply to the mitochondria of etching cells. Depressed bioerosion rates in *C. orientalis* were previously found in shaded specimens (Rosell and Uriz, 1992; Hill, 1996; Schönberg, 2006) and after short- and long-term bleaching, when the sponges eventually suffered from an unsustainable carbon budget that resulted in mortality (Fang *et al.*, 2014; 2018; Chapter 4 of the current thesis). Furthermore, photosynthetic compounds fixed by *Symbiodinium* are shared with hosting sponge cells in the outer symbiont-rich and light-exposed layer of *C. orientalis* and other photosymbiotic sponges (Weisz *et al.*, 2010; Chapter 3 of the current thesis), yet translocation of these photoassimilates to deeper etching cells remains to be directly explored.

Assuming that photosynthetic products can boost sponge bioerosion, we would have expected more intense bioerosion during the day compared to night. Bioerosion was overall higher by night than by day, however. Importantly, this diurnal difference appears to be greater for

treated rather than control sponges. Large variation in the night-time response of the control eliminates any potential to detect a significant interaction between treatment and sampling time (i.e. the treatment effect did not statistically depend on the time of the day), and therefore we could not directly compare day and night rates within treatments (post-hoc analyses were permitted only at the factor level). A previous study suggested that diurnal changes in ambient seawater acidity are of less importance in regulating the bioerosion of healthy *C. orientalis* than the input of photosynthetic energy during the day, leading to higher chemical erosion rates by day than by night (8h autumn incubations; Fang *et al.*, 2016b). According to our observations both factors play a role, but their proportional contributions can shift with the condition of the photosymbionts. In our experiment (4h summer incubations), daytime bioerosion rates under ambient conditions did not surpass the highly-variable night-time rates, but photosynthetic products appeared to enable daytime bioerosion to nearly meet night-time levels when water chemistry is generally more favourable for dissolution. Photosynthetic loss in both treatments removed this effect and coincided with a trend of higher bioerosion by night. The presence of diurnal variability in bioerosion rates of photosymbiotic sponges remains debatable to date and deserves further attention: No diurnal variability was found in chemical bioerosion of the photosymbiotic sponge *Pione* cf. *vastifica* (Zundelevich *et al.*, 2007). In the zooxanthellate sponge *Cliona caribbaea* diurnal variability of chemical bioerosion was found to depend on the level of pCO_2 and nutrients (Webb *et al.*, 2017). Clearly, variability in water column chemistry and CO_2 saturation inside the sponges complicates comparisons between studies.

When the *Symbiodinium* population was diminished or when net daytime O_2 production was significantly impeded by treatment effects, bioerosion rates decreased as compared to those of untreated sponges by day as well as by night. The decrease by night indicates that, in intact symbioses, photosynthetic products are potentially stored for night-time use. It could also be that, in intact symbioses, photosynthetically produced oxygen remains available in relatively deeper layers of the sponge, enabling an aerobic rather than anaerobic metabolism by night, in turn facilitating excavation. This is likely to be the case given the high rates of metabolism at night and the expected size of these oxygen reservoirs. In favour of the metabolic or oxygenic spill-over from day to night is the observation that under long-term darkness, bioerosion rates of *C. orientalis* decrease (Pineda *et al.*, 2016; Fang *et al.*, 2017). Reductions in the contribution and acidifying effect of respired CO_2, potentially due to reductions in symbiont biomass or symbiont derived carbohydrates, may also contribute to the observed reduction in night-time chemical erosion for treated compared to control sponges. In

particular, healthy *Symbiodinium* invoke a substantial amount of chlororespiration at night to supplement basal respiration of the mitochondria (e.g. Hill and Ralph, 2008), but since DCMU does not allow PQ to accept electrons (Suggett *et al.*, 2003; 2011), this respiration and any bioerosion it may have induced would likely be diminished. The observed differences in night-time bioerosion rates among the treatments were only partially explained by daytime net O_2 production (33%) and to an even lesser extent by night-time respiration (8%), however, leaving the principal driver of night-time bioerosion undiscovered. Oxygen consumption and alkalinity changes measured in incubation seawater may not accurately describe the actual local respiration or bioerosion activity in the deeper sponge tissues, which may be better targeted in future studies by the use of micro-sensors. Furthermore, since heterotrophic rates did not differ between the treatments, our experiment was not suitable for testing the impact of heterotrophic feeding on bioerosion rates, but previous studies have established a strong link between the two (e.g. Holmes *et al.*, 2009; Webb *et al.*, 2017; Chapter 4 of the current thesis).

Interestingly, the alkalinity of the culture water decreased during the daytime incubation of the DCMU-treated sponge holobionts. In combination with the lowering of the chemical bioerosion rate, the decrease in alkalinity may be explained by the release of protons due to enhanced microbial calcification or other metabolic processes (e.g. Riding, 2000; Reyes-Nivia *et al.*, 2013). For example, calcifying alphaproteobacteria as reported in *Cliona viridis* are not affected by DCMU since their photosystem structure does not allow binding of the algaecide (Sinning, 1992; Sadekar *et al*., 2006; Garate *et al.*, 2017). Such microbes may have photosynthesized, calcified and/or grown relatively more in the absence of competition with the disabled *Symbiodinium*, thereby influencing alkalinity. Additionally, algaecide-related photodamage may have led to some degradation of the symbiont-hosting cell structures, accompanied by a larger abundance of microorganisms, possibly also stimulating relatively more HNO_3 release due to aerobic respiration of organic matter, and hence a decrease in alkalinity (Wolf-Gladrow *et al.*, 2007; Kim and Lee, 2009). Alkalinity shifts due to shifts in the composition of the microbiome of treated *C. orientalis* are plausible, since the microbiome is known to be unstable and it changes under different light and temperature (and hence photosynthetic) environments (Pineda *et al.*, 2016; Ramsby *et al.*, 2018). Further research is necessary to fully explain the alkalinity decrease in question.

Treatment effects on holobiont

The observed differences in autotrophic activity and hence bioerosion between the treatments can be explained by photostress that resulted either in reductions of the photosymbiont density (expulsion, or even digestion of photosymbionts by the host; Rosell, 1993; Hill and Hill, 2012), or reductions of their photosynthetic efficiencies, or both (schematic summary in Fig. 2.7). In comparison to the heat treatment, DCMU allowed the persistence of a larger, yet relatively photochemically inactive population of resident symbionts (per cell net photosynthesis decreased by roughly 150% relative to control). The few symbionts that persisted under elevated temperature remained active photosynthetically (oxygen production per cell almost met respiratory costs), perhaps taking advantage of the larger availability of light in the bleached tissue (Enríquez *et al.*, 2005; Hoogenboom *et al.*, 2010). When applied at high concentrations and over several days such as in the present study, DCMU causes photochemical changes that lead to the disruption of the endosymbiosis between scleractinian corals and their resident dinoflagellates, resulting in near-complete bleaching (e.g. Jones, 2004; Negri *et al.*, 2005; Underwood *et al.*, 2006). We did not directly compare the sponges to corals, and the actual dose of algaecide that interacts with the endosymbionts will be affected by very different dynamics in the two symbioses. Nevertheless, in the sponges just over half of the dinoflagellate population remained in place, despite the saturating DCMU concentration and despite photosynthetic impairment, as evidenced by the depressed fluorescence and the net oxygen consumption in the light. In the heat-stressed sponges (MMM + 3.1°C), there was no gradual decline in photosynthetic potential of individual symbionts as typically seen at the onset of coral bleaching (Jones *et al.*, 1998; Jones, 2004). Instead, symptoms of the loss of photosynthetic capacity during the short-term warming were delayed until a sudden collapse occurred, when not enough functional symbionts remained.

The above observations reinforce the conclusion that the partnership between clionaid sponges and *Symbiodinium* responds differently to photosynthetic stress as compared to the coral-*Symbiodinium* partnership (Schönberg *et al.*, 2008; Hill *et al.*, 2011; Schönberg and Wisshak, 2012). The different response may in part stem from the sponge holobiont's ability to regulate the positioning of the symbionts inside the thick three-dimensional sponge body, the overall body temperature via active pumping and rapid water replenishment (Schönberg and Suwa, 2007; Schönberg *et al.*, 2017b) and the composition and thus thermal tolerance of the lipid bilayer of cell membranes (Bennett *et al.*, 2018). In these ways, temporary control or reduction of light and/or heat stress is offered, enabling the sponge to cope with short-term stress, although this protection is not limitless (see also Fang *et al.*, 2018a and Chapter 4 of

the current thesis) and the potential of host cell damage due to experimental heat stress cannot be excluded. At the same time, the persistence of a relatively large fraction of the *Symbiodinium* population inside the algaecide-treated sponges may indicate that symbiont survival in *C. orientalis* does not necessarily require constant active photosynthesis (Pineda *et al.*, 2016; Fang *et al.*, 2017).

The persistence of *Symbiodinium* cells within stressed corals may be related to differences in tolerance among different dinoflagellates (Berkelmans *et al.,* 2006; Sampayo *et al.,* 2008; Wang *et al.*, 2017). However, preliminary analysis of remnant *Symbiodinium* from our sponges comparing the chloroplast large-subunit rDNA marker cp23S and high resolution psbA^{ncr} (LaJeunesse and Thornhill, 2011) did not find differences between the symbionts from control samples and those in reduced populations that remained in treated samples (T. LaJeunesse, unpubl. data). In other words, there was no indication of the presence of a different kind of *Symbiodinium* to explain the persistence of these symbionts. Therefore, variation in the response of these symbionts to DCMU or heat most likely reflects physiological heterogeneity of the symbiont population affected by location in the sponge tissue (see also Chapter 3). Symbionts in the uppermost, sunlit layer are exposed to greater algaecide, thermal and light stressors and are likely to be physiologically compromised and, therefore, are more vulnerable to expulsion from the host (Jones *et al.*, 2003; Jones, 2004).

Although a number of *Symbiodinium* cells persisted in the DCMU-treated sponges, photophysiology and chlorophyll fluorescence was clearly affected in these specimens. Since all photosynthesis reaction centres are "closed" or saturated under the DCMU treatment, minimum and maximum fluorescence will approach each other, and therefore $\Delta F/F_m$' is expected to decrease as observed in our measurements (Suggett *et al.*, 2011). Ultimately, and faster under high light, the build-up of electrons within photosystem II may lead to the generation of the longer-lived triplet chlorophyll state, leading to the production of reactive singlet oxygen and other free radicals that are detrimental to the photosystems and other physiological processes (Osmond *et al.*, 1999; Krause and Weis, 1991; Jones, 2004; Krieger-Liszkay, 2004). As mentioned above, an oxidized plastoquinone pool under DCMU may partially quench chlorophyll fluorescence, thereby reducing F_v/F_m (Hohmann-Marriott *et al.*, 2010). Photoinactivation caused by DCMU may further explain the observed reduction in F_v/F_m despite the fact that in the dark the photosystems could eventually return to the ground state. Photoinactivation may also explain the expulsion of symbionts found in the DCMU treatment, in a similar way to potential oxidative stress and host cell detachment experienced

under the elevated temperature treatment. Such responses to heat stress are established in *Symbiodinium* that reside in Cnidaria (Gates *et al.*, 1992; Hoegh-Guldberg, 1999; Jones and Hoegh-Guldberg, 2001; Paxton *et al.*, 2013).

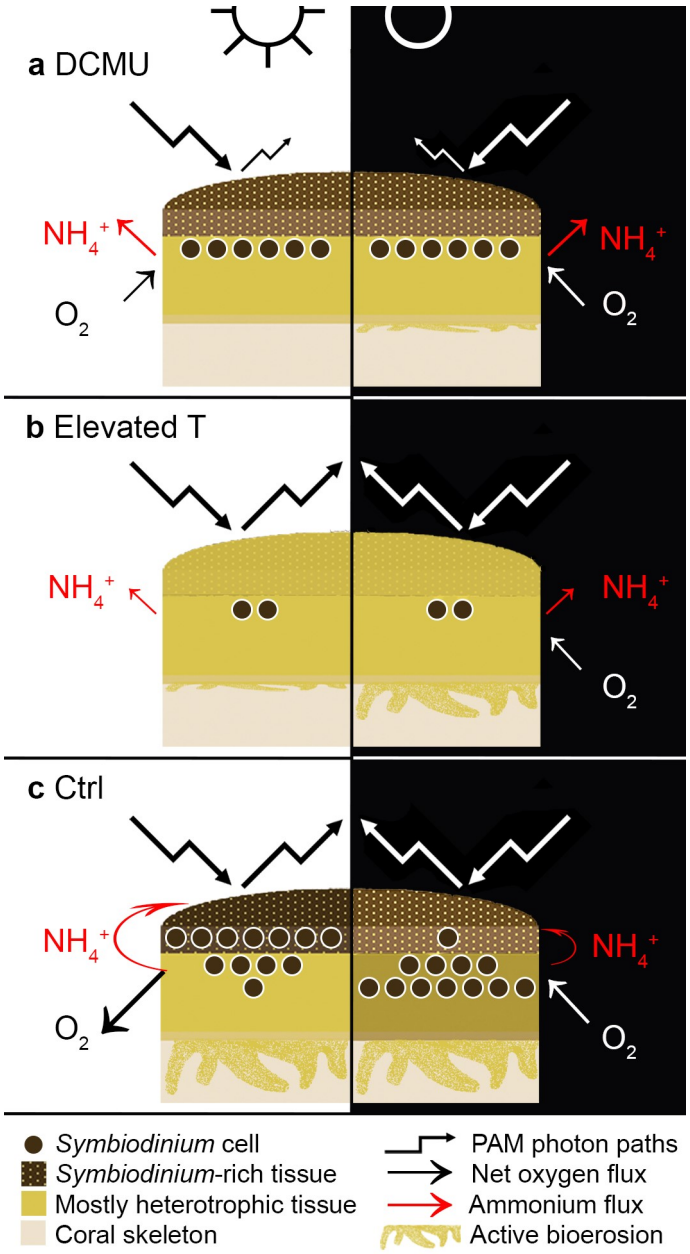

Figure 2.7: Schematic representation summarizing the main physiological responses monitored in experimental cores of *Cliona orientalis* by day (left panels, in white) and by night (right panels, in black) after **(a)** exposure to the algaecide DCMU and **(b)** exposure to elevated temperature (T) over 9 days relative to control sponges **(c)**. Cross sections of sponge cores display a heterogeneous distribution of symbiont densities (varying colours representing the corresponding *Symbiodinium* abundance; while colouration suggests zones, there is no clear separation, but one merges into the other). Close to the surface the sponge contains the densest distribution of the photosymbionts and the most intensive daytime oxygen production. Further into the sponge

Symbiodinium become less abundant and the heterotrophic sponge cells become increasingly more dominant in comparison. Bioeroding cells most likely occur throughout the sponge, but they are concentrated at the etching front at the interface with the underlying coral skeleton. The etching front contains the fewest *Symbiodinium*, and none of them could fit into the bioerosion fissures that release the substrate chips. The abundance of *Symbiodinium* cells (not to scale), the saturating pulse of light and resulting yields of Photosystem II (incoming and outgoing PAM Photon paths respectively, pulse- amplitude modulated fluorometry), the net oxygen and ammonium flux, and the chemical bioerosion rates are schematically represented by day and by night. The size of the symbols displays the approximate intensity of the corresponding function. For example, in DCMU-treated sponges **(a)**: i) The saturating pulse of light during the PAM measurement (incoming Photon path) results in low chlorophyll fluorescence (outgoing Photon path) indicative of poor photosynthetic potential. ii) Since photosynthesis is inhibited, the sponge holobiont is a net consumer of O_2 both by day and by night. iii) The *Symbiodinium* population is halved compared to the control and kept lower in the sponge body by day for protection from light and algaecide. iv) Ammonium is released by the host as a metabolic waste product without interception by *Symbiodinium* v) Reduced bioerosion takes place, and only by night.

Experimental loss of symbionts in *C. orientalis* as a result of thermal stress has been observed before, and can cause longer-term energetic deprivation and mortality to the holobiont (Fang *et al.*, 2013a, 2014; Chapter 4 of the present thesis). Cnidaria that are symbiotic with *Symbiodinium* may compensate for the loss of phototrophic capacity by increasing their heterotrophic potential (Grottoli *et al.*, 2006; Dove *et al.*, 2013), but the presence of such plasticity in photosymbiotic sponges is debatable and could not be confirmed here (Fang *et al.*, 2014, 2017, 2018; Pineda *et al.*, 2017b; Chapter 4 of the present thesis). In our experiment, heterotrophic uptake of carbon was generally higher by day than by night regardless of the treatment, which is in accordance with higher pumping rates of *C. orientalis* by day (Strehlow *et al.*, 2016). Higher pumping activity by day may serve to regulate internal temperatures and to diffuse photosynthetic oxygen before it reaches harmful levels. Lower pumping by night – in combination with withdrawal of *Symbiodinium* to deeper layers (Schönberg and Suwa, 2007) – results in added respiration and possibly in saturation of the sponge tissue with CO_2, a condition that would likely stimulate bioerosion via an acidification effect (Schläppy *et al.*, 2007).

The removal and/or inhibition of the main photosymbiotic player in *C. orientalis* allowed examination of other nutrient cycles that are linked to photosynthesis. Ammonium is commonly excreted by sponges as a metabolic waste product (Hentschel *et al.*, 2012; Maldonado *et al.*, 2012), but the *Symbiodinium* community of *C. orientalis* "intercepts" and rapidly reassimilates ammonium (Chapter 3). This can also be seen in *Cliona varians* and in various Cnidarian hosts (Corredor *et al.*, 1988; Wang and Douglas, 1998; Rädecker *et al.*,

2015). Our control sponges demonstrated net uptake of ammonium, likely because photosynthesis provided the necessary energy and carbon substrates to accept ammonium ions and produce amino acids, potentially through the costly glutamine synthetase/glutamate synthase (GOGAT) pathway of *Symbiodinium* (Muscatine and D'Elia, 1978; Rahav *et al*., 1989; Foyer *et al.*, 2003). Accordingly, with loss of *Symbiodinium* and/or their photosynthetic ability, ammonium was no longer taken up by day or by night, and a net excretion was measured, as previously shown in bleached or DCMU-exposed symbiotic corals (e.g. Muscatine *et al.*, 1979; Rahav *et al.*, 1989; Falkowski *et al.*, 1993).

In conclusion, the present study demonstrates that photosynthetic activity is a driver of bioerosion rates in photosymbiotic clionaid sponges, and that symbiont presence strongly supports the metabolic functioning of the holobiont on a diurnal basis. Further investigations of the photo-bleaching behaviour and thresholds of these understudied organisms can be performed, as demonstrated, with the aid of the photosystem II herbicide DCMU, and will advance understanding of their susceptibility to warming waters. With photosynthesis being crucial to the metabolic needs of photosymbiotic clionaids, their ecological prevalence may depend on the continued maintenance of a functional mutualism with co-evolved symbionts (Achlatis *et al*., 2017; Fang *et al*., 2018a). Animal-photosymbiont associations on tropical coral reefs have exploited solar energy to power decalcification as well as calcification for millions of years, yet this energetic benefit comes with the price of an increased vulnerability to the abrupt environmental changes accompanying current and projected shifts in global climate.

Chapter 3

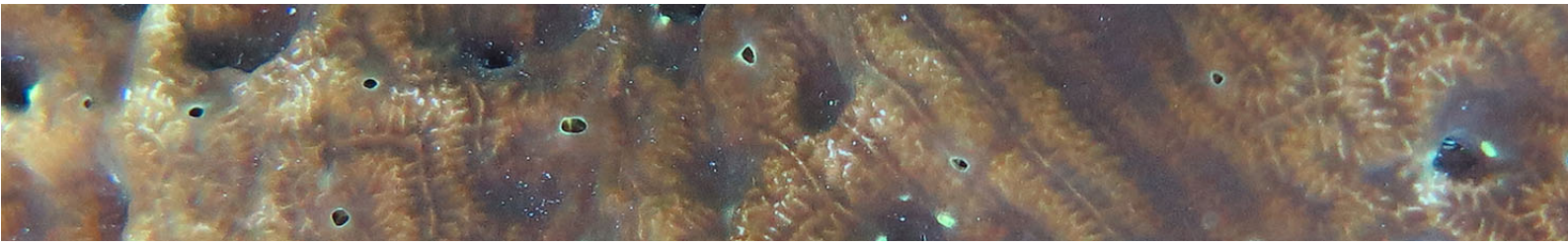

Single-cell measurement of ammonium and bicarbonate uptake within a photosymbiotic bioeroding sponge

Published as: Achlatis M, Pernice M, Green K, Guagliardo P, Kilburn MR, Hoegh-Guldberg O, Dove S. (2018). Single-cell measurement of ammonium and bicarbonate uptake within a photosymbiotic bioeroding sponge. *ISME J* **12**: 1308-1318.

Abstract

Some of the most aggressive coral-excavating sponges host intracellular dinoflagellates from the genus *Symbiodinium*, which are hypothesized to provide the sponges with autotrophic energy that powers bioerosion. Investigations of the contribution of *Symbiodinium* to host metabolism and particularly inorganic nutrient recycling are complicated, however, by the presence of alternative prokaryotic candidates for this role. Here, novel methods are used to study nutrient assimilation and transfer within and between the outer-layer cells of the Indo-pacific bioeroding sponge *Cliona orientalis*. Combining stable isotope labelling, transmission electron microscopy (TEM) and nanoscale secondary ion mass spectrometry (NanoSIMS), we visualize and measure metabolic activity at the individual cell level, tracking the fate of ^{15}N-ammonium and ^{13}C-bicarbonate within the intact holobiont. We found strong uptake of both inorganic sources (especially ^{13}C-bicarbonate) by *Symbiodinium* cells. Labelled organic nutrients were translocated from *Symbiodinium* to the *Symbiodinium*-hosting sponge cells within 6 hours, and occasionally to other sponge cells within 3 days. By contrast, prokaryotic symbionts were not observed to participate in inorganic nutrient assimilation in the outer-layers of the sponge. Our findings strongly support the metabolic interaction between the sponge and dinoflagellates, shedding light on the ecological advantages and adaptive capacity of photosymbiotic bioeroding sponges in oligotrophic marine habitats.

3.1. Introduction

Coral reefs are among the most productive and biodiverse ecosystems, and are the result of a fragile balance between accretion of calcium carbonate by calcifying organisms, and its loss by physical, chemical or biological erosion (bioerosion). At the heart of reef accretion is the mutualistic symbiosis between scleractinian corals and dinoflagellates of the genus *Symbiodinium* (Muscatine, 1990; Gattuso *et al.*, 1999). Interestingly, *Symbiodinium* have also been linked to the opposite side of the carbonate balance, potentially powering the activities of a prominent group of bioeroding sponges from the genus *Cliona* (Rosell and Uriz, 1992; Hill, 1996; Schönberg, 2006; Weisz *et al.*, 2010).

Bioeroding sponges contribute substantially to the excavation of coral skeletons, accounting often for 40-70% and up to >90% of macroborer activity on coral reefs (Schönberg *et al.*, 2017b). They chemically etch and mechanically remove calcium carbonate ($CaCO_3$) chips from the skeletons of organisms such as corals (Pomponi, 1980; Zundelevich *et al.*, 2007), adopting an endolithic lifestyle that often results in the death of the calcareous host (Glynn,

1997; Schönberg, 2000). The photosymbiotic *Cliona viridis* species complex consists of competitive and fast-spreading bioeroding sponges that host intracellular *Symbiodinium* in archaeocyte-like cells of the sponge pinacoderm (or outer layer) where light levels are highest (Vacelet, 1981; Rutzler, 1990). This symbiosis is hypothesized to explain observations of enhanced growth and bioerosion rates in the light (Rosell & Uriz, 1992; Hill, 1996; Schönberg, 2006; Fang *et al.*, 2016b). Besides *Symbiodinium,* photosymbiotic clionaids belong to the "low microbial abundance" sponges, harbouring sparse prokaryotic communities in their mesohyl, typically to a similar concentration as in the surrounding seawater (Gloeckner *et al.*, 2014; Poppell *et al.*, 2014). "High microbial abundance" sponges on the contrary can host communities that are 2-4 orders of magnitude more concentrated (Hentschel *et al.*, 2006). In addition, these clionaid prokaryotic communities are perhaps phylogenetically less diverse in comparison to those of other sponge holobionts (i.e. the collective community of the host and its microbial symbionts) (Poppell *et al.*, 2014; Thomas *et al.*, 2016).

The presence of a small prokaryotic community complicates definitive attribution of metabolic involvement by *Symbiodinium* in host performance, despite evidence that seawater spiked with $NaH^{13}CO_3$ leads to initial ^{13}C enrichment of the pinacoderm of *Cliona varians* followed by translocation to the choanosome (or inner layer that contains sponge choanocytes) (Weisz *et al.*, 2010). The complication is driven by the observations that: (1) the marine sponge literature strongly supports a metabolic role for intracellular (or intercellular) prokaryotic communities in the fixation of inorganic carbon and transfer of glycerol or small organic phosphates for host growth and reproductive capacity (Wilkinson, 1979; Usher, 2008; Poppell *et al.*, 2014); and, (2) it appears that it is microbial identity, not quantity, that determines the quantity of organic carbon translocated to sponge hosts with some photo-autotrophic cyanobacteria found not to translocate fixed products to their host (Freeman *et al.*, 2013; Thacker, 2005; López-Legentil *et al.*, 2008).

Attributing assimilation of inorganic nitrogen to *Symbiodinium* within a clionaid holobiont is likewise complicated by multiple potential candidates for this role. Freshly isolated *Symbiodinium* avail themselves of inorganic and organic forms of nitrogen (D'Elia *et al.*, 1983), and within a coral host *Symbiodinium* acquire ammonium [mainly through the glutamine synthetase/ glutamate synthase (GS/GOGAT) pathway (Rahav *et al.*, 1989)] or nitrate from the seawater surrounding their host (Kopp *et al.*, 2013). Prokaryotic symbionts, however, are also associated with moderating nitrogen availability within sponges (Fan *et al.*,

2012; Fiore *et al.*, 2010). For example, some assimilate ammonium into glutamate via the GS/GOGAT pathway, and this assimilation proceeds irrespective of the presence of autotrophic-eukaryotic symbionts such as diatoms (Hentschel *et al.*, 2012; Fiore *et al.*, 2015; Moitinho-Silva *et al.*, 2017). At the same time, the enzyme glutamate dehydrogenase (GDH) provides an alternate pathway for converting ammonium into amino acids, leading to the conclusion that a range of invertebrate phyla also have the capacity to directly assimilate inorganic nitrogen (Bender, 1985; Lee *et al.*, 1999; Hansen and Moran, 2011; Pernice *et al.*, 2012). In Porifera, genomic domains of GDH and GS are putative (Srivastava *et al.*, 2010), with evidence of GS expression in a clionaid sponge (Riesgo *et al.*, 2014). Whilst to date there is no evidence for a GOGAT enzyme in sponge genomes (see Supplementary Table S3.1 in the Appendix), it is nonetheless possible that sponge cells, that are not evolutionarily far removed from a Protist origin (King *et al.*, 2008), can directly assimilate ammonium via GDH.

While a metatranscriptomic analysis in the diatom harbouring sponge *Cymbastela concentrica* revealed the functional potential of the diatoms in terms of carbon (fixed through photosynthesis) and nitrogen (assimilated or produced) contributed to other members of the holobiont (Moitinho-Silva *et al.*, 2017), similar studies are lacking in bioeroding sponges. Here, we use the prominent Indopacific bioeroding sponge *Cliona orientalis* as a model system to examine the realized rather than potential metabolic contributions of the host and symbiont community to holobiont energetics, and to assess the ability of such sponges to directly assimilate inorganic carbon (as bicarbonate) and nitrogen (as ammonium). Following a pulse-chase experiment, we capitalized on the integration of isotopic labelling, transmission electron microscopy (TEM) and nanoscale secondary ion mass spectrometry (NanoSIMS) to detect *in situ* metabolic activity at the subcellular level while targeting cell types of interest (e.g. Musat *et al.*, 2012; Pernice *et al.*, 2012; Pernice and Levy, 2014; Kopp *et al.*, 2013). We quantitatively and qualitatively mapped the uptake, assimilation and distribution of the isotopically labelled materials over time at the single-cell level of the outer sponge layer, exploring whether the dinoflagellates form the primary site of inorganic assimilation into organic material, and whether this assimilated material is subsequently translocated to sponge cells.

3.2. Materials and Methods

Collection and maintenance of sponges

Cliona orientalis sponges in encrusting "beta" morphology (Schönberg *et al*, 2017a) were collected at 5m depth at Tenements 2 (151.9302°E, 23.4326°S), Heron Reef slope, Great Barrier Reef in February 2016. To standardize the specimen size, cylindrical cores of 35 mm in diameter were extracted using a circular pneumatic drill from 7 different individuals. The species identity was confirmed upon examination of the sponge spicules under the light microscope (Schönberg, 2000). The sponge cores were transferred to the outdoor flow-through seawater system at the Heron Island Research Station for 2 weeks of healing, and were then randomly distributed to three experimental aquaria (40L each) and acclimated for 10 days. The aquaria and lids were covered with Marine Blue 131 light filters (Lee Filters, Andover, UK) to mimic the typical light spectrum of the collection depth (Sampayo *et al.*, 2016). Over the duration of the experiment noon irradiance was 520 ± 73 µmol quanta m^{-2} s^{-1} and noon temperature was 27.2 ± 0.3 ºC in the experimental tanks (mean ± SD measured by Odyssey and HOBO Pendant loggers).

Pulse-chase labelling experiment

To examine the assimilation of inorganic nitrogen and carbon within the holobiont, sponge cores were exposed to a labelling treatment with isotopically enriched artificial seawater (Supplementary Fig. S3.1). The seawater contained enriched ammonium chloride powder ($^{15}NH_4Cl$, ^{15}N isotopic abundance of 98%) and enriched sodium bicarbonate powder ($NaH^{13}CO_3$, ^{13}C isotopic abundance of 99%) to a final concentration of 5µM and 2mM respectively. The $^{15}NH_4Cl$ concentration was based on ecological [summer concentrations of 0.9-9.1µM NH_4^+ at the Heron reef slope (Staunton Smith and Johnson, 1995) and NH_4^+-rich pulses frequently contributed by reef fish (Meyer and Schultz, 1985)] and methodological relevance (same concentration used by Pernice *et al.*, 2014). Both powders were supplied by Sigma Castle Hill, NSW, Australia and the enriched treatment was prepared according to Pernice *et al.* (2014). The sponge cores were incubated over a 6h pulse (starting at 06:30 am) in three independent closed-water chambers filled to 3L and equipped with a small wave maker. Each chamber was partially submerged into the 40L aquaria, which served as water baths for temperature regulation, and was covered by the aquarium lid. After the pulse phase (0h to 6h), labelled cores were moved back to the natural flow-through seawater of the 40L aquaria (without exposing them to air) for the chase phase (6h to 72h). Sponge replicates were randomly sampled at t=0h, 6h and 72h respectively. Background enrichment levels were

determined at t=0h from sponges in non-enriched artificial seawater containing $^{14}NH_4Cl$ and $NaH^{12}CO_3$ powder to the same concentration as the labelling treatment. Sampled sponge cores were vertically halved, the first half being snap-frozen and stored at -80°C for *Symbiodinium* extractions, and *Symbiodinium*-rich sponge material from the upper surface of the second half being fixed for further TEM and NanoSIMS analysis.

Sample fixation and TEM analysis

$CaCO_3$ from the coral substrate was carefully removed to isolate intact sponge material, remove non-assimilated inorganics, and embed the samples for TEM (details in Supplementary Methods in the Appendix). Sponges were cut into 120nm sections using an Ultracut UC6 microtome (Leica Microsystems, Australia). Selected sections were stained with uranyl acetate and lead citrate on finder grids (Electron Microscopy Sciences, Hatfield, PA, USA) and viewed at 80kV accelerating voltage using a JEOL 1011 Transmission Electron Microscope at the Centre for Microscopy and Microanalysis (University of Queensland, Brisbane). Sponge regions (approx. 35 x 35 µm) of high-embedment quality that contained cellular structures of interest (I, II and III defined below) were identified and marked on a separate digital map of the grid so that they could be located by the instrument camera during the NanoSIMS analysis.

NanoSIMS analysis

In order to examine the ^{15}N and ^{13}C organic enrichment in the sponge holobiont over time and space, the selected regions of the same sections were imaged with a NanoSIMS ion probe (NanoSIMS 50, CAMECA, Paris, France) at the Centre for Microscopy, Characterisation, and Analysis (University of Western Australia, Perth) using methodology previously established in Cnidaria (Supplementary Methods in the Appendix) (Pernice *et al.*, 2012, 2014; Wangpraseurt *et al.*, 2015). Analysis of the NanoSIMS results (Fig. 3.1) focused on three areas of interest (AOI) all within the outer sponge layer, namely (I) *Symbiodinium* cells (typical diameter 7-10 µm), (II) surrounding cytoplasm of the host archaeocyte-like cells that contain *Symbiodinium* (selections of approximately 5 µm in diameter), hereafter termed *Symbiodinium*-hosting cells, and (III) random selections of unidentified sponge or microbial cells and intercellular space of the mesohyl matrix in the same field of view as the *Symbiodinium* cells (diameter 5µm) (Fig. 3.1b,f,j and 3.2a). *Symbiodinium*-hosting cells were not observed to host other microorganisms, which were overall sparse in the examined sponge layer. In total we analysed 5 individual sponges, with on average 6 raster regions containing 70 AOI per sponge (see Supplementary Table S3.2 for details). Consulting the

corresponding TEM images, all AOI were drawn onto the $^{12}C^{14}N^-$ maps which do not display the enrichment levels for an unbiased selection. Once the $^{15}N/^{14}N$ and $^{13}C/^{12}C$ ratio maps were obtained (Fig. 3.1c,g,k and d,h,l), the AOI were superimposed on the NanoSIMS maps allowing extraction and quantification of the mean $^{15}N/^{14}N$ and $^{13}C/^{12}C$ ratios of the selected cells. Enrichments levels were expressed using delta notations ($\delta^{15}N$ and $\delta^{13}C$ in ‰) as follows:

$$\delta^{15}\mathrm{N} = \left(\frac{N_{mes}}{N_{nat}} - 1\right) \times 10^3$$

$$\delta^{13}\mathrm{C} = \left(\frac{C_{mes}}{C_{nat}} - 1\right) \times 10^3$$

where N_{mes} is the $^{15}N/^{14}N$ ratio measured in labelled sponges and N_{nat} is the natural $^{15}N/^{14}N$ ratio measured in AOI of non-labelled control sponge samples. Similarly, C_{mes} is the $^{13}C/^{12}C$ ratio measured in the AOI of the labelled sponges and C_{nat} is the natural $^{13}C/^{12}C$ ratio. Using the same NanoSIMS methodology and resolution, enriched prokaryotic cells have been detected in the *C. orientalis* choanosome after a pulse of organic compounds (Achlatis *et al*., unpublished data), demonstrating the capacity of the current methodology to detect enrichment of cells that are more than 10-fold smaller than *Symbiodinium*. After the enrichment levels were determined, enriched versus non-enriched AOI were distinguished for each time-point and their proportions as fractions of the measured AOI population were determined. Only the enriched AOI were considered when calculating mean enrichment levels.

Symbiodinium-specific ^{15}N-ammonium and ^{13}C-bicarbonate uptake rates

Since uptake by *Symbiodinium* was found to be dominant (see Results), the sponge material of the remaining halves of the cores was used to determine the surface areas of the sponge, the *Symbiodinium* population density and the nitrogen and carbon content of the *Symbiodinium* fraction as detailed in the Supplementary Methods in the Appendix. These parameters were then used to determine the ammonium and bicarbonate assimilatory capacity of the dinoflagellate symbionts.

Statistical analysis

Statistical analyses were done in Primer v6 (Clarke and Gorley, 2006) with permutational analysis of variance (PERMANOVA) add-on. PERMANOVA is a semiparametric test that

offers both the flexibility of distribution-free tests and the partitioning to analyse complex designs while considering interaction terms (Anderson *et al*., 2008). While typically used in multivariate approaches, it provides useful tools for univariate datasets (Anderson *et al*., 2008) generated by low-throughput methods, such as NanoSIMS (Musat *et al.*, 2012; Gao *et al.*, 2016). The pseudo-*F* statistic was derived from dissimilarity matrices constructed with Euclidean distance and the $P_{(perm)}$ value was based on 4999 permutations under a full model using type III sums of squares to account for the unbalanced design. A two-factor design with Treatment (Pre-pulse t=0h, Post-pulse t=6h and Post-chase t=72h) and AOI [(I), (II), (III)] was used to test for differences in ^{15}N or ^{13}C enrichment levels of each AOI over time, and between the AOI of each time-point. Pairwise post-hoc comparisons were conducted using permutational pseudo-*t* tests when significant factor effects were found. Detailed statistical outputs are given in Supplementary Table S3.3. For each AOI type, two-proportion z-tests (Fleiss *et al.*, 2003) computed in Statistica v13 (Dell, California, USA) were used to compare a) the proportion of enriched AOI at t=6h to the proportion enriched at t=72h for both nitrogen and carbon and b) the proportion of ^{15}N-enriched cells to that ^{13}C-enriched cells and both t=6h and t=72h (Supplementary Table S3.4). Throughout the paper, results are considered significant at the $p<0.05$ level.

3.3. Results and Discussion[2]

Single-cell enrichments through NanoSIMS analysis

The NanoSIMS analysis detected nitrogen and carbon enrichment in the sponge and/or symbiont cells on thin surface planes, allowing for visualization of the enrichment levels in the intact holobiont (Fig. 3.1). The enrichment images were compared to the TEM images of the same sponge areas and therefore the corresponding cell structures were accurately identified (Fig. 3.1a,e,i). The isotopic ratios ($^{15}N/^{14}N$ and $^{13}C/^{12}C$) were separately measured and compared to natural abundance ratios of unlabelled control samples for each area of interest (AOI, Fig. 3.3a; individual values in Supplementary Table S3.2).

The nitrogen enrichment levels of the examined AOI differed between the treatment time-points (Pseudo-F=4.483, $P_{(perm)}=0.032$). Dinoflagellate cells present in the outer layer of the sponge displayed a substantial ^{15}N-enrichment of 1416 ± 360‰ (mean ± SEM) after the 6h pulse of enriched seawater [pair-wise comparison between pre-pulse samples and treated samples at t=6h (abbreviated hereafter as "t=0h versus t=6h"), $P_{(perm)}<0.001$, Fig. 3.3a].

[2] Results and Discussion are merged in this Chapter as in the published article.

During the chase over the next 3 days, dinoflagellates remained enriched at an enrichment

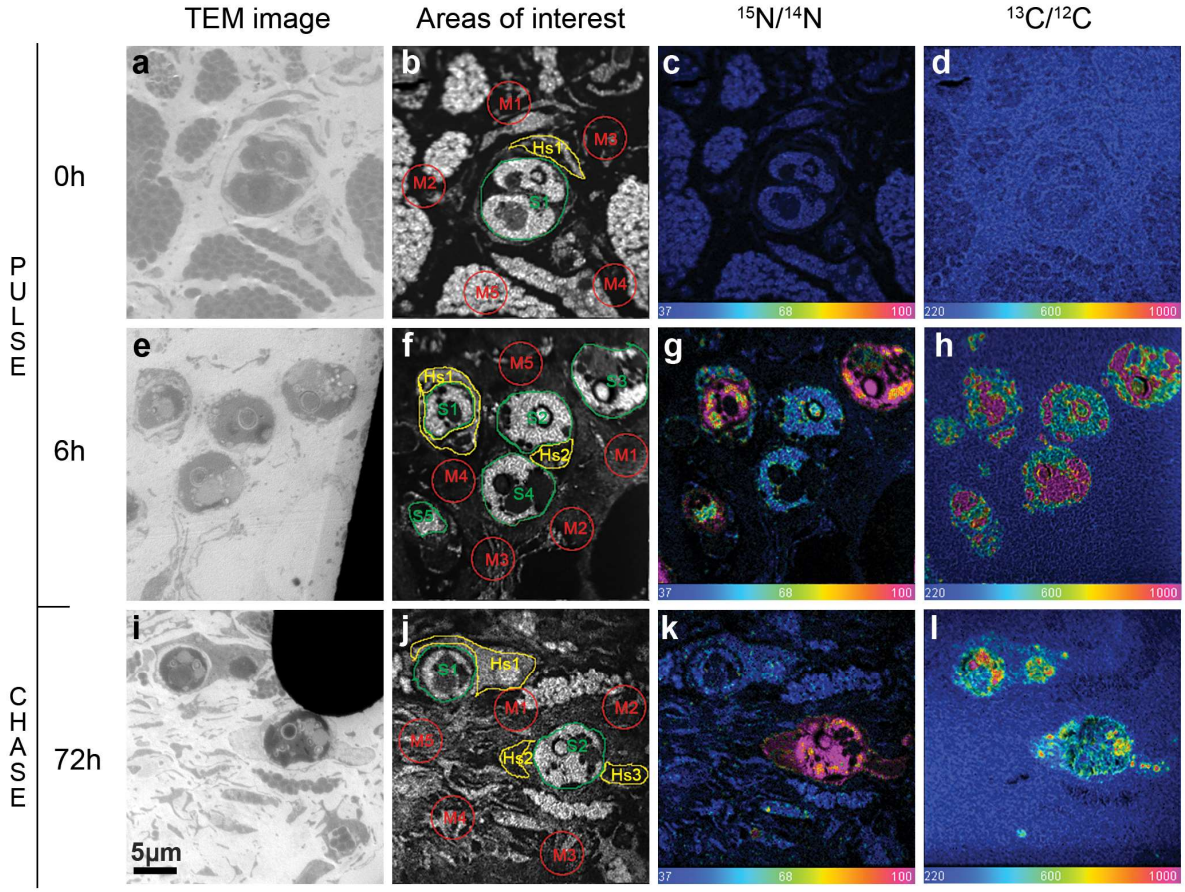

Figure 3.1: Visualization of ^{15}N-ammonium and ^{13}C-bicarbonate assimilation in the photosymbiotic bioeroding sponge holobiont *Cliona orientalis*, with a focus on the resident dinoflagellates of the genus *Symbiodinium*. **(a, e, i)** TEM images of three selected holobiont samples before the addition of label (t=0h), at the end of the pulse period (t=6h) and at the end of the chase period (t=72h). **(b, f, j)** NanoSIMS $^{12}C^{14}N^-$ image displaying the selection of the areas of interest (AOI) for enrichment quantification: (I) *Symbiodinium* (in green, S, total measured n=113), (II) Cytoplasm of *Symbiodinium*-hosting sponge cells (in yellow, Hs, n=82) and (III) nearby mesohyl cells and intercellular space (in red, M, n=150) (see also Fig. 3.2a). **(c, g, k)** Distribution of $^{15}N/^{14}N$ ratio and (d, h, l) of $^{13}C/^{12}C$ ratio over the same selected areas as obtained through NanoSIMS analysis at each of the three time-points. The images show the deviation of the ratios from the natural abundance ratio, using a rainbow scale in hue saturation intensity. The rainbow scale ranges from natural abundance in blue (0.0037 for $^{15}N/^{14}N$ and 2x 0.0110 for $^{13}C/^{12}C$) to several-fold enrichment above natural abundance in red (approx. 3-fold for $^{15}N/^{14}N$ and 5-fold for $^{13}C/^{12}C$). Heterogeneity in label incorporation is exemplified by **(k)** and **(l)**, where *Symbiodinium* cell S1 that was measured simultaneously to *Symbiodinium* cell S2 shows disproportionately low nitrogen uptake in comparison to carbon. Individual isotopic ratios per AOI are given in the Supplementary Table S3.2.

level of 667 ± 224‰ (t=0h versus t=72h, $P_{(perm)}$=0.012). The dinoflagellates hosted within *Cliona orientalis* cells are thus able to rapidly absorb and assimilate ammonium from the surrounding seawater, as known for coral dinoflagellates where ammonium is the preferred

source of dissolved inorganic nitrogen due to its ease of access and uptake *in hospite* (Grover *et al.*, 2008; Pernice *et al.*, 2012, 2014; Kopp *et al.*, 2013). In the sponge, water movement through the canal network may allow for the rapid diffusion of ammonium to the intracellular dinoflagellates, possibly stimulated by photosynthetic energy during the pulse phase (Leys *et al.*, 2011; Strehlow *et al.*, 2016a). During photosynthesis, the profusion of energy and carbon compounds as acceptors for ammonium ions may facilitate direct incorporation of ammonium into amino acids potentially through the efficient yet energetically-demanding GS/GOGAT pathway (Muscatine and D'Elia, 1978; Rahav *et al.*, 1989; Foyer *et al.*, 2003). Intriguingly, the *Symbiodinium*-rich pinacoderm also directly takes up particulate organic nitrogen (shown in *Cliona varians* by Weisz *et al.*, 2010).

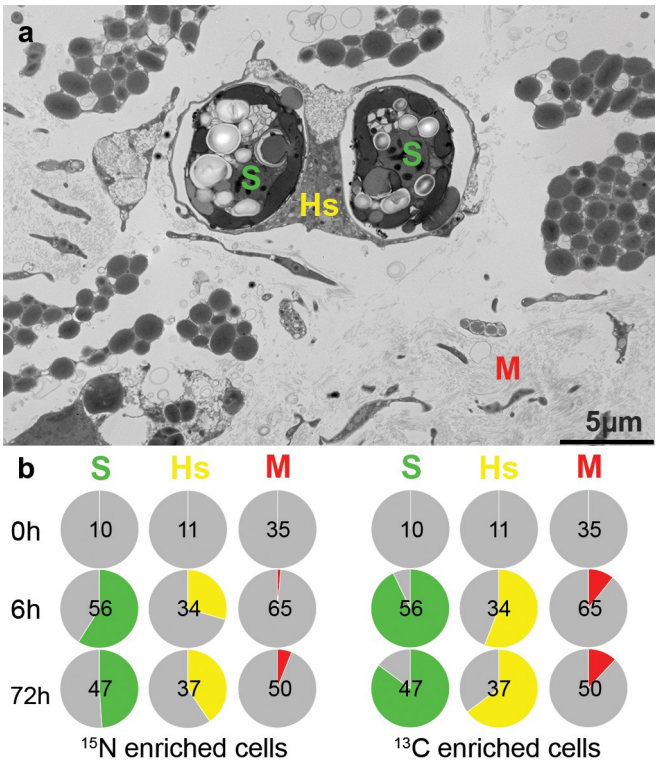

Figure 3.2: Distribution of ^{15}N and ^{13}C enriched and non-enriched cells of three cellular structures of interest in the bioeroding sponge holobiont *Cliona orientalis*, with a focus on its resident dinoflagellates of the genus *Symbiodinium*. **(a)** TEM displaying examples of the cellular areas of interest (AOI) examined: (I) *Symbiodinium* (in green, S), (II) *Symbiodinium*-hosting sponge cells (in yellow, Hs) and (III) nearby mesohyl cells and intercellular material (in red, M). **(b)** Pie-charts illustrating the distribution of ^{15}N and ^{13}C enriched and non-enriched cells for each of the AOI displayed in **(a)** as obtained from NanoSIMS quantification. The numbers on the pie charts correspond to the AOI replicates (n=…) analysed at each timepoint.

The carbon enrichment levels also differed between the treatment time-points, but the response depended on the AOI in question (2-way interaction, Pseudo-F=5.052, $P_{(perm)}$= 0.001). As expected, ^{13}C-bicarbonate was taken up rapidly by the photosynthetic

dinoflagellates, which displayed an organic enrichment of 2172 ± 272‰ at t=6h (Fig. 3.3b, t=0h versus t=6h, $P_{(perm)}$<0.001). At the end of the chase (t=72h), the enrichment had dropped significantly to 1055 ± 116‰ (t=0h versus t=72h, as well as between t=6h and t=72h, all $P_{(perm)}$<0.001). At both time-points, carbon enrichment was strongest in the dinoflagellates compared to the two other AOI (pair-wise comparisons between the three AOI at t=6h and at t=72h, all $P_{(perm)}$<0.01 and $P_{(perm)}$<0.05 respectively). The nitrogen and carbon enrichments found are comparable if not higher to enrichment previously found in clade C *Symbiodinium* of a symbiotic coral that was incubated in the same concentrations of the same sources (Pernice *et al.*, 2014), when the different incubation times are taken into account (48h labelling pulse for the coral versus 6h pulse in the current experiment).

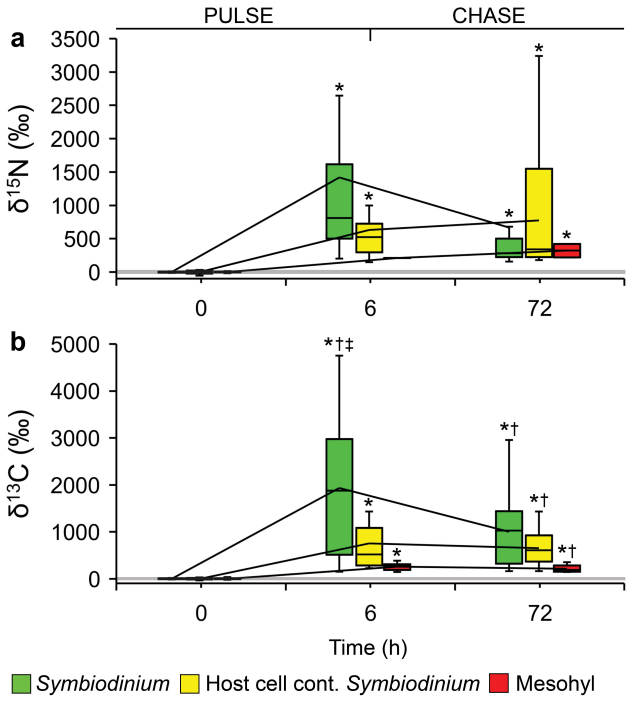

Figure 3.3: Quantification of (a) nitrogen and (b) carbon assimilation in enriched host and symbiont cells of the bioeroding sponge *Cliona orientalis* in response to a pulse of seawater enriched in ^{15}N-ammonium and ^{13}C-bicarbonate. Through NanoSIMS isotopic analysis, the mean ^{15}N and ^{13}C enrichments were quantified in three areas of interest (AOI): (I) *Symbiodinium* (in green), (II) Cytoplasm of *Symbiodinium*-hosting sponge cells (in yellow) and (III) nearby mesohyl cells and intercellular space (in red). Individual values are given in Supplementary Table S3.2. Significant differences ($P_{(perm)}$<0.05) are marked between t=0h and enriched samples (*), between enriched samples from t=6h to t=72h (‡) and between different AOI within the same time-point (†) (Supplementary Table S3.3). The grey lines and their width depict the range of the natural ^{15}N **(a)** and ^{13}C levels **(b)** measured in control unlabelled sponges (δ^{15}N = 0 ± 30‰ and δ^{13}C = 0 ± 35‰). The box-whisker plots display the data in quartiles, with the bottom of the box corresponding to the 25th percentile, the line within the box marking the median and the top of the box corresponding to the 75th percentile. The black lines outside the

boxes connect the means of the time-points to each other, but the median and frequency distribution allow for a clearer depiction of the data variability.

The isotopic ratios of the cytoplasm of *Symbiodinium*-hosting cells revealed a less strong ^{15}N-enrichment at t=6h (631 ± 167‰) (t=0h versus t=6h, $P_{(perm)}$<0.001, Fig. 3.3a), and showed high variability at t=72h (773 ± 235‰) (t=0h versus t=72 h, $P_{(perm)}$= 0.012). Similarly, these cells were enriched in carbon, with enrichment ranging from 750 ± 153‰ at t=6h to 653 ± 65‰ at t=72h (t=0h versus t=6h and t=72h, both $P_{(perm)}$<0.001, Fig. 3.3b). At t=72h, the ^{13}C-enrichment level of the *Symbiodinium*-hosting cells was higher than that of mesohyl material (pair-wise comparisons between the two AOI at t=72h, $P_{(perm)}$=0.0028).

Mesohyl areas near *Symbiodinium* were scarcely enriched in nitrogen throughout the experiment, with at most 6% strongly enriched at t=72h (t=0h versus t=72h, $P_{(perm)}$=0.012, Fig. 3.2b and 3.3a). Mesohyl areas were more frequently enriched in carbon (~12% of the mesohyl AOI, Fig. 3.2b, with enrichment levels stable at approx. 250 ± 31‰ (t=0h versus t=6h and t=72h, both $P_{(perm)}$<0.001, Fig. 3.3b). All enriched mesohyl material (both for nitrogen and carbon) was of host origin and no enriched prokaryotes were observed under the present experimental conditions, indicating that these sparse microorganisms most likely don't have an active role or at least have a lesser role in ammonium and bicarbonate assimilation in the outer layer of this sponge species.

Invertebrate hosts such as clams, jellyfish and sponges may infrequently digest their symbionts when under stress (Rosell, 1994; Hill and Hill, 2012; Strehlow *et al.*, 2016b), yet here the dinoflagellate cell membranes and thylakoids of the examined cells appeared intact and without signs of digestion throughout the experiment. Given the lack of evidence of algal digestion, we argue that in the present case the NanoSIMS quantification supports translocation of both nitrogen and carbon compounds incorporated by the dinoflagellates to the host cells that contain the dinoflagellates for a number of reasons: For nitrogen specifically, translocation is evident because only the hosting cells that contained enriched *Symbiodinium* were found to be enriched in nitrogen, and no other sponge cells took up ammonium during the pulse phase of the experiment. For carbon, since there are no pathways of direct inorganic carbon assimilation in animal cells, we suggest that bicarbonate was incorporated into photosynthates by *Symbiodinium* (Trench, 1993) and was then transported or leached out into the cytoplasm of the *Symbiodinium*-hosting cell. Already at 6h, one third of *Symbiodinium*-hosting cells were enriched in nitrogen and almost twice as many were enriched in carbon (Fig. 3.2b, two-proportions test, p=0.027). At each time-point,

dinoflagellates enriched in nitrogen and/or carbon were in approx. 70% of the cases hosted by enriched sponge cells i.e. translocation was a common phenomenon. Furthermore, *Symbiodinium*-hosting cells were never enriched unless they hosted an enriched dinoflagellate, which provides additional evidence for the autotrophic origin of the enrichment. The most parsimonious explanation for both tracers would be that translocation to the *Symbiodinium*-hosting cells already started during the 6h pulse, rendering further translocation during the chase phase less pronounced.

In other symbiotic invertebrates such as Cnidaria and tridacnid clams, translocation of amino acids and photosynthates (principally glucose but also glycerol and organic acids) from *Symbiodinium* to non-*Symbiodinium*-hosting cells is well-established (Wang and Douglas, 1998; Yellowlees *et al.*, 2008; Burriesci *et al.*, 2012). In the porous sponge body that is subject to constant water flow, it is more likely that enrichment signals may weaken over large surface areas away from the uptake site as compounds are processed by cellular metabolism and/or indirectly transferred to other cells through the mesohyl. However, the relatively low translocation we observed in non-*Symbiodinium*-hosting cells may also indicate that nitrogen or carbon-derived compounds are rapidly consumed to support basal metabolic rates, or are not used for host growth (and/or metabolism) in the outer sponge layer within the first 72-hours after capture. Instead, the compounds may serve as a direct source to the amoeboid *Symbiodinium*-hosting cells: these cells have a high metabolic demand since they purportedly migrate vertically in the sponge body on a daily basis, transporting the symbiont to deeper layers at night to protect them from sponge predators and back to the surface by day for energy capture via photosynthetic activity (Schönberg and Suwa, 2007). It is unclear how the symbiont migration is controlled; potentially, all the symbiont energy is burnt in the migration and hence symbiont cells may have "hijacked" host cells to improve their photosynthetic ability, without necessarily contributing to other energetically expensive activities of the host. Alternatively, this migration simultaneously serves for transportation of fixed materials to deeper layers of the host (e.g. translocation of carbon to the choanosome as shown by Weisz *et al.*, 2010) not examined here.

The little nitrogen mesohyl enrichment that we found was only present during the chase phase (Fig. 3.3a), again implicating an indirect uptake of the enriched material through translocation. Symbiotic invertebrates are also able to directly assimilate ammonium (e.g. shown by Pernice *et al.*, 2012 under 20µM $^{15}NH_4Cl$), yet our results suggest that such a pathway was not generally active in the sponge under the experimental conditions. The

ammonium concentration during the pulse (5µM) may have favoured GS/GOGAT pathways of *Symbiodinium* over GDH of the host; the latter pathway requires less energy yet higher ammonium loads due to lower ammonium affinity (Harper *et al.*, 2008), which could imply a slower response time for direct assimilation by host cells. If the mechanism of ammonium assimilation is concentration-dependent (Kopp *et al.*, 2013), it would be of interest to determine whether a higher ammonium spike would lead to greater/faster activation of potential animal GDH. Under oligotrophic conditions, it appears that the dinoflagellates are chiefly responsible for incorporation of ammonium potentially into uric acid, urea or amino acids, as is the role of (prokaryotic) symbionts in other sponges (Kopp *et al.*, 2013; Fiore *et al.*, 2010, 2015; Moitinho-Silva *et al.*, 2017).

Heterogeneity in ^{15}N and ^{13}C enrichment

The incorporation of ^{15}N and ^{13}C was apparent in the majority of the dinoflagellates, yet some had incorporated one of the tracers only, or showed little incorporation of the tracers (Fig. 3.2b, Supplementary Table S3.4). This was particularly true for nitrogen, with enrichment in 59% of the *Symbiodinium* population measured after the 6h-pulse, as opposed to 93% of the population for carbon (two-proportions test, $p<0.0001$, $n=56$ cells). Although rates of carbon fixation by *Symbiodinium in hospite* do not appear to depend on nitrogen availability (Falkowski *et al.*, 1993), fixation products may differ; dinoflagellate cells enriched in carbon but not in nitrogen may imply production of sugars and lipids. We acknowledge that distinguishing between sugar/lipid and amino acid production (the latter being dependent on the nitrogen availability and therefore potentially stimulated by the provided pulse of ammonium) is beyond the scope of our study.

While part of the observed heterogeneity in isotopic enrichment could be linked to the orientation of the thin sectioning across specific subcellular structures of dinoflagellates (Pernice *et al.*, 2014), it is far too prevalent to be caused by sample bias or measurement noise only, especially since (i) it was occasionally observed in the same field of view (e.g. Fig. 3.1k,l) and (ii) each NanoSIMS analysis included several layers and was therefore representative of a few tens of nm depth in the cellular material. Alternatively, variability could be caused by intercladal or interspecies metabolic heterogeneity (Pernice *et al.*, 2014), but only one species of *Symbiodinium* (*S. endoclionum*; Ramsby *et al.*, 2017b) belonging to clade G (Schönberg *et al.*, 2005; Hill *et al.*, 2011) has so far been described in *Cliona orientalis*. Within a lineage, variability in nutritional strategies may arise due to different microenvironments inside the sponge body, divergent life histories or cell cycle stages (e.g.

dissipation of enrichment signals upon cellular division), or stochastic gene expression of cellular transporters or assimilation pathways amongst cells (Matantseva *et al.*, 2016). Ultimately, the cell-to-cell metabolic heterogeneity found within the *Symbiodinium* population (undetectable in bulk studies but revealed with NanoSIMS) may have important implications for stability and competitive advantage inside the host microenvironment, as shown for a number of microorganisms (Kaern *et al.*, 2005).

The NanoSIMS technique furthermore revealed spatial heterogeneity in ^{15}N and ^{13}C-enrichment within single *Symbiodinium* cells, in addition to that observed between cells. Subcellular enrichment hotspots are commonly observed in NanoSIMS analyses and they contribute to the large standard deviations produced for each per cell measurement (e.g. Pernice *et al.*, 2012, 2014). Similarly to coral dinoflagellates, this heterogeneity may reflect temporary storage of nitrogen in cytosolic crystalline structures (Kopp *et al.*, 2013) and carbon in intracellular lipid droplets and starch granules of the chloroplast pyrenoid or the cytosol (Kopp *et al.*, 2015).

***Symbiodinium*-specific ^{15}N-ammonium and ^{13}C-bicarbonate uptake rates**

During the 6h-pulse, *Symbiodinium* fixed nitrogen and carbon at specific uptake rates of 122 ± 32 ng N h^{-1} cm^{-2} and 7901 ± 853 ng C h^{-1} cm^{-2} respectively (Fig. 3.4). Variability in the duration and concentration of the labelling pulse makes it difficult to compare to existing NanoSIMS uptake rates, but our results fall in the same order of magnitude as previously reported for *Symbiodinium* in coral [504 ± 28 ng N h^{-1} mg^{-1} (standardized to mass of dinoflagellates) which is equivalent to 385 ± 21 ng N h^{-1} cm^{-2}; Pernice *et al.*, 2012] and for a free living dinoflagellate (~2 pg C h^{-1} $cell^{-1}$ which would be equivalent to 2816 ng C h^{-1} cm^{-2} in the sponge; Matantseva *et al.*, 2016). Despite rapid osmium post-fixation before rinsing and while avoiding acetone storage of the samples, low-molecular weight compounds that are soluble and poor in amino-groups may not always be successfully immobilized during the fixation protocol used in this study. Therefore, absolute uptake rates especially of bicarbonate represent mostly incorporation into macromolecules and may be an underestimate of the total uptake of the tracer.

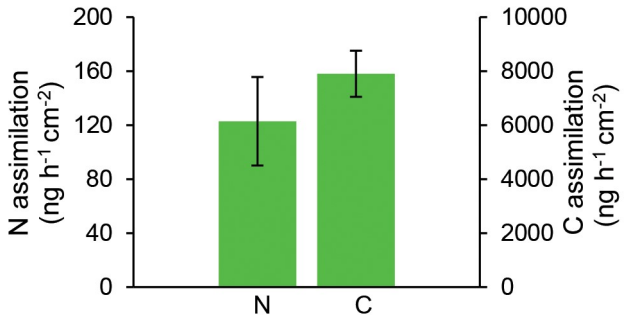

Figure 3.4: Single-cell nitrogen and carbon assimilatory capacity of the dinoflagellate symbionts residing in the bioeroding sponge *Cliona orientalis*. Assimilation was quantified in n=56 *Symbiodinium* cells with NanoSIMS after a 6h pulse of ^{15}N-ammonium and ^{13}C-bicarbonate enriched seawater. Cellular uptake rates were normalized to the average N or C content of the symbiont cells and the pulse time according to the calculations provided by Dugdale and Wilkerson (1986) and expressed per surface area of the sponge holobiont. Bars display mean ± SEM.

Ecological significance

Stimulation of bioerosion by light has been suggested for a number of photosymbiotic bioeroding species (Rosell & Uriz, 1992; Hill, 1996; Schönberg, 2006), including *C. orientalis* (Fang *et al.*, 2016b). Accordingly, the bioerosion rates of *C. orientalis* decrease after prolonged bleaching due to heat stress (Chapter 4) or after artificial inhibition of photosynthesis (Chapter 2). Our NanoSIMS results provide evidence of strong fixation of carbon and nitrogen by *Symbiodinium* in the light and transfer of carbon and nitrogen-compounds at least to specific cell types, but we did not examine potential translocation of these nutrients to the etching cells in deeper sponge layers. Although direct or indirect stimulation of bioerosion by *Symbiodinium*-harvested energy is most likely, we cannot exclude the potential that (auto)trophic bacteria deeper in the sponge (also) supply energy for etching. Future studies may clarify the abundance and function of prokaryotic symbionts or migrating *Symbiodinium* with regards to (chemo)autotrophic or non-photosynthetically-driven assimilation of nitrogen and carbon.

While calcifying corals are in decline worldwide (De'ath *et al.*, 2009; Hughes *et al.*, 2017), the prevalence and excavating activity of photosymbiotic bioeroding sponges has been observed to increase on disturbed reefs (Rützler, 2002; Schönberg and Ortiz, 2008). The upper thermal limit of the partnership between *Symbiodinium* and bioeroding sponges is considered higher than that of the respective scleractinian symbiosis, possibly enabling bioerosion to temporarily persist as global warming impairs rates of calcification (Fang *et al.*, 2014; Schönberg *et al.*, 2017b). Understanding the metabolic interaction between bioeroding

sponges and their symbiotic dinoflagellates will enhance projections of the response of bioeroding sponges and their excavating activity to warming, acidification and eutrophication of reef environments. This provides valuable insight into the competition dynamics between calcifying corals and decalcifying sponges, with important implications for the carbonate budgets of coral reefs.

In conclusion, we have provided imaging and quantification of nitrogen and carbon assimilation at the single-cell level in the bioeroding sponge *Cliona orientalis*, using NanoSIMS analysis in combination with TEM ultrastructural observations. In a novel application of NanoSIMS to (bioeroding) sponges, we provide a qualitative and quantitative baseline of the metabolic integration and translocation of nutrients within the outer layer of a sponge holobiont. In this regard, NanoSIMS is a powerful tool that bridges the functional potential of symbiotic partners to experimental evidence of realized metabolic pathways. The metabolism of carbon-containing photosynthates is well established in other symbiotic invertebrates and the fate of nitrogen-containing compounds is also being explored (Rädecker *et al.*, 2015); for both these pathways, we provide a reference description inside a less studied symbiosis. Our data show clear differences in the roles of the host and microbial cells, stressing the precedence of the dinoflagellate symbiont over prokaryotic symbionts in the outer layers of *C. orientalis* for the efficient uptake of inorganic nutrients in oligotrophic reef waters. All in all, our results provide new insights into how light-dependent symbioses in sponges enable both hosts and symbionts to function in microhabitats that would otherwise be unfavourable.

Chapter 4

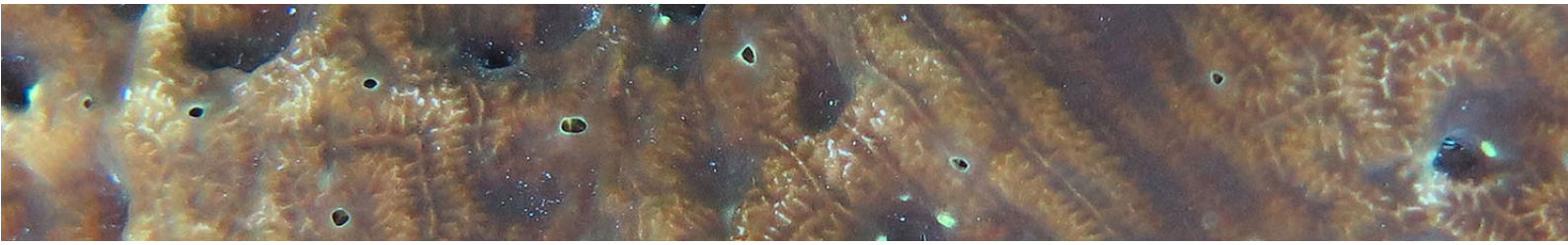

Sponge bioerosion on changing reefs: ocean warming poses physiological constraints to the success of a photosymbiotic excavating sponge

Published as: Achlatis M, van der Zande RM, Schönberg CHL, Fang JKH, Hoegh-Guldberg O, Dove S. (2017). Sponge bioerosion on changing reefs: ocean warming poses physiological constraints to the success of a photosymbiotic excavating sponge. *Sci Rep* **7**: 10705.

Abstract

Excavating sponges are prominent bioeroders on coral reefs that in comparison to other benthic organisms may suffer less or may even benefit from warmer, more acidic and more eutrophic waters. Here, the photosymbiotic excavating sponge *Cliona orientalis* from the Great Barrier Reef was subjected to a prolonged simulation of both global and local environmental change: future seawater temperature, partial pressure of carbon dioxide (as for 2100 summer conditions under "business-as-usual" emissions), and diet supplementation with particulate organics. The individual and combined effects of the three factors on the bioerosion rates, metabolic oxygen and carbon flux, biomass change and survival of the sponge were monitored over the height of summer. Diet supplementation accelerated bioerosion rates. Acidification alone did not have a strong effect on total bioerosion or survival rates, yet it co-occurred with reduced heterotrophy. Warming above 30°C (+2.7°C above the local maximum monthly mean) caused extensive bleaching, lower bioerosion, and prevailing mortality, overriding the other factors and suggesting a strong metabolic dependence of the sponge on its resident symbionts. The growth, bioerosion capacity and likelihood of survival of *C. orientalis* and similar photosymbiotic excavating sponges could be substantially reduced rather than increased on end-of-the-century reefs under "business-as-usual" emission profiles.

4.1. Introduction

To date approximately 30% of the anthropogenic carbon dioxide (CO_2) emissions have been absorbed by the oceans (IPCC, 2013). Since the beginning of the Industrial Revolution, ocean pH has decreased by 0.1 units (Raven *et al.*, 2005). In combination with ocean acidification, ocean warming caused by the CO_2-driven enhancement of the greenhouse effect, and eutrophication are threatening the distribution and abundance of coral reefs worldwide (Burke *et al.*, 2011; Hoegh-Guldberg *et al.,* 2014; Pörtner *et al.*, 2014). Projections conclude that these changes will reduce calcium carbonate ($CaCO_3$) accretion on reefs due to increased mortality and decreased calcification potential of reef-building organisms (Fabricius, 2005; Orr *et al.*, 2005; Kroeker *et al.*, 2013). Compared to calcification, responses of decalcification and especially biological erosion (bioerosion) to environmental change remain less well studied (Fang and Schönberg, 2015), even though bioerosion is of equal significance to the carbonate balance on coral reefs (Schönberg *et al.,* 2017a; 2017b).

Bioeroding taxa on coral reefs include internal bioeroders that excavate and inhabit $CaCO_3$ materials (e.g. certain poriferan, molluscan, annelid, algal, fungal and cyanobacterial genera) and external bioeroders (e.g. certain echinoderm, crustacean, molluscan and fish genera) (Glynn, 1997). As it is predominantly the internal bioeroders that employ chemical means to rework the substrate, and as they are mostly sessile, changes to seawater chemistry may be directly reflected in their bioerosion capacity (Schönberg *et al.,* 2017a). Attention on internal bioerosion has focused more specifically on coral-excavating sponges (Fang and Schönberg, 2015), which often account for 40-70% and up to >90% of macroborer activity on coral reefs (Schönberg *et al.*, 2017b and references therein). Excavating sponges influence seawater carbonate cycling and they play important ecological roles by breaking down and sculpting the reef framework, thereby changing the heterogeneity and availability of space (Schönberg *et al.*, 2017b). In contrast to many calcifiers, the abundance, activity and competitive vigour of certain excavating sponges has been observed to increase on perturbed reefs (e.g. Rützler, 2002; Schönberg and Ortiz, 2008; Marulanda-Gómez *et al.*, 2017; Kelmo *et al.*, 2013).

As excavating sponges are demosponges that have a siliceous skeleton, their skeletogenesis is unlikely to be as strongly impacted by carbonate saturation changes as that of calcifiers (Vicente *et al.*, 2016). However, ocean warming, acidification and eutrophication may still affect these sponges for several reasons. Sponge bioerosion proceeds through chemical etching of $CaCO_3$ chips, which purportedly involves acid regulation, followed by mechanical removal of the chips from the substrate (Pomponi, 1980; Zundelevich *et al.*, 2007). The energetic cost of chemical bioerosion may be reduced in more acidified oceans, as the $CaCO_3$ dissolution threshold will be more easily met (Wisshak *et al.*, 2012; Enochs *et al.*, 2015). As a result, bioerosion may be enhanced on future reefs (Hoegh-Guldberg *et al.*, 2007), as has been suggested after observing bioerosion patterns in $CaCO_3$ materials from naturally low-pH waters (Manzello *et al.*, 2008; Crook *et al.*, 2013; DeCarlo *et al.*, 2015; Silbiger *et al.*, 2016). Some dominant bioeroding sponges are aggressive space competitors capable of overgrowing living corals (López-Victoria *et al.*, 2006; González-Rivero *et al.*, 2011a), and reduced competitive pressure caused by increased weakness and mortality of corals may further elevate their abundances (Rützler, 2002; López-Victoria *et al.*, 2005; Schönberg and Ortiz, 2008; Carballo *et al.*, 2013). Moreover, bioeroding sponges are filter feeders with an efficient pumping system (Lynch and Phlips, 2000; Strehlow *et al.*, 2016) and they have been observed to thrive in eutrophic waters (Rose and Risk, 1985; Holmes, 1997; Ward-Paige *et al.*, 2005). Eutrophication may result in greater access to food and thereby increase energetic

availability, which may not only affect sponge abundances and growth, but may also increase their bioerosion rates (Holmes *et al.*, 2009).

Apart from their heterotrophic filter feeding, certain bioeroding sponges also benefit from photoautotrophic inputs provided by symbiotic dinoflagellates of the genus *Symbiodinium* (Weisz *et al.*, 2010). The *Cliona viridis* species complex consists of such species, which are very competitive and destructive to the $CaCO_3$ framework (Schönberg *et al*, 2017b). Presumably, this is due to the symbiosis providing greater access to energy and hence promoting greater sponge growth, survival and bioerosion (Rosell and Uriz, 1992; Hill, 1996; Schönberg, 2006). In comparison to corals, these sponges are also thought to be relatively resilient to *in situ* bleaching (Schönberg *et al.*, 2017b), which suggests that they are well-positioned to dominate newly available space should corals decline (Rützler, 2002; Schönberg and Ortiz, 2008; Marulanda-Gómez *et al.*, 2017).

The potential of increased bioerosion by excavating sponges in changing environments implies a growing threat to the three-dimensional framework of future reefs and the organisms that inhabit them (Bozec *et al.*, 2015). However, the physiological limits to the enhanced performance of excavating sponges remain to be explored. Research on photosymbiotic bioeroding sponges under experimentally elevated partial pressure of CO_2 (pCO_2) displayed only little adverse response or accelerated bioerosion (reviewed in Schönberg *et al.,* 2017a). Experiments observing effects of elevated temperature have either not shown a strong response (Stubler *et al.*, 2015; Schönberg *et al.*, 2008), or led to bleaching (Fang *et al.*, 2013a; BD Ramsby, pers. comm.) or partial necrosis or mortality (Wisshak *et al.*, 2013). Combined exposure of the Indo-Pacific photosymbiotic sponge *Cliona orientalis* to temperature and pCO_2 anomalies under two future scenarios over eight weeks (Austral spring to summer transition) dramatically enhanced both the growth and bioerosion of the sponge (Fang *et al.*, 2013a). However, under spring business-as-usual conditions *C. orientalis* bleached and showed energetic deficiencies (Fang *et al.*, 2013a, 2014) that are likely to lead to mortality in the longer term over summer (JKH Fang, pers. comm.).

The current study assessed the capacity of *C. orientalis* to erode and survive over the summer on future reefs through a 10-week simulation of both independent and concurrent warming and acidification predicted for the year 2100. To explore the influence of local nutrient availability on the outcome of globally changing climate conditions, supplementation of the diet of the sponges with nitrogen-rich particulate organics was also included as a factor. The diurnally and seasonally variable simulation was based on a “business-as-usual” greenhouse

gas concentration trajectory called the Representative Concentration Pathway 8.5 (RCP8.5) (IPCC, 2013). As opposed to previous experiments, the individual and combined effects of temperature, pCO_2 and diet supplementation on bioerosion rates, biomass, oxygen flux, carbon flux and survivorship were studied in an orthogonal design. Such designs permit the unravelling of independent effects, which is crucial to fully understand the physiological mechanisms underpinning an organism's response. The key questions of the current study were: (1) Do simulated warming and/or acidification and/or diet supplementation accelerate or decelerate bioerosion rates and growth of *C. orientalis*? (2) What changes to the carbon budget of the sponge drive the observed responses? (3) Which of the three factors or which of the combinations is most likely to impact the sponge's survival in future oceans under RCP8.5 emissions?

4.2. Materials and Methods

Experimental design and sample collection

Experiments were conducted at the Heron Island Research Station on the southern Great Barrier Reef over the Austral summer 2014-2015 using the ocean warming and acidification simulation system (Dove *et al.*, 2013; Fang, 2013) (see also Supplementary Information in the Appendix). This system allows computer-controlled manipulation of seawater chemistry while mimicking natural diurnal and seasonal variability of the reef. Four different flow-through scenarios were produced in 4 mixing sumps under a fully orthogonal combination of temperature and pCO_2 according to the greenhouse gas concentration trajectory RCP8.5 (IPCC, 2013) (Fig. 4.1a and Supplementary Fig. S4.1 and S4.2):

a) Baseline simulation, reproducing conditions at the reference site, with present-day (PD) levels of both temperature and pCO_2.

b) Elevated pCO_2 only, with RCP8.5 pCO_2 levels (set at 572 ± 11 µatm above PD) while maintaining PD temperature levels.

c) Elevated temperature only, with RCP8.5 temperature (3.5°C above PD) while maintaining PD pCO_2 levels.

d) Concurrent elevation of temperature and pCO_2 to RCP8.5 levels.

Dietary supplementation was superimposed on these scenarios in orthogonal setup, dividing the experiment into supplemented and unsupplemented treatments, with three replicate 40 L

experimental aquaria ascribed to each treatment (24 aquaria in total, see text below and Fig. 4.1a). Seawater supplying the aquaria contained dissolved organics and picoplankton cells up to 10 µm diameter that comprise the main part of sponges' diets, including clionaids (Maldonado *et al.*, 2012; Mueller *et al.*, 2014; Lynch and Phlips, 2000). The water flow to the aquaria (1L/min in each aquarium) was interrupted for one hour daily and diet-supplemented aquaria received a dose of protein-rich microalgal mix to a final concentration of 25 µL L^{-1} (non-viable, 9% algal biomass, N-rich High Pro, Reed Mariculture, Campbell, USA). Sunset was chosen as the feeding time, since it follows the period of maximum mucus production by corals triggering bacterial enrichment and increased food supply for reef organisms (Wild *et al.*, 2004; Rix *et al.*, 2016a). The sponges in the present experiment were still pumping actively at sunset (confirmed with fluorescent dye) and their oscula were open.

The experiment was performed with *Cliona orientalis* Thiele, 1900 in encrusting "beta" morphology (Schönberg *et al.,* 2017a; 2017b). Apart from *Symbiodinium*, *C. orientalis* hosts a low abundance of other microorganisms (Poppell *et al.*, 2013) [such as alpha and gamma proteobacteria (Pineda *et al.*, 2016)]. In the current study, treatment responses were addressed at the holobiont level. Samples were collected from *C. orientalis* individuals inhabiting dead coral substrates at 5 m depth at Harry's Bommie (151.9357°E, 23.4675°S), Heron Island in November 2014. Sponge spicules were examined to confirm the species identity (Schönberg, 2000). The sponges were cored to produce standardized cylinders of 35 mm diameter. Each core was then horizontally divided into 15 mm slices. The upper slice contained the sponge tissue plus a ca. 3 mm-thin underlying disc of non-infested $CaCO_3$ to allow downward growth and expansion (sponge core), whereas the lower slice consisted of entirely sponge-free $CaCO_3$ substrate (control core). Control cores were bleached for 6 h in 12.5% sodium hypochlorite to remove organic matter, thoroughly washed in distilled water and then reconditioned in running seawater for at least 48h. Control cores served throughout the experiment to quantify background weight loss due to passive $CaCO_3$ dissolution, abrasion from cleaning and bioerosion by re-colonizing microborers. To eliminate variation in bioerosion rates caused by substrate properties (Schönberg, 2002), only material sampled from six sponges excavating $CaCO_3$ of similar bulk density was selected (measured as outlined in Supplementary Information and Fig. S4.3 in the Appendix). The sponge-free $CaCO_3$ of the selected individuals had a higher initial bulk density (2.30 ± 0.02 g/cm^3, mean ± SEM) compared to the massive *Porites* sp. [<1.6 g/cm^3, e.g. (Smith *et al.*, 2007)] eroded by *C. orientalis* in previous experiments (Wisshak *et al.*, 2012; Fang *et al.*, 2013a).

The sponge cores (n=12 per treatment) and control cores (n=12 per treatment) from the six genotypes were labelled and randomly distributed (Maldonado *et al.*, 2008) across the 24 aquaria (4 sponge cores and 4 control cores per aquarium), with each of the 8 treatments receiving two cores of each genotype where possible. The contents of each aquarium were then assigned a group label (A through X). After collection, the sponge cores recovered for 2 weeks to allow full healing (open oscula on all core surfaces) before being exposed to a stepwise acclimation to the experimental treatments (progressive weekly steps of 0, 25, 50, 75 and 100% treatment water mixed with ambient seawater). Subsequently, full treatment conditions were maintained for 10 weeks (Fig. 4.1b). During the experiment, the preassigned groups of cores were rotated every 4th day between replicate aquaria (after water renewal) of the same treatment to minimize localized variations in light intensity and other positional effects (Hughes *et al.*, 2010; Grottoli *et al.*, 2013; Schoepf *et al.*, 2014). Upstream temperature and pCO_2 were continuously monitored in the four mixing sumps, while downstream temperature and pH were continuously monitored in the experimental tanks, with

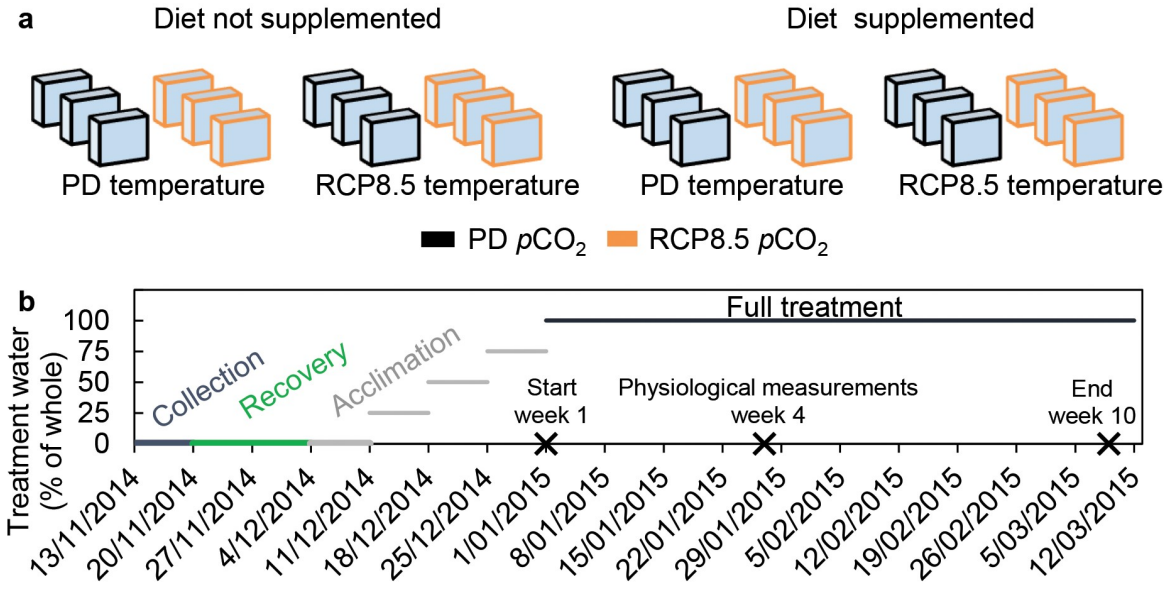

Figure 4.1: Schematic illustration of experimental design and timeline. (a) The orthogonal setup of the experiment produced 8 different combinations using three factors (temperature, pCO_2 and diet, with 2 levels each) and 3 replicate aquaria for each combination (i.e. 2 temperatures × 2 pCO_2 levels × 2 diets × 3 replicate aquaria = 24 aquaria in total). These aquaria were randomly assorted on the experimental table, so as not to bias the amount of light that specific treatments received. A total of 96 sponge cores and 96 controls cores from different sponge-invaded dead coral substrates were distributed across the aquaria (n=12 per treatment which equals to n=4 per aquarium). The cores were rotated in preassigned groups between replicate aquaria of the same treatment every 4th day to minimize localized variations in light intensity and other positional effects

(Hughes *et al.*, 2010; Schoepf *et al.*, 2014; Grottoli *et al.*, 2013). All aquaria were equipped with temperature loggers, light loggers and small wave makers and covered with light filters (Lee Filters #131) to mimic the light spectrum of the collection depth (Sampayo *et al.*, 2016) **(b)** After collection, the sponge cores recovered for 2 weeks to allow full healing before being exposed to a stepwise acclimation to the experimental treatments (progressive weekly steps of 0, 25, 50, 75 and 100% treatment water). Full treatment (100% treatment water) was reached on the 1st of January (start) and maintained until the 9th of March 2015 (end). Physiological measurements were performed with a subset of the sponges in the 4th week after the onset of full treatment conditions (week 4 of the experiment).

additional weekly pH measurements made inside each of the 24 aquaria (see Supplementary Methods in the Appendix for details). The use of a single sump per experimental treatment is technically a pseudo-replicated design (Cornwall and Hurd, 2016). The flow rate and dimensions of the dark sump however significantly limit the potential for confounding effects (see Supplementary Methods). Replicating sumps would necessitate a counterproductive reduction in sump size, significant increases to the energy budget on an offshore island, and would prove to be impractical for an experiment that aims to deliver in situ diurnal fluctuations for multiple factors in reef water of high quality.

Four weeks after the onset of full treatment conditions (hereafter referred to as "week 4", Fig. 4.1b), physiological measurements were performed with a subset of the specimens, which were subsequently sacrificed (n=7 out of 12 per treatment). At this point in time the top surfaces of all cores were still entirely covered by sponge tissue and oscula were open. The remaining specimens (n=5) were retained until the end of the summer period. During the experiment, aerial exposure of the sponges was prevented and epibionts were removed regularly using a pair of forceps and/or a soft brush, taking care not to damage the sponge tissue.

Bleaching and mortality

Bleaching, partial and complete mortality of the sponge cores were scored throughout the experiment. Bleaching was assessed by the colour change of the sponges from dark brown to pale yellow (Fig. 4.2a,b) and confirmed upon dissection to eliminate the possibility that symbionts were relocated deeper inside the core (Schönberg and Suwa, 2007). As a measure of photoinactivation during bleaching, the maximum potential quantum yield of photosystem II (Fv/Fm) of the sponge symbionts was measured once a week at 20:00 h using pulse amplitude modulated (PAM) chlorophyll fluorometry (Genty *et al.*, 1989) (dark-acclimated; Diving-PAM, Walz, Effeltrich, Germany). The PAM measurements (in combination with the oxygen flux assay, see below) further confirmed the observed bleaching (Fang *et al.*, 2014;

2016b). Towards the end of the experiment, some sponge cores (only in the treatments where diet was not supplemented) experienced partial mortality, defined here as the loss of sponge tissue from areas of the core, partially exposing the $CaCO_3$ substrate but without the appearance of black patches. The assessment of complete mortality was based on blackening of all sponge tissue, decaying odour and absence of oscula (Wisshak *et al.*, 2013).

Bioerosion rates

To measure total sponge bioerosion over time, all sponge and control cores were buoyant-weighed (Fang *et al.*, 2013b) at the onset of the full-treatments, at week 4 and at the end of the experiment. The decrease in the buoyant mass (BM) of the sponge cores was calibrated for seawater density and corrected for residual mass loss using the control cores. Changes in BM were converted to changes in $CaCO_3$ mass of the cores (see Supplementary Methods in the Appendix). The upper surface areas of sacrificed sponge explants were estimated using a standard aluminium foil method (Marsh, 1970) and total bioerosion rates were expressed as mg $CaCO_3$ cm^{-2} day^{-1} in reference to this surface.

Metabolic oxygen and carbon flux

Photosynthetic and respiratory activities of the sponge cores (n=7 replicates per treatment) were assessed at week 4 of the experiment, using an OXY-10 oxygen meter (PreSens, Regensburg, Germany) as described in detail previously (Fang *et al.*, 2014). Sponges were 30-min dark-acclimated before being placed -without exposing them to air- inside sealable chambers (250 ml) filled with respective scenario seawater (filtered to 0.45 µm to remove most microorganisms from the seawater), and non-viable algal mix was added to supplement half of the treatments to the same per sponge concentration as during daily supplementation of the experimental aquaria. The sponges were subjected to a cycle of 30 min darkness followed by 20 min light at 450 µmol quanta m^{-2} s^{-1} (Aqua Medic Ocean lights, Bissendorf, Germany), with oxygen levels logged every 15 s. Dark respiration (R_{dark}) and maximum net photosynthesis [max P_{net} at saturating light intensity (Fang *et al.*, 2016b)] were quantified based on the oxygen depletion or evolution (µM O_2 cm^{-2} h^{-1}) during the dark and light phase of the cycle respectively. R_{dark} reflects changes in holobiont metabolism as well as pumping rates (not measured here). The same procedure was performed with the control cores, which generated minimal non-sponge metabolic rates that were used to correct the sponge results. Corrected photosynthetic values were ascribed to *Symbiodinium*. The hourly respiratory and net photosynthetic rates were scaled up to daily rates and converted into carbon equivalents (see Supplementary Methods).

To measure the uptake or excretion of particulate and dissolved organic carbon by the sponges (POC and DOC respectively), incubations in confined seawater (5 L) were performed (Fang *et al.*, 2014). Dietary supplementation of the incubated sponges took place in the same manner as daily in the experimental aquaria. Seawater samples were collected and analysed as detailed in the Supplementary Methods. Uptake rates of DOC and POC were expressed as mg C cm^{-2} day^{-1} and added to the carbon flux that was calculated from photosynthesis and respiration. In that manner, the daily net carbon surplus (C_{net}) available to the sponge holobiont was estimated.

Biomass

After completion of the week 4 physiological measurements, analysed sponge and control cores were snap-frozen in liquid nitrogen and stored at -80°C. The sponge cores were later vertically divided into 4 quarters (A, B, C and D), three of which were subjected to different analyses. To quantify total organic mass of the core, spicular mass of *C. orientalis* and $CaCO_3$ mass (M_{CaCO3}), a loss after combustion method was performed on quarter A with correction factors applied (Fang *et al.*, 2013b); to quantify organic mass of other endo/epilithic organisms that could inhabit the sponge holobiont, an acid decalcification method was conducted with quarter B (Fang *et al.*, 2013b). The organic mass of *C. orientalis* was estimated by subtracting the organic mass of other organisms from the total organic mass. All biomass data were standardized to $CaCO_3$ mass of the whole core ($mg_{(biomass)}/g_{(core)}$). Quarter C was used to quantify the bulk density of the sponge core (Supplementary Methods and Fig. S4.3).

Data analysis

Preliminary analysis did not detect group-specific effects for any of the variables and therefore replicate groups of each treatment were pooled (Underwood, 1997). No single genotype or group of genotypes deviated from the others in a way that would substantially bias the analysis (Fig. S4.4). Dependent variables were analysed using a factorial, fully crossed analysis of variance (ANOVA) with three categorical factors having two levels each, resulting in a 2 × 2 × 2 matrix: temperature (PD and RCP8.5), pCO_2 (PD and RCP8.5), diet (supplemented and unsupplemented; Fig. 4.1a). Datasets were tested for normality (Shapiro-Wilk test) and homogeneity of variances (Levene's test). Log or square root transformations were applied if normality was violated, and heteroscedastic datasets were assesed at a reduced alpha level of 0.01 (Underwood, 1997) (Table S4). Main effects were reported when there were no significant three-way or two-way interactive effects. Differences in the case of

significant three-way interactions were explored using simple two-way interactions at each level of the third factor whilst using the error term (sum of squares and degrees of freedom) of the three-way ANOVA (Keppel and Wickens, 2004). If such simple two-way interactions were significant, pairwise comparisons with Bonferroni adjustments (to reduce type I errors) were performed to determine the effect of a factor at each level of the other factor (Keppel and Wickens, 2004). Chlorophyll fluorescence data were analysed with a three-way repeated measures ANOVA examining the effects and interactions of the categorical factors over time. Partial and complete mortality of the sponge cores were assessed at the end of the experiment with a two-way ANOVA and a two-proportions z-test. Statistical analyses were evaluated at a 0.05 level of significance (unless otherwise stated) and were performed using SPSS Statistics software (IBM, New York).

4.3. Results

Treatment conditions

Mean pCO_2 levels across the experiment were 493 ± 20 µatm (mean ± SEM hereafter, unless otherwise specified) for treatments with PD levels and 982 ± 17 µatm for treatments with RCP8.5 levels, thus approximately denoting a doubling from PD to RCP8.5. Peak temperature levels of 28.3 ± 0.1°C for the PD scenarios and 31.6 ± 0.1°C for the elevated scenarios [+1 and +4.3°C above the maximum monthly mean (MMM) respectively (NOAA, 2016)] were reached four weeks after the onset of full treatment conditions (Fig. S4.1). Details of the experimental conditions are given in the Supplementary Methods of the Appendix (Fig. S4.1 and S4.2 and Table S4.1 and S4.2).

Bleaching of sponge cores

Sponges in the heated treatments began to pale 24 days after the onset of acclimation, when midday temperature was 29.4 ± 0.06°C (MMM+2.1°C) and midday pCO_2 was 452 µatm in the low pCO_2 treatment and 903 µatm in the high pCO_2 treatment. By the onset of full treatment conditions, approximately one third of all the sponges exposed to simulated warming were visibly bleached (Fig. 4.2a,b). Bleaching of 100% of the sponge population in each heated treatment was reached after approximately the same number of full treatment days, regardless of diet (arrows in Fig. 4.2d,e). In line with the bleaching observations, maximum potential quantum yield of fluorescence for photosystem II of *Symbiodinium* decreased significantly in all heated treatments ($F=53.76$, $p<0.001$; Fig. 4.2c). Throughout the experiment, bleaching occurred only in the heated treatments.

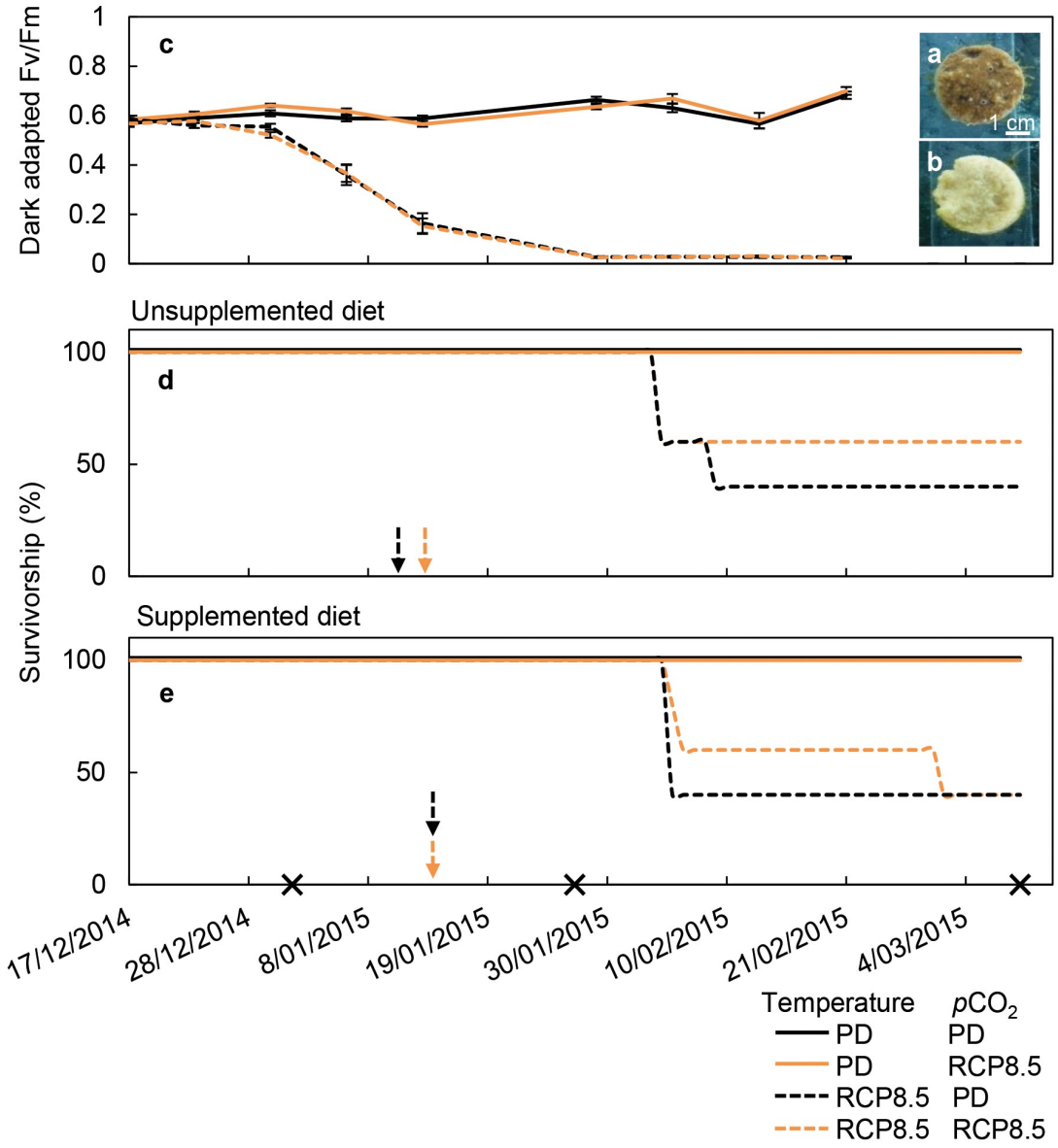

Figure 4.2: Photophysiology and survival of the *Cliona orientalis* holobiont under independent and concurrent simulation of warming and acidification from present-day (PD) summer conditions to Representative Concentration Pathway 8.5 (RCP8.5) conditions of the year 2100. Insets **(a)** and **(b)** show typical colours of healthy (brown) and bleached (pale yellow) sponges as observed in the treatments with PD versus RCP8.5 temperature levels respectively. **(c)** Dark-acclimated Fv/Fm of *Symbiodinium* in the sponge cores over the course of the experiment reflects the bleaching observations (mean ± SEM). Data are averaged across diet, since diet did not influence Fv/Fm ratios. Survival of *C. orientalis* decreased over the summer in all heated treatments, both for treatments with unsupplemented **(d)** and supplemented diets **(e)**. Only complete mortality was considered for this comparison. Crosses represent the arrival at full treatment conditions, the 4th week thereafter when physiological measurements were performed and the end of the experiment respectively. Arrows indicate the points in time when 100% bleaching of sponge cores in heated treatments were reached.

Bioerosion rates

Total sponge bioerosion corrected for control values ranged between 2.64 to 4.39 mg $CaCO_3$ cm^{-2} day^{-1} over the first 4 weeks of full treatment and was on average 35% higher for sponges with supplemented diets compared to unsupplemented sponges ($F_{(1,48)}$=8.07, p=0.007; Fig. 4.3a,b; Table S4.4). Simulated warming lowered total bioerosion rates by 20% ($F_{(1,48)}$=4.54, p=0.038), whereas acidification on its own did not have a strong effect on total bioerosion. Rates of weight loss in the sponge-free control cores were an order of magnitude lower than sponge bioerosion rates (0.28-0.59 mg $CaCO_3$ cm^{-2} day^{-1}) and did not differ between the treatments.

The bulk densities of the sponge cores at week 4 ranged from 1.67 to 1.82 g cm^{-3} across the different treatments with the average porosity being 35.90 ± 0.94%. The lowest densities and highest porosities were found in the treatments with both PD temperature and PD pCO_2, yet these differences were not significant.

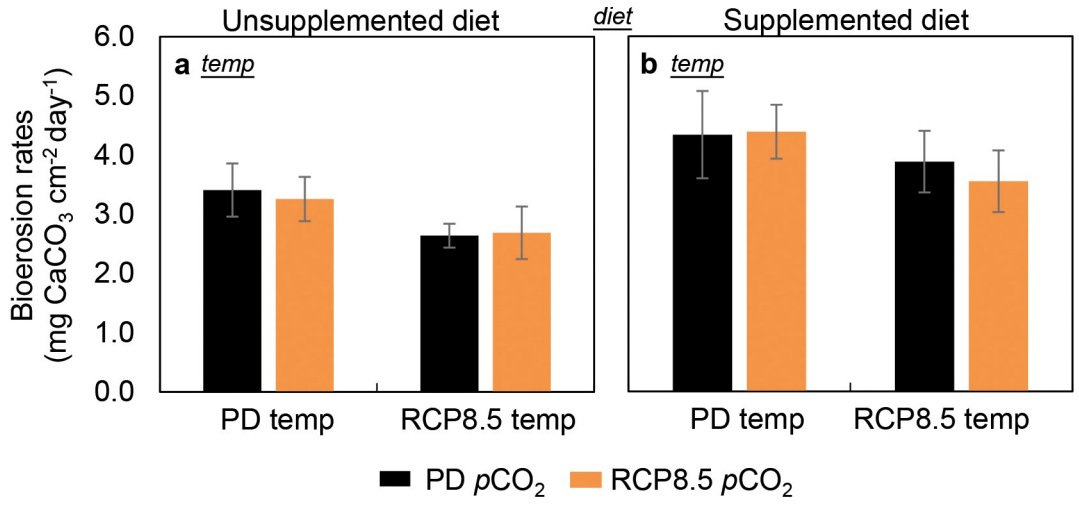

Figure 4.3: Total bioerosion rates of *Cliona orientalis* at Heron Island on the southern Great Barrier Reef receiving an unsupplemented **(a)** and supplemented diet **(b)** under independent and concurrent simulation of warming and acidification from present-day (PD) summer levels to Representative Concentration Pathway 8.5 (RCP8.5) levels of the year 2100 (mean ± SEM). The rates represent the loss of $CaCO_3$ measured as buoyant mass change over the first 4 weeks of full treatment conditions. The designations *diet* or *temp* indicate significant main effects of diet supplementation or temperature respectively. Buoyant mass at the end of the experiment (week 10) is not presented here due to prevalent mortality in the heated treatments from week 6 onwards.

Metabolic oxygen and carbon flux

Photosynthesis in week 4 of the experiment exceeded respiration rates only in the absence of simulated warming where the sponges did not bleach (max P_{net}, Fig. 4.4a,b and Table S4.4).

When the diet was not supplemented, acidification enhanced photosynthesis by 80% ($F_{(1,48)}$=5.96, p=0.018), but this effect was absent when the diet was supplemented. Warming, acidification and diet interactively drove the response of photosynthesis (3-way interaction, $F_{(1,48)}$=6.48, p=0.014). Dark respiration ($R_{dark,}$ Fig. 4.4c,d) of the sponge cores was affected only by temperature, with sponges under RCP8.5 temperature respiring at a slower rate ($F_{(1,48)}$=36.44, p=0.00).

Diet supplementation caused increased uptake of dissolved organic carbon (DOC, Fig. 4.4e,f and Table S4.4), but this food source appeared to be only half consumed when the sponges were under PD temperature and pCO_2 levels ($F_{(1,48)}$=26.06, p<0.001, Fig. 4.4e). Warming led to a decrease in DOC uptake ($F_{(1,48)}$=141.76, p<0.001 and $F_{(1,48)}$=13.09, p=0.001 for unsupplemented and supplemented treatments respectively, Fig. 4.4e,f). Acidification lowered uptake rates at PD temperatures, regardless of diet (95% decrease, $F_{(1,48)}$=95.43, p<0.001 and 65% decrease, $F_{(1,48)}$=11.41, p=0.001 for unsupplemented and supplemented sponges respectively, Fig. 4.4e,f). Uptake rates of DOC were driven by a 3-way interaction between the factors ($F_{(1,48)}$=11.39, p=0.001). Uptake rates of particulate organic carbon showed similar trends, yet without statistically robust support (POC, Table S4.3 and S4.4).

At PD temperature and $pCO_{2,}$ supplemented sponges had a lower daily net carbon surplus than unsupplemented sponges (C_{net}, Fig. 4.5 and Table S4.4; $F_{(1,48)}$=15.19, p<0.001 and $F_{(1,48)}$=20.13, p<0.0001). Regardless of diet or pCO_2, only the sponges exposed to warming were net consumers of metabolic carbon i.e. the metabolic demand of bleached sponges surpassed the carbon that could be autotrophically or heterotrophically harvested. Acidification led to reduced C_{net} surplus at PD temperature levels when the sponges were not supplemented ($F_{(1,48)}$=28.78, p<0.0001), reflecting the loss in DOC uptake despite the increase in photosynthetic activity which only contributes carbon during light hours.

Biomass

Regardless of diet or $pCO_{2,}$ the sponges were able to build or maintain more organic biomass under PD temperature than under RCP8.5 temperature (on average 41.74 and 36.69 $mg_{(biomass)}/g_{(core)}$ respectively, $F_{(1,48)}$=13.16, p<0.001, Table S4.3 and S4.4). Non-sponge organics were found to be on average 1.94 ± 0.3% of total organics (no difference between treatments) and were therefore considered negligible in this study. The spicular mass of the sponge cores formed a large fraction of the sponge biomass (approx. 35% of total sponge biomass) and did not differ between treatments.

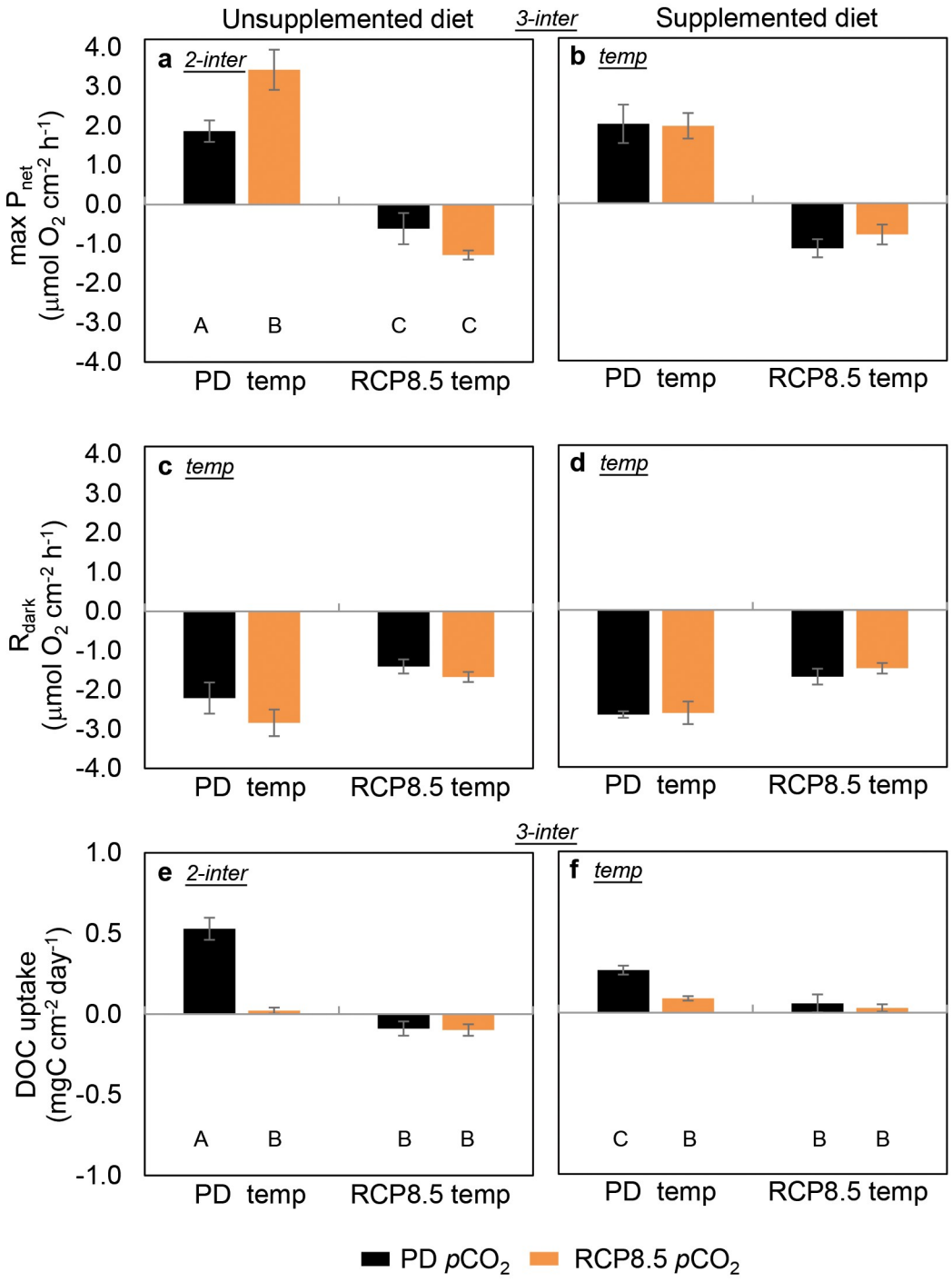

Figure 4.4: Maximum net photosynthesis (max P_{net}), dark respiration (R_{dark}) and dissolved organic carbon (DOC) uptake of *Cliona orientalis* at Heron Island on the southern Great Barrier Reef receiving an unsupplemented (**a, c** and **e** respectively) and supplemented diet (**b, d** and **f** respectively) under independent and concurrent simulation of warming and acidification from present-day (PD) summer levels to Representative Concentration Pathway 8.5 (RCP8.5) levels of the year 2100 (mean ± SEM). All parameters were measured 4 weeks after the onset of full treatment conditions. Max P_{net} and R_{dark} rates represent hourly rates of oxygen evolution and depletion, whereas DOC uptake was measured over a 24 h period. The designations *inter*, *temp*, or pCO_2 indicate significant 3-way or 2-way interactive effects as specified, or (simple) main effects for temperature or pCO_2 respectively within each panel. When interactive effects are present, the capitalized letters

beneath the bars indicate statistical differences. When standardized to sponge biomass, reported R_{dark} rates (**c** and **d**) range between 14.46 ± 1.22 and 24.60 ± 1.49 µmol O_2 g^{-1} h^{-1} (mean ± SEM).

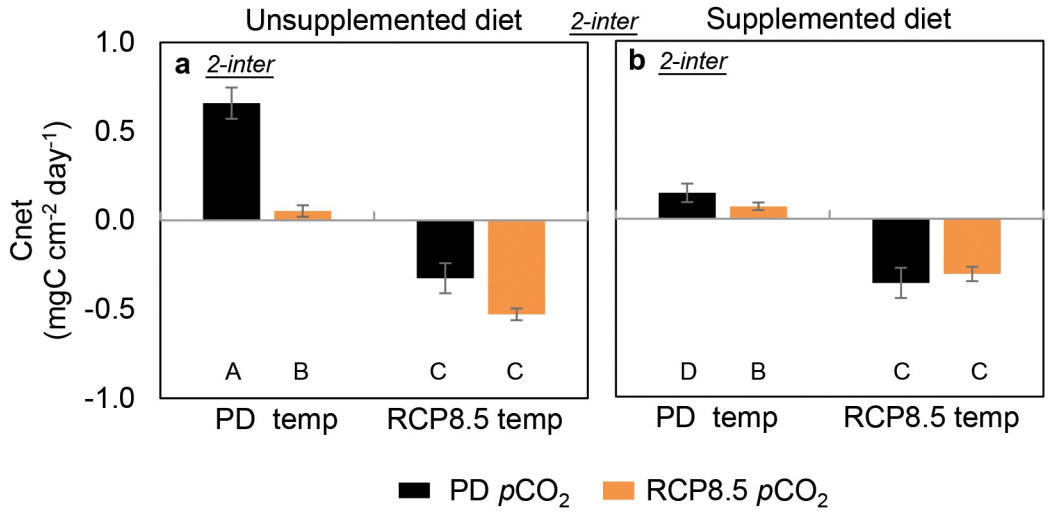

Figure 4.5: Daily net carbon surplus (C_{net}) of *Cliona orientalis* at Heron Island on the southern Great Barrier Reef receiving an unsupplemented **(a)** and supplemented diet **(b)** under independent and concurrent simulation of warming and acidification from present-day (PD) levels to Representative Concentration Pathway 8.5 (RCP8.5) summer levels of the year 2100 (mean ± SEM). The carbon surplus incorporates autotrophic inputs (photosynthetically fixed carbon), heterotrophic inputs (net uptake of dissolved and particulate organic carbon) and respiratory output (carbon used for maintenance, growth etc) over a 24h period after 4 weeks of exposure to full treatment conditions. The response of C_{net} to the treatments was driven by 2-way interactive effects (*2-inter*) for each combination of the 3 factors. The capitalized letters beneath the bars indicate statistical differences. When interactive effects are present, the capitalized letters beneath the bars indicate statistical differences.

Sponge mortality

After physiological responses had been measured at week 4 and during the second half of the experiment, the tissue of all bleached sponges increasingly retracted to a small surface area of the core, despite regular removal of epibionts. Bare parts of the core were colonized by a diverse algal community consisting mainly of crustose coralline algae (CCA), *Derbesia* sp., *Ulva* sp., pennate diatoms and free-living dinoflagellates (D Bender-Champ, pers. comm.). In approximately half of the specimens exposed to simulated warming, bleaching resulted in complete mortality ($z=3.65$, $p<0.001$) (Fig. 4.2d,e). The first cases of complete mortality co-occurred amongst PD pCO_2 and RCP8.5 pCO_2 treatments 6 weeks after the onset of full treatment, regardless of dietary supplementation. Complete mortality was always preceded by bleaching, occurring between 3-6 weeks post bleaching. Dead sponge cores were inhabited by fungi and cyanobacteria (*Spirulina* sp.) in addition to the algal community described above (D Bender-Champ, pers. comm.).

Regardless of diet and pCO_2, all specimens exposed to PD temperatures survived beyond the end of the summer in the experiment, without any signs of bleaching. However, in the unsupplemented treatment the substrate of some of these specimens had become partly exposed by the end of the experiment due to sponge tissue loss (partial mortality, Fig. 4.6). Here, partial mortality and consecutive algal settlement was found in 2 out of 5 of the PD pCO_2 and 3 out of 5 of the RCP8.5 pCO_2 sponges (z= 1.5806, p=0.057 and z=2.0698, p=0.019, respectively) and was an independent effect of diet. Supplemented sponges retained their tissue, but unsupplemented sponges lost about one third of their tissue cover, resulting in 5.20 ± 0.78 cm^2 live tissue compared to 8.23 ± 0.65 cm^2 in supplemented sponges at the end of the experiment (two-way ANOVA, $F_{(1,16)}$=7.96, p=0.015). The surface tissue of supplemented sponges also appeared healthier and thicker.

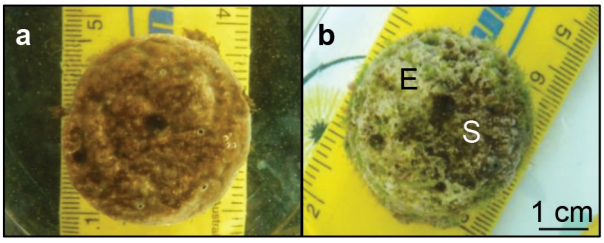

Figure 4.6: An example of partial mortality observed in a number of *Cliona orientalis* cores in the present-day temperature treatments that did not receive a supplemented diet. At the start of the experiment and at week 4 during the physiological measurements, sponge tissue covered the entire surface of the core **(a)**. At the end of the experiment 10 weeks later, the tissue of several cores had retracted to a smaller surface area, exposing the $CaCO_3$ substrate **(b)**. This process may be a reversible result of stress as indicated by similar observations in other species (Luter *et al.*, 2012). Partial mortality was not observed in any of the sponges that received a supplemented diet. E = Exposed $CaCO_3$ substrate, S = Sponge tissue

4.4. Discussion

Exposure of the photosymbiotic sponge *Cliona orientalis* to RCP8.5 summer projections for the year 2100 at Heron Island led to decreases in biomass and rates of bioerosion, autotrophy, heterotrophy and survival. These responses were driven by resource deprivation of both the host and the symbiont and were primarily caused by impacts of simulated warming, but also acidification, even when additional heterotrophic food sources were provided. Excavating sponges are often regarded as "winners" on disturbed coral reefs under projected future conditions (Schönberg *et al.,* 2017a). However, based on the combined results of the current experiment, under "business-as-usual" CO_2 emissions *C. orientalis* and possibly other similar

photosymbiotic excavating sponges are expected to suffer losses at the end of the current century comparable to those projected for scleractinian corals (Hoegh-Guldberg *et al.*, 2007).

Extrapolating measured present-day summer rates of substrate removal by *C. orientalis* to an annual mean resulted in a total bioerosion rate of 12.4 kg $CaCO_3$ m^{-2} $year^{-1}$ when the diet was not supplemented, which is consistent with earlier results from similarly dense substrates (Schönberg, 2002). Our study demonstrated a 35% stimulation of total sponge bioerosion by the availability of food, purportedly also allowing faster expansion as would be expected in nutrient-rich environments such as inshore reefs (Ward-Paige *et al.*, 2005). Our results do not imply a sustained increase in bioerosion performance by photosymbiotic sponges in future oceans however, mainly due to observed adverse impacts of simulated warming. We suggest that bioerosion rates were mainly reduced by the failure of the photosynthesis of the symbionts, highlighting the importance of the symbiosis to supply energy for bioerosion (Rosell and Uriz, 1992; Hill, 1996; Schönberg, 2006). Previously documented temperature effects on bioerosion of *Cliona* species have shown variable responses (Márquez *et al.*, 2006; Duckworth and Peterson, 2013; Wisshak *et al.*, 2013; Stubler *et al.*, 2015). Our results are in accordance with the reduction of bioerosion rates under warming reported from a short-term experiment using the same species (Wisshak *et al.*, 2013). Simulated acidification co-occurred with heterotrophic carbon losses in our study, which may have resulted in the loss of a clear response through bioerosion as opposed to previous studies: Bioerosion by *C. orientalis* significantly increased under similar acidification in a 3-day closed system experiment (chemical bioerosion measured through alkalinity changes) (Wisshak *et al.*, 2013), in a 10-day flow-through experiment (total bioerosion measured through buoyant mass changes) (Wisshak *et al.*, 2012) and in a 8-week flow-through experiment over Austral spring (both of the above measures) (Fang *et al.*, 2013a). We hypothesize that in our study over Austral summer, the longer-term losses to the sponge's carbon budget under acidification may have lessened the energy invested into bioerosion, thereby decoupling acidification effects from erosion enhancement. We measured bioerosion through buoyant mass changes, but identifying chemical and mechanical rates in future studies could better elucidate potential acidification impacts.

Bleaching of *C. orientalis* tissues has previously been shown under concurrent simulation of RCP8.5 warming and acidification (Fang *et al.*, 2013a). Here, we provide evidence that our observation of bleaching was caused by warming above the mean summer water temperature. Whether the bleaching is a result of oxidative stress and mechanisms similar to those

established for the cnidarian-*Symbiodinium* partnership (Hoegh-Guldberg, 1999; Brown and Dunne, 2016; Oakley and Davy, 2018) remains to be explored, but our results show that the bleached sponges experience reduced holobiont productivity and increased mortality, as is known for bleached corals (Hoegh-Guldberg, 1999; Brown and Dunne, 2016; Oakley and Davy, 2018). The decrease of photosynthetic activity translates into reduced access to resources, yet even though bleached specimens had lower biomass and no symbiont population, they maintained a considerable respiratory demand (metabolic needs increase inherently with temperature rise), which would have represented an additional resource drain. To date, bleaching of *Cliona* spp. has been considered a rare event *in* or *ex situ* (Schönberg *et al.*, 2017b). In October 2015 a natural bleaching event was reported for the first time for a clionaid sponge in the lower Florida Keys (Hill *et al.*, 2016), but the sponges were only partially bleached and appeared to survive and recover (M Hill, pers. comm.). An unknown encrusting *Cliona* sp. exhibited impaired photosynthesis during a heating event in March 2013 (Lafratta *et al.*, 2016) (MMM+1°C or more) in depths down to 15 m near Onslow, NW Australia (CHL Schönberg, pers.comm.). In our experiment, the sponges began to pale prior to the full establishment of the 2100 climate scenarios, indicating that at least partial or occasional bleaching could become more common in natural populations under similar warming events before the end of the current century.

Acidification may have stimulated higher photosynthetic rates in unbleached specimens that were not diet-supplemented, possibly because less resources had to be invested into the conversion of HCO_3^- to CO_2 for use by the Rubisco enzyme (Cornwall *et al.*, 2012). *Symbiodinium* phylotypes are known to respond differentially to acidification (Brading *et al.*, 2011; 2013), and perhaps the carbon concentrating mechanism of the present *Cliona*-associated phylotype is relatively inefficient and therefore enhanced by the greater potential for passive, diffusive uptake of CO_2 under acidification (Brading *et al.*, 2011). No enhancing effect was found when the sponges received a supplemented diet since they may have been less dependent on autotrophic inputs, despite stable respiration that could otherwise provide an alternative source of CO_2 to the symbiont (Cornwall *et al.*, 2012).

With regards to organic carbon uptake, an increase in heterotrophic feeding of the bleached sponges could have served to compensate for the loss of autotrophic carbon. However, sponges in the heated treatments had reduced rather than increased carbon uptake rates. Filter feeding is an energetically costly process (Leys *et al.*, 2011) that could be rendered unsustainable in the bleached sponges. Negative effects of temperature on sponge feeding

have been reported for the Great Barrier Reef (GBR) sponge *Rhopaloeides odorabile*, with filtration efficiency, pumping rate and choanocyte chamber density and size reduced at 31°C (MMM+2°C) (Massaro *et al.*, 2012). POC uptake in our sponges was only insignificantly reduced, yet choanocyte functioning and water pumping may also facilitate DOC uptake (De Goeij *et al.*, 2008), which could explain the losses observed here under simulated warming. Acidification similarly reduced uptake of DOC, which may point towards a trade-off between autotrophy (due to stimulation of photosynthesis under elevated pCO_2) and heterotrophy. Alternatively, prolonged high levels of H^+ may have had deleterious effects on the filter-feeding capacity of the sponge, for example by affecting mitochondrial ATP recycling which is crucial to the flagellar beating (Lukik-Bilela *et al.*, 2011). Further investigations are necessary to confirm what caused the observed decrease in carbon uptake under acidification.

In treatments with either warming or acidification, dietary supplementation slightly ameliorated the effect of the other factors; the sponges took advantage of the elevated concentration of organics and more organic carbon was incorporated. Sponges in present-day conditions did not respond in the same way. Compared to supplemented sponges that were not in need of food, unsupplemented sponges may have been relatively starved (only particles up to 10 μm in diameter were retained in unsupplemented tanks) and were therefore filtering more actively (i.e. taking up more carbon from the seawater) when assessed over a 24h-period at the height of summer. The assumption of resource deficiency is also supported by the partial mortality found towards the end of the experiment in unbleached sponges that did not receive a supplemented diet.

All bleached sponges had lower organic biomass, which will in part explain the reduction in total bioerosion rates and respiration in the heated treatments. Bleached *C. orientalis* in previous experiments increased biomass (Fang *et al.*, 2013a, 2014), but this may have been due to a lag effect after an initial stimulation of growth earlier in spring when the symbionts were still present (JKH Fang, pers. comm.). The duration and the severity of our experimental warming went beyond physiological thresholds, and bleached sponges suffered biomass losses due to reduced autotrophy and heterotrophy. Supplementary feeding with protein-rich organics was expected to stimulate growth, since the extent to which the sponge holobiont can utilize photosynthetically transferred or heterotrophically attained carbon beyond its respiratory needs in the oligotrophic reef waters may depend on the availability of commonly limiting nutrients such as nitrogen (Falkowski *et al.*, 1993). No such effect was observed, but instead the resources gained from the extra nutrition may have been redirected towards

bioerosion activity. Alternatively, the sponges may have not been nitrogen-limited in the first place, yet the partial mortality observed in the unsupplemented treatments is contraindicative.

Even though spiculogenesis is considered energy-demanding (Frøhlich and Barthel, 1997; Uriz *et al.*, 2003), the mass of siliceous spicule was not affected by any of the treatments, which confirms previous results (Fang *et al.*, 2013a; Vicente *et al.*, 2016). The formation of one demosponge spicule may take approximately one week and an even longer lag period needs to be considered when looking for environmental effects on spicules (Schönberg and Barthel, 1997).

A daily net carbon surplus was only realized under present-day temperatures, and that surplus was significantly reduced with acidification, since organic carbon uptake decreased. Overall, the physiological measurements revealed carbon deprivation in the bleached sponges, which explains their subsequent mortality. Heterotrophy by itself does not appear to be sufficient for the energetic needs of *C. orientalis* [also shown by (Fang *et al.*, 2014)]. We conclude that the symbiosis between the sponge and its dinoflagellates is neither facultative nor merely beneficial to bioerosion performance alone, but it is vital to the survival of the holobiont in several ways.

For marine sponges, interactive effects of environmental factors such as warming, acidification and food availability remain largely unknown and vary between species depending on the natural conditions that they are adapted to (Duckworth *et al.*, 2012; Wisshak *et al.*, 2013). The lack of and the need for related studies has recently been highlighted in order to quantify present trends of carbonate budgets and to provide modelled trajectories for different scenarios to facilitate management (Schönberg *et al.,* 2017a). Our experiment assessed the effects of simulated warming, acidification and diet supplementation on the bioerosion efficiency and survival of *C. orientalis* separately and in combination. Overall, warming appears to be a more important factor in determining the physiological thresholds of the sponge, and increased bioerosion rates observed in previous short-term acidification-only experiments (Schönberg *et al.,* 2017a) may not realistically reflect future developments under coexisting ocean warming and acidification. In non-bioeroding sponges from the GBR, the effects of RCP8.5 warming were also shown to be physiologically more important than acidification effects (Bennett *et al.*, 2016), but Caribbean sponges exposed to similar warming and acidification for 24 days remained largely unaltered (Duckworth *et al.*, 2012). Our study suggests that future climate conditions may temporarily incur increased bioerosion rates at intermediate levels of environmental change, but that ultimately escalating

environmental conditions under presently predicted "business-as-usual" fossil fuel usage will cause photosymbiotic clionaids to fail along with other benthic organisms. This supports a parabolic rather than a linear response of bioeroding sponges to future change (Schönberg *et al.,* 2017a). Bioerosion and biomass maintenance are not the only energetically-costly activities of *C. orientalis*; other costly processes such as reproduction or competition for space (Hill, 1996) could also be impacted by climate change, thereby possibly further reducing the likelihood of survival in this species.

Climate simulations on coral reef assemblages from the southern GBR have provided evidence that firstly, there has been little adjustment of corals to changes over the past 100 years, and secondly, 100 years from now corals are unlikely to calcify or survive over RCP8.5 summers (when temperatures and seawater pCO_2 concentrations are at their seasonal highest) and beyond (Dove *et al.*, 2013). To date, excavating sponges were often considered more tolerant to future changes than scleractian corals (Schönberg *et al.*, 2017b). However, our study stresses that there are limits especially to the temperature but also the pCO_2 conditions that *C. orientalis* can tolerate, and that, despite subtle benefits from higher food availability, future summers can be expected to have adverse effects on the bioerosion capacity, general physiology and ultimately survival of the sponge. Keeping in mind the limitations of extrapolating from simulations to the field, we nevertheless cannot support that excavating sponges such as *C. orientalis* are still likely to be 'winners' in 2100.

Dinoflagellate sponges have evolved a tight and highly specialized relationship with their symbionts (Schönberg and Loh, 2005; Schönberg *et al.*, 2005; Hill *et al.*, 2011; Pochon *et al.*, 2014; Ramsby *et al.*, 2017b) which, however beneficial, also renders them vulnerable to environmental stressors that disrupt the symbiosis. We acknowledge therefore that the present results may only be relevant for excavating sponges that are symbiotic with *Symbiodinium* and that other excavating sponges might show different response patterns. This remains an essential area to explore if we are to gain a complete understanding of the implications of a warmer, more acidic and more eutrophic ocean for these key reef organisms. It is also important to note that our study did not identify the temperature threshold for the loss of *C. orientalis* from coral reefs like those of Heron Island and the southern Great Barrier Reef, or how well *C. orientalis* is performing as climate change intensifies in the interim, causing mass coral mortality events (Hughes *et al.*, 2017) and thus increasing the availability of bioerosion substrate.

Chapter 5

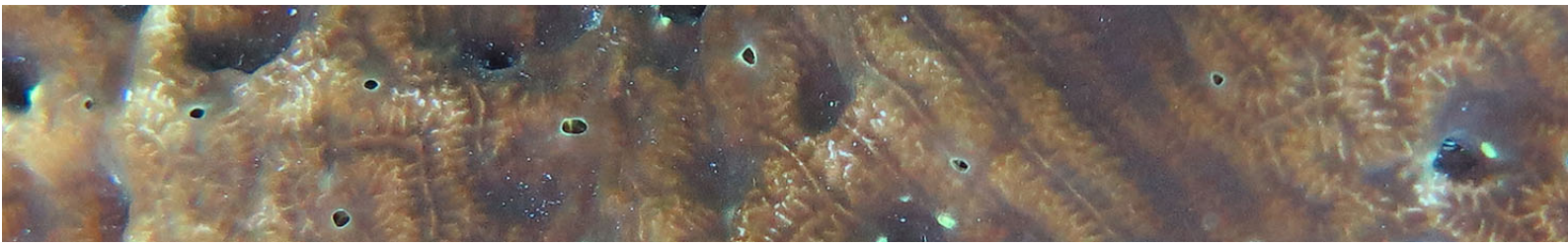

General Discussion

5.1. Chapter Summaries

Bioeroding sponges are predicted to be "winners" on future reefs with important negative implications for maintaining coral growth and thus maintaining positive carbonate budgets. However, there is urgent need to understand how some of the most efficient and fast-growing bioeroding sponges, namely the species that host photosynthetic symbionts, will respond to future conditions. The present thesis explored the interplay between the photosynthetic and excavating activity of an aggressive photosymbiotic coral-eroding sponge that hosts dinoflagellates of the genus *Symbiodinium*. Before addressing the response of such sponges to future changes, a better understanding of the physiological and metabolic processes that define the present success of such bioeroding sponges on coral reefs is needed. Armed with this better understanding, it was hoped that the present thesis would contribute to a growing body of studies that address the current and future role of sponge bioerosion on changing reefs, and will add novel insights into the drivers of bioerosion (Chapter 1). Along the way, we discovered a strong link between photosynthesis and bioerosion of the *Cliona orientalis* holobiont (Chapter 2), and we pinpointed its endosymbiotic dinoflagellates as the major site of photosynthetic fixation and subsequent distribution of fixed materials to the sponge host (Chapter 3). However, we also discovered that the "chemistry" of the partnership between sponge and dinoflagellates depends strongly on the chemistry of the seawater they inhabit. The symbiotic partnership was disrupted when exposed to seawater typical of an average summer at the end of the current century (IPCC RCP8.5), lest we tackle climate change. We were able to tease apart that heat stress, rather than acidosis, was the major driver of this disruption and of the subsequent mortality (Chapter 4). If our findings hold for other *Cliona viridis* species, then the very partnership that enables the competitive growth and erosion of photosymbiotic sponges may decrease their fitness on warmer reefs by the year 2100. Decreased fitness may lead to future evolutionary losses, similar to those predicted to occur even sooner for scleractinian corals (e.g. Dove *et al.*, 2013).

Before moving on to discuss the findings of this thesis in the light of current constraints and new directions in sponge bioerosion research and beyond, we would like to remind the reader of the major outcomes of Chapters 2 to 4:

In Chapter 2, we set out to examine the relationship between symbiont photosynthesis and bioerosion activity of the Indo-Pacific sponge holobiont *Cliona orientalis.* To do so, we first manipulated the quality and quantity of photosynthetic activity in the holobiont by exposing sponge specimens to a) the photosynthetic inhibitor diuron (DCMU), which led to a reduced

symbiont population that was photosynthetically inactive and b) heat stress known to cause disruption of the symbiosis, which led to a larger reduction of the symbiont population but allowed remnant symbionts to photosynthesize. Once the treatments were established, we measured daytime and night-time chemical bioerosion rates and correlated these to the photosynthetic rates obtained in the same treatments. We found a strong positive link between the photosynthetic activity of the symbionts and the bioerosion rates of the sponge during the daytime. Even during night, bioerosion rates were higher in holobionts that were able to photosynthesize during the day. These results support the model in which photosynthates and/or oxygen production stimulate the etching activity of the sponge.

Having established that symbiont photosynthesis is an important driver of sponge bioerosion, in Chapter 3 we wanted to identify the component of the holobiont to which (most of) the photosynthetic activity can be ascribed. Apart from examining the site of uptake of inorganic carbon via photosynthesis, we also wanted to examine the site of uptake of inorganic nitrogen, as well as the subsequent fate of both nutrients in sponge tissue and metabolism. To do so, we combined a pulse-chase experiment (using isotopically enriched ^{13}C-bicarbonate and ^{15}N-ammonium) with transmission electron microscopy and nanoscale secondary ion mass spectrometry. In that way, we pinpointed how the *Symbiodinium* dinoflagellates of the *C. orientalis* holobiont functioned as the primary source of inorganic assimilation into organic material in the outer sponge body, and we illustrated that assimilated material was subsequently translocated to proximate sponge cells, in the absence of symbiont digestion. *Symbiodinium* was very efficient in taking up both inorganic sources, even though this uptake was not uniform across individual *Symbiodinium* cells, especially with regards to nitrogen. Other less abundant prokaryotic symbionts were not observed to participate in nutrient assimilation in the outer layer of the sponge.

Finally, in Chapter 4, we examined the response of the *C. orientalis* holobiont to projected ocean conditions for non-El Niño summer conditions of the year 2100, if humanity fails to reduce emissions of greenhouse gasses. We simulated ocean warming, acidification and eutrophication both concurrently and independently in a fully-crossed design that mimicked diurnal and seasonal variability in temperature and pCO_2 for an average non-El Niño summer. We found that acidification did not strongly affect erosion rates, while simulated eutrophication (diet supplementation with particulate organic material) increased bioerosion rates. Warming above 30°C (+2.7°C above the local maximum monthly mean, MMM) had the most severe effect on the sponge holobiont, as it led to extensive bleaching (i.e. expulsion

and disintegration of *Symbiodinium*) followed by prevailing mortality. Under elevated temperature, the holobiont was physiologically impaired and the carbon budget as well as the bioerosion rates of the sponge were diminished. What is more, warming effects were not ameliorated by diet supplementation. These findings demonstrate that the tight and obligate relationship that has evolved between certain bioeroding sponges and *Symbiodinium* is largely beneficial to the hosts under present-day ocean conditions, but it might also be their Achilles' heel in future warmer oceans.

5.2. Synthesis of results, limitations and suggestions for future research

Sponge bioerosion on present-day reefs is clearly still on the rise (Schönberg *et al.*, 2017a, 2017b; Chaves-Fonnegra *et al.*, 2017), and therefore there is a need for more experimental and observational studies that fill the important gaps in our current knowledge of the physiology and ecology of these sponges. Such efforts are needed in most areas of sponge bioerosion research, ranging, for instance, from improvements to taxonomy and *in situ* species identification, to standardization of common metrics that will enable more accurate comparisons among studies, and to the development of superior methodology to quantify bioerosion inside $CaCO_3$ substrates (e.g. microcomputed tomography, X-radiography or pH microprobes) or in the seawater of incubation chambers (Schönberg *et al.*, 2017b; De Bakker *et al.*, 2018). While synthesizing the main findings of the current thesis in the following paragraphs, we would like to point out a number of new directions that we believe would be largely beneficial to the advancement of the sponge bioerosion field (Fig. 5.1).

Photophysiology and holobiont health

A first topic of interest is the bleaching susceptibility of photosymbiotic clionaid sponges. Both short term (Chapter 2) and relatively longer term (Chapter 4) experimental temperature stress led to near complete bleaching of *C. orientalis*, as has been demonstrated previously (Fang *et al.*, 2013a, 2014). The relatively high temperature offset that was necessary to bleach the sponges, however, warrants further investigation of their bleaching behaviour in experiments as well as field validations that can identify bleaching thresholds, ideally in direct comparison to corals (Schönberg *et al.*, 2008). In Chapter 2, we demonstrated that the photosystem II herbicide diuron (DCMU) can be effectively used in photosymbiotic sponges, opening new opportunities for describing photo-bleaching models in sponges as has been previously achieved in other benthic organisms (e.g. Jones, 2004; Murata *et al.*, 2007; Takahashi *et al.*, 2013).

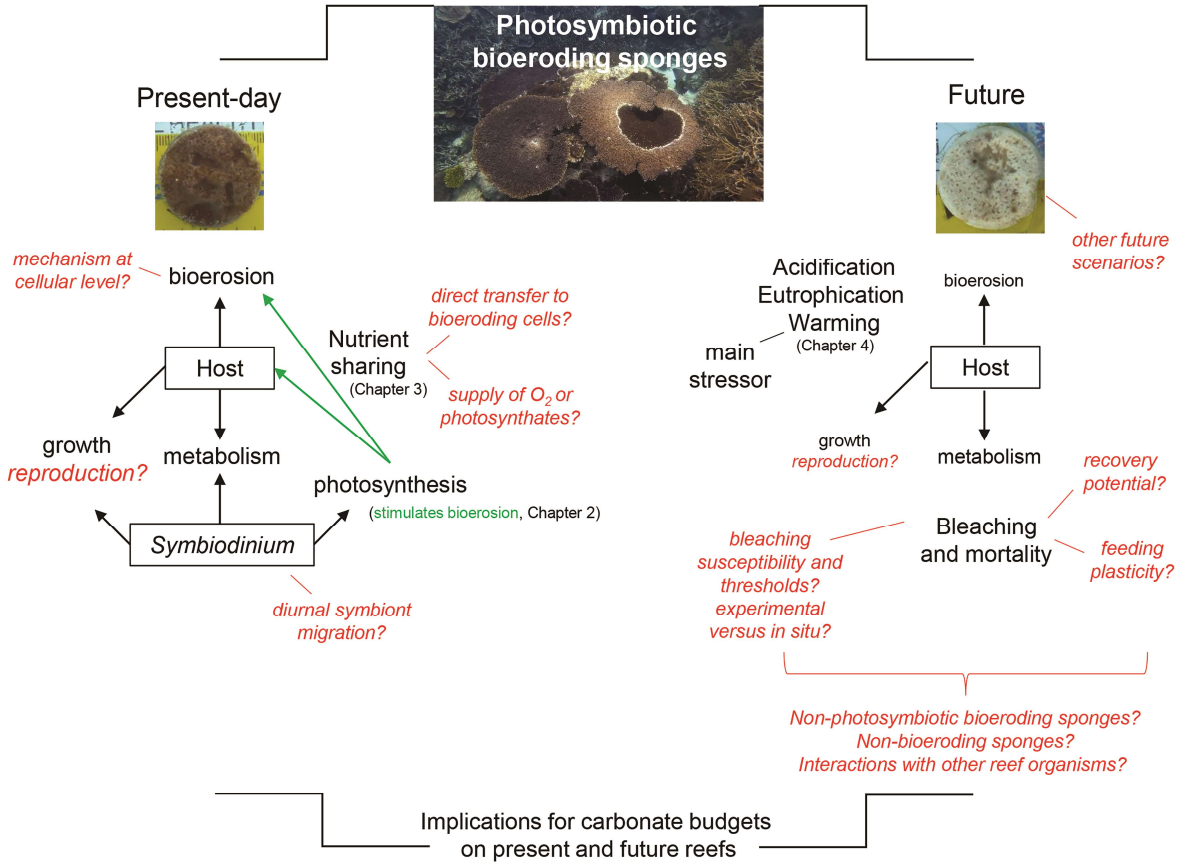

Figure 5.1: Schematic summary of the current thesis, integrating the main experimental findings (in black) and the identified gaps in knowledge that can spur future research (in red). Chapters 2 and 3 mainly addressed the dynamic interplay between photosymbiotic bioeroding sponges and their resident symbionts under present-day seawater conditions (left panel), whereas Chapter 4 extrapolated these findings to future conditions (right panel, defined as end of the century conditions under business-as-usual CO_2 emissions). Changes in font sizes from the left to the right panel reflect changes to the efficiency of the displayed processes.

Importantly, to determine to what extent tank-based experimental observations apply to real-world ecological patterns, bleaching susceptibility and the potential for post-bleaching recovery need to be studied *in situ*. In experimental settings, persistent loss of symbiont photochemical activity under heat stress and holobiont bleaching were observed, yet *in situ* other factors might help to offset (or, on the other hand, exacerbate) such impacts. Preliminary genetic testing discussed in Chapter 2 (T. LaJeunesse, unpubl. data) pointed towards a restricted symbiont diversity association in *C. orientalis*, which could imply a limited capacity for adaptation and resilience. However, we do not know whether there is potential for symbiont type reshuffling and enhanced resilience under *in situ* conditions where the vast 'free living pool' of *Symbiodinium* is available to the sponges. The diversity

and plasticity of sponge-*Symbiodinium* associations clearly deserves further attention. Little is know about the response of photosymbiotic sponges to the recent global coral bleaching event (Hughes *et al.*, 2017a; 2017b), but a study of Caribbean *Cliona viridis* complex spp. showed that, in contrast to 30% bleaching in the local coral population, all sponges maintained intact symbioses (Fang *et al.*, 2018b).

In the light of bleaching susceptibility, the mechanism that enables symbiont relocation from the upper surface of the sponge to deeper tissues and back to the surface also deserves further attention. This mechanism can shelter the symbionts from the light and heat stress of the surface layer (Chapter 2), and it may be key to the bleaching tolerance of the sponge. Since *Symbiodinium* are intracellular, one would expect that sponge cells are their vehicle for relocation, yet it remains unclear to what extent the symbiont relocation is a phototactic response or a host-controlled response, or a combination of both. There is a clear need for detailed investigations of the relocation process at the cellular level, as done for example in symbiotic Foraminifera (Petrou *et al.*, 2016). Ideally, these investigations should be accompanied by detailed *in vivo* mapping of the internal light, heat and metabolic regimes of tissue layers of the sponge, moving stepwise from the surface to deeper internal tissues using state of the art micro-sensor technology (as done in corals; e.g. Wangprausert *et al.*, 2015; 2017). Such micro-sensors could even directly measure oxygen and calcium fluxes. In that way, symbiont relocation as well as bioerosion and metabolic potential can be linked to specific micro-environments of each tissue layer.

Our findings demonstrated that a crucial factor in defining the well-being of photosymbiotic clionaid sponges is the photosynthetic activity of their symbionts (Chapters 2, 3 and 4). Since photosynthetic activity is maintained only in intact symbioses, and intact symbioses are maintained only under certain temperature conditions, it follows that the well-being of the host is closely linked to the heat tolerance of the holobiont. However, keeping the symbiosis intact does not necessarily guarantee host well-being. For example, a large proportion of photosynthetically inhibited *Symbiodinium* persisted in sponges treated with DCMU, even though they had lost their ability to contribute photosynthetic products to the host metabolism i.e. they no longer contributed to the well-being of the host (Chapter 2). Similarly, even though *Symbiodinium* may avoid heat or light stress by moving deeper into the sponge, unless they acclimate to the lower light levels, they will not be deriving the same amount of photosynthetic products for their host. In other words, the mechanisms that enable *Symbiodinium* to tolerate heat stress may nonetheless result in negative impacts on the energy

budget of the sponge, and therefore heat tolerance of *Symbiodinium* should not be regarded as a strict synonym of host well-being.

Rather than simply keeping the symbiosis intact, the significance of uninterrupted symbiont photosynthesis for the overall energy requirements and, importantly, the bioerosion performance of the holobiont was clear in all three chapters of this thesis. Photosynthesis served as an important source of inorganic nutrient uptake (Chapter 3), and when impaired, the bioerosion rates (Chapters 2 and 4) and overall health conditions of the sponge (Chapter 4) decreased. Prolonged loss of photosynthesis resulted in an unsustainable carbon budget, which eventually led to prevalent sponge mortality (Chapter 4).

The mystery of the bioerosion mechanism

Evidence of direct translocation of photosynthetic products (photosynthates and/or oxygen) to the etching cells of the sponge is needed to solidify the argument that photosynthesis stimulates bioerosion (Chapters 2 and 3). Without this evidence, the facet of photosynthesis (photosynthates versus oxygen) that assisted with the bioerosion process remains unclear. If the movement of protons into the space of decalcification requires energy, then this needs to be delivered to the pseudopodia of the etching cells. In that respect, it would be very informative to examine whether the etching cells are sites of high energy use by measuring ATP consumption, as has been done for the choanocytes of non-bioeroding sponges (Lukik-Bilela *et al.*, 2011). At the same time, photosynthesis may not only supply sugars, but it may also supersaturate sponge tissues with oxygen, enabling the activation of mitochondria for ATP production in these deep tissues. Experiments supersaturating bleached sponges with oxygen, in the presence and absence of glucose, may enable these roles to be partially teased apart, as has been done for corals (Colombo-Pallotta *et al.*, 2010). Similarly, it would be interesting to bubble saturated O_2 through the base of a thinned down skeleton to examine whether decalcification rates of bleached or photosynthetically inhibited sponges can be recovered.

Many photosynthetic organisms facilitate the transport of oxygen to deep anaerobic tissue to power mitochondria to grow this tissue, to take up nutrients, or to bring about other metabolic functions that require active respiration. For instance, marsh grasses, mangroves and seagrasses maintain microaerobic zones around their otherwise anaerobic or even anoxic roots, and these zones are supplied primarily with photosynthetic oxygen from the above-ground compartments (Teal and Kanwisher, 1966; Fry et al., 1982; Hemminga, 1998; Hogarth, 2015). One could perhaps draw parallels to such organisms to imagine how

bioerosion could be stimulated by photosynthetic oxygen that is transported to deeper, relatively anaerobic (due to microbial activity) layers of the sponge. Alternatively, even though live cover by the sponge prevents new colonization by endoliths (Schönberg and Loh, 2005; Fang *et al*., 2013b), it is plausible that microendolithic algae residing beneath the sponge zone could serve as a potential oxygen source deeper inside the skeleton. The role that endolithic algae play in fuelling coral metabolism is rapidly gaining interest (Thompson *et al.*, 2015 and references therein), and likewise the potential for provision of resources (or chemical properties associated with sponge erosion) from organisms residing in the underlying layers of the coral skeleton deserves further attention.

It is clear that perhaps the most crucial hurdle to our understanding of sponge bioerosion, in both photosymbiotic and non-photosymbiotic species, remains the lack of precise understanding of the excavating mechanism on the cellular level (reviewed by Schönberg, 2008). We came up against this hurdle a number of times, throughout this thesis, when wanting to interpret our findings or their implications for bioerosion rates, as will other studies if the mechanisms remain unresolved. To develop a comprehensive model of how photosynthesis stimulates bioerosion, understanding of the physicochemical processes and the structural properties of the site of decalcification is a necessary prerequisite. Technical difficulties in the histological examination of the etching front, for example, impeded us from analysing its isotopic composition though nanoscale secondary ion mass spectrometry (NanoSIMS), meaning that direct translocation of photosynthetic products to the etching cells could not be examined (Chapter 3). There is an urgent need for more sophisticated experiments that will allow direct, real time observation of the process of excavation and identification of the associated chemical/enzymatic agents in non-photosymbiotic bioeroding sponges to begin with. For instance, tracer experiments targeting the fate of Ca^{+2} during the bioerosion process can elucidate whether calcium pumps play a role in chemical etching. Staining for Ca^{2+}/H^{+} ATPases in the small but deep recesses of etching cells may be informative, while the effect of inhibition of Ca^{2+} ATPases on bioerosion can be studied using specific inhibitors such as Ruthenium red (Al-Horani *et al.*, 2003).

Photosymbiotic bioeroding sponges and future reefs

Bleaching and mortality occurred when we exposed the sponges to climate conditions that are likely to occur annually in 2100, and beyond, if society continues to emit large amounts of greenhouse gasses in a "business-as-usual" fashion (IPCC, 2013) (Chapter 4). Between now and the end of our century, climate change will intensify unless measures to curb emissions

are adhered to internationally. At the same time, thermal conditions such as those tested [DHW<4ºC-weeks during the first two weeks of "full treatment" (Fig. 4.1b), followed by 4<DHW<8 during the next two weeks, and DHW>8 over the remaining 6 weeks of the experiment, reaching a maximum of 18 DHW at the end of the experiment] may be associated with sporadic El Niño events that are also expected to intensify in the future (Cai *et al.*, 2014). Therefore, our findings of sponge mortality with regards to warming may apply *in situ* before mid-Century, on reefs during El Niño years. Recently coral reefs have suffered severely from mass coral bleaching and mortality, with over one fourth of the GBR experiencing between 8-16 DHW over a three month period in 2016, particularly in the northern region (Hoegh-Guldberg, 2012; Hughes *et al.*, 2017a, 2017b; NOAA Coral Reef Watch, 5 km satellite data). Similar widespread bleaching or losses of photosymbiotic sponges have not yet been documented (Schönberg *et al.*, 2017b), and so far no data on the response of sponges to the recent warming event on the GBR have been presented. An individual report from the Caribbean suggests that sponge bleaching may become frequent sooner than we currently appreciate (Hill *et al.*, 2016). On the other hand, ocean acidification seems to be building up steadily without abrupt acidification events, and therefore our findings relating to acidification alone do not directly apply to reefs prior to the end of the century.

Overall, the response of bioeroding sponges (including photosymbiotic species) to changing seawater conditions might be parabolic (i.e. initial linear response followed by a maximum and eventually a decay): in the near future these opportunistic sponges will most likely prosper, taking advantage of reduced competition, increased acidity, nutrients and availability of bioerosion substrate due to coral mortality; at a yet unidentified point in time their success will plateau; if stressors persist, their trajectory may eventually (sooner rather than later for photosymbiotic species, Chapter 4) proceed downhill from there (Schönberg *et al.*, 2017a). To a certain extent photosymbiotic bioeroding sponges may benefit from weaker, more readily erodible coral skeletons (due to ocean acidification) in the near future, but it remains to be explored whether this benefit will compensate for losses to their bioerosion capacity caused by reduced metabolism.

Sponge survival rates will also be modulated by their ability to re-acquire photosymbionts when heat stress is alleviated during cooler seasons of the year. Summer heat stress caused sponge bleaching and approximately 50% population mortality 3-6 weeks post initial bleaching in our study (with bleaching occurring at MMM+2.7°C or more, Chapter 4), but we

did not examine the potential for recovery of the sponges. The post-bleaching survival and recovery rates of photosymbiotic sponges deserve further attention in more comprehensive studies spanning autumn and winter projections, along with *in situ* studies that will document the current trajectory of bioeroding sponges as their well-being increases and eventually plateaus. Such studies could draw parallels from recent methodology and findings concerning the post-bleaching survival of corals (e.g. Grottoli *et al*., 2014; Levas *et al.*, 2018).

Sponge survival rates will also depend on their ability to increase their heterotrophic feeding when autotrophic feeding is impaired. Heterotrophic feeding did not increase after short-term photosynthetic impairment in heat- or algaecide-treated *C. orientalis* sponges (Chapter 2). Likewise, supplementing the sponges' diet with particulate organics led to enhanced bioerosion rates, but the boost from heterotrophic feeding was not sufficient to maintain a positive carbon budget in longer-term bleached sponges (Chapter 4). The stimulation of bioerosion by particulate organics helps to explain why *C. orientalis* fares well on inshore, nutrient-rich reefs of the GBR (provided that macroalgal competition is not strong; Ramsby *et al.*, 2017a). Different populations of the sponge may have acclimated to different heterotrophy to autotrophy ratios depending on whether they inhabit inshore, nutrient-rich reefs with poor water clarity versus offshore, nutrient-poor reefs with high water clarity. Trade-offs between heterotrophy and autotrophy within single individuals however remain debatable (Fang *et al*., 2014, 2017, 2018; Pineda *et al*., 2017b). Future experiments addressing the feeding plasticity of photosymbiotic sponges are clearly of need.

Studies addressing the capacity of photosymbiotic sponges to acclimate or adapt to prolonged warming and/or acidification over the next decade are also missing. Perhaps there are populations that naturally occur in extreme habitats and/or are more tolerant to environmental fluctuations. Such populations of bioeroding sponges have been described in high-CO_2 environments (e.g. CO_2 seeps; Fabricius *et al.*, 2011), but to our knowledge populations with enhanced thermal capacity have not been described so far.

While the research undertaken in this thesis demonstrated that loss of photosynthesis in a *Cliona viridis* sponge species has important consequences at the organismal level, it was unable to map out the repercussions of such a loss for reef productivity. This is because primary productivity by photosymbiotic sponges on coral reefs has only been poorly quantified so far (as pointed out by Wilkinson, 1983; Thacker and Freeman, 2012; Pawlik *et al.*, 2015b; De Goeij *et al.*, 2017), and estimates of the contributions of specific taxa such as the photosymbiotic bioeroding sponges to reef productivity are lacking. With increasing

abundance of sponges on both present and future degraded reefs, their contribution to primary productivity as well as to organic nutrient cycling warrants revision of classic reef food webs (De Goeij *et al.*, 2017). More studies on the productivity of photosymbiotic bioeroding sponges are needed to determine their role in benthic food webs.

Considerations for future studies

In the light of future changes on reefs (warming, acidification and eutrophication examined here), we have shown that warming had the largest impact due to the changes it brought about to the photosynthetic potential of the holobiont (Chapter 4). The fact that we could tease apart the independent effects of warming, acidification and eutrophication and confirm that warming alone was sufficient to diminish photosynthetic health, serves as a strong argument in favour of experimental designs that enable the examination of interaction effects of multiple factors. It is true that future seawater conditions will encompass a combination of stressors (Meehl *et al.*, 2007), and therefore experiments are more realistic when the joint impact of these factors is studied (Wernberg *et al.*, 2012). Yet ideally, an experiment should also have the power to identify the driving force behind the changes observed, and therefore we argue for more crossed-design studies where independent and concurrent effects are equally considered. Unravelling independent effects is particularly important in the context of climate change, where intensifying El Niño events will cause sudden seawater temperature changes, but acidification will remain milder. As demonstrated in Chapter 4, a deeper understanding of independent effects will help assess whether controlling local stressors can ameliorate the impact of global stressors and *vice versa*. It will also help prioritize management efforts by laying the focus on mitigating the stressor with the most critical effect.

As important as testing multiple factors is the inclusion of multiple species in future experiments (Fang *et al*., 2018a). Depending on the natural conditions they are adapted to, sponge taxa from the Indo-Pacific and the Caribbean have been shown to respond differentially to warming and/or acidification (Duckworth *et al.*, 2012; Wisshak *et al.*, 2013; Bennet *et al.*, 2016). Our approach focused on a single species (Chapter 4), but other bioeroding sponges and other sponges in general need to be investigated before our results can be meaningful at the ecosystem level. What is more, competition and other ecological interactions with non-sponge reef species will be decisive to future outcomes. Excavating sponges are opportunistic competitors of not only corals but also algae, which are in turn controlled by other reef organisms (e.g. Chaves-Fonnegra and Zea, 2011; González-Rivero *et*

al., 2016). This dynamic competition may be especially important to the reproduction of excavating sponges, for example by exerting pressure on sponge recruitment. We did not include sexual or asexual reproductive output as a response variable in our study, but this remains another important area to explore in order to describe population changes of excavating sponges in reef communities (Schönberg *et al.*, 2017b).

In most of the present thesis, we have discussed sponge health through the lens of symbiont population and productivity. Inevitably, this has meant that a number of conclusions that we draw are not readily applicable to non-photosymbiotic sponges. These organisms deserve similar attention in future studies. Some of the methodologies developed in this thesis can be instrumental in studying such species, and in studying sponges in general. In this regard, we would like to particularly stress the applicability of the methodologies presented in Chapter 3 for studying realized trophic interactions and metabolic processes within sponge holobionts, or even between sponges and other reef organisms. The integration of isotopic labelling, electron microscopy and NanoSIMS is a powerful tool to study feeding strategies and metabolic interactions at the single-cell level, while keeping the holobiont intact (Musat *et al.*, 2012; Pernice and Levy, 2014). NanoSIMS can have numerous applications in the field of sponge research (and beyond), and we anticipate that it will be widely used as a tool in future studies of sponges, especially given the current interest in the functional potential of the sponge microbiome (Hill and Sacristán-Soriano, 2017; Pita *et al.*, 2018) and the role of sponges as nutrient cyclers in food webs of coral reefs (de Goeij *et al.*, 2013; 2017; Rix *et al.*, 2016a, 2016b, 2017). For example, one could examine closely what role certain symbionts play in holobiont trophic behaviour, or one could ascertain which cellular structures are responsible for uptake of various nutritious sources, be it inorganic or organic, dissolved or particulate. And as these novel technologies develop even further so will our ability to listen in on the conversations between marine sponges and their symbiotic players even more closely and precisely.

Exploring *Symbiodinium*-invertebrate symbioses

Last but not least, by focusing on the dynamics of the sponge-*Symbiodinium* symbiosis, we have not only contributed to the understanding of photosymbiosis in sponges, but we have also contributed to a more generic body of knowledge on the interaction of heterotrophic hosts and ancient dinoflagellate symbionts such as *Symbiodinium* (Stanley *et al.*, 2003; Muscatine *et al.*, 2005). Currently, the nature of such interactions remains ambiguous. For example, even in the better studied partnership of Cnidaria and *Symbiodinium*, the fine

dynamics and the selective pressures that favour its existence have not been satisfactorily explained (Yellowlees *et al.*, 2008; Hill and Hill, 2012). Bioeroding sponges in that respect present a useful framework for studying why *Symbiodinium* forms symbioses with invertebrates, and how these are maintained. The exclusive association of *Symbiodinium* with bioeroding sponges over other sponges may hold answers with regards to the properties that make a host hospitable to these dinoflagellates (Hill and Hill, 2012). For example, experiments where aposymbiotic sponges are reinfected with *Symbiodinium* under active versus inhibited bioerosion can elucidate the role of Ca^{2+} availability in host hospitability, providing evidence for or against the magnesium inhibition hypothesis (Hill and Hill, 2012). Analysis of non-cnidarian holobionts such as sponges can shed light on the nuanced areas of various *Symbiodinium* associations, including the cnidarian one that in the long run subsidizes the existence of coral reefs (Muscatine and Porter, 1977). This knowledge is essential as the scientific community strives to respond to the challenges that present-day reefs face.

5.3. Significance for coral reefs

Apart from their intrinsic value, coral reefs such as Australia's Great Barrier Reef provide a large number of ecological goods and services that are important to human livelihoods, well-being and economies (Moberg and Folke, 1999; Carr and Mendelsohn, 2003; Marshall and Johnson, 2007). If changing climatic conditions come to favour decalcification mechanisms such as bioerosion, then the degradation of the already weakened coral frameworks is likely to be exacerbated (Fang *et al.*, 2013a; Kennedy *et al.*, 2013; IPCC, 2014). These changes need to also be placed with the context of the increasingly intense storms that are expected as part of climate change (Peduzzi *et al*., 2012). The two drivers, stronger storms and weakened coral reefs structures, are likely to combine to have major impacts on the availability of coral reef habitat. In turn, loss of coral reef habitat will detrimentally impact other reef-dependent species and the physical foundations of reef ecosystems as a whole (Marshall and Johnson, 2007; Hoegh-Guldberg, 2012).

The significance of the current study thus lays in the provision of a deeper understanding of the role of clionaid sponges in present and future dynamics of coral reefs, which is an urgent prerequisite for responding to the challenge of changing $CaCO_3$ balances. Bioerosion is crucial to understanding the decline of corals, coral reefs and their 3-D structures, but is often overlooked by legislators and coastal resource managers. Reef-wide models of carbonate

budgets are increasing our understanding of the dynamic existence of reef frameworks, and of the appropriate management strategies to secure their existence into the future, but bioerosion data are often missing (Perry *et al.*, 2012; 2014). By studying a prominent eroding sponge, we hope to have provided further valuable information on the manner in which bioeroders sustain their metabolism, erode and flourish under intermediate disturbance events, thereby altering $CaCO_3$ balances. Such information can be applied in a predictive management context for coral reefs worldwide, and is ever more crucial for the protection of GBR habitats themselves, especially given the current threats to habitat quality both on inshore and offshore reefs. Global climate stressors as well as local agriculture runoff and plans for dredging to allow harbour expansions and increased coal export activity have led to a controversy on the continuation of the UNESCO status of the GBR (Grech *et al.*, 2016; UNESCO, 2016a, 2016b). In a time like this, understanding how future changes will influence the $CaCO_3$ balance on protected reefs –favouring organisms such as excavating sponges, or not– is of great significance to management efforts. It is hoped that some of the extreme scenarios explored in the present thesis will not come to pass and that global society will rapidly decarbonise in order to avoid these scenarios. Only time, however, will tell.

……

All in all, the current thesis has used a number of novel techniques to provide insights into the biology of bioeroding sponges and the carbonate balance of coral reefs, focusing on the interaction between photosynthesis and bioerosion inside the sponge *Cliona orientalis*. In this regard, the intimate relationship between the sponge host and its photosynthetic microbes was literally "put under the microscope", always in the context of the even more intimate relationship of this holobiont with the calcium carbonate that it vigorously erodes. It was the fascination for such reworking of carbonates by living organisms that kick-started this thesis. Coming to an end, it is hoped that this fascination has grown in the reader as it has in the author, together with an increased appreciation of the need for interdisciplinary research on these intriguing interactions between the animate and the inanimate realms of coral reefs.

Bibliography

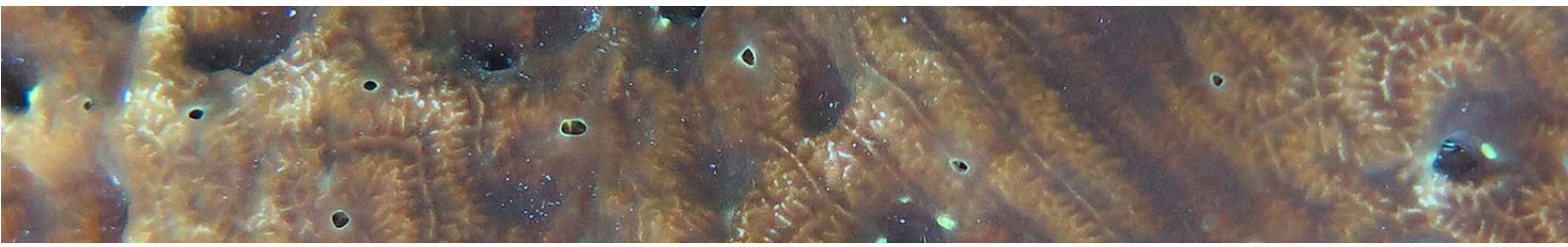

A

Acker KL, Risk MJ. (1985). Substrate destruction and sediment production by the boring sponge *Cliona caribbaea* on Grand Cayman Island. *J Sediment Res* **55**: 705-711.

Adey WH, Steneck RS. (1985). Highly productive eastern Caribbean reefs: synergistic effects of biological, physical and geological factors. In: Reaka, M.L. (Ed.), The Ecology of Coral Reefs. National Oceanic and Atmospheric Administration, Rockville, Maryland, pp. 163–187

Aerts LAM. (1999). Sponge/coral interactions in Caribbean reefs: analysis of overgrowth patterns in relation to species identity and cover. *Mar Ecol Prog Ser* **175**: 241–249.

Al-Horani FA. (2016). Physiology of skeletogenesis in scleractinian coral, in Cheryl M. Woodley, Craig A. Downs, Andrew W. Bruckner, James W. Porter, S. B. G. (ed.) *Diseases of Coral*. John Wiley & Sons, New Jersey.

Al-Horani FA, Al-Moghrabi SM, De Beer D. (2003). The mechanism of calcification and its relation to photosynthesis and respiration in the scleractinian coral *Galaxea fascicularis*. *Mar Biol* **142:** 419-426.

Allemand D, Ferrier-Pagès C, Furla P, Houlbrèque F, Puverel S, Reynaud S, *et al.* (2004). Biomineralisation in reef-building corals: From molecular mechanisms to environmental control. *CR Paleovol* **3**: 453–467.

Allemand D, Tambutté É, Zoccola D, Tambutté S. (2011). Coral calcification, cells to reefs. In: *Coral reefs: an ecosystem in transition*. Springer, pp 119–150.

Anderson MJ, Gorley RN, Clarke KR. (2008). *PERMANOVA+ for PRIMER: guide to software and statistical methods*. PRIMER-E Ltd: Plymouth, UK.

Anderson MJ, Walsh DC. (2013) PERMANOVA, ANOSIM, and the Mantel test in the face of heterogeneous dispersions: what null hypothesis are you testing? *Ecol Monograph* **83**: 557-74.

Andersson AJ, Gledhill D. (2013). Ocean acidification and coral reefs: effects on breakdown, dissolution, and net ecosystem calcification. *Ann Rev Mar Sci* **5**: 321–348.

Andersson AJ, Mackenzie FT, Bates NR. (2008). Life on the margin: implications of ocean acidification on Mg-calcite, high latitude and cold-water marine calcifiers. *Mar Ecol Prog Ser* **373:** 265-274.

Angly FE, Pantos O, Morgan TC, Rich V, Tonin H, Bourne DG *et al.* (2016). Diuron tolerance and potential degradation by pelagic microbiomes in the Great Barrier Reef lagoon, *PeerJ*, **4:** e1758.

Astier C, Boussac A, Etienne AL. (1984). 'Evidence for different binding sites on the 33-kDa protein for DCMU, atrazine and QB', *FEBS Lett*. **167**: 321–326.

Atkins P, De Paula J. (2009) Physical chemistry. 9th edn. WH Freeman, New York, NY.

B

Bell JJ, Davy SK, Jones T, Taylor MW, Webster NS. (2013). Could some coral reefs become sponge reefs as our climate changes? *Glob Chang Biol* **19**: 2613–2624.

Bender DA. (1985). *Amino Acid Metabolism*. Wiley Interscience: New York.

Bennett HM, Altenrath C, Woods L, Davy SK, Webster NS, Bell JJ. (2016). Interactive effects of temperature and pCO_2 on sponges: From the cradle to the grave. *Glob Chang Biol* **23***:* 2031-2046.

Bennett H, Bell JJ, Davy SK, Webster NS, Francis DS (2018). Elucidating the sponge stress response;

lipids and fatty acids can facilitate survival under future climate scenarios. *Glob Chang Biol* **24***:* 3130–3144.

Berkelmans R, Van Oppen MJ. (2006). The role of zooxanthellae in the thermal tolerance of corals: a 'nugget of hope'for coral reefs in an era of climate change. *Proc Royal Soc Lond B* **273**: 2305-12.

Berman-Frank I, Lundgren P, Chen Y-B, Küpper H, Kolber Z, Begman B, Falkowski P. (2001). Segregation of nitrogen fixation and oxygenic photosynthesis in the marine cyanobacterium *Trichodesmium*. *Nature* **294**: 1534–1537.

Bozec YM, Alvarez-Filip L, Mumby PJ. (2015). The dynamics of architectural complexity on coral reefs under climate change. *Glob Chang Biol* **21**: 223–235.

Brading P, Warner ME, Davey P, Smith DJ, Achterberg EP, Suggett DJ. (2011). Differential effects of ocean acidification on growth and photosynthesis among phylotypes of *Symbiodinium* (Dinophyceae). *Limnol Oceanogr* **56**: 927-938.

Brading P, Warner ME, Smith DJ, Suggett DJ. (2013). Contrasting modes of inorganic carbon acquisition amongst *Symbiodinium* (Dinophyceae) phylotypes. *New Phytol* **200**: 432-442.

Brown BE, Dunne RP. (2016). Coral Bleaching: the roles of sea temperature and solar radiation. In: *Woodley CM, Downs CA, et al. Diseases of Coral*, Wiley, New Jersey, p266-283.

Bryant DA, Frigaard NU. (2006). Prokaryotic photosynthesis and phototrophy illuminated. *Trends Microbiol* **14**: 488–496.

Burke LM, Reytar K, Spalding M, Perry A. (2011). *Reefs at Risk Revisited*. World Resources Institute, Washington.

Burriesci MS, Raab TK, Pringle JR. (2012). Evidence that glucose is the major transferred metabolite in dinoflagellate-cnidarian symbiosis. *J Exp Biol* **215**: 3467–3477.

Butler, W. L. (1978) Energy distribution in the photochemical apparatus of photosynthesis, *Ann Rev Plant Physiol* **29**: 345–78.

C

Cai W, Borlace S, Lengaigne M, van Rensch P, Collins M, Vecchi G, *et al.* (2014). Increasing frequency of extreme El Niño events due to greenhouse warming. *Nat Clim Chang* **5**: 1–6.

Cantin NE, Negri AP, Willis BL. (2007). Photoinhibition from chronic herbicide exposure reduces reproductive output of reef-building corals. *Mar Ecol Prog Ser* **344**: 81–93.

Carballo JL, Bautista E, Nava H, Cruz-Barraza JA, Chávez JA. (2013). Boring sponges, an increasing threat for coral reefs affected by bleaching events. *Ecol Evol* **3**: 872–886.

Carl-Friedrich Schleussner BC, Lissner TK, Fischer EM, Wohland J, Perrette M, Golly A, *et al.* (2016). Differential climate impacts for policy-relevant limits to global warming: the case of 1.5 ºC. *Earth Syst Dynam* **7**: 327–351.

Carr L, Mendelsohn R. (2003). Valuing coral reefs: a travel cost analysis of the Great Barrier Reef. *Ambio* **32**: 353–357.

Chaves-Fonnegra A, Castellanos L, Zea S, Duque C, Rodríguez J, Jiménez C. (2008). Clionapyrrolidine A—a metabolite from the encrusting and excavating sponge *Cliona tenuis* that kills coral tissue upon contact. *J Chem Ecol* **34:** 1565-1574.

Chaves-Fonnegra A, Riegl B, Zea S, Lopez J V., Smith T, Brandt M, *et al.* (2017). Bleaching events regulate shifts from corals to excavating sponges in algae-dominated reefs. *Glob Chang Biol* **24**: 773-

85.

Chaves-Fonnegra A, Zea S, Gómez ML. (2007). Abundance of the excavating sponge *Cliona delitrix* in relation to sewage discharge at San Andrés Island, SW Caribbean, Colombia. *Boletín Investig Mar y Costeras-INVEMAR* **36**: 63–78.

Chaves-Fonnegra A, Zea S. (2011). Coral colonization by the encrusting excavating Caribbean sponge *Cliona delitrix*. *Mar Ecol* **32**: 162–173.

Chaves-Fonnegra, A. Zea, S. (2007) Observations on reef coral undermining by the Caribbean excavating sponge *Cliona delitrix* (Demospongiae, Hadromerida). *Proc 7th Int Sponge Symp, Río de Janeiro, Brazil*, 247–254.

Clarke, KR, Gorley, RN. (2006). *PRIMER v6: User Manual/Tutorial*. PRIMER-E Ltd: Plymouth, UK.

Cohen AL, McConnaughey TA. (2003). Geochemical perspectives on coral mineralization. Rev. Mineral. Geochem **54**: 151-187.

Colombo-Pallotta MF, Rodríguez-Román A, Iglesias-Prieto R. (2010). Calcification in bleached and unbleached *Montastraea faveolata*: Evaluating the role of oxygen and glycerol. *Coral Reefs* **29**: 899–907.

Colvard NB, Edmunds PJ. (2011). Decadal-scale changes in abundance of non-scleractinian invertebrates on a Caribbean coral reef. *J Exp Mar Bio Ecol* **15**:153-60.

Consalvey M, Perkins RG, Paterson DM, Underwood GJ (2005). PAM fluorescence: a beginners guide for benthic diatomists. *Diatom Research* **20**:1-22.

Cooper TF, De'Ath G, Fabricius KE, Lough JM. (2008). Declining coral calcification in massive *Porites* in two nearshore regions of the northern Great Barrier Reef. *Glob Chang Biol* **14**: 529–538.

Cornwall CE, Hepburn CD, Pritchard D, Currie KI, Mcgraw CM, Hunter KA, *et al.* (2012). Carbon-use strategies in macroalgae: Differential responses to lowered pH and implications for ocean acidification. *J Phycol* **48**: 137–144.

Cornwall CE, Hurd CL. (2016). Experimental design in ocean acidification research: problems and solutions. *ICES J Mar Sci* **73**: 572–581.

Corredor JE, Wilkinson CR, Vicente VP, Morell JM, Otero E. (1988). Nitrate release by Caribbean reef sponges. *Limnol Oceanogr* **33**: 114-20.

Crain CM, Kroeker K, Halpern BS. (2008). Interactive and cumulative effects of multiple human stressors in marine systems. *Ecol Lett* **11**: 1304–1315.

Crook ED, Cohen AL, Rebolledo-Vieyra M, Hernandez L, Paytan A. (2013). Reduced calcification and lack of acclimatization by coral colonies growing in areas of persistent natural acidification. *Proc Natl Acad Sci* **110**: 11044–9.

CSIRO (Commonwealth Scientific and Industrial Research Organisation) and PMEL (Pacific Marine Environmental Laboratory) Carbon Program. Available at: https://www.pmel.noaa.gov/co2/story/Heron+Island (date of access Nov 2016).

D

D'Elia CF, Domotor SL, Webb KL. (1983). Nutrient uptake kinetics of freshly isolated zooxanthellae. *Mar Biol* **75**: 157–167.

De Bakker DM, van Duyl FC, Bak RPM, Nugues MM, Nieuwland G, Meesters EH. (2017). 40 Years

of benthic community change on the Caribbean reefs of Curaçao and Bonaire: the rise of slimy cyanobacterial mats. *Coral Reefs* **36**: 1–13.

De Bakker DM, Webb AE, van den Bogaart LA, van Heuven SMAC, Meesters EH, van Duyl FC. (2018) Quantification of chemical and mechanical bioerosion rates of six Caribbean excavating sponge species found on the coral reefs of Curaçao. *PLoS ONE* **13**: e0197824.

De Goeij JM, Lesser MP, Pawlik JR. (2017). Nutrient fluxes and ecological functions of coral reef sponges in a changing ocean. In: Bell JJ and Carballo JL (eds). *Climate Change, Ocean Acidification and Sponges*. Springer, pp 373–410.

De Goeij JM, Moodley L, Houtekamer M, Carballeira NM, Duyl FC van. (2008). Tracing ^{13}C-enriched dissolved and particulate organic carbon in the bacteria-containing coral reef sponge *Halisarca caerulea*: Evidence for DOM-feeding. *Limnol Oceanogr* **53**: 1376.

De Goeij JM, Van Den Berg H, van Oostveen MM, Epping EHG, Van Duyl FC. (2008). Major bulk dissolved organic carbon (DOC) removal by encrusting coral reef cavity sponges. *Mar Ecol Prog Ser* **357**: 139-151.

De Goeij JM, van Oevelen D, Vermeij MJ, Osinga R, Middelburg JJ, de Goeij AF, *et al.* (2013). Surviving in a marine desert: the sponge loop retains resources within coral reefs. *Science* **342**: 108–110.

De'ath G, Lough JM, Fabricius KE. (2009). Declining coral calcification on the Great Barrier Reef. *Science* **323**: 116–119.

DeCarlo TM, Cohen AL, Barkley HC, Cobban Q, Young C, Shamberger KE, *et al.* (2015). Coral macrobioerosion is accelerated by ocean acidification and nutrients. *Geology* **43**: 7–10.

Delosme R, Olive J, Wollman FA. (1996). Changes in light energy distribution upon state transitions: an in vivo photoacoustic study of the wild type and photosynthesis mutants from *Chlamydomonas reinhardtii*. *Biochim Biophys Acta* **1273**: 150-8.

Diaz MC, Rützler K. (2001). Sponges: An essential component of Caribbean coral reeds. *Bull Mar Sci* **69**: 535–546.

Diaz MC, Thacker RW, Rützler K, Piantoni Dietrich C. (2007) Two new haplosclerid sponges from Caribbean Panama with symbiotic filamentous cyanobacteria, and an overview of sponge-cyanobacteria associations. *Porifera Research Biodiversity, Innovation and Sustainability* pp. 31–39.

Dove SG, Kline DI, Pantos O, Angly FE, Tyson GW, Hoegh-Guldberg O. (2013). Future reef decalcification under a business-as-usual CO_2 emission scenario. *Proc Natl Acad Sci* **110**: 15342–15347.

Duckworth AR, Peterson BJ. (2013). Effects of seawater temperature and pH on the boring rates of the sponge *Cliona celata* in scallop shells. *Mar Biol* **160**: 27–35.

Duckworth AR, West L, Vansach T, Stubler A, Hardt M. (2012). Effects of water temperature and pH on growth and metabolite biosynthesis of coral reef sponges. *Mar Ecol Prog Ser* **462**: 67–77.

Dugdale R, Wilkerson F. (1986). The use of ^{15}N to measure nitrogen uptake in eutrophic oceans; experimental considerations. *Limnol Oceanogr* **31**: 673–689.

Durnford DG, Prasil O, Escoubas JM, Falkowski PG. (1998) Assessing the potential for chloroplast redox regulation of nuclear gene expression. In: *Methods in enzymology*, Academic Press **297**: 220-234.

E

Enochs IC, Manzello DP, Carlton RD, Graham DM, Ruzicka R, Colella MA. (2015). Ocean acidification enhances the bioerosion of a common coral reef sponge: Implications for the persistence of the Florida Reef Tract. *Bull Mar Sci* **91**: 271–290.

Enríquez S, Méndez ER, Iglesias-Prieto R. (2005). Multiple scattering on coral skeletons enhances light absorption by symbiotic algae. *Limnol Oceanogr* **50**: 1025-1032.

Erwin PM, Thacker RW. (2007). Incidence and identity of photosynthetic symbionts in Caribbean coral reef sponge assemblages. *J Mar Biol Assoc UK* **87**: 1683–1692.

Erwin PM, Thacker RW. (2008) Phototrophic nutrition and symbiont diversity of two Caribbean sponge-cyanobacteria symbioses. *Mar Ecol Prog Ser* **362**: 139–147.

F

Fabricius K, De'ath G, McCook L, Turak E, Williams DM. (2005). Changes in algal, coral and fish assemblages along water quality gradients on the inshore Great Barrier Reef. *Mar Pollut Bull* **51**: 384–398.

Fabricius KE. (2005). Effects of terrestrial runoff on the ecology of corals and coral reefs: Review and synthesis. *Mar Pollut Bull* **50**: 125–146.

Fabry VJ, Seibel BA, Feely RA, Orr JC. (2008). Impacts of ocean acidification on marine fauna and ecosystem processes. *ICES J Mar Sci* **65**: 414–432.

Falkowski PG, Dubinsky Z, Muscatine L, McCloskey L. (1993) Population control in symbiotic corals. *Bioscience* **43**: 606–611.

Falkowski PG, Raven JA. (2007). *Aquatic photosynthesis*. 2nd edition. Princeton: Princeton University Press.

Fan L, Reynolds D, Liu M, Stark M, Kjelleberg S, Webster NS, *et al.* (2012). Functional equivalence and evolutionary convergence in complex communities of microbial sponge symbionts. *Proc Natl Acad Sci* **109**: E1878–E1887.

Fang JKH, Mason RAB, Schönberg CHL, Hoegh-Guldberg O, Dove S. (2016a). Studying interactions between excavating sponges and massive corals by the use of hybrid cores. *Mar Ecol* **38**: 1–8.

Fang JKH, Mello-Athayde MA, Schönberg CHL, Kline DI, Hoegh-Guldberg O, Dove S. (2013a). Sponge biomass and bioerosion rates increase under ocean warming and acidification. *Glob Chang Biol* **19**: 3581–3591.

Fang JKH, Schönberg CHL, Hoegh O, Dove S. (2017). Symbiotic plasticity of *Symbiodinium* in a common excavating sponge. *Mar Biol* **164**: 1–11.

Fang JKH, Schönberg CHL, Hoegh-Guldberg O, Dove S. (2016). Day/night ecophysiology of the photosymbiotic bioeroding sponge *Cliona orientalis* Thiele, 1900. *Mar Biol* **163**: 1-12.

Fang JKH, Schönberg CHL, Kline DI, Hoegh-Guldberg O, Dove S. (2013b). Methods to quantify components of the excavating sponge *Cliona orientalis* Thiele, 1900. *Mar Ecol* **34**: 193–206.

Fang JKH, Schönberg CHL, Mello-Athayde MA, Achlatis M, Hoegh-Guldberg O, Dove S. (2018a). Bleaching and mortality of a photosymbiotic bioeroding sponge under future carbon dioxide emission scenarios. *Oecologia* **187**: 25-35.

Fang JKH, Schönberg CHL, Mello-Athayde MA, Hoegh-Guldberg O, Dove S. (2014). Effects of ocean warming and acidification on the energy budget of an excavating sponge. *Glob Chang Biol* **20**:

1043–1054.

Fang JKH, Schönberg CHL, Ormond RF. (2018b) Are some photosymbiotic bioeroding sponges more bleaching-tolerant than hard corals? *J Mar Biol Oceanogr* **7**: 2.

Fang JKH, Schönberg CHL. (2015). Carbonate budgets of coral reefs: recent developments in excavating sponge research. *Reef Encounter* **30:** 43–46.

Fang JKH. (2013). Combined effects of ocean warming and acidification on the marine excavating sponge *Cliona orientalis* Thiele, 1900. PhD Thesis, The University of Queensland.

Feely RA, Sabine CL, Lee K, Berelson W, Kleypas J, Fabry VJ, *et al.* (2004). Impact of anthropogenic CO_2 on the $CaCO_3$ system in the oceans. *Science* **305**: 362–366.

Finazzi G, Rappaport F, Furia A, Fleischmann M, Rochaix JD, Zito F, Forti G. (2002). Involvement of state transitions in the switch between linear and cyclic electron flow in *Chlamydomonas reinhardtii*. *EMBO reports*. **3**: 280-285.

Findlay S, McDowell WH, Fischer D, Pace ML, Caraco N, Kaushal SS, Weathers KC. (2010). Total carbon analysis may overestimate organic carbon content of fresh waters in the presence of high dissolved inorganic carbon. *Limnol Oceanogr Methods* **8:** 196–201.

Fiore CL, Jarett JK, Olson ND, Lesser MP. (2010). Nitrogen fixation and nitrogen transformations in marine symbioses. *Trends Microbiol* **18**: 455–463.

Fiore CL, Labrie M, Jarett JK, Lesser MP. (2015). Transcriptional activity of the giant barrel sponge, *Xestospongia muta* Holobiont: Molecular evidence for metabolic interchange. *Front Microbiol* **6**: 364.

Fisher R, O'Leary RA, Low-Choy S, Mengersen K, Knowlton N, Brainard RE, *et al.* (2015). Species richness on coral reefs and the pursuit of convergent global estimates. *Curr Biol* **25**: 500–505.

Fleiss JL, Levin B, Paik MC. (2003). Statistical methods for rates and proportions. Wiley: New Jersey.

Foyer CH, Parry M, Noctor G. (2003). Markers and signals associated with nitrogen assimilation in higher plants. *J Exp Bot* **54**: 585–593.

Freeman CJ, Easson CG, Baker DM. (2014). Metabolic diversity and niche structure in sponges from the Miskito Cays, Honduras. *PeerJ* **2**: e695.

Freeman CJ, Thacker RW, Baker DM, Fogel ML. (2013). Quality or quantity: is nutrient transfer driven more by symbiont identity and productivity than by symbiont abundance? *ISME J* **7**: 1116–1125.

Freeman CJ, Thacker RW. (2011). Complex interactions between marine sponges and their symbiotic microbial communities. *Limnol Oceanogr* **56**: 1577–1586.

Frieler K, Meinshausen M, Golly A, Mengel M, Lebek K, Donner SD, *et al.* (2013). Limiting global warming to 2 °C is unlikely to save most coral reefs. *Nat Clim Chang* **3**: 165–170.

Frøhlich H; Barthel D. (1997). Silica uptake of the marine sponge *Halichondria panicea* in Kiel Bight. *Mar Biol* **128**: 115–125.

Fry B, Scalan RS, Winters JK, Parker PL. (1982). Sulphur uptake by salt grasses, mangroves, and seagrasses in anaerobic sediments. *Geoch et Cosmoch Acta* **46**: 1121-4.

Furla PA, Galgani I, Durand IS, Allemand DE.(2000). Sources and mechanisms of inorganic carbon transport for coral calcification and photosynthesis. *J Exp Biol* **203**: 3445-57.

Futterer DK. (1974). Significance of the boring sponge *Cliona* for the origin of fine grained material

of carbonate sediments. *J Sediment Res* **44:** 79-84.

G

Gaino E, Manconi R, Pronzato R. (1995). Organizational plasticity as a successful conservative tactics in sponges. *Anim Biol* **4**: 31-43.

Gao D, Huang X, Tao Y. (2016) A critical review of NanoSIMS in analysis of microbial metabolic activities at single-cell level. *Crit Rev Biotechnol* **36:** 884-90.

Garate L, Sureda J, Agell G, Uriz MJ. (2017) Endosymbiotic calcifying bacteria across sponge species and oceans. *Sci Rep* **7**:43674.

Garcia-Pichel F. (2006). Plausible mechanisms for the boring on carbonates by microbial phototrophs. *Sediment Geol* **185**: 205–213.

Gates RD, Baghdasarian G, Muscatine L. (1992) Temperature stress causes host-cell detachment in symbiotic Cnidarians: implications for coral bleaching. *Biol Bull* **182**: 324–332.

Gattuso J, Allemand D, Frankignoulle M. (1999). Photosynthesis and calcification at cellular, organismal and community levels in coral reefs: a review on interactions and control by carbonate chemistry. *Am Zool* **39:** 160-183.

Genty B, Briantais J-M, Baker NR. (1989). The relationship between the quantum yield of photosynthetic electron transport and quenching of chlorophyll fluorescence. *Biochim Biophys Acta* **990**: 87–92.

Girden ER. (1992). *ANOVA : repeated measures*. Sage Publications. Newbury Park, USA

Gloeckner V, Wehrl M, Moitinho-Silva L, Gernert C, Schupp P, Pawlik JR, *et al*. (2014). The HMA-LMA dichotomy revisited: an electron microscopical survey of 56 sponge species. *Biol Bull* **227**:78-88.

Glynn PW. (1997). Bioerosion and coral-reef growth: a dynamic balance. In: *Life and death of coral reefs,* Chapmann and Hall: New York, pp 68–95.

González-Rivero M, Bozec YM, Chollett I, Ferrari R, Schönberg CHL, Mumby PJ. (2016). Asymmetric competition prevents the outbreak of an opportunistic species after coral reef degradation. *Oecologia* **181**: 161–173.

González-Rivero M, Ferrari R, Schönberg CHL, Mumby PJ. (2011a). Impacts of macroalgal competition and parrotfish predation on the growth of a common bioeroding sponge. *Mar Ecol Prog Ser* **444**: 133–142.

González-Rivero M, Yakob L, Mumby PJ. (2011b). The role of sponge competition on coral reef alternative steady states. *Ecol Modell* **222**: 1847–1853.

Grech A, Pressey RL, Day JC. (2016). Coal, cumulative impacts, and the Great Barrier Reef. *Conserv Lett* **9**: 200–207.

Grottoli AG, Rodrigues LJ, Palardy JE. (2006) Heterotrophic plasticity and resilience in bleached corals, *Nature* **440**: 1186–1189.

Grottoli AG, Warner ME, Levas SJ, Aschaffenburg MD, Schoepf V, McGinley M, Baumann J, Matsui Y. (2014). The cumulative impact of annual coral bleaching can turn some coral species winners into losers. *Glob Chang Biol* **12**: 3823-3833.

Grover R, Maguer JF, Allemand D, Ferrier-Pages C. (2008). Uptake of dissolved free amino acids by the scleractinian coral *Stylophora pistillata*. *J Exp Biol* **211**: 860–865.

H

Hansen AK, Moran NA. (2011). Aphid genome expression reveals host-symbiont cooperation in the production of amino acids. *Proc Natl Acad Sci* **108**: 2849–2854.

Harper C, Hayward D, Wiid I, Helden P van. (2008). Regulation of nitrogen metabolism in *Mycobacterium tuberculosis*: a comparison with mechanisms in *Corynebacterium glutamicum* and *Streptomyces*. *IUBMB Life* **60:** 643-650.

Hatch WI. (1980). The implication of carbonic anhydrase in the physiological mechanism of penetration of carbonate substrata by the marine burrowing sponge *Cliona celata* (Demospongiae). *Biol Bull* **159**: 135–147.

Hemminga MA. (1998) The root/rhizome system of seagrasses: an asset and a burden. *Journal of Sea Research.* **39**: 183-96.

Hentschel U, Piel J, Degnan SM, Taylor MW. (2012). Genomic insights into the marine sponge microbiome. *Nat Rev Microbiol* **10**: 641–654.

Hentschel U, Usher KM, Taylor MW. (2006). Marine sponges as microbial fermenters. *FEMS Microbiol Ecol* **55**: 167–177.

Hentschel U, Fieseler L, Wehrl M, Gernert C, Steinert M, Hacker J, Horn M. (2003). Microbial diversity of marine sponges. In: *Sponges (Porifera)*, Springer, Berlin-Heidelberg. pp. 59-88.

Hill R, Ralph PJ. (2008). Dark-induced reduction of the plastoquinone pool in zooxanthellae of scleractinian corals and implications for measurements of chlorophyll a fluorescence. *Symbiosis* **46**: 45-56.

Hill MS, Allenby A, Ramsby B, Schönberg C, Hill A. (2011). *Symbiodinium* diversity among host clionaid sponges from Caribbean and Pacific reefs: Evidence of heteroplasmy and putative host-specific symbiont lineages. *Mol Phylogenet Evol* **59**: 81–88.

Hill MS, Hill A. (2012). The magnesium inhibition and arrested phagosome hypotheses: New perspectives on the evolution and ecology of *Symbiodinium* symbioses. *Biol Rev* **87**: 804–821.

Hill MS, Sacristán-Soriano O. (2017). Molecular and Functional Ecology of Sponges and Their Microbial Symbionts. In: Bell JJ and Carballo JL (ed). *Climate Change, Ocean Acidification and Sponges*. Springer, pp 105–141.

Hill MS, Walter C, Bartels E. (2016). A mass bleaching event involving clionaid sponges. *Coral Reefs* **35**: 153.

Hill MS. (1996). Symbiotic zooxanthellae enhance boring and growth rates of the tropical sponge *Anthosigmella varians* forma *varians*. *Mar Biol* **125**: 649–654.

Hill MS. (2014). Production possibility frontiers in phototroph: heterotroph symbioses: Trade-offs in allocating fixed carbon pools and the challenges these alternatives present for understanding the acquisition of intracellular habitats. *Front Microbiol* **5**: 1–11.

Hoegh-Guldberg O, Cai R PE et al. (2014). The Ocean. In: *Climate Change 2014: Impacts, adaptation, and vulnerability, Part B: Regional aspects, Contribution of working group II to the fifth assessment report of the Intergovernmental Panel on Climate Change*. Cambridge University Press, Cambridge.

Hoegh-Guldberg O, Mumby PJ, Hooten AJ, Steneck RS, Greenfield P, Gomez E, *et al.* (2007). Coral reefs under rapid climate change and ocean acidification. *Science* **318**: 1737–1742.

Hoegh-Guldberg O. (1999). Climate change, coral bleaching and the future of the world's coral reefs.

Mar Freshw Res **50**: 839–866.

Hoegh-Guldberg O. (2012). Coral reefs, climate change, and mass extinction. In: *Saving a Million Species*. Springer, pp 261–283.

Hogarth PJ. The biology of mangroves and seagrasses. Oxford University Press; 2015.

Hohmann-Marriott MF, Takizawa K, Eaton-Rye JJ, Mets L, Minagawa J. (2010). The redox state of the plastoquinone pool directly modulates minimum chlorophyll fluorescence yield in *Chlamydomonas reinhardtii*. *FEBS Lett* **584**:1021-1026.

Holmes G, Ortiz J-C, Schönberg CHL. (2009). Bioerosion rates of the sponge *Cliona orientalis* Thiele, 1900: spatial variation over short distances. *Facies* **55**: 203–211.

Holmes KE. (1997). Eutrophication and its effect on bioeroding sponge communities. In: *Proc 8th Int Coral Reef Symp*. Panama City, pp 1411–1416.

Hoogenboom M, Beraud E, Ferrier-Pagès C. (2010). Relationship between symbiont density and photosynthetic carbon acquisition in the temperate coral *Cladocora caespitosa*. *Coral Reefs* **29:** 21-29.

Hughes AD, Grottoli AG, Pease TK, Matsui Y. (2010). Acquisition and assimilation of carbon in non-bleached and bleached corals. *Mar Ecol Prog Ser* **420**: 91–101.

Hughes TP, Anderson KD, Connolly SR, Heron SF, Kerry JT, Lough JM, *et al.* (2018). Spatial and temporal patterns of mass bleaching of corals in the Anthropocene. *Science* **359**: 80–83.

Hughes TP, Barnes ML, Bellwood DR, Cinner JE, Cumming GS, Jackson JBC, *et al.* (2017a). Coral reefs in the Anthropocene. *Nature* **546**: 82–90.

Hughes TP, Kerry J, Álvarez-Noriega M, Álvarez-Romero J, Anderson K, Baird A, *et al.* (2017b). Global warming and recurrent mass bleaching of corals. *Nature* **543:** 373-377.

Hutchings PA. (1986). Biological destruction of coral reefs - A review. *Coral Reefs* **4**: 239–252.

I

IPCC. (2000) Special report on emissions scenarios (eds Nakicenovic N, Swart R), Cambridge University Press, Cambridge.

IPCC. (2013). Climate Change 2013: The physical science basis. Contribution of working group I to the fifth assessment report of the Intergovernmental Panel on Climate Change. (eds Stocker T.F. *et al*.), Cambridge University Press, Cambridge.

IPCC. (2014). Climate Change 2014: Impacts, adaptation, and vulnerability. Contribution of working group II to the fifth assessment report of the Intergovernmental Panel on Climate Change. (eds Field C.B. *et al*.), Cambridge University Press, Cambridge.

J

Jackson DJ, Thiel V, Wörheide G. (2010). An evolutionary fast-track to biocalcification. *Geobiology* **8**:191-196.

Jackson RB, Le Quéré C, Andrew RM, Canadell JG, Peters GP, Roy J, *et al.* (2017). Warning signs for stabilizing global CO_2 emissions. *Environ Res Lett* **12**: 110202.

Jones RJ, Hoegh-Guldberg O, Larkum AWD, Schreiber U. (1998). Temperature-induced bleaching of corals begins with impairment of the CO_2 fixation mechanism in zooxanthellae. *Plant, Cell & Environment* **21**: 1219–1230.

Jones, R. J. (2004). Testing the “photoinhibition” model of coral bleaching using chemical inhibitors. *Mar Ecol Prog Ser* **284**: 133–145.

Jones RJ, Hoegh-Guldberg O. (2001). Diurnal changes in the photochemical efficiency of the symbiotic dinoflagellates (Dinophyceae) of corals: Photoprotection, photoinactivation and the relationship to coral bleaching. *Plant, Cell & Environment* **24**: 89–99.

Jones RJ. (2003). Effects of herbicides diuron and atrazine on corals of the Great Barrier Reef, Australia. *Mar Ecol Progr Ser* **251**: 153–167.

Jones RJ, Hoegh-Guldberg O. (1999). Effects of cyanide on coral photosynthesis: implications for identifying the cause of coral bleaching and for assessing the environmental effects of cyanide fishing. *Mar Ecol Prog Ser* 11:83-91.

K

Kaern M, Elston TC, Blake WJ, Collins JJ. (2005). Stochasticity in gene expression: from theories to phenotypes. *Nat Rev Genet* **6**: 451–464.

Kanayama M, Kamishima Y. (1990). Role of symbiotic algae in hatching of gemmules of the freshwater sponge, *Radiospongilla cerebellata*. *Zoological science* **7**: 649-655.

Kelmo F, Bell JJ, Attrill MJ. (2013). Tolerance of sponge assemblages to temperature anomalies : Resilience and proliferation of sponges following the 1997-8 El-Niño Southern Oscillation. *PLoS One* **8:** e76441

Kennedy EV, Perry CT, Halloran PR, Iglesias-Prieto R, Schönberg CHL, Wisshak M, *et al.* (2013). Avoiding coral reef functional collapse requires local and global action. *Curr Biol* **23**: 912–918.

Keppel G, Wickens, T.D. (2004). Design and analysis: A researcher’s handbook. Prentice Hall: Upper Saddle River.

Kim H C, Lee, K. (2009). Significant contribution of dissolved organic matter to seawater alkalinity. *Geophys Res Lett* **36**: 1–5.

King N, Westbrook MJ, Young SL, Kuo A, Abedin M, Chapman J, *et al.* (2008). The genome of the choanoflagellate *Monosiga brevicollis* and the origin of metazoans. *Nature* **451**: 783–788.

Kleczkowski LA. (1994). Glucose activation and metabolism through UDP-glucose pyrophosphorylase in plants. *Phytochemistry* **37**: 1507-1515.

Kleypas JA, Langdon C. (2006). Coral reefs and changing seawater carbonate chemistry. *Coast Estuar Stud* **61**: 73–110.

Kline DI, Teneva L, Schneider K, Miard T, Chai A, Marker M, Headley K, Opdyke B, Nash M, Valetich M, Caves JK. (2012). A short-term in situ CO_2 enrichment experiment on Heron Island (GBR). *Sci Rep* **2:** 413.

Knowlton N, Brainard RE, Fisher R, Moews M, Plaisance L, Caley MJ. (2010). Coral reef biodiversity. In: *Life in the World’s Oceans: Diversity Distribution and Abundance*. John Wiley & Sons **18**: 65-74.

Kopp C, Domart-Coulon I, Escrig S, Humbel BM, Hignette M, Meibom A. (2015). Subcellular investigation of photosynthesis-driven carbon and nitrogen assimilation and utilization in the symbiotic reef coral *Pocillopora damicornis*. *MBio* **6**: e02299-14.

Kopp C, Pernice M, Domart-Coulon I, Djediat C, Spangenberg JE, Alexander DTL, *et al.* (2013). Highly dynamic cellular-level response of symbiotic coral to a sudden increase in environmental nitrogen. *MBio* **4**: e00052-13.

Kovačevic G, Kalafatic M, Ljubešic N, Šunjic H. (2001). The effect of chloramphenicol on the symbiosis between alga and hydra. *Biologia, Bratislava* 56: 605-610.

Krause GH, Weis E. (1991) Chlorophyll Fluorescence and Photosynthesis: The Basics. In: *Annu Rev Plant Physiol Plant Mol Biol* 42: 313–349.

Krieger-Liszkay A. (2004). Singlet oxygen production in photosynthesis. *J Exp Bot* **56**: 337–346.

Kroeker KJ, Kordas RL, Crim R, Hendriks IE, Ramajo L, Singh GS, Duarte CM, Gattuso JP. (2013). Impacts of ocean acidification on marine organisms: quantifying sensitivities and interaction with warming. *Glob Chang Biol* **19**: 1884–1896.

Kübler JE, Jonston AM, Raven JA. (1999). The effects of reduced and elevated CO_2 and O_2 on the seaweed *Lomentaria articulata*. *Plant Cell Environ* **22**:1303–10.

Kunert KJ, Dodge AD. (1989). Herbicide-induced radical damage and antioxidative systems. Target sites of herbicide action. CRC Press, Boca Raton, USA **31**:45-63.

L

Lafratta A, Fromont J, Speare P SC. (2016). Coral bleaching in turbid waters of north-western Australia. *Mar Freshw Res* **68:** 65-75.

LaJeunesse, TC, Thornhill DJ. (2011). Improved resolution of reef-coral endosymbiont (*Symbiodinium*) species diversity, ecology, and evolution through psbA non-coding region genotyping. *PLoS ONE* **6:** doi: 10.1371/journal.pone.0029013.

Le Campion Alsumard T, Golubic S, Hutchings P. (1995). Microbial endoliths in skeletons of live and dead corals: *Porites lobata* (Moorea, French Polynesia). *Mar Ecol Prog Ser* **117**: 149–158.

Le Quéré C, Andrew RM, Friedlingstein P, Sitch S, Pongratz J, Manning AC, *et al.* (2018). Global Carbon Budget 2017. *Earth Syst Sci Data* **10***:* 405-448.

Lee R, Robinson J, Cavanaugh C. (1999). Pathways of inorganic nitrogen assimilation in chemoautotrophic bacteria-marine invertebrate symbioses: expression of host and symbiont glutamine synthetase. *J Exp Biol* **202**: 289–300.

Lesser MP, Slattery M. (2013). Ecology of caribbean sponges: Are top-down or bottom-up processes more important? *PLoS One* **8**: 1–9.

Lesser MP. (2006). Benthic–pelagic coupling on coral reefs: feeding and growth of Caribbean sponges. *J Exp Mar Bio Ecol* **328***:* 277-88.

Levas SJ, Grottoli G, Hughes A, Osburn CL, Matsui Y. (2013). Physiological and biogeochemical traits of bleaching and recovery in the mounding species of coral *Porites lobata* : Implications for resilience in mounding corals. *PLoS One* **8:** e63267.

Levas S, Schoepf V, Warner ME, Aschaffenburg M, Baumann J, Grottoli AG. (2018) Long-term recovery of Caribbean corals from bleaching. *J Exp Mar Bio Ecol* **506**: 124-34.

Leys SP, Yahel G, Reidenbach MA, Tunnicliffe V, Shavit U, Reiswig, HM. (2011). The sponge pump: the role of current induced flow in the design of the sponge body plan. *PLoS One* **6:** e27787.

Lide, DR. (2006). *CRC Handbook of Chemistry and Physics*. CRC Press. Boca Raton, USA

Lipps JH, Stanley GD. (2016). Photosymbiosis in past and present reefs. In: *Coral Reefs at the Crossroads*, Springer, Dordrecht, pp. 47–68.

López-Legentil S, Song B, McMurray SE, Pawlik JR. (2008). Bleaching and stress in coral reef

ecosystems: *hsp70* expression by the giant barrel sponge *Xestospongia muta*. *Mol Ecol* **17**: 1840–1849.

López-Victoria M, Zea S, Weil E. (2006). Competition for space between encrusting excavating Caribbean sponges and other coral reef organisms. *Mar Ecol Prog Ser* **312**: 113–121.

López-Victoria M, Zea S. (2005). Current trends of space occupation by encrusting excavating sponges on Colombian coral reefs. *Mar Ecol* **26**: 33–41.

Lukić-Bilela L, Perović-Ottstadt S, Walenta S, Natalio F, Pleše B, Link T, Müller WE. (2011). ATP distribution and localization of mitochondria in *Suberites domuncula* (Olivi 1792) tissue. *J Exp Biol* **214**: 1748–1753.

Luter HM, Whalan S, Webster NS. (2012). The marine sponge *Ianthella basta* can recover from stress-induced tissue regression. *Hydrobiologia* **687**: 227–235.

Lynch TC, Phlips EJ. (2000). Filtration of the bloom-forming cyanobacteria *Synechococcus* by three sponge species from Florida Bay, USA. *Bull Mar Sci* **67**: 923–936.

M

MacGeachy JK. (1977). Factors controlling sponge boring in Barbados reef corals. In: *Proc 3rd Int Coral Reef Symp* pp 477–483.

Macintyre IG. (1984). Preburial and shallow-subsurface alteration of modern scleractinian corals. *Palaeontogr Am* **54**: 229–244.

Maldonado M, Giraud K, Carmona C. (2008). Effects of sediment on the survival of asexually produced sponge recruits. *Mar Biol* **154**: 631–641.

Maldonado M, Ribes M, van Duyl FC. (2012). Nutrient fluxes through sponges: Biology, budgets, and ecological implications. In: *Advances in Marine Biology,* Elsevier, Amsterdam, **62**: p113.

Mallela J, Perry CT. (2007). Calcium carbonate budgets for two coral reefs affected by different terrestrial runoff regimes, Rio Bueno, Jamaica. *Coral Reefs* **26**: 129–145.

Manzello DP, Joan A. Kleypas, David A. Budd, C. Mark Eakin, Peter W. Glynn, Langdon C. (2008). Poorly cemented coral reefs of the eastern tropical Pacific: Possible insights into reef development in a high-CO_2 world. *Proc Natl Acad Sci* **105**: 10450–10455.

Mariani S, Uriz MJ, Turon X. (2000). Larval bloom of the oviparous sponge Cliona viridis: Coupling of larval abundance and adult distribution. *Mar Biol* **137**: 783–790.

Márquez JC, Zea S, López-Victoria M. (2006). Is competition for space between the encrusting excavating sponge *Cliona tenuis* and corals influenced by higher-than-normal temperatures? *Boletín Investig Mar y Costeras-INVEMAR* **35**: 259–265.

Marsh JA. (1970). Primary productivity of reef-building calcareous red algae. *Ecology* **51**: 255–263.

Marshall P, Johnson J. (2007). The Great Barrier Reef and climate change: vulnerability and management implications. Townsville, Australia: Great Barrier Reef Marine Park Authority and Australian Greenhouse Office. p773–801.

Marulanda-Gómez Á, López-Victoria M, Zea S. (2017). Current status of coral takeover by an encrusting excavating sponge in a Caribbean reef. *Mar Ecol* **38**: e12379.

Massaro AJ, Weisz JB, Hill MS, Webster NS. (2012). Behavioral and morphological changes caused by thermal stress in the Great Barrier Reef sponge *Rhopaloeides odorabile*. *J Exp Mar Bio Ecol* **416**: 55–60.

Matantseva O, Skarlato S, Vogts A, Pozdnyakov I, Liskow I, Schubert H, *et al.* (2016). Superposition of individual activities: Urea-mediated suppression of nitrate uptake in the dinoflagellate *Prorocentrum minimum* revealed at the population and single-cell levels. *Front Microbiol* **7**: 1310.

McConnaughey TA, Whelan JF. (1997). Calcification generates protons for nutrient and bicarbonate uptake. *Earth-Sci Rev* **42:** 95-117.

McElhany, P. (2016). CO_2 sensitivity experiments are not sufficient to show an effect of ocean acidification. *ICES J Mar Sci* **74:** 926-8.

McMurray SE, Henkel TP, Pawlik JR. (2010). Demographics of increasing populations of the giant barrel sponge *Xestospongia muta* in the Florida Keys. *Ecology* **91**: 560-70.

Meehl GA, Stocker TF, Collins WD, Friedlingstein P, Gaye AT, Meehl GA, *et al*. (2007). Global climate projections. In: Solomon S, Qin D, Manning M, Chen Z, Marquis M, Averyt KB, Tignor M MH (ed). *Climate Change 2007: The Physical Science Basis. Contribution of Working Group I to the Fourth Assessment Report of the Intergovernmental Panel on Climate Change*. Cambridge University Press, Cambridge and New York, pp 747–845.

Mehrbach C, Culberson CH, Hawley JE, Pytkowicx RM. (1973). Measurement of the apparent dissociation constants of carbonic acid in seawater at atmospheric pressure. *Limnol Oceanogr* **18**: 897–907.

Meyer JL, Schultz ET. (1985) Migrating haemulid fishes as a source of nutrients and organic matter on coral reefs. *Limnol Oceanogr* **30**: 146-56.

Moberg F, Folke C. (1999). Ecological goods and services of coral reef ecosystems. *Ecol Econ* **29**: 215–233.

Moitinho-Silva L, Díez-Vives C, Batani G, Esteves AI, Jahn MT, Thomas T. (2017). Integrated metabolism in sponge–microbe symbiosis revealed by genome-centered metatranscriptomics. *ISME J* **11**: 1651-1666.

Mote S, Schönberg CHL, Samaai T, Gupta V, Ingole B. (in review). A new clionaid sponge infests live corals on the West Coast of India (Porifera, Demospongiae, Clionaida). *Zool J Linn Soc*.

Mueller B, de Goeij JM, Vermeij MJA, Mulders Y, van der Ent E, Ribes M, *et al.* (2014). Natural diet of coral-excavating sponges consists mainly of dissolved organic carbon (DOC). *PLoS One* **9**: e90152.

Murata N, Takahashi S, Nishiyama Y, Allakhverdiev SI. (2007). Photoinhibition of photosystem II under environmental stress. *Biochim Biophys Acta* **1767**: 414–421.

Musat N, Foster R, Vagner T, Adam B, Kuypers MM. (2012) Detecting metabolic activities in single cells, with emphasis on NanoSIMS. *FEMS Microbiol Rev* **36**:486-511.

Muscatine L, Masuda H, Burnap R. (1979). Ammonium uptake by symbiotic and aposymbiotic reef corals. *Bull of Mar Sci* **1**: 572-575.

Muscatine L, D'Elia C. (1978). The uptake, retention, and release of ammonium by reef corals. *Limnol Oceanogr* **23:** 725-734.

Muscatine L, Goiran C, Land L, Jaubert J, Cuif JP, Allemand D. (2005). Stable isotopes (delta^{13}C and delta^{15}N) of organic matrix from coral skeleton. *Proc Natl Acad Sci USA* **102**: 1525–1530.

Muscatine L, McCloskey LR, Marian, RE. (1981). Estimating the daily contribution of carbon from zooxanthellae to coral animal respiration. *Limnol Oceanogr* **26:** 601–611.

Muscatine L, Porter JW. (1977). Reef corals: mutualistic symbioses adapted to nutrient-poor

environments. *Bioscience* **27**: 454–460.

Muscatine L. (1990). The role of symbiotic algae in carbon and energy flux in reef corals. *Ecosyst world* **25:** 75-87.

N

Nava H, Carballo JL. (2008). Chemical and mechanical bioerosion of boring sponges from Mexican Pacific coral reefs. *J Exp Biol* **211**: 2827–2831.

Negri A, Vollhardt C, Humphrey C, Heyward A, Jones R, Eaglesham G, Fabricius K. (2005). Effects of the herbicide diuron on the early life history stages of coral. *Mar Poll Bull* **51**: 370-383.

Neumann AC. (1966). Observations on coastal erosion in Bermuda and measurements of the boring rate of the sponge *Cliona lampa*. *Limnol Oceanogr* **11**: 92–108.

Nielsen C. (2008). Six major steps in animal evolution: Are we derived sponge larvae? *Evol Dev* **10**: 241–257.

Niyogi KK. (1999). Photoprotetcion revisited: Genetic and molecular approaches. *Annu. Rev. Plant Physiol. Plant Mol. Biol* **50**: 333–59.

NOAA Coral Reef Watch. 2013, updated daily. NOAA Coral Reef Watch Daily Global 5-km Satellite Coral Bleaching Degree Heating Week Product, Jun. 3, 2013-Jun. 2, 2014. College Park, Maryland, USA: NOAA Coral Reef Watch. Data set accessed 14th March 2018 at http://coralreefwatch.noaa.gov/satellite/hdf/index.php

NOAA National Oceanic and Atmospheric Administration Coral Reef Watch. 50-km pixel satellite data Available at: http://coralreefwatch.noaa.gov (date of access Nov 2016).

Norström AV, Nyström M, Lokrantz J, Folke C. (2009). Alternative states on coral reefs: beyond coral-macroalgal phase shifts. *Mar Ecol Prog Ser* **376**: 295–306.

O

Oakley CA, Davy SK (2018). Cell biology of coral bleaching. In: *van Oppen M., Lough J. (eds) Coral Bleaching.* Ecological Studies (Analysis and Synthesis), vol 233. Springer, Cham, pp. 189-211.

Oettmeier W, Masson K, Johanningmeier U. (1980) Photoaffinity labelling of the photosystem II herbicide binding protein. *FEBS Lett* **118:** 267–270.

Orr JC, Fabry VJ, Aumont O, Bopp L, Doney SC, Feely RA, Gnanadesikan A, Gruber N, Ishida A, Joos F, Key RM (2005). Anthropogenic ocean acidification over the twenty-first century and its impact on calcifying organisms. *Nature* **437**: 681–686.

Osmond CB, Anderson JM, Ball MC, Egerton JJ. (1999). Compromising efficiency: the molecular ecology of light-resource utilization in plants. In: *Physiological Plant Ecology,* Blackwell Science, p.1-25.

P

Page C, Willis B. (2006). Distribution, host range and large-scale spatial variability in black band disease prevalence on the Great Barrier Reef, Australia. *Dis Aquat Organ* **69**: 41–51.

Papageorgiou G, Isaakidou J, Argoudelis C. (1972). Structure dependent control of chlorophyll a excitation density: the role of oxygen. *FEBS Lett* **25**: 139-42.

Parrin AP, Somova EL, Kern PM, Millet TA, Bross LS, Blackstone NW. (2017). The use of *in vivo* microscopy to image the cnidarian stress response in three octocoral species. *Invert Biol* **136**: 330-

344.

Parsons TR, Maita Y, Lalli CM. (1984). A manual of chemical and biological methods for seawater analysis. Pergamon Press, Oxford, New York, Sydney.

Pawlik J, McMurray S, Erwin P, Zea S. (2015a). No evidence for food limitation of Caribbean reef sponges: Reply to Slattery and Lesser (2015). *Mar Ecol Prog Ser* **527**: 281–284.

Pawlik JR, Loh T-L, McMurray SE, Finelli CM. (2013). Sponge communities on Caribbean coral reefs are structured by factors that are top-down, not bottom-up. *PLoS One* **8**: e62573.

Pawlik JR, McMurray SE, Erwin P, Zea S. (2015b). A review of evidence for food limitation of sponges on Caribbean reefs. *Mar Ecol Prog Ser* **519**: 265–283.

Paxton CW, Davy SK, Weis VM. (2013). Stress and death of cnidarian host cells play a role in cnidarian bleaching, *J Exp Biol* **216**: 2813–2820.

Peduzzi PB, Chatenoux H, Dao A, De Bono C, Herold J, Kossin F *et al*. (2012) Global trends in tropical cyclone risk. *Nat Climate Change* **2**: 289–294.

Pernice M, Dunn SR, Tonk L, Dove S, Domart-Coulon I, Hoppe P, *et al.* (2014). A nanosims study of dinoflagellate functional diversity in reef-building corals. *Environ Microbiol* **17:** 3570-3580.

Pernice M, Levy O. (2014). Novel tools integrating metabolic and gene function to study the impact of the environment on coral symbiosis. *Front Microbiol* **5**: 448.

Pernice M, Meibom A, Van Den Heuvel A, Kopp C, Domart-Coulon I, Hoegh-Guldberg O, *et al.* (2012). A single-cell view of ammonium assimilation in coral–dinoflagellate symbiosis. *ISME J* **6**: 1314–1324.

Perry CT, Edinger EN, Kench PS, Mumby PJ, Murphy G, Steneck RS, Smithers SG. (2012). Estimating rates of biologically driven coral reef framework production and erosion: a new census-based carbonate budget methodology and applications to the reefs of Bonaire. *Coral Reefs* **31**: 853-868.

Perry CT, Murphy GN, Kench PS, Edinger EN, Smithers SG, Steneck RS, *et al.* (2014). Changing dynamics of Caribbean reef carbonate budgets: emergence of reef bioeroders as critical controls on present and future reef growth potential. *Proc Biol Sci* **281**: 20142018.

Peters GP, Le Quéré C, Andrew RM, Canadell JG, Friedlingstein P, Ilyina T, *et al.* (2017). Towards real-time verification of CO_2 emissions. *Nat Clim Chang* **7**: 848–850.

Petrou K, Ralph PJ, Nielsen DA. (2016). A novel mechanism for host-mediated photoprotection in endosymbiotic foraminifera. *ISME J* **11**: 453–462.

Pineda MC, Strehlow B, Sternel M, Duckworth A, Den Haan J, Jones R, Webster NS (2017a). Effects of sediment smothering on the sponge holobiont with implications for dredging management. *Sci Rep* **7**: 5156.

Pineda MC, Strehlow B, Sternel M, Duckworth A, Jones R, Webster NS. (2017b). Effects of suspended sediments on the sponge holobiont with implications for dredging management. *Sci Rep* **7**: 4925.

Pineda MC, Strehlow B, Duckworth A, Doyle J, Jones R, Webster NS. (2016). Effects of light attenuation on the sponge holobiont- implications for dredging management. *Sci Rep* **6:** 39038.

Pita L, Rix L, Slaby BM, Franke A, Hentschel U. (2018). The sponge holobiont in a changing ocean: from microbes to ecosystems. *BMC Microbiome* **6:** 1–18.

Pochon X, Putnam HM, Gates RD. (2014). Multi-gene analysis of *Symbiodinium* dinoflagellates: a perspective on rarity, symbiosis, and evolution. *Peer J* **2**: e394.

Pomponi SA. (1979a). Ultrastructure and cytochemistry of the etching area of boring sponges. *Coll Int CNRS* **291**: 317–332.

Pomponi SA. (1979b). Ultrastructure of cells associated with excavation of calcium carbonate substrates by boring sponges. *J Mar Biol Assoc UK* **59**: 777–784.

Pomponi SA. (1979c). Cytochemical studies of acid phosphatase in etching cells of boring sponges. *J Mar Biol Assoc UK* **59**: 785–790.

Pomponi SA. (1980). Cytological Mechanisms of Calcium Carbonate Excavation by Boring Sponges. *Int Rev Cytol* **65**: 301–319.

Poppell E, Weisz J, Spicer L, Massaro A, Hill A, Hill MS. (2013). Sponge heterotrophic capacity and bacterial community structure in high-and low-microbial abundance sponges. *Mar Ecol* **35**: 414–424.

Pörtner HO, Karl DM, Boyd PW *et al*. (2014). Ocean systems. In: Climate Change 2014: Impacts, adaptation, and vulnerability. Part A: Global and sectoral aspects. Contribution of working group II to the fifth assessment report of the Intergovernmental Panel on Climate Change (eds Field C. B. et al.) Cambridge University Press, pp 411–484.

R

Rädecker N, Pogoreutz C, Voolstra CR, Wiedenmann J, Wild C. (2015). Nitrogen cycling in corals: The key to understanding holobiont functioning? *Trends Microbiol* **23**: 490–497.

Rahav O, Dubinsky Z, Archituv Y FP. (1989). Ammonium metabolism in the zooxanthellate coral, *Stylophora pistillata*. *Proc R Soc B* **337**: 325–337.

Ralph PJ, Schreiber U, Gademann R, Kühl M, Larkum AW. (2005). Coral photobiology studied with a new imaging pulse amplitude modulated fluorometer. *J Phycol* **41**: 335-42.

Ramsby BD, Hill MS, Thornhill DJ, Steenhuizen SF, Achlatis M, Lewis AM, *et al.* (2017). Sibling species of mutualistic *Symbiodinium* clade G from bioeroding sponges in the western Pacific and western Atlantic oceans. *J Phycol* **53**: 951-960.

Ramsby BD, Hoogenboom MO, Whalan S, Webster NS, Thompson A. (2017). A decadal analysis of bioeroding sponge cover on the inshore Great Barrier Reef. *Sci Rep* **7**: 2706.

Ramsby BD, Hoogenboom MO, Whalan S, Webster NS. (2018). Elevated seawater temperature disrupts the microbiome of an ecologically important bioeroding sponge. *Mol Ecol*. e-pub ahead of print, doi: 10.1111/mec.14544.

Rasheed M, Wild C, Franke U, Huettel M. (2004). Benthic photosynthesis and oxygen consumption in permeable carbonate sediments at Heron Island, Great Barrier Reef, Australia. *Estuar Coast Shelf Sci* **59**: 139–150.

Raven J, Caldeira K, Elderfield H, Hoegh-Guldberg O, Liss P, Riebesell U, *et al.* (2005). Ocean acidification due to increasing atmospheric carbon dioxide. Policy document 12/05, The Royal Society, London.

Reaka-Kudla ML. (1997). The global biodiversity of coral reefs: a comparison with rain forests. In: *Biodiversity II: Understanding and protecting our biological resources*. **2**: 551.

Renger G. (1976). Studies on the structural and functional organization of system II of photosynthesis. The use of trypsin as a structurally selective inhibitor at the outer surface of the thylakoid membrane. *Biochim Biophys Acta* **440**: 287–300.

Stanley Jr GD. (2003). The evolution of modern corals and their early history. *Earth-Sci Rev* **60**: 195-225.

Reyes-Nivia C, Diaz-Pulido G, Kline D, Guldberg OH, Dove S. (2013). Ocean acidification and warming scenarios increase microbioerosion of coral skeletons. Glob Change Biol **19**: 1919-29.

Riding R. (2000). Microbial carbonates: the geological record of calcified bacterial–algal mats and biofilms. *Sedimentology* **47**: 179-214.

Riesgo A, Peterson K, Richardson C, Heist T, Strehlow B, McCauley M, *et al.* (2014). Transcriptomic analysis of differential host gene expression upon uptake of symbionts: a case study with *Symbiodinium* and the major bioeroding sponge *Cliona varians*. *BMC Genomics* **15**: 376.

Risk MJ, Sammarco PW, Edinger EN. (1995). Bioerosion in *Acropora* across the continental shelf of the Great Barrier Reef. *Coral Reefs* **14**: 79–86.

Rix L, de Goeij J, van Oevelen D, Struck U, Al-Horani F, Wild C, *et al.* (2017). Reef sponges facilitate the transfer of coral-derived organic matter to their associated fauna via the sponge loop. *Mar Ecol Prog Ser* **589**: 85-96.

Rix L, De Goeij JM, Mueller CE, Struck U, Middelburg JJ, van Duyl FC, *et al.* (2016a). Coral mucus fuels the sponge loop in warm-and cold-water coral reef ecosystems. *Sci Rep* **6**: 18715.

Rix L, de Goeij JM, van Oevelen D, Struck U, Al-Horani FA, Wild C, *et al.* (2016b). Differential recycling of coral and algal dissolved organic matter via the sponge loop. *Funct Ecol* **31**: 778-89.

Robbins LL, Hansen ME, Kleypas JA, Meylan SC. (2010) CO_2calc - A user-friendly seawater carbon calculator for Windows, Max OS X, and iOS (iPhone). *U.S. Geological Survey Open-File Report*.

Roberts JM, Fixter LM, Davies PS. (2001). Ammonium metabolism in the symbiotic sea anemone *Anemonia viridis. Hydrobiologia* **461**: 25–35.

Rose CS, Risk MJ. (1985). Increase in *Cliona delitrix* infestation of *Montastrea cavernosa* heads on an organically polluted portion of the Grand Cayman fringing reef. *Mar Ecol* **6**: 345–363.

Rosell D, Uriz MJ. (1992). Do associated zooxanthellae and the nature of the substratum affect survival, attachment and growth of *Cliona viridis* (Porifera: Hadromerida)? An experimental approach. *Mar Biol* **114**: 503–507.

Rosell D. (1993). Effects of reproduction in *Cliona viridis* (Hadromerida) on zooxanthellae. *Sci Mar* **57**: 405–413.

Rützler K, Rieger G. (1973). Sponge burrowing: fine structure of *Cliona lampa* penetrating calcareous substrata. *Mar Biol* **21**: 144-62.

Rützler K. (1974). The burrowing sponges of Bermuda. *Smiths Contr Zool* **165**: 1–32.

Rützler K. (1975). The role of burrowing sponges in bioerosion. *Oecologia* **19**: 203–216.

Rützler K. (2002). Impact of crustose clionid sponges on Caribbean reef corals. *Acta Geol Hisp* **37**: 61–72.

Rützler K. (1990). Associations between Caribbean sponges and photosynthetic organisms. In: Rützler K. (ed.) *New Perspectives in Sponge Biology*. Smithsonian Institution Press, Washington, DC, pp 455–466.

Ruzicka RR, Colella MA, Porter JW, Morrison JM, Kidney JA, Brinkhuis V, *et al.* (2013). Temporal changes in benthic assemblages on Florida Keys reefs 11 years after the 1997/1998 El Niño. *Mar Ecol Progr Ser* **489**: 125-41.

S

Sadekar S, Raymond J, Blankenship RE. (2006). Conservation of distantly related membrane proteins: photosynthetic reaction centers share a common structural core. *Mol Biol Evol* **23***:* 2001-2007.

Sammarco PW, Risk MJ. (1990). Large-scale patterns in internal bioerosion of *Porites*: cross continental shelf trends on the Great Barrier Reef. *Mar Ecol Progr Ser* **11**: 145-56.

Sampayo EM, Ridgway T, Franceschinis L, Roff G, Hoegh-Guldberg O, Dove S. (2016). Coral symbioses under prolonged environmental change: living near tolerance range limits. *Sci Rep* **6**: 36271.

Sampayo EM, Ridgway T, Bongaerts P, Hoegh-Guldberg O. (2008). Bleaching susceptibility and mortality of corals are determined by fine-scale differences in symbiont type. *Proc Natl Acad Sci USA* **105:** 10444-9.

Sara M, Liaci L. (1964). Symbiotic association between zooxanthellae and two marine sponges of the genus *Cliona*. *Nature* **4942**: 321.

Schindelin J, Arganda-Carreras I, Frise E, Kaynig V, Longair M, Pietzsch T, *et al.* (2012). Fiji: an open-source platform for biological-image analysis. *Nat Methods* **9**: 676–682.

Schläppy ML, Hoffmann F, Røy H, Wijffels RH, Mendola D, Sidri M, de Beer D. (2007). Oxygen dynamics and flow patterns of *Dysidea avara* (Porifera: Demospongiae). *J Mar Biol Assoc UK* **87**: 1677-82.

Schneider K, Silverman J, Woolsey E, Eriksson H, Byrne M, Caldeira K. (2011). Potential influence of sea cucumbers on coral reef $CaCO_3$ budget: A case study at One Tree Reef. *J Geophys Res* **116**: 2-7.

Schoepf V, Levas SJ, Rodrigues LJ, Mcbride MO, Aschaffenburg MD, Matsui Y, *et al.* (2014). Kinetic and metabolic isotope effects in coral skeletal carbon isotopes: A re-evaluation using experimental coral bleaching as a case study. **146**: 164–178.

Schönberg CE, Wilkinson C. (2001). Induced colonization of corals by a clionid bioeroding sponge. *Coral Reefs* **20**: 69-76.

Schönberg CHL, Loh WKW. (2005). Molecular identity of the unique symbiotic dinoflagellates found in the bioeroding demosponge *Cliona orientalis*. *Mar Ecol Prog Ser* **299**: 157–166.

Schönberg CHL, Barthel D. (1997). Inorganic skeleton of the demosponge *Halichondria panicea*. Seasonality in spicule production in the Baltic Sea. *Mar Biol* **130**: 133–140.

Schönberg CHL, Fang JKH, Carreiro-Silva M, Tribollet A, Wisshak M. (2017a). Bioerosion: the other ocean acidification problem. *ICES J Mar Sci* **74**: 895-925.

Schönberg CHL, Fang JKH CJ. Carballo, J. L. (2017b). Bioeroding sponges and the future of coral reefs. In: *Climate change, ocean acidification, and sponges* (eds. Bell, J. J., Carballo, J. L.), Springer Berlin / Heidelberg.

Schönberg CHL, Ortiz JC. (2008). Is sponge bioerosion increasing? In: *Proc 11th Int Coral Reef Symp*, Ft. Lauderdale, pp 520–523.

Schönberg CHL, Shields G. (2008). Micro-computed tomography for studies on Entobia: transparent substrate versus modern technology. In: *Current Developments in Bioerosion*. Springer, pp 147–164.

Schönberg CHL, Suwa R, Hidaka M, Loh WKW. (2008). Sponge and coral zooxanthellae in heat and light: Preliminary results of photochemical efficiency monitored with pulse amplitude modulated fluorometry. *Mar Ecol* **29**: 247–258.

Schönberg CHL, Suwa R. (2007). Why bioeroding sponges may be better hosts for symbiotic dinoflagellates than many corals. *Porifera Res Biodiversity, Innov Sustain Mus Nac Rio Janeiro* 569–580.

Schönberg CHL, Wisshak M. (2012). The perks of being endolithic. *Aquat Biol* **17**: 1–5.

Schönberg CHL. (2000). Bioeroding sponges common to the Central Australian Great Barrier Reef: descriptions of three new species, two new records, and additions to two previously described species. *Senck marit* **30**: 161–221.

Schönberg CHL. (2002). Substrate effects on the bioeroding demosponge *Cliona orientalis*. 1. Bioerosion rates. *Mar Ecol* **23**: 313–326.

Schönberg CHL. (2003). Substrate effects on the bioeroding demosponge *Cliona orientalis*. 2. Susbtrate colonisation and tissue growth. *Mar Ecol* **24**: 59–74.

Schönberg CHL. (2006). Growth and erosion of the zooxanthellate Australian bioeroding sponge *Cliona orientalis* are enhanced in light. In: *Proc 10th Int Coral Reef Symp, Okinawa*. pp 168–174.

Schönberg CHL. (2008). A history of sponge erosion: from past myths and hypotheses to recent approaches. In: *Current Developments in Bioerosion*. Springer, pp 165–202.

Schönberg CHL. (2001). Small-scale distribution of Great Barrier Reef bioeroding sponges in shallow water. *Ophelia* **1**: 39-54.

Schönberg CHL, De Beer D, Lawton A. (2005). Oxygen microsensor studies on zooxanthellate clionaid sponges from the Costa Brava, Mediterranean sea. *J Phycol* **41**: 774–779.

Schreiber U. (2004). Pulse-Amplitude-Modulation (PAM) fluorometry and saturation pulse method: An overview. In: *Chlorophyll a Fluorescence*. Dordrecht: Springer Netherlands, pp. 279–319.

Schreiber U, Kühl M, Klimant I, Reising H. (1996). Measurement of chlorophyll fluorescence within leaves using a modified PAM Fluorometer with a fiber-optic microprobe. *Photosynth Res* **47**: 103–109.

Schwab D, Shore R. (1971). Fine structure and composition of a siliceous sponge spicule. *Biol Bull* **140**: 125-136.

Seckbach J. (2004). *Symbiosis: Mechanisms and Model Systems.* Kluwer Academic Publishers, Dordrecht, The Netherlands.

Silbiger NJ, Guadayol O, Thomas FOM, Donahue MJ. (2016). A novel μCT analysis reveals different responses of bioerosion and secondary accretion to environmental variability. *PLoS One* **11**: 11–16.

Simister RL, Deines P, Botté ES, Webster NS, Taylor MW. (2012). Sponge-specific clusters revisited: a comprehensive phylogeny of sponge-associated microorganisms. *Environ Microbiol* **14**: 517-24.

Sinning, I. (1992). Herbicide binding in the bacterial photosynthetic reaction center. *Trends Biochem Sci* **17**: 150–154.

Slattery M, Lesser MP. (2015). Trophic ecology of sponges from shallow to mesophotic depths (3 to 150 m): comment on Pawlik *et al*.(2015). *Mar Ecol Progr Ser* **527**: 275-279.

Smith LW, Barshis D, Birkeland C. (2007). Phenotypic plasticity for skeletal growth, density and calcification of *Porites lobata* in response to habitat type. *Coral Reefs* **26**: 559–567.

Srivastava M, Simakov O, Chapman J, Fahey B, Gauthier MEA, Mitros T, *et al.* (2010). The *Amphimedon queenslandica* genome and the evolution of animal complexity. *Nature* **466**: 720–726.

Stal LJ, Krumbein WE. (1987). Temporal separation of nitrogen fixation and photosynthesis in the filamentous, non-heterocystous cyanobacterium *Oscillatoria* sp. *Arch Microbiol* **149:** 76–80.

Staunton Smith J, Johnson CR. (1995). Nutrient inputs from seabirds and humans on a populated coral cay. *Mar Ecol Prog Ser* **10:** 189-200.

Strehlow B, Friday S, McCauley M, Hill MS. (2016b). The potential of azooxanthellate poriferan hosts to assess the fundamental and realized *Symbiodinium* niche: evaluating a novel method to initiate *Symbiodinium* associations. *Coral Reefs* **35**: 1201–1212.

Strehlow BW, Jorgensen D, Webster NS, Pineda M-C, Duckworth A. (2016). Using a thermistor flowmeter with attached video camera for monitoring sponge excurrent speed and oscular behaviour. *PeerJ* **4**: e2761.

Stubler AD, Furman BT, Peterson BJ. (2015). Sponge erosion under acidification and warming scenarios: differential impacts on living and dead coral. *Glob Chang Biol* **21**: 4006–4020.

Suggett DJ, Oxborough K, Baker NR, MacIntyre HL, Kana TM, Geider RJ. (2003). Fast repetition rate and pulse amplitude modulation chlorophyll a fluorescence measurements for assessment of photosynthetic electron transport in marine phytoplankton. *Eur J Phycol* 2003 **38**: 371-384.

Suggett DJ, Prašil O, Borowitzka, MA. (2011). *Chlorophyll a fluorescence in aquatic sciences: Methods and applications*. Springer, Dordrecht, The Netherlands.

T

Takahashi S, Yoshioka-Nishimura M, Nanba D, Badger MR. (2013). Thermal acclimation of the symbiotic alga *Symbiodinium* spp. alleviates photobleaching under heat stress. *Plant Physiol* **161**: 477–485.

Takahashi S, Nakamura T, Sakamizu M, Woesik RV, Yamasaki H. (2004). Repair machinery of symbiotic photosynthesis as the primary target of heat stress for reef-building corals. *Plant & Cell Physiol* **45**: 251–255.

Taylor MW, Radax R, Steger D, Wagner M. (2007). Sponge-associated microorganisms: evolution, ecology, and biotechnological potential. *Microbiol Mol Biol Rev* **71**: 295-347.

Teal JM, Kanwisher JW. (1966). Gas transport in the marsh grass, *Spartina alterniflora*. *J Exp Bot* 17: 355-361.

Thacker RW. (2005). Impacts of shading on sponge-cyanobacteria symbioses: a comparison between host-specific and generalist associations. *Integr Comp Biol* **45**: 369–376.

Thacker RW, Freeman CJ. (2012). Sponge–microbe symbioses: recent advances and new directions. In: *Advances in Marine Biology* **62**: 57-111. Academic Press. Elsevier.

Thomas T, Moitinho-Silva L, Lurgi M, Björk JR, Easson C, Astudillo-García C, *et al.* (2016). Diversity, structure and convergent evolution of the global sponge microbiome. *Nat Commun* **7**: 11870.

Thompson JR, Rivera HE, Closek CJ, Medina M. (2015). Microbes in the coral holobiont: partners through evolution, development, and ecological interactions. *Front Cell Infect Microbiol* **4**: 176.

Tolosa I, Treignier C, Grover R, Ferrier-Pagès C. (2011). Impact of feeding and short-term temperature stress on the content and isotopic signature of fatty acids, sterols, and alcohols in the scleractinian coral *Turbinaria reniformis*. *Coral Reefs* **30**: 763.

Trebst A. (2007). Inhibitors in the functional dissection of the photosynthetic electron transport system. *Photosynth Res* **92**: 217–224.

Tremblay P, Gori A, Maguer JF, Hoogenboom M, Ferrier-Pagès C. (2016). Heterotrophy promotes the re-establishment of photosynthate translocation in a symbiotic coral after heat stress. *Sci Rep* **6**: 38112.

Trench RK. (1993). Microalgal-invertebrate symbioses-a review. *Endocytobiosis Cell Res*. **9**: 135-175.

Trench RK, Wethey DS, Porter JW. (1981). Observations on the symbiosis with zooxanthellae among the Tridacnidae (Mollusca, Bivalvia). *Biol Bull* **161**: 180-198.

Tribollet A, Golubic S. (2011). Reef bioerosion: agents and processes. In: *Coral reefs: An ecosystem in transition*. Springer, pp 435–449.

Trussell GC, Lesser MP, Patterson MR, Genovese SJ. (2006). Depth-specific differences in growth of the reef sponge *Callyspongia vaginalis*: role of bottom-up effects. *Mar Ecol Progr Ser* **323**: 149-58.

U

Underwood AJ. (1997). Experiments in ecology, their logical design and interpretation using analysis of variance. Cambridge University Press: Cambridge, UK.

Underwood JN, Souter PB, Ballment ER, Lutz AH, Van Oppen MJ. (2006). Development of 10 polymorphic microsatellite markers from herbicide-bleached tissues of the brooding pocilloporid coral *Seriatopora hystrix*. *Mol Ecol Res* **6**: 176-178.

Unesco. (2016a). Damage to Great Barrier Reef assessed; stricter shipping surveillance proposed. http://whc.unesco.org/en/news/606. [21 December 2016].

Unesco. (2016b). Director-general meets with experts responsible for health of Great Barrier Reef. http://whc.unesco.org/en/news/1199. [21 December 2016].

Uriz MJ, Agell G, Blanquer A, Turon X, Casamayor EO. (2012). Endosymbiotic calcifying bacteria: a new cue to the origin of calcification in metazoa? *Evolution* **66**: 2993-2999.

Uriz MJ; Turon X; Becerro MA; Agell G. (2003). Siliceous spicules and skeleton frameworks in sponges: origin, diversity, ultrastructural patterns, and biological functions. *Microsc Res Tech* **62**: 279–299.

Usher KM. (2008). The ecology and phylogeny of cyanobacterial symbionts in sponges. *Mar Ecol* **29**: 178–192.

V

Vacelet J. (1981). Algal-sponge symbioses in the coral reefs of New Caledonia: A morphological study. *Proc 4th Int Coral Reef Symp*, *Manila* **2**: 713–719.

Venn AA, Loram JE, Douglas AE. (2008). Photosynthetic symbioses in animals. *J Exp Bot* **59**: 1069–1080.

Vicente J, Silbiger NJ, Beckley BA, Raczkowski CW, Hill RT. (2016). Impact of high pCO_2 and warmer temperatures on the process of silica biomineralization in the sponge *Mycale grandis*. *ICES J Mar Sci* **73:** 704-714.

Vicente VP. (1990). Response of sponges with autotrophic endosymbionts during the coral-bleaching episode in Puerto Rico. *Coral Reefs* **8**: 199–202.

Vicente VP. (1978). An ecological evaluation of the West Indian demosponge *Anthosigmella varians* (Hadromerida: Spirastrellidae). *Bull Mar Sci* **28**: 771-779.

Villamizar E, Díaz MC, Rützler K, Nóbrega R. (2014). Biodiversity, ecological structure, and change in the sponge community of different geomorphological zones of the barrier fore reef at Carrie Bow Cay, Belize. *Mar Ecol* **35**: 425-35.

Vogel K. (1993). Bioeroders in fossil reefs. *Facies* **28**: 109–113.

W

Walz (2014) Imaging-PAM M-Series chlorophyll fluorometer: instrument description and information for users, 5th edn. Heinz Walz GmbH, Effeltrich, Germany.

Wang J-T, Douglas AE. (1998). Nitrogen recycling or nitrogen conservation in an alga-invertebrate symbiosis? *J Exp Biol* **201**: 2445–2453.

Wang J-T, Keshavmurthy S, Chu TY, Chen CA. (2017). Diverse responses of *Symbiodinium* types to menthol and DCMU treatment. *PeerJ* **5**: e3843.

Wangpraseurt D, Pernice M, Guagliardo P, Kilburn MR, Clode PL, Polerecky L, *et al.* (2015). Light microenvironment and single-cell gradients of carbon fixation in tissues of symbiont-bearing corals. *ISME J* **10**: 788–792.

Wangpraseurt D, Holm JB, Larkum AWD, Pernice M, Ralph PJ, Suggett DJ, Kühl M. (2017). *In vivo* microscale measurements of light and photosynthesis during coral bleaching: evidence for the optical feedback loop. *Front Microbiol* **8**: 59-.

Ward P, Risk MJ. (1977). Boring pattern of the sponge *Cliona vermifera* in the coral *Montastrea annularis*. *J Paleontol* **51**: 520−526.

Ward-Paige CA, Risk MJ, Sherwood OA, Jaap WC. (2005). Clionid sponge surveys on the Florida Reef Tract suggest land-based nutrient inputs. *Mar Pollut Bull* **51**: 570–579.

Warner ME, Fitt WK, Schmidt GW. (1999). Damage to photosystem II in symbiotic dinoflagellates: a determinant of coral bleaching. *Proc Natl Acad Sci USA* **96**: 8007-12.

Watanabe T, Yuyama I, Yasumura S. (2006). Toxicological effects of biocides on symbiotic and aposymbiotic juveniles of the hermatypic coral *Acropora tenuis*. *J Exp Mar Biol Ecol* **339**: 177-88.

Webb AE, van Heuven SM, de Bakker DM, van Duyl FC, Reichart GJ, de Nooijer LJ. (2017). Combined effects of experimental acidification and eutrophication on reef sponge bioerosion rates. *Front Mar Sci*. **26**: 311.

Webster NS, Thomas T. (2016). Defining the Sponge Hologenome. *MBio* **7**: 1–14.

Weis VM. (2008). Cellular mechanisms of Cnidarian bleaching: stress causes the collapse of symbiosis. *J Exp Biol* **211**: 3059–3066.

Weisz JB, Massaro AJ, Ramsby BD, Hill MS. (2010). Zooxanthellar symbionts shape host sponge trophic status through translocation of carbon. *Biol Bull* **219**: 189–197.

Wernberg T, Smale DA, Thomsen MS. (2012). A decade of climate change experiments on marine organisms: procedures, patterns and problems. *Glob Chang Biol* **18**: 1491–1498.

Wild C, Huettel M, Klueter A, Kremb, SG., Rasheed, MY JB. (2004). Coral mucus functions as an energy carrier and particle trap in the reef ecosystem. *Nature* **428**: 66–70.

Wilkinson CR. (1979). Nutrient translocation from symbiotic cyanobacteria to coral reef sponges. In:

Biologie des spongiaires, Colloques International du Centre National de la Recherche Scientifique: Paris **291**: 373-380.

Wilkinson CR. (1983). Net primary productivity in coral reef sponges. *Science* **219**: 410–412.

Wilkinson CR. (1984). Immunological evidence for the Precambrian origin of bacterial symbioses in marine sponges. *Proc R Soc B* **220**: 509-518.

Wilkinson CR. (1987). Interocean differences in size and nutrition of coral reef sponge populations. *Science* **236**: 1654–1657.

Wilkinson CR, Fay, P. (1979). Nitrogen fixation in coral reef sponges with symbiotic cyanobacteria. *Nature* **279**: 527–529.

Wisshak M, Schönberg CHL, Form A, Freiwald A. (2012). Ocean acidification accelerates reef bioerosion. *PLoS One* **7**: e45124.

Wisshak M, Schönberg CHL, Form A, Freiwald A. (2013). Effects of ocean acidification and global warming on reef bioerosion-lessons from a clionaid sponge. *Aquat Biol* **19**: 111–127.

Wisshak M, Schönberg CHL, Form A, Freiwald A. (2014). Sponge bioerosion accelerated by ocean acidification across species and latitudes? *Helgol Mar Res* **68**: 253–262.

Wolf-Gladrow DA, Zeebe RE, Klaas C, Körtzinger A, Dickson AG. (2007). Total alkalinity: The explicit conservative expression and its application to biogeochemical processes. *Mar Chem* **106**: 287-300.

Y

Yahel G, Sharp JH, Marie D, Hase C., Genin A. (2003). *In situ* feeding and element removal in the symbiont-bearing sponge *Theonella swinhoei*: Bulk DOC is the major source for carbon. *Limnol Oceanogr* **48:** 141–149.

Yaakoubd B, Andersen R, Desjardins Y, Samson G. (2002). Contributions of the free oxidized and QB-bound plastoquinone molecules to the thermal phase of chlorophyll-a fluorescence. *Photosynth Res* **74**: 251.

Yellowlees D, Rees TA V, Leggat W. (2008). Metabolic interactions between algal symbionts and invertebrate hosts. *Plant Cell Environ* **31**: 679–694.

Z

Zea S, Weil E. (2003). Taxonomy of the Caribbean excavating sponge species complex *Cliona caribbaea* - *C. aprica* - *C. langae* (Porifera, Hadromerida, Clionaidae). *Caribb J Sci* **39**: 348–370.

Zundelevich A, Lazar B, Ilan M. (2007). Chemical versus mechanical bioerosion of coral reefs by boring sponges-lessons from *Pione cf. vastifica*. *J Exp Biol* **210**: 91–96.

Appendix

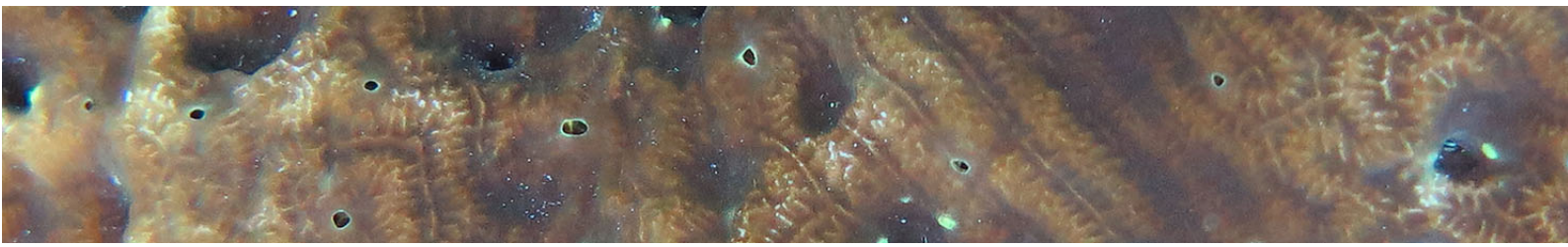

Supplementary Information – Chapter 2

Supplementary pilot study - Materials and Methods

A pilot study was done in August 2014 to determine the treatment conditions used in the main experiment to inhibit the photosynthetic activity and/or photosymbiont abundance of the *Cliona orientalis* holobiont. Besides the herbicide diuron (DCMU), the pilot study considered the use of the antibiotic chloramphenicol (CAP). CAP hinders *de novo* synthesis of proteins, including the chloroplast D1 protein of Photosystem II (PSII) (Warner *et al.*, 1999; Kovačevic *et al.*, 2001; Takahashi *et al.*, 2004). DCMU and CAP have been commonly used to study Cnidarian and *Symbiodinium* photophysiology (e.g. DCMU: Jones *et al.*, 2003; Jones, 2004; Murata *et al.*, 2007; Takahashi *et al.*, 2013; CAP: Warner *et al.*, 1999; Kovačevic *et al.*, 2001; Takahashi *et al.*, 2004), but similar studies are lacking in photosymbiotic Porifera. DCMU has previously been applied to suppress photosynthesis of the symbiotic cyanobacteria of the marine sponge *Haliclona (Reniera) tabernacula* (Wilkinson and Fay, 1979; as *Siphonochalina*) and the zoochlorellae living in symbiosis with the freshwater sponge *Radiospongilla cerebellata* (Kanayama and Kamishima, 1990). To our knowledge, there are no reports of previous use of DCMU on sponge-*Symbiodinium* associations.

Initially, the concentrations of DCMU and CAP needed to inhibit photosynthesis in the bioeroding sponge *Cliona orientalis* had to be identified. Encrusting "beta" morphology sponges (Schönberg *et al.*, 2017a) inhabiting dead coral substrates (massive corals) were sampled by SCUBA diving at 5-8m depth at "Tenements 2" (151.9302°E, 23.4326°S). Sponges were exposed in triplet to confined seawater containing 0, 50, 100 and 200 µg/L DCMU over 10 days. Tanks were aerated with small wave makers and treatment seawater was renewed daily. The ratio of variable chlorophyll fluoresence (F_v) to maximum (F_m) chlorophyll fluoresence was simultaneously monitored using 30 min dark-adapted pulse amplitude modulation (PAM, Walz, Effeltrich, Germany). The optimal concentration that caused the largest decreases in F_v/F_m but without detrimental effects on the sponges was 100 µg/L DCMU. The same concentration has been used to bleach corals in previous studies (Negri *et al.*, 2005; Underwood *et al.*, 2006). Stock solutions of DCMU were made up with ethanol as the carrier solvent (4.2 mg DCMU in 2.5 ml ethanol; Underwood *et al.*, 2006; Suggett *et al.*, 2011). Therefore, a separate test was performed comparing sponges treated over 5 days in triplet with 100 µg/L DCMU (dissolved in ethanol) or an equivalent volume of plain ethanol to control untreated sponges (Negri *et al.*, 2005). Unlike DCMU-treated

sponges, F_v/F_m of ethanol-treated sponges did not deviate from that of controls, confirming that observed responses were caused by the herbicide and not the carrier solvent. Based on previous studies (Kovačevic *et al.*, 2001), 250 mg/L CAP (dissolved in seawater) were applied to sponges in triplet for an initial period of 24h, leading to decreases in F_v/F_m and paling of the sponge tissues.

After determining the suitable treatments, 21 sponge cores from 3 genotypes were randomly distributed over three 5L-holding tanks (n=7 pseudoreplicates) and treated as follows: 100 µg/L DCMU, 250 µg/L CAP and control treatment, all in confined seawater mixed with a wave maker. Treatments ran over 3 days (15th to 17th August 2014), with seawater solutions replenished daily. Average midday temperature, pH and light levels across the holding tanks ranged between 19.7-23.1°C, 7.82-8.16 pH units, and 160-390 µmol quanta m^{-2} s^{-1} (integrated over 15s intervals) respectively.

At the end of the treatment phase and after returning treated sponges to chemical-free running seawater for one hour, photosynthetic activity of the sponges was measured at midday as described in the main text (see daytime incubations, but the water bath was set at 21°C to mimic winter conditions). Finally, the sponge cores were examined using an Imaging-PAM fluorometer (Pulse Amplitude Modulated fluorometry –i.e. PAM), which allows measurements and visualization of the spatial heterogeneity of chlorophyll fluorescence (principally as photosynthetic efficiency) on a detailed two-dimensional scale (Schreiber, 2004; Ralph *et al.*, 2005). Light absorption (Abs, apparent absorptivity, in this case an estimate of absorption of PAR; Walz, 2014), minimum fluorescence yield (F_o, used as a proxy for the distribution of chlorophyll or symbionts) and F_v/F_m of the surface of dark-adapted cores were determined using the software ImagingWin v2.41a (Walz, Effeltrich, Germany) based on methodology described previously (Fang *et al.*, 2016b).

All photosynthetic parameters of the pilot study were analysed by means of a one-way analysis of variance (ANOVA, Statistica 13, StatSoft) with treatment as a categorical factor, after testing the assumptions of normality (Shapiro-Wilk test) and homogeneity of variances (Levene's test).

Supplementary pilot Study - Results

Exposure of *Cliona orientalis* to the herbicide diuron (DCMU) and the antibiotic chloramphenicol (CAP) over 3 days led to a decrease in photosynthetic activity in both treatmens (Fig. S2.1, $F_{(2,18)}=163.27$, $p<0.0001$). Net oxygen production (net photosynthesis) decreased by approximately 68% in the CAP treatment and by 140% in the DCMU treatment

in comparison to the control treatment (Tukey's post-hoc, $p<0.001$ for both comparisons). Apparent absorptivity (Abs) and maximum quantum yield (efficiency) of photosystem II (F_v/F_m) also decreased in DCMU-treated sponges in comparison to the controls (Fig. S2.2, Tukey's post-hoc, $p<0.001$ for both comparisons). Dark acclimated minimum fluoresence (F_o) showed a similar decreasing (yet not significant) trend in DCMU-treated sponges, but not in CAP-treated sponges where F_o appeared to increase compared to controls (Fig. S2.2, Tukey's post-hoc, $p=0.079$ and $p=0.001$ respectively). In both treatments and especially in the CAP treatment the sponges appeared paled (Fig. S2.2a,b) but their oscula remained open and they were actively pumping (confirmed with fluorescent dye).

In conclusion, DCMU appeared to be a more effective inhibitor of photosynthesis, and since it only affects specific photosynthetic properties, it was chosen as a more suitable treatment for the main experiment. The antibiotic CAP was not used given it could potentially have considerable effects on the host and its microbiome (Kovačevic et al., 2001). Since after 3 days of exposure to the herbicide diuron (DCMU) the sponges appeared healthy, it was decided to carefully increase the duration of exposure in the main experiment towards achieving a potentially stronger inhibition of photosynthesis.

Supplementary Figures

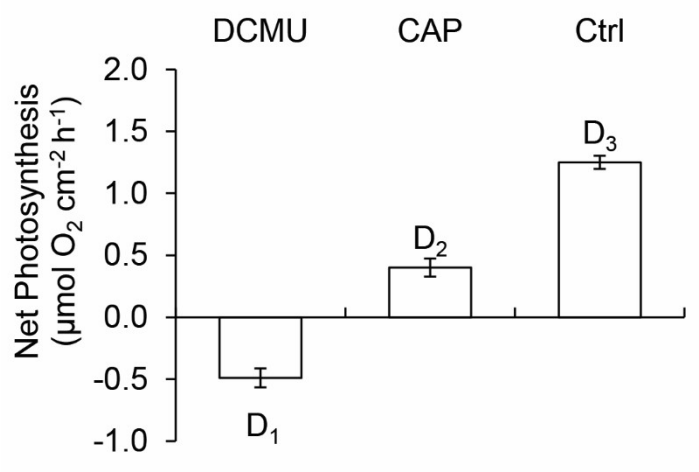

Figure S2.1: Oxygen production of the *Cliona orientalis* holobiont in the day (net photosynthesis) after a 3-day exposure to three different treatments: exposure to the herbicide DCMU, exposure to the antibiotic chloramphenicol, and control treatment (Ctrl). Bars display means ± SEM, n=7 sponges per treatment.

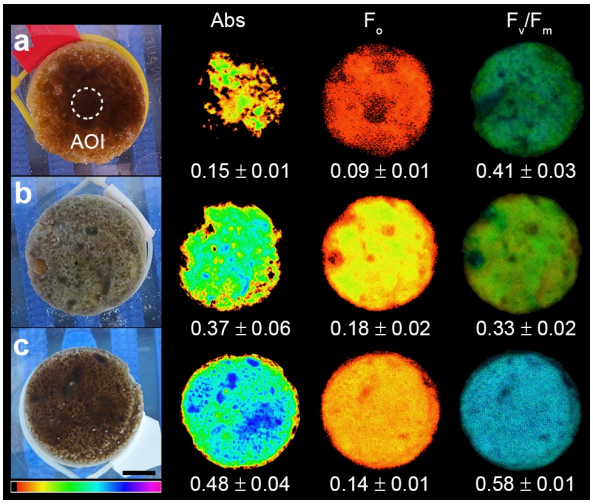

Figure S2.2: Tissue colour (first column, a-c) and photosynthetic indicators (columns 2-4) measured in the photosymbiotic bioeroding sponge holobiont *Cliona orientalis* after 3 days of exposure to the herbicide diuron (DCMU) **(a)** and the antibiotic chloramphenicol (CAP) **(b)** in comparison to the control treatment **(c)**. For each treatment, relative values of apparent absorptivity (Abs), dark-acclimated minimum fluorescence yield (F_o) and maximum potential quantum yield of photosystem II (F_v/F_m) measured on areas of interest (AOI) of the top surface of the sponges are displayed (mean±SEM, n=7 sponges per treatment). The intensity of Abs, F_o and F_v/F_m ranges from 0 (in black) to 1 (in purple), as shown in the rainbow scale. The scale bar in **(c)** equals 1 cm.

Supplementary Information – Chapter 3

Supplementary Methods

Fixation and embedment of sponge material

Thin slices of *Symbiodinium*-rich tissue were isolated from the upper layer of the halved sponge cores. The slices were immediately fixed in 3% glutaraldehyde and 1% paraformaldehyde in 0.1M sodium cacodylate in filtered seawater on a rocker for 3h at RT. The fixed material was decalcified in 5% HNO_3 for 4h to separate the sponge tissue from the coral skeleton that it was infesting. The sponge tissue was then placed in 5% HF for 1.5h to break down the siliceous spicules that form the sponge's skeleton. The sponge samples were returned to 0.1M sodium cacodylate buffer and cut into 1mm pieces. Post-fixation followed in 1% osmium tetroxide in sodium cacodylate buffer under vacuum at 80W (2 x sequence of 2min on- 2min off- 2 min on) using a Pelco Biowave (Ted Pella, CA, USA). The samples were then rinsed in ultrapure water and stained to increase contrast using 2% uranyl acetate under vacuum at 150W (sequence of 1min on- 1min off- 1min on). Samples were dehydrated in an increasing series of ethanol concentrations (30%, 50%, 70%, 90% and 2x 100%) in the Biowave at 250W for 40 sec at each concentration. To ensure embedment of all cells, resin infiltration was performed stepwise increasing the resin to ethanol ratio in 7 steps (1:3, 1:2, 1:1, 2:1, 3:1 and finally 2x 100% resin). At each step, the samples were microwaved at 250W for 10min under vacuum and then centrifuged for 10min at low speed. Samples were left overnight on a rotary tube mixer before resin polymerisation at 60°C in a convection oven. Note that fixation and embedment remove all inorganic label from the sample and therefore only fixed organic isotopic enrichment is monitored through NanoSIMS.

NanoSIMS analysis

The isotopic enrichments of the sponge sections were examined using a NanoSIMS ion probe (NanoSIMS 50, CAMECA, Paris, France) according to previous studies (Pernice *et al.*, 2012, 2014; Wangpraseurt *et al.*, 2015). The finder grids were mounted onto the instrument holder and coated with gold. Once inside the instrument, the samples were bombarded by a Cs^+ primary ion beam (1-3 pA) with a net impact energy of 16keV, and a spot size of approx. 100nm on the sample surface. Under the impact of the beam, secondary molecular ions ($^{12}C^{14}N^-$, $^{12}C^{15}N$, $^{-12}C^{12}C^-$ and $^{12}C^{13}C^-$,) were extracted from the sample surface (to a depth of tens of nm) and simultaneously detected using electron multipliers, at a mass resolution ($\Delta M/M$, following the manufacturer's guidelines) of about 9000, enough to resolve the ion

peaks from mass interferences. Compensation for local charging effects was unnecessary. The beam moved across the surface of the sample with a dwell-time of 20ms per pixel, producing 2D images of 256 x 256 pixels with a typical raster size of 35 x 35 µm for each of the secondary molecular ions. The images were dead-time corrected, stacked and aligned using the OpenMIMS data analysis software (www.nano.bwh.harvard.edu/openmims) in Fiji platform (Schindelin *et al.*, 2012). Division of the $^{12}C^{15}N^-$ by the $^{12}C^{14}N^-$ image and the $^{12}C^{13}C^-$ by the $^{12}C^{12}C^-$ image generated the $^{15}N/^{14}N$ and $^{13}C/^{12}C$ ratio images (Figure 3.1 in main text).

***Symbiodinium*-specific ^{15}N-ammonium and ^{13}C-bicarbonate uptake rates**

Remaining halves of the sampled sponge cores were thawed and upper surface areas were estimated using a standard aluminium foil method (Marsh, 1970). Using the acid decalcification method (Fang *et al.*, 2013b), all $CaCO_3$ was removed from the samples and the wet sponge material was homogenized with a tissue tearor. The homogenate was filtered sequentially through a 200 µm, 40 µm and 10 µm cell strainer (Pluriselect, Leipzig, Germany) to remove most of the sponge spicules and centrifuged at 4000g for 5 min at 4°C. The pellet containing *Symbiodinium* cells was then washed repeatedly to minimize contamination from sponge material and resuspended in phosphate buffer solution. A subsample was used to quantify the number of *Symbiodinium* cells using a haemocytometer (Laboroptik, Lancing, UK) under a microscope at 400x magnification (BX43, Olympus, Tokyo, Japan) as detailed by Fang *et al.* (2013a). The number of *Symbiodinium* cells counted per unit volume was normalized to the original surface area of the sponge core (cells cm^{-2}). The remaining cell suspension was centrifuged again, washed with deionized water to remove salts, and re-pelleted. The dried pellets were weighed and analysed in triplicate using a standard combustion (950°C) method with a LECO TruSpec analyser (Leco, St. Joseph, MI, USA). Pellets may have contained a small fraction of sponge spicules, yet these did not influence the measurements since their organic content is negligible (~0.4‰ of spicule weight, Schwab and Shore, 1971). Resulting nitrogen and carbon content (% dry mass) were normalized to the incubation time and the *Symbiodinium* population density as modified from Dugdale and Wilkerson (1986):

$$\text{N uptake rate} = ((N_{mes}-N_{nat})/((N_{enr}-N_{nat}) \times T_{inc})) \times N_{content} \times 10^3$$

$$\text{C uptake rate} = ((C_{mes}-C_{nat})/((C_{enr}-C_{nat}) \times T_{inc})) \times C_{content} \times 10^3, \text{ where}$$

N_{mes} and C_{mes}: $^{15}N/^{14}N$ and $^{13}C/^{12}C$ respectively, measured in labelled samples by NanoSIMS

N_{nat} and C_{nat}: natural abundance of $^{15}N/^{14}N$ and $^{13}C/^{12}C$ respectively, measured in unlabelled samples by NanoSIMS

N_{enr} and C_{enr}: ^{15}N and ^{13}C enrichment of the incubation medium

T_{inc}: incubation time

$N_{content}$ and $C_{content}$: average nitrogen and carbon content of the dinoflagellate cells per surface area as measured by combustion (950°C)

Supplementary Figures

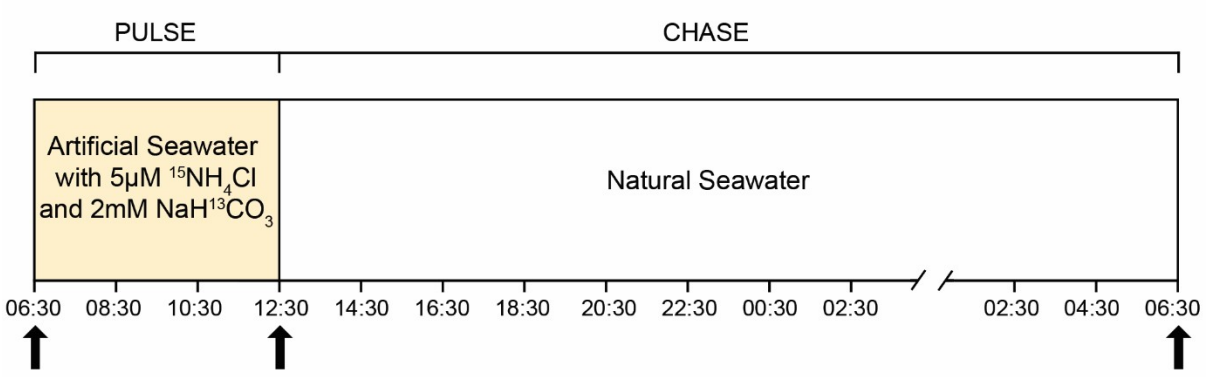

Figure S3.1: Experimental design of sponge pulse-chase labelling. The 6h-pulse of enriched artificial seawater was performed on the 25th of February 2016 (sunrise at 5:45 and sunset at 18:25), with the chase extending until 3 days later. Arrows indicate the sampling times (t=0h, 6h and 72h).

Supplementary Tables

Table S3.1: Best hits found when searching glutamate synthase (GOGAT) derived from over 20 animal species against Poriferan sequences (taxid: 6040) using psi-BLAST algorithm and Blastx. Even though sponges are early-diverging metazoa (Nielsen, 2008), no evidence of a GOGAT homolog in sponges was found. Instead, all hits returned a conserved region of the predicted protein dihydropyrimidine dehydrogenase $NADP^+$ (DPD) -which does not correspond to GOGAT- from the sponge *Amphimedon queenslandica*.

Query Sequence = GOGAT		Closest Poriferan hit = DPD		
Species	GenBank accession nr	Query cover	E-value	GenBank accession nr
Drosophila melanogaster	NP_648922.1	21%	7×10^{-24}	XP_003385906.1
Pediculus humanus	XP_002428593.1	24%	3×10^{-23}	XP_003385906.1
Acyrthosiphon pisum	XP_001948786.2	21%	4×10^{-23}	XP_003385906.1
Ixodes scapularis	XP_002435411.1	24%	2×10^{-21}	XP_003385906.1
Nematostella vectensis	XP_001630774.1	25%	3×10^{-21}	XP_003385906.1
Harpegnathos saltator	EFN86827.1	22%	3×10^{-18}	XP_003385906.1
Acromyrmex echinatior	EGI70214.1	14%	6×10^{-18}	XP_003385906.1
Bombus impatiens	XP_003487604.1	21%	2×10^{-17}	XP_003385906.1
Trichinella spiralis	XP_003377159.1	20%	3×10^{-17}	XP_003385906.1
Apis mellifera	XP_396817.3	23%	2×10^{-15}	XP_003385906.1

Table S3.2: Nitrogen and carbon isotopic ratios and enrichment levels of three individual areas of interest [AOI: (I) *Symbiodinium*=S, (II) Cytoplasm of *Symbiodinium*-hosting sponge cells=Hs and (III) nearby mesohyl cells or intercellular areas=M] in the photosymbiotic bioeroding sponge *Cliona orientalis* after a pulse of ^{15}N-ammonium and ^{13}C-bicarbonate. AOI displayed in Figure 3.1 (3.1b, f and j respectively) are marked with an asterisk.

Sponge replicate	AOI	Sampling time (h)	Section	Raster regions	AOI name	$^{15}N/^{14}N$	$\delta^{15}N$ (‰)	$^{13}C/^{12}C$	$\delta^{13}C$ (‰)
Sponge A 7 raster regions n=10 AOI (S)	S	0	1	B_1	2	0.00366	3.75	0.02113	5.82
	S	0	1	B_2	1	0.00367	5.67	0.02132	15.03
	S	0	1	B_2	2	0.00360	-13.08	0.02132	15.00
	S	0	1	B_3	S1*	0.00367	7.91	0.02116	7.26
	S	0	1	B_4	10	0.00362	-6.57	0.02109	4.00
	S	0	2	D_1	1	0.00364	-0.76	0.02078	-10.64
	S	0	2	D_1	2	0.00366	4.33	0.02071	-14.18
	S	0	2	D_2	1	0.00362	-6.48	0.02092	-4.04
	S	0	2	D_3	1	0.00365	2.45	0.02083	-8.29
	S	0	2	D_3	2	0.00366	2.79	0.02079	-9.97
Sponge B 6 raster regions n=16 AOI (S)	S	6	1	E_1	19	0.00660	811.60	0.02459	170.77
	S	6	1	E_1	21	0.00954	1616.55	0.02581	228.85
	S	6	2	F_1	19	0.00541	482.75	0.02543	210.67
	S	6	2	F_1	20	0.00551	510.66	0.02815	340.18
	S	6	2	F_1	21	0.00645	769.54	0.03064	458.73
	S	6	2	F_2	19	0.00847	1323.95	0.02421	152.45
	S	6	1	E_1	18	0.00366	3.58	0.02783	325.14
	S	6	1	E_1	20	0.00393	77.80	0.02840	352.36
	S	6	3	H_1	18	0.00400	96.56	0.02440	161.78
	S	6	3	H_1	21	0.00372	20.23	0.02489	185.22
	S	6	4	J_1	20	0.00368	8.43	0.02528	203.65
	S	6	4	J_1	22	0.00388	64.22	0.02493	187.09
	S	6	5	G_1	19	0.01208	2314.94	0.02284	87.36
	S	6	3	H_1	19	0.00406	112.84	0.02300	95.24
	S	6	3	H_1	20	0.00401	98.93	0.02271	81.16
	S	6	4	J_1	21	0.00395	83.44	0.02309	99.45
Sponge C 7 raster regions n=40 AOI (S)	S	6	1	A_1	S1*	0.00969	1659.42	0.08001	2809.23
	S	6	1	A_1	S2*	0.00515	412.35	0.08293	2948.58
	S	6	1	A_1	S3*	0.00953	1615.38	0.07818	2722.26
	S	6	1	A_1	S4*	0.00472	295.35	0.10043	3781.61
	S	6	1	A_1	S5*	0.00731	1004.63	0.11404	4429.61
	S	6	2	D_1	21	0.00463	270.13	0.05205	1478.07
	S	6	3	F_1	17	0.00624	710.39	0.09777	3654.90
	S	6	3	F_1	18	0.00543	490.32	0.10537	4016.94
	S	6	3	F_1	19	0.00569	561.48	0.10564	4029.68
	S	6	3	F_1	20	0.01329	2646.94	0.12081	4751.81
	S	6	3	F_1	21	0.01254	2440.96	0.11858	4645.67
	S	6	3	F_1	22	0.00697	912.52	0.09258	3407.96
	S	6	3	F_1	23	0.00668	833.19	0.10223	3867.15

	S	6	3	F_1	24	0.01233	2383.00	0.09977	3749.95
	S	6	3	F_2	18	0.00651	787.00	0.07028	2346.07
	S	6	3	F_2	19	0.00741	1031.73	0.08371	2985.53
	S	6	3	F_2	20	0.00438	201.72	0.07822	2723.92
	S	6	3	F_2	21	0.00566	553.66	0.05244	1496.49
	S	6	4	G_1	18	0.00708	943.40	0.08920	3246.65
	S	6	4	G_1	19	0.00481	318.12	0.04320	1056.87
	S	6	4	G_1	20	0.01616	3433.37	0.06246	1973.76
	S	6	4	G_1	21	0.04769	12083.09	0.06684	2182.21
	S	6	4	G_1	23	0.00627	721.20	0.04280	1037.95
	S	6	4	G_2	18	0.00545	494.58	0.03860	837.63
	S	6	4	G_2	21	0.00851	1334.92	0.05985	1849.60
	S	6	4	G_2	22	0.00652	789.86	0.05446	1593.10
	S	6	2	D_1	16	0.00367	7.10	0.06843	2258.24
	S	6	2	D_1	17	0.00381	46.28	0.06240	1970.95
	S	6	2	D_1	18	0.00387	61.58	0.05059	1408.67
	S	6	2	D_1	19	0.00408	119.04	0.07080	2370.73
	S	6	2	D_1	20	0.00395	84.31	0.07629	2632.04
	S	6	3	F_1	16	0.00412	129.15	0.10671	4080.74
	S	6	4	G_1	22	0.00415	137.66	0.07485	2563.58
	S	6	4	G_2	19	0.00389	67.44	0.06087	1898.22
	S	6	4	G_2	20	0.00390	68.80	0.03167	507.89
	S	6	5	K_1	1	0.00368	10.65	0.04668	1222.49
	S	6	5	K_1	2	0.00369	13.24	0.04336	1064.60
	S	6	5	K_1	3	0.00373	23.86	0.03207	526.67
	S	6	5	K_1	4	0.00382	49.20	0.03839	827.64
	S	6	5	K_1	5	0.00370	15.23	0.03290	566.16
Sponge D 6 raster regions n=22 AOI (S)	S	72	1	H_1	7	0.00458	257.42	0.04996	1378.82
	S	72	1	H_1	8	0.00432	184.49	0.02456	169.34
	S	72	2	J_1	1	0.00537	472.37	0.02452	167.53
	S	72	2	J_1	2	0.00465	275.67	0.02526	202.80
	S	72	2	J_1	3	0.00495	356.59	0.02447	164.88
	S	72	2	J_1	4	0.00444	217.11	0.02484	182.64
	S	72	2	J_1	5	0.00471	292.61	0.04660	1218.48
	S	72	3	K_1	1	0.00608	668.42	0.05422	1581.40
	S	72	3	K_1	2	0.01025	1811.34	0.04916	1340.53
	S	72	3	K_2	S1*	0.00422	157.20	0.05445	1592.48
	S	72	3	K_2	S2*	0.01161	2185.78	0.04670	1223.48
	S	72	3	K_3	7	0.00547	501.33	0.04253	1024.84
	S	72	3	K_3	8	0.00450	233.50	0.04054	930.23
	S	72	3	K_3	9	0.00613	682.64	0.08303	2953.10
	S	72	4	M_1	12	0.00467	281.49	0.02485	183.06
	S	72	4	M_1	13	0.00470	290.59	0.03717	769.47
	S	72	4	M_1	14	0.00446	224.37	0.03651	738.16
	S	72	3	K_1	3	0.00369	11.88	0.02805	335.47
	S	72	3	K_1	5	0.00391	73.92	0.03253	548.56
	S	72	3	K_3	6	0.00398	92.87	0.05450	1595.02

	S	72	3	K_1	4	0.00415	138.07	0.02267	79.14
	S	72	3	K_3	5	0.00373	23.43	0.02340	114.11
Sponge E 4 raster regions n=25 AOI (S)	S	72	1	J_1	20	0.00430	180.70	0.04246	1021.73
	S	72	1	J_1	21	0.00430	179.88	0.04289	1042.09
	S	72	2	L_1	20	0.00462	268.28	0.06747	2212.41
	S	72	2	L_1	21	0.00449	230.73	0.06461	2075.93
	S	72	2	L_1	26	0.02197	5027.62	0.04679	1227.88
	S	72	2	L_2	32	0.00502	377.65	0.04668	1222.31
	S	72	1	J_1	22	0.00380	42.54	0.03583	705.76
	S	72	1	J_2	20	0.00384	52.48	0.05083	1420.01
	S	72	1	J_2	21	0.00371	18.75	0.05904	1810.79
	S	72	1	J_2	22	0.00376	30.49	0.03680	752.03
	S	72	1	J_2	23	0.00364	-1.54	0.05143	1448.63
	S	72	1	J_2	24	0.00298	-182.22	0.05329	1537.39
	S	72	2	L_1	22	0.00386	57.79	0.03436	635.79
	S	72	2	L_1	23	0.00363	-4.20	0.03024	439.91
	S	72	2	L_1	24	0.00371	16.78	0.06457	2074.33
	S	72	2	L_1	25	0.00381	46.47	0.02597	236.66
	S	72	2	L_2	20	0.00365	1.78	0.02772	319.80
	S	72	2	L_2	21	0.00366	4.71	0.02517	198.15
	S	72	2	L_2	33	0.00412	129.90	0.04678	1227.38
	S	72	2	L_2	34	0.00365	0.32	0.02507	193.68
	S	72	1	J_2	25	0.00368	8.54	0.02061	-18.74
	S	72	2	L_2	22	0.00371	17.16	0.02340	114.18
	S	72	2	L_2	23	0.00385	55.81	0.02273	82.20
	S	72	2	L_2	35	0.00377	34.33	0.02230	61.87
	S	72	2	L_2	36	0.00375	30.03	0.02320	104.33
Sponge A 7 raster regions n=11 AOI (Hs)	Hs	0	1	B_1	3	0.00365	10.96	0.02102	7.32
	Hs	0	1	B_2	3	0.00369	22.31	0.02142	26.54
	Hs	0	1	B_2	4	0.00353	-22.01	0.02117	14.88
	Hs	0	1	B_3	Hs1*	0.00369	21.41	0.02106	9.65
	Hs	0	1	B_4	11	0.00372	30.80	0.02115	13.83
	Hs	0	1	B_4	12	0.00360	-4.78	0.02102	7.68
	Hs	0	2	D_1	3	0.00362	1.46	0.02060	-12.39
	Hs	0	2	D_1	5	0.00343	-51.53	0.02045	-19.88
	Hs	0	2	D_1	6	0.00349	-34.12	0.02015	-34.22
	Hs	0	2	D_2	2	0.00368	19.77	0.02084	-1.15
	Hs	0	2	D_3	3	0.00363	5.73	0.02061	-12.27
Sponge B 6 raster regions n=12 AOI (Hs)	Hs	6	1	F_1	23	0.00398	101.86	0.02917	398.12
	Hs	6	1	F_1	22	0.00418	157.20	0.02304	104.34
	Hs	6	1	F_2	26	0.00544	506.58	0.02191	50.33
	Hs	6	2	G_1	20	0.00486	343.87	0.02165	37.49
	Hs	6	3	E_1	22	0.00346	-41.78	0.02251	78.78
	Hs	6	3	E_1	23	0.00394	90.73	0.02148	29.38
	Hs	6	3	E_1	24	0.00380	51.37	0.02168	39.32
	Hs	6	4	H_1	22	0.00366	13.40	0.02068	-8.60
	Hs	6	4	H_1	23	0.00376	39.27	0.02119	15.89

	Hs	6	4	H_1	24	0.00364	8.16	0.02124	18.01
	Hs	6	5	J_1	23	0.00376	40.86	0.02099	6.25
	Hs	6	5	J_1	24	0.00367	16.67	0.02166	38.09
Sponge C 7 raster regions n=22 AOI (Hs)	Hs	6	1	A_1	Hs1*	0.00722	997.31	0.05080	1434.95
	Hs	6	1	A_1	Hs2*	0.00415	148.94	0.02581	237.02
	Hs	6	2	F_1	27	0.00590	632.88	0.04350	1085.01
	Hs	6	2	F_1	28	0.00578	598.83	0.03769	806.30
	Hs	6	3	G_1	24	0.00557	541.97	0.08414	3032.90
	Hs	6	3	G_1	25	0.00514	422.27	0.02962	419.59
	Hs	6	3	G_1	26	0.01070	1961.28	0.04394	1106.06
	Hs	6	4	D_1	22	0.00360	-3.95	0.04065	948.42
	Hs	6	4	D_1	25	0.00382	57.06	0.03338	599.74
	Hs	6	2	F_1	25	0.00397	98.18	0.02678	283.82
	Hs	6	2	F_1	26	0.00408	128.75	0.03718	781.88
	Hs	6	2	F_2	22	0.00405	121.27	0.02845	363.85
	Hs	6	2	F_2	23	0.00391	82.95	0.02558	226.04
	Hs	6	3	G_2	23	0.00391	80.92	0.04569	1189.96
	Hs	6	5	K_1	6	0.00372	29.41	0.02707	297.73
	Hs	6	5	K_1	7	0.00353	-23.80	0.03168	518.66
	Hs	6	5	K_1	8	0.00365	9.02	0.02613	252.55
	Hs	6	5	K_1	9	0.00356	-15.70	0.02667	278.54
	Hs	6	4	D_1	23	0.00379	48.48	0.02267	86.68
	Hs	6	4	D_1	24	0.00370	23.11	0.02294	99.47
	Hs	6	3	G_2	24	0.00383	58.78	0.02237	72.19
	Hs	6	3	G_2	25	0.00410	133.27	0.02314	109.28
Sponge D 6 raster regions n=18 AOI (Hs)	Hs	72	1	H_1	6	0.00464	284.28	0.02924	401.42
	Hs	72	2	J_1	11	0.00433	199.03	0.02833	357.91
	Hs	72	3	K_1	6	0.00485	341.76	0.02877	379.04
	Hs	72	3	K_2	Hs1*	0.00413	142.93	0.03661	754.75
	Hs	72	3	K_2	Hs2*	0.01062	1938.18	0.04339	1079.82
	Hs	72	3	K_2	Hs3*	0.00990	1740.59	0.04284	1053.52
	Hs	72	3	K_1	7	0.00922	1550.61	0.04007	920.37
	Hs	72	3	K_3	3	0.00477	321.19	0.02741	314.03
	Hs	72	4	M_1	9	0.00465	285.66	0.02965	421.15
	Hs	72	2	J_1	13	0.00402	113.36	0.02430	164.51
	Hs	72	2	J_1	12	0.00428	184.66	0.02237	72.13
	Hs	72	1	H_1	9	0.00383	61.27	0.02172	41.15
	Hs	72	3	K_1	8	0.00382	57.32	0.02383	142.00
	Hs	72	3	K_1	9	0.00398	100.57	0.02216	61.97
	Hs	72	3	K_3	2	0.00371	25.95	0.02256	81.21
	Hs	72	3	K_3	4	0.00408	128.28	0.02359	130.52
	Hs	72	4	M_1	10	0.00365	11.09	0.02284	94.60
	Hs	72	4	M_1	11	0.00406	124.35	0.02288	96.55
	Hs	72	1	J_1	23	0.00443	224.93	0.03120	495.60
	Hs	72	1	J_2	27	0.00426	179.72	0.03132	501.28
	Hs	72	2	L_1	27	0.00489	352.96	0.03540	696.75

Sponge E 4 raster regions n=19 AOI (Hs)	Hs	72	2	L_1	31	0.01532	3238.68	0.03268	566.36
	Hs	72	2	L_2	25	0.00486	345.59	0.03746	795.57
	Hs	72	2	L_2	38	0.00509	407.92	0.03449	653.07
	Hs	72	1	J_1	24	0.00349	-35.38	0.04022	928.02
	Hs	72	1	J_2	26	0.00365	9.47	0.04192	1009.17
	Hs	72	1	J_2	28	0.00400	105.97	0.04191	1008.76
	Hs	72	1	J_2	29	0.00385	66.18	0.03624	736.84
	Hs	72	2	L_1	28	0.00397	98.65	0.02713	300.21
	Hs	72	2	L_1	29	0.00321	-112.04	0.02833	357.75
	Hs	72	2	L_1	30	0.00400	106.92	0.02817	350.35
	Hs	72	2	L_2	39	0.00379	48.02	0.05069	1429.72
	Hs	72	1	J_1	25	0.00376	41.60	0.02149	29.83
	Hs	72	1	J_2	30	0.00374	34.15	0.02278	91.77
	Hs	72	2	L_2	24	0.00357	-11.20	0.02275	90.51
	Hs	72	2	L_2	26	0.00359	-7.16	0.02152	31.43
	Hs	72	2	L_2	37	0.00381	54.39	0.02379	140.10
Sponge A 7 raster regions n=35 AOI (M)	M	0	1	B_1	4	0.00357	-26.72	0.02102	0.99
	M	0	1	B_1	5	0.00367	-0.24	0.02130	14.35
	M	0	1	B_1	6	0.00369	4.14	0.02116	7.40
	M	0	1	B_1	7	0.00367	-0.43	0.02085	-7.49
	M	0	1	B_1	8	0.00368	1.27	0.02113	5.93
	M	0	1	B_2	5	0.00368	2.59	0.02084	-7.97
	M	0	1	B_2	10	0.00369	4.60	0.02128	13.44
	M	0	1	B_2	11	0.00368	2.94	0.02090	-4.93
	M	0	1	B_2	12	0.00367	-2.09	0.02106	2.93
	M	0	1	B_2	14	0.00367	-2.02	0.02120	9.51
	M	0	1	B_3	M1*	0.00365	-7.14	0.02130	14.17
	M	0	1	B_3	M2*	0.00365	-5.86	0.02122	10.27
	M	0	1	B_3	M3*	0.00369	5.88	0.02115	6.84
	M	0	1	B_3	M4*	0.00376	24.14	0.02120	9.31
	M	0	1	B_3	M5*	0.00371	9.99	0.02170	33.30
	M	0	1	B_4	13	0.00369	5.07	0.02090	-4.70
	M	0	1	B_4	14	0.00363	-12.87	0.02137	17.71
	M	0	1	B_4	15	0.00368	1.73	0.02141	19.57
	M	0	1	B_4	21	0.00371	9.64	0.02096	-2.11
	M	0	1	B_4	22	0.00367	-2.07	0.02139	18.28
	M	0	2	D_1	7	0.00364	-8.31	0.02026	-35.48
	M	0	2	D_1	8	0.00367	-0.26	0.02080	-9.46
	M	0	2	D_1	9	0.00378	28.78	0.02065	-16.89
	M	0	2	D_1	10	0.00356	-31.79	0.02102	0.67
	M	0	2	D_1	11	0.00360	-19.28	0.02061	-18.61
	M	0	2	D_2	3	0.00370	8.32	0.02085	-7.28
	M	0	2	D_2	4	0.00366	-3.68	0.02111	5.15
	M	0	2	D_2	5	0.00367	-2.01	0.02068	-15.26
	M	0	2	D_2	6	0.00361	-16.09	0.02094	-2.81
	M	0	2	D_2	7	0.00371	9.71	0.02082	-8.88
	M	0	2	D_3	7	0.00369	4.74	0.02090	-4.98
	M	0	2	D_3	8	0.00372	12.27	0.02099	-0.76
	M	0	2	D_3	9	0.00365	-5.73	0.02070	-14.21

	M	0	2	D_3	10	0.00362	-13.42	0.02096	-2.17
	M	0	2	D_3	11	0.00369	4.84	0.02074	-12.60
Sponge B 6 raster regions n=30 AOI (M)	M	6	1	E_1	25	0.00375	20.26	0.02135	16.61
	M	6	1	E_1	26	0.00383	41.76	0.02113	6.26
	M	6	1	E_1	27	0.00361	-16.11	0.02133	15.82
	M	6	1	E_1	28	0.00374	18.64	0.02102	1.00
	M	6	1	E_1	29	0.00393	70.53	0.02105	2.14
	M	6	2	F_1	24	0.00385	47.13	0.02168	32.37
	M	6	2	F_1	25	0.00369	5.31	0.02104	1.55
	M	6	2	F_1	26	0.00372	13.01	0.02114	6.33
	M	6	2	F_1	27	0.00377	27.70	0.02141	19.37
	M	6	2	F_1	28	0.00364	-8.05	0.02118	8.52
	M	6	2	F_2	21	0.00376	24.25	0.02144	20.74
	M	6	2	F_2	22	0.00370	7.68	0.02160	28.24
	M	6	2	F_2	23	0.00373	15.37	0.02149	23.18
	M	6	2	F_2	24	0.00365	-6.28	0.02138	18.16
	M	6	2	F_2	25	0.00374	17.39	0.02157	26.96
	M	6	3	G_1	21	0.00363	-12.53	0.02133	15.42
	M	6	3	G_1	22	0.00372	11.62	0.02137	17.65
	M	6	3	G_1	23	0.00375	20.63	0.02148	22.88
	M	6	3	G_1	24	0.00370	8.15	0.02144	20.93
	M	6	3	G_1	25	0.00376	22.63	0.02125	12.00
	M	6	4	H_1	25	0.00384	44.28	0.02080	-9.87
	M	6	4	H_1	26	0.00383	42.38	0.02151	24.24
	M	6	4	H_1	27	0.00371	8.96	0.02127	12.96
	M	6	4	H_1	28	0.00377	27.09	0.02121	9.95
	M	6	4	H_1	29	0.00366	-3.95	0.02127	12.94
	M	6	5	J_1	25	0.00367	-0.24	0.02153	25.21
	M	6	5	J_1	26	0.00373	14.17	0.02135	16.57
	M	6	5	J_1	27	0.00374	19.26	0.02179	37.27
	M	6	5	J_1	28	0.00374	18.84	0.02119	8.85
	M	6	5	J_1	29	0.00358	-24.56	0.02106	2.50
Sponge C 7 raster regions n=35 AOI (M)	M	6	1	G_1	27	0.00445	210.29	0.02752	310.51
	M	6	2	D_1	27	0.00378	28.51	0.02671	271.67
	M	6	3	F_1	31	0.00373	16.32	0.02492	186.41
	M	6	3	F_1	32	0.00397	81.37	0.02700	285.70
	M	6	3	F_2	24	0.00393	71.16	0.02406	145.48
	M	6	1	G_1	31	0.00407	109.02	0.02909	385.00
	M	6	4	K_1	16	0.00376	23.09	0.02516	197.87
	M	6	5	A_1	M1*	0.00369	5.19	0.02073	-13.19
	M	6	5	A_1	M2*	0.00370	7.14	0.01912	-89.57
	M	6	5	A_1	M3*	0.00381	38.51	0.01817	-134.69
	M	6	5	A_1	M4*	0.00408	110.32	0.02329	108.82
	M	6	5	A_1	M5*	0.00388	56.94	0.02089	-5.51
	M	6	2	D_1	26	0.00364	-7.98	0.02151	23.96
	M	6	2	D_1	29	0.00368	1.37	0.02264	78.13
	M	6	2	D_1	30	0.00387	54.93	0.02201	47.94
	M	6	2	D_1	31	0.00353	-39.18	0.02120	9.57
	M	6	3	F_1	29	0.00389	58.62	0.02253	72.88

	M	6	3	F_1	30	0.00379	31.59	0.02225	59.60
	M	6	3	F_1	33	0.00380	35.44	0.02272	81.81
	M	6	3	F_2	25	0.00385	46.93	0.02343	115.55
	M	6	3	F_2	27	0.00368	2.14	0.02108	3.53
	M	6	3	F_2	28	0.00388	55.04	0.02339	113.57
	M	6	3	F_2	29	0.00368	1.38	0.02111	5.08
	M	6	1	G_1	29	0.00375	21.31	0.02127	12.81
	M	6	1	G_1	30	0.00371	8.72	0.02105	2.35
	M	6	1	G_1	32	0.00386	50.20	0.02124	11.41
	M	6	1	G_2	26	0.00371	10.83	0.02111	5.07
	M	6	1	G_2	27	0.00359	-22.26	0.02321	105.05
	M	6	1	G_2	28	0.00371	10.02	0.02169	32.88
	M	6	1	G_2	29	0.00380	33.39	0.02282	86.30
	M	6	1	G_2	30	0.00372	11.69	0.02118	8.27
	M	6	4	K_1	15	0.00390	62.57	0.02101	0.24
	M	6	4	K_1	17	0.00362	-13.91	0.02133	15.54
	M	6	4	K_1	18	0.00379	31.90	0.02150	23.73
	M	6	4	K_1	19	0.00366	-3.06	0.02172	34.25
Sponge D 6 raster regions n=30 AOI (M)	M	72	1	M_1	1	0.00521	419.71	0.02293	91.86
	M	72	2	H_1	1	0.00376	23.90	0.02165	31.06
	M	72	2	H_1	2	0.00361	-17.46	0.02139	18.37
	M	72	2	H_1	3	0.00364	-8.64	0.02188	41.91
	M	72	2	H_1	4	0.00371	10.38	0.02133	15.63
	M	72	2	H_1	5	0.00364	-8.21	0.02113	5.96
	M	72	3	J_1	6	0.00344	-64.79	0.02207	50.64
	M	72	3	J_1	7	0.00370	6.06	0.02161	28.77
	M	72	3	J_1	8	0.00371	10.69	0.02212	53.28
	M	72	3	J_1	9	0.00410	116.46	0.02073	-12.83
	M	72	3	J_1	10	0.00371	10.75	0.02174	34.99
	M	72	4	K_1	15	0.00366	-2.63	0.02198	46.77
	M	72	4	K_1	16	0.00394	73.54	0.02200	47.50
	M	72	4	K_1	17	0.00411	117.96	0.02352	119.87
	M	72	4	K_1	18	0.00363	-10.66	0.02137	17.31
	M	72	4	K_1	19	0.00374	18.22	0.02275	83.12
	M	72	4	K_2	M1*	0.00382	38.97	0.02228	60.95
	M	72	4	K_2	M2*	0.00362	-14.73	0.02199	46.91
	M	72	4	K_2	M3*	0.00378	29.66	0.02132	15.20
	M	72	4	K_2	M4*	0.00375	20.32	0.02206	50.53
	M	72	4	K_2	M5*	0.00373	15.00	0.02201	47.80
	M	72	4	K_3	1	0.00390	62.03	0.02147	22.30
	M	72	4	K_3	2	0.00377	26.38	0.02168	32.36
	M	72	4	K_3	3	0.00364	-9.86	0.02171	33.76
	M	72	4	K_3	4	0.00357	-27.46	0.02124	11.47
	M	72	4	K_3	5	0.00368	1.54	0.02205	49.83
	M	72	1	M_1	2	0.00408	111.38	0.02153	25.15
	M	72	1	M_1	3	0.00360	-19.94	0.02150	23.76
	M	72	1	M_1	4	0.00349	-49.21	0.02117	7.90
	M	72	1	M_1	5	0.00400	89.30	0.02195	45.18
	M	72	1	J_2	35	0.00448	220.41	0.02535	206.88

Sponge E 4 raster regions n=20 AOI (M)	M	72	1	J_1	26	0.00395	75.71	0.02418	151.32
	M	72	1	J_1	28	0.00361	-17.36	0.02835	350.04
	M	72	1	J_1	29	0.00365	-6.80	0.02643	258.29
	M	72	1	J_2	34	0.00359	-22.62	0.02453	167.74
	M	72	2	L_2	27	0.00416	131.44	0.02407	146.13
	M	72	1	J_1	27	0.00485	321.27	0.02340	114.02
	M	72	1	J_1	30	0.00389	60.15	0.02166	31.14
	M	72	1	J_2	31	0.00357	-28.11	0.02181	38.46
	M	72	1	J_2	32	0.00367	-0.51	0.02249	70.65
	M	72	1	J_2	33	0.00346	-58.58	0.02171	33.71
	M	72	2	L_1	32	0.00337	-83.73	0.02185	40.47
	M	72	2	L_1	33	0.00375	19.66	0.02152	24.48
	M	72	2	L_1	34	0.00376	24.04	0.02154	25.45
	M	72	2	L_1	36	0.00361	-18.13	0.02216	54.90
	M	72	2	L_1	37	0.00349	-48.55	0.02167	31.57
	M	72	2	L_2	28	0.00371	9.92	0.02177	36.52
	M	72	2	L_2	29	0.00363	-10.90	0.02193	44.18
	M	72	2	L_2	30	0.00372	12.10	0.02218	56.22
	M	72	2	L_2	31	0.00358	-26.13	0.02127	12.56

Table S3.3: Results of permutational analysis of variance testing the Euclidean dissimilarities between the levels of ^{15}N- and ^{13}C-enrichment of each area of interest [AOI: (I) *Symbiodinium*=S, (II) Cytoplasm of *Symbiodinium*-hosting sponge cells=Hs and (III) nearby mesohyl cells or intercellular areas=M] and between treatment timepoints (0h, 6h and 72h). df=degrees of freedom; SS=sum of squares; MS=mean sum of squares; Pseudo-F=F value by permutation, $P_{(perm)}$=P-value by permutation. Bold face indicates statistical significance ($P < 0.05$). Dispersions differed amongst the compared groups, with the greatest dispersion found in the largest group, rendering the permutational tests relatively conservative (Anderson and Walsh, 2013).

		Main Permanova Test					Pairwise Comparisons			
Parameter	Source	df	SS	MS	Pseudo-F	$P_{(perm)}$	Level	Groups	T	$P_{(perm)}$
^{15}N-enrichment	Treatment	2	**1.20E+07**	**6.01E+06**	**4.4832**	**0.0318**	-	**0h versus 6h**	**2.9647**	**0.0004**
	AOI	2	1.46E+06	7.31E+05	0.54524	0.4682		**0h versus 72h**	**3.383**	**0.012**
	Treatment x AOI	3	3.96E+06	1.32E+06	0.98592	0.3236		6h versus 72h	0.82769	0.4292
	Res	132	1.77E+08	1.34E+06						
^{13}C-enrichment	Treatment	2	**2.03E+07**	**1.02E+07**	**14.928**	**0.0002**	0h	Hs versus M	7.51E-02	0.9416
	AOI	2	**1.48E+07**	**7.41E+06**	**10.893**	**0.0002**		M versus S	8.16E-02	0.9412
	Treatment x AOI	4	**1.37E+07**	**3.44E+06**	**5.0518**	**0.001**		Hs versus S	2.64E-08	1.000
	Res	195	1.32E+08	6.80E+05			6h	Hs versus M	1.9324	0.0654
								M versus S	**3.0867**	**0.0038**
								Hs versus S	**3.4622**	**0.0012**
							72h	**Hs versus M**	**3.2851**	**0.0028**
								M versus S	**2.7979**	**0.0072**
								Hs versus S	**2.3472**	**0.0256**
							S	**0h versus 6h**	**4.2537**	**0.0002**
								0h versus 72h	**4.601**	**0.0002**
								6h versus 72h	**3.7966**	**0.0004**
							Hs	**0h versus 6h**	**3.6954**	**0.0002**
								0h versus 72h	**6.6791**	**0.0002**
								6h versus 72h	0.62926	0.569
							M	**0h versus 6h**	**17.868**	**0.0002**
								0h versus 72h	**15.593**	**0.0002**
								6h versus 72h	0.91444	0.3566

Table S3.4: Results of statistical tests comparing (a) the proportion of enriched cells between the 6h and 72h treatment timepoints for each area of interest [AOI: (I) *Symbiodinium*=S, (II) Cytoplasm of *Symbiodinium*-hosting sponge cells=Hs and (III) nearby mesohyl cells or intercellular areas=M] for nitrogen and carbon separately, and **(b)** the proportion of ^{15}N-enriched cells to the proportion of ^{13}C-enriched cells in each AOI for 6h and 72h separately. When expected frequencies in one of the groups of the statistical design were low (<5 counts), Fisher's exact test replaced the z-test (marked with an asterisk) (Fleiss *et al.*, 2003). Bold face indicates statistical significance ($p < 0.05$).

a Two-proportions z-test: 6h versus 72h

Parameter	AOI	df	z-value	p-value
^{15}N-enrichment	S	1	1.0284	0.3105
	Hs	1	0.9619	0.3267
	M	1	N/A	0.3155*
^{13}C-enrichment	S	1	N/A	0.3373*
	Hs	1	0.5986	0.4391
	M	1	0.0427	0.8363

b Two-proportions z-test: ^{15}N-enriched versus ^{13}C-enriched

Treatment	AOI	df	z-value	p-value
6h	S	1	N/A	**<0.0001***
	Hs	1	4.8700	**0.0273**
	M	1	N/A	0.0619*
72h	S	1	13.9099	**0.0002**
	Hs	1	4.3912	**0.0361**
	M	1	N/A	0.4869*

Supplementary Information – Chapter 4

Supplementary Methods

Simulation system

The ocean warming and acidification simulation system established at the Heron Island Research Station on the southern GBR employed computer control systems to replicate diel and seasonal variations of temperature and pCO_2 conditions on the reef in an experimental setting (Dove *et al.*, 2013; Fang, 2013). Projected increases of temperature and pCO_2 were applied as offsets to a baseline produced by 2 or 3 hourly measurements at a reference site on Heron Island's reef crest (Harry's Bommie) over the summer of the previous year (CSIRO and PMEL, 2016). The offsets were established according to projected conditions for the year 2100 based on the greenhouse gas concentration trajectory RCP8.5 (IPCC, 2013; 2014), the endpoint of which is equivalent to the A1FI scenario (IPCC, 2000).

The scenarios were continuously reproduced and monitored in four individual 8000 L sumps (residence time: 4-6 hours). The sumps were darkened, insulated with a rubber seal and inspected regularly. Seawater temperature in the sumps was controlled by heater-chillers (HWP017, Rheem, Rydalmere, Australia, equipped with Eurotherm 3216 temperature regulators, Invensys Process Systems, Clayton, Australia). The appropriate amounts of CO_2 gas (food grade), compressed air and "CO_2-free" air were injected into the sumps through an array of gas solenoid valves. Compressed air was stripped of CO_2 in desiccant columns containing soda lime (medical grade Spherasorb, Intersurgical, Berkshire, UK). A non-dispersive infrared (NDIR) sensor (CO_2-Pro, Pro-Oceanus, Nova Scotia, Canada, accuracy ±0.5% of CO_2 concentration, resolution 0.01ppm) measured the sumps in continuous rotation. The sensor was calibrated using Coregas (Yennora, Australia) span gases (102.3, 403.7, 613.8 and 1198 ppm CO_2). Every 24hours, an automatic zero compensation circuit removed all CO_2 from the detector prior to a zero-reference measurement, providing a stable long-term measurement baseline.

The timing and rate of heating, chilling and gas dosing in each sump were regulated by a central computer system according to the baseline from the reference site using custom-made software based on LabVIEW (National Instruments, Austin, USA). The software for temperature regulation was created by the School of Information Technology and Electrical Engineering (The University of Queensland) and the software for pCO_2 regulation by

SciWare (Brisbane, Australia). The software was also capable of triggering an alarm system if offsets deviated from the given setpoints.

The treated water flowed continuously from the sumps (20L/min per sump) through individual pipes to 40 L experimental aquaria which contained the sponge replicates and were equipped with HOBO Pendant temperature loggers (Onset, Bourne, USA), Odyssey light loggers (Dataflow Systems, Christchurch, New Zealand) and small wave makers. pH was continuously monitored in one experimental tank per treatment using InPro4501VP X pH sensors (Mettler Toledo, Victoria, Australia) connected to a monitoring system (ACQ110, Aquatronica, Reggio Emilia, Italy). These sensors were rotated between tanks of the same treatment every 4th day. In addition, weekly pH (NBS scale) measurements were made in all 24 tanks at 11:00 and at 20:00 using a pHep sensor freshly calibrated (HI 98128, Hanna Instruments, Rhode Island, USA) (Fig. S4.2). Adjacent tanks with the same scenarios contained Pt100 temperature sensors (RS components, Wetherhill Park, Australia) that provided feed-back measurements to the sump controller. No feedback measurements were provided for pH/pCO_2, allowing a minimal extent of local pCO_2 regulation due to metabolic activity of the sponges in the experimental tanks.

The experimental elevation of temperature and pCO_2 are referred to as simulated warming and acidification respectively in the main text, while acknowledging the relatively shorter timescale of the experimental elevations compared to oceanographic changes (McElhany, 2016).

Treatment conditions

During the experiment, sunrise time shifted from 05:10 to 05:50 h and sunset from 18:40 to 18:15 h, with in tank light intensities maximizing at mid-day (on average 463 ± 21 μmol quanta m^{-2} s^{-1}). After gradual adjustment of the treatments, full experimental conditions were reached on the 1st of January 2015, when daily mean water temperatures were 26.3 ± 0.3°C for the present-day (PD) temperature scenarios and 29.9 ± 0.1°C for the future (RCP8.5) temperature scenarios (mean ± SEM, Fig. S4.1). A snapshot of seawater chemistry parameters at week 4 (when most physiological measurements were performed) is given in Table S4.1, whereas Table S4.2 summarizes pH, total alkalinity and pCO_2 measurements made in the aquaria on other dates throughout the experiment. At the end of the experiment (9th of March 2015), which roughly coincided with the end of the Austral summer, temperature had decreased to approximately the same level as prevalent during week 1 (Fig.

S4.1). Upstream sump pCO_2 at midday over the 10-week experimental period ranged from 428 ± 12 µatm to 519 ± 10 µatm for the PD pCO_2 scenarios and from 924 ± 5 µatm to 1053 ± 9 µatm for the RCP8.5 pCO_2 scenarios. Downstream midday pH in the experimental aquaria ranged from 7.98 to 8.27 for the PD pCO_2 scenarios and from 7.79 to 7.99 for the RCP8.5 pCO_2 scenarios.

Total alkalinity (A_T) of the experimental aquaria was measured with Gran titration using an automated titrator (T50, Mettler Toledo, Langacher, Switzerland) calibrated daily with pH NBS scale buffers (Radiometer analytical, Lyon, France) and Dickson's Standards (University of California, San Diego, USA) (Kline *et al.,* 2012).

Buoyant mass conversion

To express total bioerosion rates of the sponge in mg $CaCO_3$ cm^{-2} core area day^{-1}, the measured changes in buoyant mass (BM) over time where converted to changes in $CaCO_3$ mass of the cores (M_{CaCO3}). This was made possible through a linear regression analysis between buoyant mass and $CaCO_3$ mass as measured from sponge and control cores at week 4 of the experiment, after having assessed the data for homoscedacity and the residuals for normality. Equation (1) expresses the regression found between the two variables (r^2=0.95, $p<0.001$, n=70):

$$\log(BM) = \log(M_{CaCO3}) - 0.196 \quad (1)$$

Metabolic oxygen and carbon flux

A theoretical curve of daily net oxygen production/ consumption was constructed based on the average daily irradiance profile during the experimental phase (see Fang *et al.*, 2014 for details). Net oxygen production by *C. orientalis* can saturate at around 300 µmol photons m^{-2} s^{-1} (Fang *et al.*, 2014), which was attained between 09:00 and 14:00 h. Oxygen production was assumed to decrease linearly from max P_{net} to R_{dark} between 14:00 and 18:00 h, maintain R_{dark} levels during darkness (18:00 to 05:00 h) and linearly increase from R_{dark} to max P_{net} between 05:00 and 09:00 h. Oxygen flux during light, dark and transitioning hours was defined as time integrals and geometrically calculated from the relevant areas of the theoretical curve (see Fig. 1 in Fang *et al.*, 2014). Oxygen flux was then summed over 24 h and converted to carbon flux (mg C cm^{-2} day^{-1}) based on the stoichiometric balance of

photosynthesis (0.375 g carbon per g oxygen), applying a photosynthetic quotient of 1.1 and a respiratory quotient of 0.9 (Muscatine *et al*., 1981; Fang *et al., 2014*).

To quantify the flux of particulate and dissolved organic carbon (POC and DOC respectively), sponges were incubated in confined seawater (5 L incubation chambers) over 24 hours. Seawater samples were collected in glass vials (pre-combusted and washed with 1N hydrochloric acid and Milli-Q water), which were sealed and immediately frozen for later analysis. Each of the defrosted seawater samples was filtered through a pre-combusted GF/F filter (pore size 0.7 μm) to separate particles >0.7 μm along with POC onto the filter while collecting the filtrate, which contains the DOC (Yahel *et al.*, 2003). Subsequently, Milli-Q water was washed through the filters to remove salts, followed by 0.1N HCl to remove any inorganic carbon and Milli-Q again before drying the filters at 60°C overnight. Dried filters were weighted to ±0.001 mg and wrapped into large tin capsules. Quantitative combustion was performed at the School of Chemistry and Molecular Biosciences at the University of Queensland with a FLASH 2000 CHNS/O Analyzer. Blank filters were used to correct the measured values. To quantify DOC, the filtrate was analysed at the Advanced Water Management Centre at the University of Queensland using a Total Organic Carbon Analyzer (TOC-L CSH with TNM-L TN unit, Shimadzu). The samples were first acidified using HCl and aerated to remove inorganics, and non-purgeable organic carbon was measured immediately thereafter (Findlay *et al.*, 2010).

Density of the sponge cores

The bulk density of the sponge cores was quantified at the beginning of the experiment and at week 4 of the experiment. Subsamples of $CaCO_3$ with sponge infestation were isolated and reconditioned overnight in distilled water on a shaker table. Without exposing the samples to air, they were transferred to 12% sodium hypochlorite for 4 h and rinsed and buoyant weighed in distilled water (buoyant mass in water = $m_{buoyant}$). Subsequently the samples were drip-dried, weighed in air (wet mass = m_{wet}) and dried at 60°C to a stable mass (dry mass = m_{dry}). Following Archimedes' principle, the volumes of the skeletal matrix of the cores ($V_{skeletal\ matrix,}$ Fig. S4.3) were estimated [Equation (2), where d_{water} is the density of distilled water (1.00 g cm^{-3} at 22°C) (Lide, 2006)]. Since the samples were perforate (Fig. S4.3), pore volumes (V_{pores}) [Equation (3)] were added to the skeletal matrix volumes in order to calculate the bulk volumes of the cores (V_{bulk}) [Equation (4)]. Bulk densities ($d_{bulk,}$ g cm^{-3}) and porosity (Por, %) were then calculated using Equation (5) and (6) respectively.

$$V_{skeletal\ matrix} = (m_{dry} - m_{buoyant}) / d_{water} \quad (2)$$

$$V_{pores} = (m_{wet} - m_{dry}) / d_{water} \quad (3)$$

$$V_{bulk} = V_{skeletal\ matrix} + V_{pores} \quad (4)$$

$$d_{bulk} = m_{dry} / V_{bulk} \quad (5)$$

$$Por = (100 \times V_{pores}) / V_{bulk} \quad (6)$$

Supplementary Tables

Table S4.1: Seawater parameters at week 4 of the experiment for each of the scenarios, irrespective of diet. PCO_2 was measured in upstream sumps (pCO_2 upstream), whereas temperature, total alkalinity (A_T) and pH_{NBS} (NBS scale) are given as means ± SEM of values measured in all downstream aquaria (n=6 for each T and pCO_2 combination, irrespective of diet). Values represent instantaneous averages at 11:00 h and at 20:00 h (light intensity 414 and 0 µmol quanta m^{-2} s^{-1} respectively) on 31/01/2015. Downstream pCO_2, aragonite saturation state (Ω_{Arag}), bicarbonate (HCO_3^-) and carbonate (CO_3^{2-}) were estimated using the software CO2calc 1.2.0 (Robbins *et al*., 2010) and therefore lack error bars. Conditions are abbreviated PD for present-day levels and RCP8.5 for future levels of temperature and pCO_2. For seawater parameters measured on other dates throughout the experiment see Table S4.2. (SW = seawater).

	PD temperature		RCP8.5 temperature	
	PD pCO_2	RCP8.5 pCO_2	PD pCO_2	RCP8.5 pCO_2
11:00 h				
pCO_2 upstream (µatm)	491 ± 2.4	919 ± 1.7	435 ± 2.5	942 ± 2.3
Temperature (°C)	28.1 ± 0.1	27.8 ± 0.1	31.3 ± 0.1	31.1 ± 0.1
A_T (µmol $kgSW^{-1}$)	2275.3 ± 0.4	2274.1 ± 0.6	2273.6 ± 1.1	2272.9 ± 1.1
pH_{NBS}	8.11 ± 0.01	7.88 ± 0.01	8.16 ± 0.01	7.90 ± 0.02
pCO_2 downstream (µatm)	488	909	429	916
HCO_3^- (µmol $kgSW^{-1}$)	1784	1961	1699	1949
CO_3^{2-} (µmol $kgSW^{-1}$)	199	127	233	133
Ω_{Arag}	3.22	2.05	3.84	2.25
20:00 h				
pCO_2 upstream (µatm)	390 ± 2.3	915 ± 1.8	406 ± 2.2	887 ± 2.1
Temperature (°C)	28.3 ± 0.1	28.6 ± 0.0	31.2 ± 0.0	31.0 ± 0.1
A_T (µmol $kgSW^{-1}$)	2227.0 ± 1.4	2229.7 ± 1.4	2228.8 ± 1.1	2229.9 ± 1.5
pH_{NBS}	8.10± 0.02	7.87± 0.01	8.14± 0.02	7.86± 0.01
pCO_2 downstream (µatm)	493	920	446	960
HCO_3^- (µmol $kgSW^{-1}$)	1755.098	1923.322	1687.998	1910.934
CO_3^{2-} (µmol $kgSW^{-1}$)	191.47	124.664	219.475	129.925
Ω_{Arag}	3.09	2.02	3.60	2.13

Table S4.2: Seawater chemistry parameters measured throughout the experiment in the downstream aquaria. pH (NBS scale) and total alkalinity (A_T, in µmol $kgSW^{-1}$) were measured using the Gran titration method (Kline *et al*., 2012). Downstream pCO_2 (in µatm) in the experimental aquaria (Aq # refers to a specific aquarium for each measurement) was estimated using the software CO2calc 1.2.0 (Robbins *et al*., 2010) and compared to upstream sump pCO_2 for each timepoint. Conditions are abbreviated PD for present-day levels and RCP8.5 for future levels of temperature and pCO_2. (SW = seawater).

	Treatment					pCO_2				
Aq #	T	pCO_2	Feeding	pH	A_T	downstream	upstream	Date	Day/ Night	Time
9	PD	PD	U	8.119	2317	482	452	7/01/2015	Day	16:00
18	PD	PD	U	8.124	2328	477		7/01/2015	Day	16:00
6	PD	PD	S	8.128	2317	470		7/01/2015	Day	16:00
13	PD	PD	S	8.140	2321	456		7/01/2015	Day	16:00
4	PD	PD	U	8.122	2248	466	459	8/01/2015	Day	16:00
9	PD	PD	U	8.105	2244	488		8/01/2015	Day	16:00
18	PD	PD	U	8.120	2247	468		8/01/2015	Day	16:00
6	PD	PD	S	8.122	2245	465		8/01/2015	Day	16:00
13	PD	PD	S	8.120	2247	468		8/01/2015	Day	16:00
23	PD	PD	S	8.121	2245	466		8/01/2015	Day	16:00
9	PD	PD	U	8.097	2280	508	451	12/01/2015	Day	13:00
18	PD	PD	U	8.095	2280	511		12/01/2015	Day	13:00
6	PD	PD	S	8.112	2287	489		12/01/2015	Day	13:00
13	PD	PD	S	8.104	2281	498		12/01/2015	Day	13:00
4	PD	PD	U	8.212	2288	369	402	13/01/2015	Day	13:00
9	PD	PD	U	8.222	2287	358		13/01/2015	Day	13:00
18	PD	PD	U	8.241	2311	342		13/01/2015	Day	13:00
6	PD	PD	S	8.222	2292	359		13/01/2015	Day	13:00
13	PD	PD	S	8.273	2297	309		13/01/2015	Day	13:00
23	PD	PD	S	8.279	2298	304		13/01/2015	Day	13:00
4	PD	PD	U	8.098	2313	511	461	15/01/2015	Day	12:00
9	PD	PD	U	8.082	2310	533		15/01/2015	Day	12:00
18	PD	PD	U	8.099	2313	509		15/01/2015	Day	12:00
6	PD	PD	S	8.082	2311	533		15/01/2015	Day	12:00
13	PD	PD	S	8.078	2310	539		15/01/2015	Day	12:00
23	PD	PD	S	8.101	2311	506		15/01/2015	Day	12:00
4	PD	PD	U	8.081	2293	531	389	16/01/2015	Day	16:00
9	PD	PD	U	8.095	2290	510		16/01/2015	Day	16:00
18	PD	PD	U	8.129	2310	468		16/01/2015	Day	16:00
6	PD	PD	S	8.138	2295	454		16/01/2015	Day	16:00
13	PD	PD	S	8.160	2296	426		16/01/2015	Day	16:00
23	PD	PD	S	8.130	2290	463		16/01/2015	Day	16:00

4	PD	PD	U	8.109	2237	480	527	12/02/2015	Day	15:00
9	PD	PD	U	8.122	2235	463		12/02/2015	Day	15:00
18	PD	PD	U	8.114	2240	474		12/02/2015	Day	15:00
4	PD	PD	U	8.144	2280	441	404	16/02/2015	Day	16:00
9	PD	PD	U	8.148	2280	436		16/02/2015	Day	16:00
18	PD	PD	U	8.151	2283	433		16/02/2015	Day	16:00
4	PD	PD	U	8.166	2263	412	380	16/02/2015	Night	21:00
9	PD	PD	U	8.150	2260	430		16/02/2015	Night	21:00
18	PD	PD	U	8.164	2262	414		16/02/2015	Night	21:00
4	PD	PD	U	8.121	2262	466	487	5/03/2015	Day	14:00
9	PD	PD	U	8.119	2271	471		5/03/2015	Day	14:00
18	PD	PD	U	8.113	2266	478		5/03/2015	Day	14:00
6	PD	PD	S	8.129	2212	446		5/03/2015	Day	14:00
13	PD	PD	S	8.169	2212	398		5/03/2015	Day	14:00
23	PD	PD	S	8.159	2212	410		5/03/2015	Day	14:00
4	PD	PD	U	8.122	2275	468	518	8/03/2015	Day	12:00
9	PD	PD	U	8.119	2291	476		8/03/2015	Day	12:00
18	PD	PD	U	8.113	2294	484		8/03/2015	Day	12:00
6	PD	PD	S	8.175	2296	407		8/03/2015	Day	12:00
23	PD	PD	S	8.143	2296	446		8/03/2015	Day	12:00
2	PD	RCP8.5	U	7.942	2281	763	947	12/01/2015	Day	13:00
14	PD	RCP8.5	U	7.922	2279	804		12/01/2015	Day	13:00
7	PD	RCP8.5	S	7.879	2276	898		12/01/2015	Day	13:00
21	PD	RCP8.5	S	7.921	2277	805		12/01/2015	Day	13:00
2	PD	RCP8.5	U	7.918	2232	802	881	24/01/2015	Night	18:00
12	PD	RCP8.5	U	7.911	2234	818		24/01/2015	Night	18:00
14	PD	RCP8.5	U	7.909	2238	824		24/01/2015	Night	18:00
7	PD	RCP8.5	S	7.909	2240	824		24/01/2015	Night	18:00
17	PD	RCP8.5	S	7.912	2243	819		24/01/2015	Night	18:00
21	PD	RCP8.5	S	7.910	2241	823		24/01/2015	Night	18:00
2	PD	RCP8.5	U	7.860	2307	969	934	26/01/2015	Day	13:00
12	PD	RCP8.5	U	7.916	2293	832		26/01/2015	Day	13:00
14	PD	RCP8.5	U	7.912	2294	841		26/01/2015	Day	13:00
7	PD	RCP8.5	S	7.871	2304	941		26/01/2015	Day	13:00
17	PD	RCP8.5	S	7.919	2289	824		26/01/2015	Day	13:00
21	PD	RCP8.5	S	7.913	2288	836		26/01/2015	Day	13:00
2	PD	RCP8.5	U	7.898	2267	873	922	13/02/2015	Day	11:00
12	PD	RCP8.5	U	7.916	2270	834		13/02/2015	Day	11:00
14	PD	RCP8.5	U	7.920	2273	826		13/02/2015	Day	11:00
2	PD	RCP8.5	U	7.845	2244	976	932	13/02/2015	Night	21:00
12	PD	RCP8.5	U	7.859	2241	939		13/02/2015	Night	21:00
14	PD	RCP8.5	U	7.875	2252	906		13/02/2015	Night	21:00

2	PD	RCP8.5	U	7.875	2256	925	912	14/02/2015	Day	15:00
12	PD	RCP8.5	U	7.904	2261	858		14/02/2015	Day	15:00
14	PD	RCP8.5	U	7.894	2258	880		14/02/2015	Day	15:00
2	PD	RCP8.5	U	7.887	2278	884	1008	23/02/2015	Night	21:00
12	PD	RCP8.5	U	7.879	2284	905		23/02/2015	Night	21:00
14	PD	RCP8.5	U	7.891	2284	878		23/02/2015	Night	21:00
7	PD	RCP8.5	S	7.871	2342	946	1006	3/03/2015	Day	10:00
17	PD	RCP8.5	S	7.823	2342	1071		3/03/2015	Day	10:00
21	PD	RCP8.5	S	7.848	2346	1006		3/03/2015	Day	10:00
7	PD	RCP8.5	S	7.861	2283	950	945	3/03/2015	Night	22:00
17	PD	RCP8.5	S	7.885	2275	889		3/03/2015	Night	22:00
21	PD	RCP8.5	S	7.865	2274	936		3/03/2015	Night	22:00
2	PD	RCP8.5	U	7.869	2249	904	1047	4/03/2015	Day	12:00
12	PD	RCP8.5	U	7.860	2262	931		4/03/2015	Day	12:00
14	PD	RCP8.5	U	7.866	2250	911		4/03/2015	Day	12:00
7	PD	RCP8.5	S	7.877	2222	875		4/03/2015	Day	12:00
17	PD	RCP8.5	S	7.862	2265	928		4/03/2015	Day	12:00
8	RCP8.5	PD	U	8.237	2338	352	398	15/01/2015	Day	14:00
15	RCP8.5	PD	U	8.201	2342	392		15/01/2015	Day	14:00
24	RCP8.5	PD	U	8.255	2346	335		15/01/2015	Day	14:00
3	RCP8.5	PD	S	8.189	2295	398		15/01/2015	Day	14:00
11	RCP8.5	PD	S	8.192	2295	394		15/01/2015	Day	14:00
20	RCP8.5	PD	S	8.164	2293	427		15/01/2015	Day	14:00
8	RCP8.5	PD	U	8.124	2312	482	427	17/01/2015	Day	11:00
15	RCP8.5	PD	U	8.147	2295	447		17/01/2015	Day	11:00
24	RCP8.5	PD	U	8.132	2316	472		17/01/2015	Day	11:00
3	RCP8.5	PD	S	8.155	2316	442		17/01/2015	Day	11:00
11	RCP8.5	PD	S	8.183	2319	408		17/01/2015	Day	11:00
20	RCP8.5	PD	S	8.156	2327	442		17/01/2015	Day	11:00
8	RCP8.5	PD	U	8.144	2258	445	463	5/02/2015	Day	15:00
15	RCP8.5	PD	U	8.148	2255	439		5/02/2015	Day	15:00
24	RCP8.5	PD	U	8.140	2255	449		5/02/2015	Day	15:00
8	RCP8.5	PD	U	8.129	2301	473	450	7/02/2015	Day	17:00
15	RCP8.5	PD	U	8.131	2301	471		7/02/2015	Day	17:00
24	RCP8.5	PD	U	8.142	2301	456		7/02/2015	Day	17:00
8	RCP8.5	PD	U	8.132	2246	458	459	9/02/2015	Night	21:00
15	RCP8.5	PD	U	8.146	2247	440		9/02/2015	Night	21:00
24	RCP8.5	PD	U	8.138	2245	450		9/02/2015	Night	21:00
8	RCP8.5	PD	U	8.150	2262	434	479	11/02/2015	Night	22:00
15	RCP8.5	PD	U	8.217	2259	357		11/02/2015	Night	22:00
24	RCP8.5	PD	U	8.200	2261	376		11/02/2015	Night	22:00
3	RCP8.5	PD	S	8.110	2300	498	430	2/03/2015	Day	16:00

11	RCP8.5	PD	S	8.142	2306	455		2/03/2015	Day	16:00
20	RCP8.5	PD	S	8.139	2306	460		2/03/2015	Day	16:00
3	RCP8.5	PD	S	8.158	2227	419	373	2/03/2015	Night	23:00
11	RCP8.5	PD	S	8.185	2225	387		2/03/2015	Night	23:00
20	RCP8.5	PD	S	8.141	2229	440		2/03/2015	Night	23:00
5	RCP8.5	RCP8.5	U	7.991	2316	694	954	7/01/2015	Day	16:00
16	RCP8.5	RCP8.5	U	7.982	2319	712		7/01/2015	Day	16:00
5	RCP8.5	RCP8.5	U	7.913	2292	857	950	20/01/2015	Day	13:00
16	RCP8.5	RCP8.5	U	7.910	2291	864		20/01/2015	Day	13:00
22	RCP8.5	RCP8.5	U	7.915	2290	852		20/01/2015	Day	13:00
1	RCP8.5	RCP8.5	S	7.923	2290	834		20/01/2015	Day	13:00
10	RCP8.5	RCP8.5	S	7.910	2289	863		20/01/2015	Day	13:00
19	RCP8.5	RCP8.5	S	7.917	2286	855		20/01/2015	Day	13:00
5	RCP8.5	RCP8.5	U	7.877	2281	933	938	22/01/2015	Day	17:00
16	RCP8.5	RCP8.5	U	7.879	2284	929		22/01/2015	Day	17:00
22	RCP8.5	RCP8.5	U	7.939	2282	791		22/01/2015	Day	17:00
1	RCP8.5	RCP8.5	S	7.921	2280	830		22/01/2015	Day	17:00
10	RCP8.5	RCP8.5	S	7.899	2282	880		22/01/2015	Day	17:00
19	RCP8.5	RCP8.5	S	7.895	2285	891		22/01/2015	Day	17:00
5	RCP8.5	RCP8.5	U	7.910	2258	851	958	5/02/2015	Day	15:00
16	RCP8.5	RCP8.5	U	7.899	2262	878		5/02/2015	Day	15:00
22	RCP8.5	RCP8.5	U	7.898	2259	879		5/02/2015	Day	15:00
5	RCP8.5	RCP8.5	U	7.893	2297	907	956	6/02/2015	Day	15:00
16	RCP8.5	RCP8.5	U	7.908	2297	872		6/02/2015	Day	15:00
22	RCP8.5	RCP8.5	U	7.890	2296	914		6/02/2015	Day	15:00
5	RCP8.5	RCP8.5	U	7.918	2245	824	944	8/02/2015	Night	22:00
16	RCP8.5	RCP8.5	U	7.925	2245	808		8/02/2015	Night	22:00
22	RCP8.5	RCP8.5	U	7.915	2244	830		8/02/2015	Night	22:00
1	RCP8.5	RCP8.5	S	7.921	2255	822	961	10/02/2015	Night	21:00
10	RCP8.5	RCP8.5	S	7.913	2259	842		10/02/2015	Night	21:00
19	RCP8.5	RCP8.5	S	7.915	2260	837		10/02/2015	Night	21:00
1	RCP8.5	RCP8.5	S	7.840	2342	1054	1113	21/02/2015	Day	11:00
10	RCP8.5	RCP8.5	S	7.818	2341	1116		21/02/2015	Day	11:00
19	RCP8.5	RCP8.5	S	7.873	2341	966		21/02/2015	Day	11:00

Table S4.3: Particulate organic carbon (POC) uptake and sponge biomass of *Cliona orientalis* at Heron Island on the southern Great Barrier Reef. Total sponge bioerosion, maximum net photosynthesis, dark respiration and dissolved organic carbon uptake are displayed in Fig. 4.3 and 4.4 of the main article. Outputs of statistical analyses of all variables are displayed in Table S4.4. Data were generated after 4 weeks of exposure to full treatment conditions of present day and RCP8.5 temperature and pCO_2, while receiving an unsupplemented or supplemented diet (mean ± SEM, n=7). The levels of temperature and pCO_2 are abbreviated PD for present-day levels and RCP8.5 for levels predicted for 2100.

		Unsupplemented diet		Supplemented diet	
		PD Temperature	RCP8.5 Temperature	PD Temperature	RCP8.5 Temperature
POC uptake (mg C cm^{-2} day^{-1})					
	PD pCO_2	0.25 ± 0.19	0.04 ± 0.03	0.05 ± 0.03	-0.03 ± 0.02
	RCP8.5 pCO_2	0.11 ± 0.07	-0.03 ± 0.02	0.11 ± 0.02	-0.02 ± 0.01
Sponge organic biomass ($mg_{(biomass)}/g_{(core)}$)					
	PD pCO_2	40.95 ± 1.76	38.28 ± 2.29	42.36 ± 2.12	36.66 ± 1.10
	RCP8.5 pCO_2	39.27 ± 1.32	36.25 ± 1.86	44.37 ± 2.72	35.60 ± 1.99
Spicular mass ($mg_{(biomass)}/g_{(core)}$)					
	PD pCO_2	22.84 ± 2.45	26.69 ± 2.69	23.16 ± 2.04	22.07 ± 3.69
	RCP8.5 pCO_2	24.96 ± 1.84	24.45 ± 1.30	23.47 ± 1.71	18.17 ± 2.89

Table S4.4: Results of 3-way factorial ANOVA and follow up tests where applicable for the key parameters presented in Figures 4.3-4.5 of the main article and Table S4.3. Temperature (T), pCO_2 and diet were the independent factors of the analysis. Simple main effects are reported following significant interactions of the factors, whereas main effects are reported when there is no interaction of the factors at the given level of comparison. The absolute width of the 95% confidence interval (CI) of the effect size of the single factors is shown for each variable. Temperature and pCO_2 are abbreviated PD for present-day levels and RCP8.5 for levels predicted for 2100. Max P_{net} = maximum net photosynthesis, R_{dark} = dark respiration, DOC = dissolved organic carbon, POC = particulate organic carbon, C_{net} = daily net carbon surplus, S = Supplemented diet, U = Unsupplemented diet. Data transformations: [a]log, [b]sqrt(x+3). *Indicates datasets with non-homogeneous variances where the significance level was reduced to 0.01 to minimize the risk of a Type I error (Underwood, 1997). All other data were evaluated at a 0.05 level of significance.

		ANOVA	Source of variation	DF	MS	F	P	Conclusions	Width of CI of effect size
Sponge bioerosion rates (mg $CaCO_3$ cm^{-2} d^{-1})									
1	Total[a]	3-way	T	1	0.115	4.54	0.038	PD>RCP8.5	0.023
			pCO_2	1	0.002	0.08	0.78		0.019
			Diet	1	0.205	8.07	0.007	S>U	0.006
			T × pCO_2	1	0.011	0.42	0.52		
			T × Diet	1	0.006	0.24	0.63		
			pCO_2 × Diet	1	0.000	0.00	0.98		
			T × pCO_2 × Diet	1	0.003	0.11	0.75		
			Error	48	0.025				
Weight loss of control cores (mg $CaCO_3$ cm^{-2} d^{-1})									
4	Total	3-way	T	1	0.120	0.93	0.34		0.022
			pCO_2	1	0.008	0.06	0.80		0.117
			Diet	1	0.004	0.03	0.86		0.083
			T × pCO_2	1	0.029	0.23	0.64		
			T × Diet	1	0.000	0.00	0.96		

			pCO_2 × Diet	1	0.130	1.00	0.32		
			T × pCO_2 × Diet	1	0.000	0.00	0.99		
			Error	48	0.129				
Sponge biomass ($mg_{(biomass)}/g_{(core)}$)									
5	Organic mass	3-way	T	1	335.004	13.16	<0.001	PD>RCP8.5	0.241
			pCO_2	1	6.261	0.25	0.62		0.698
			Diet	1	14.771	0.58	0.45		1.029
			T × pCO_2	1	9.583	0.38	0.54		
			T × Diet	1	63.383	2.49	0.12		
			pCO_2 × Diet	1	17.913	0.70	0.41		
			T × pCO_2 × Diet	1	6.106	0.24	0.63		
			Error	48	25.456				
6	Spicular mass	3-way	T	1	8.153	0.20	0.66		1.953
			pCO_2	1	12.087	0.29	0.59		1.111
			Diet	1	127.751	3.09	0.08		1.199
			T × pCO_2	1	64.148	1.55	0.22		
			T × Diet	1	82.977	2.00	0.16		
			pCO_2 × Diet	1	10.487	0.25	0.62		
			T × pCO_2 × Diet	1	0.018	0.00	0.98		
			Error	48	41.394				
Oxygen flux ($\mu mol\ O_2\ cm^{-2}\ h^{-1}$)									
7	$P_{net}{}^{b}$	3-way	T	1	10.754	189.11	<0.001		0.055
			pCO_2	1	0.051	0.89	0.35		0.007
			Diet	1	0.069	1.22	0.27		0.020

			T × pCO_2	1	0.136	2.39	0.13		
			T × Diet	1	0.065	1.14	0.29		
			pCO_2 × Diet	1	0.000	0.00	0.99		
			T × pCO_2 × Diet	1	0.369	6.48	0.014		
			Error	48	0.057				
7.1	Unsupplemented	Simple 2-way	T × pCO_2	1	0.467	8.21	0.006		
			Error	48	0.057				
7.1.1	PD pCO_2	Simple main effect	T	1	1.669	29.36	<0.0001	PD>RCP8.5	
			Error	48	0.057				
7.1.2	RCP8.5 pCO_2	Simple main effect	T	1	4.791	84.25	<0.0001	PD>RCP8.5	
			Error	48	0.057				
7.2	Unsupplemented	Main effect	pCO_2	1	0.339	5.96	0.018	PD<RCP8.5	
			Error	48	0.057				
7.3	Supplemented	Simple 2-way	T × pCO_2	1	0.029	0.51	0.48		
			Error	48	0.057				
7.3.1	PD pCO_2	Main effect	T	1	2.718	47.80	<0.0001	PD>RCP8.5	
			Error	48	0.057				
7.3.2	RCP8.5 pCO_2	Main effect	T	1	1.982	34.85	<0.0001	PD>RCP8.5	
			Error	48	0.057				
8	R_{dark}*	3-way	T	1	14.229	36.44	<0.0001	PD>RCP8.5	0.252
			pCO_2	1	0.354	0.91	0.35		0.027
			Diet	1	0.104	0.27	0.61		0.115
			T × pCO_2	1	0.243	0.62	0.43		
			T × Diet	1	0.014	0.04	0.85		
			pCO_2 × Diet	1	1.145	2.93	0.09		
			T × pCO_2 × Diet	1	0.032	0.08	0.78		
			Error	48	0.391				

Carbon flux (mg C cm^{-2} d^{-1})

9	DOC uptake*	3-way	T	1	0.883	93.49	<0.001		0.075
			pCO_2	1	0.453	48.02	<0.001		0.135
			Diet	1	0.005	0.54	0.46		0.120
			T × pCO_2	1	0.365	38.66	<0.001		
			T × Diet	1	0.196	20.71	<0.001		
			pCO_2 × Diet	1	0.086	9.09	0.004		
			T × pCO_2 × Diet	1	0.108	11.39	0.001		
			Error	48	0.009				
9.1	Unsupplemented	Simple 2-way	T × pCO_2	1	0.434	46.01	<0.001		
			Error	48	0.009				
9.1.1	PD pCO_2	Simple main effect	T	1	1.338	141.76	<0.001	PD>RCP8.5	
			Error	48	0.009				
9.1.2	RCP8.5 pCO_2	Simple main effect	T	1	0.051	5.35	0.02		
			Error	48	0.009				
9.2	Supplemented	Simple 2-way	T × pCO_2	1	0.038	4.04	0.05		
			Error	48	0.009				
9.2.1	PD and RCP8.5 pCO_2	Main effect	T	1	0.124	13.10	0.001	PD>RCP8.5	
			Error	48	0.009				
9.3	PD T and pCO_2	Main effect	Diet	1	0.246	26.06	<0.001	S<U	
			Error	48	0.009				
9.4.1	PD T and U	Simple main effect	pCO_2	1	0.901	95.43	<0.001	PD>RCP8.5	
			Error	48	0.009				
9.4.2	PD T and S	Simple main effect	pCO_2	1	0.108	11.42	0.001	PD>RCP8.5	
			Error	48	0.009				
10	POC uptake*	3-way	T	1	0.021	5.62	0.02		0.166
			pCO_2	1	0.001	0.25	0.62		0.183
			Diet	1	0.001	0.38	0.54		0.203
			T × pCO_2	1	0.009	2.48	0.12		

			T × Diet	1	0.000	0.11	0.74		
			pCO_2 × Diet	1	0.000	0.12	0.73		
			T × pCO_2 × Diet	1	0.003	0.83	0.37		
			Error	48	0.004				
11	C_{net}	3-way	T	1	5.049	193.41	<0.0001		0.004
			pCO_2	1	0.585	22.43	<0.0001		0.011
			Diet	1	0.082	3.14	0.08		0.022
			T × pCO_2	1	0.235	9.01	0.004		
			T × Diet	1	0.387	14.81	<0.001		
			pCO_2 × Diet	1	0.516	19.76	<0.0001		
			T × pCO_2 × Diet	1	0.065	2.48	0.12		
			Error	48	0.026				
11.1	PD pCO_2	Simple main effect	T	1	3.887	148.91	<0.0001	PD>RCP8.5	
			Error	48	0.026				
11.2	RCP8.5 pCO_2	Simple main effect	T	1	1.493	57.18	<0.0001	PD>RCP8.5	
			Error	48	0.026				
11.3	PD temp	Simple main effect	pCO_2	1	0.751	28.78	<0.0001	PD>RCP8.5	
			Error	48	0.026				
11.4	RCP8.5 Temp	Simple main effect	pCO_2	1	0.041	1.57	0.21		
			Error	48	0.026				
11.5	PD temp	Simple main effect	Diet	1	0.396	15.19	<0.001	U>S	
			Error	48	0.026				
11.6	PD pCO_2	Simple main effect	Diet	1	0.526	20.13	<0.0001	U>S	
			Error	48	0.026				

Supplementary Figures

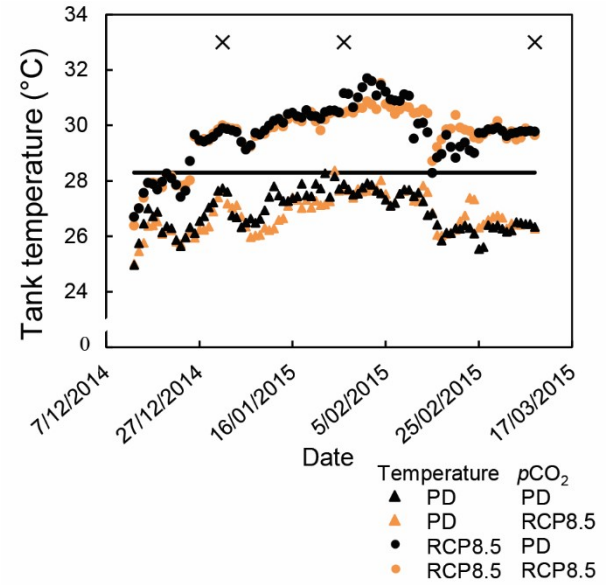

Figure S4.1: Daily temperature profiles obtained throughout the course of the experiment, pooled together for treatments supplemented with additional particulate food and unsupplemented treatments. Mean pCO_2 levels across the experiment were 493 ± 20 µatm (± SEM) for treatments with present day (PD) levels and 982 ± 17 µatm for treatments with Representative Concentration Pathway 8.5 (RCP8.5) levels. The solid line represents 1°C above the maximum monthly mean (MMM+1) established for the Heron Island region based on 50-km pixel satellite data (NOAA, 2016). Crosses represent the start of full treatment, the 4th week thereafter (when the physiological measurements described in the main text were performed) and the end of the experiment respectively.

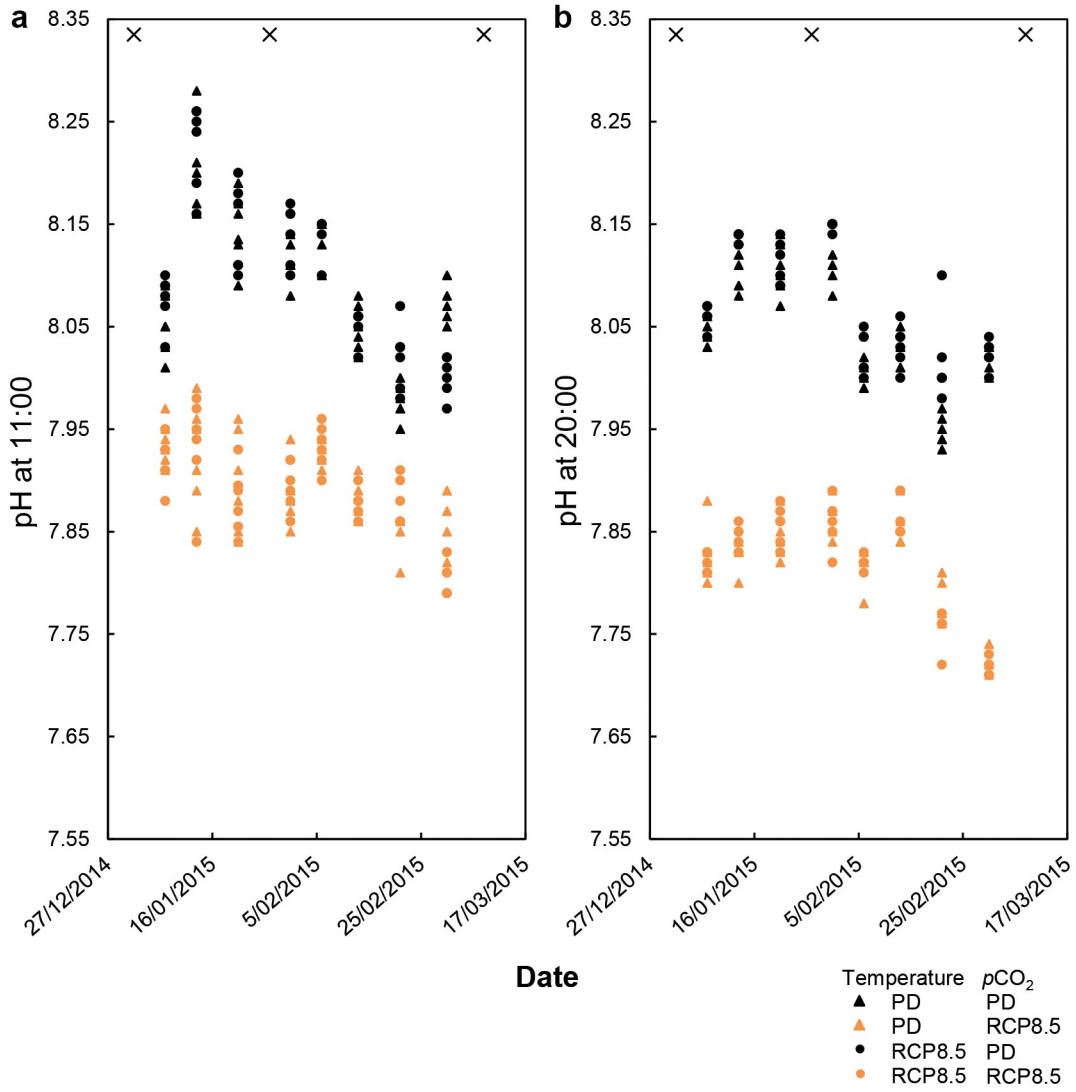

Figure S4.2: Weekly pH profiles (NBS scale) obtained throughout the course of the experiment, pooled together for treatments supplemented with additional particulate food and unsupplemented treatments. Measurements were made at **(a)** 11:00 h and **(b)** 20:00 h in each experimental aquarium. Crosses represent the start of full treatment, the 4th week thereafter (when the physiological measurements described in the main text were performed) and the end of the experiment respectively. The levels of temperature and pCO_2 are abbreviated PD for present-day levels and RCP8.5 for levels predicted for 2100.

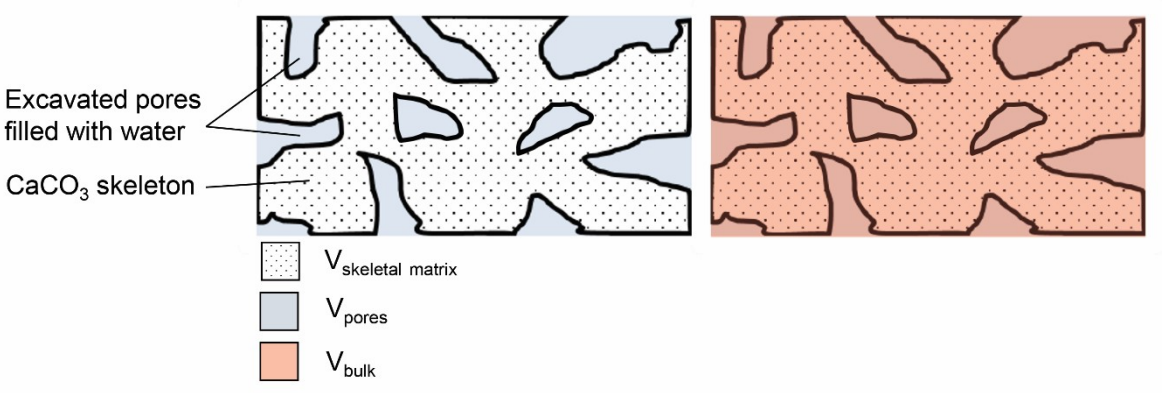

Figure S4.3: Schematic illustration of a $CaCO_3$ sample eroded by an excavating sponge. When submerged, pores created by excavation will be filled with water (in blue) after the sponge tissue has been removed. According to Archimedes' principle, a submerged object will appear to weigh less (buoyant mass in water = $m_{buoyant}$) than it would when dry in air (dry mass =m_{dry}) by an amount equal to the mass of the liquid it displaces (mass of displaced water= $V_{displaced\ water} \times d_{water,}$ where $V_{displaced\ water}$ and d_{water} are the volume and density of the displaced water respectively). Buoyant weighing an object thus allows calculation of the volume of water that the object displaces, if the density of the water is known:

$$V_{displaced\ water} = (m_{dry} - m_{buoyant}) / d_{water}$$

For water-tight objects, the volume of the displaced water equals the volume of the object. Because the sponge is perforate, the volume of the displaced water equals the volume of the skeletal matrix of the sponge core only ($V_{skeletal\ matrix}$). Thus the pore volume must be added to the volume of the skeletal matrix before the bulk volume (V_{bulk}), and by this bulk density of the $CaCO_3$ eroded by the sponge can be measured.

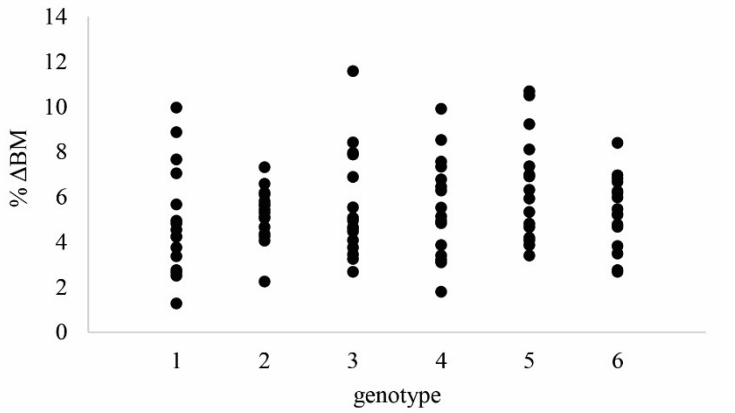

Figure S4.4: An example of overlapping responses produced by the 6 genotypes used in the experiment. For all variables, no single genotype or group of genotypes deviated from the others in response to the treatments in a way that would substantially bias the analysis. This example illustrates the percentage change in buoyant mass (%ΔBM) of the 6 different genotypes over the first 4 weeks of the experiment.